



City Research Online

City, University of London Institutional Repository

Citation: Beyer, U. (1992). Use of vane and air jet vortex generators in a thrust augmenting ejector. (Unpublished Doctoral thesis, City, University of London)

This is the accepted version of the paper.

This version of the publication may differ from the final published version.

Permanent repository link: <https://openaccess.city.ac.uk/id/eprint/29037/>

Link to published version:

Copyright: City Research Online aims to make research outputs of City, University of London available to a wider audience. Copyright and Moral Rights remain with the author(s) and/or copyright holders. URLs from City Research Online may be freely distributed and linked to.

Reuse: Copies of full items can be used for personal research or study, educational, or not-for-profit purposes without prior permission or charge. Provided that the authors, title and full bibliographic details are credited, a hyperlink and/or URL is given for the original metadata page and the content is not changed in any way.

Use of vane and air jet vortex generators
in a thrust augmenting ejector

by

Uwe Beyer

This thesis is submitted for the degree of
Doctor of Philosophy

City University

Mechanical Engineering and Aeronautics Department

November 1992

020250659

A) ABSTRACT:

The beneficial application of vortex generators to control boundary layers in the sub- and supersonic flow regime has been shown in the past. In this thesis the use of vortex generators is extended beyond boundary layer control by using them within an ejector-diffuser type augmentor. During the course of the research work it was established that the vortex generators could be used as effective 'mixers' between the primary air stream and the secondary entrained air stream.

A previously developed mathematical model of ejector-diffuser flow, incorporating parameters such as pressure ratio, nozzle to duct area ratio and diffuser area ratio, was extended and refined. With the help of that model the above mentioned parameters were defined and according to these parameters a test rig was designed and manufactured. The primary ejector was driven by either a peripheral slit jet or eight individual air jets or the combination of both. The major task of the project was to design a rig which was short but produced a good thrust augmentation based on the bare nozzle thrust. A good thrust augmentation ratio was obtainable by ensuring rapid mixing between the primary and secondary air streams.

The test programme was split into two major parts, namely the use of vane vortex generators in conjunction with the peripheral jet and then the application of air jet vortex generators again with the peripheral jet. The vanes and also the air jets were configured either as eight co-rotating vortices or as four contra-rotating vortex pairs. A special case which was also considered involved the air jet vortex generators on their own without peripheral blowing. This test was possible because the eight air jets could be used as primary air injectors and vortex generators at the same time. It emerged that this configuration was particularly revealing because it highlighted the essential difference between co- and contra-rotating vortices.

Near the design primary pressure ratio of 5.0 the bare nozzle thrust was augmented by a maximum of 30 per cent with the vanes installed. This was a considerable advance on the augmentation for the bare augmentor, i.e. the same configuration as above but without vortex generators installed, which came to 1.15 at the same pressure ratio of 5.0. The results of augmentation for the air jets were more complex due to the way in which the air was injected. Elevation and skew angle were responsible for the enlarged complexity. As a general trend it can be stated that the augmentation ratios were high for low pressure ratios, as high as 1.7 at a pressure ratio of 2.0, but fell off as the pressure was increased. Dynamic pressure contour plots in the exit plane gave good indications of the vortex movements produced by the co- and contra-rotating vortex generators.

This project showed that considerable thrust augmentations could be achieved by using vortex generators.

B) CONTENTS:

	pages
A) Abstract	2
B) Contents	3
C) List of Tables	5
D) List of Figures	6
E) Acknowledgement	12
F) Declaration	13
G) Notation	14
1.) Introduction	16 -- 24
1.1.) General	16
1.2.) Historical development of rig	17
1.3.) Vortex formation	18
1.4.) Aims and purpose of this project	21
2.) Preliminary Investigation	25 -- 31
2.1.) Theoretical model	25
2.2.) Results from model	29
3.) Experimental Arrangements and Procedures	33 -- 48
3.1.) Design of experimental rig	33
3.1.1.) Diffuser design	
3.1.2.) Mixing section	
3.1.3.) The mounting stand	
3.1.4.) Working section	
3.1.5.) Vane design	
3.1.6.) Air jet vortex generator design	
3.2.) Commissioning of rig	38
3.2.1.) Dead weight load cell calibration	
3.2.2.) Pressure transducer calibration	
3.2.3.) Tare thrust evaluation	
3.2.4.) Data acquisition	
3.2.5.) Pitot rake assembly	
3.2.6.) Noise tests	
3.3.) Experimental Errors	44
3.3.1.) Experimental setup	
3.3.2.) Accuracy of instruments	
3.3.3.) Loads caused by air supply tubes	
3.3.4.) Random errors	

4.) Thrust measurements using load cells	49 -- 62
4.1.) Bare augmentor	51
4.2.) Modified augmentor with vane vortex generators	52
4.2.1.) Co-rotating vortices	
4.2.2.) Contra-rotating vortices	
4.3.) Modified augmentor with air jet vortex generators	54
4.3.1.) Co-rotating vortices	
4.3.2.) Contra-rotating vortices	
5.) Thrust measurements using pitot rake	63 -- 79
5.1.) Bare augmentor	63
5.2.) Modified augmentor with vane vortex generators	66
5.2.1.) Co-rotating vortices	
5.2.2.) Contra-rotating vortices	
5.3.) Modified augmentor with air jet vortex generators	69
5.3.1.) Co-rotating vortices	
5.3.2.) Contra-rotating vortices	
6.) Comparison of various configurations	80 -- 103
6.1.) Comments on vane vortex generators	80
6.2.) Co-rotating versus contra-rotating	82
6.2.1.) Vane vortex generators	
6.2.2.) Air jet vortex generators	
6.3.) Vane versus air jet thrust	89
6.3.1.) General features using model and load cells	
6.3.2.) Concentrating on pitot rake results	
6.4.) Thrust augmentation: scientific versus engineering	97
7.) Conclusions	103 -- 107
8.) References	108 -- 109
9.) Figures	110 -- 161
10.) Appendices	162 -- 194
10.1.1.) Appendix IA	163
10.1.2.) Appendix IB	169
10.1.3.) Appendix IC	173
10.2.) Drawings	175

C) List of Tables:

	page
Table I : Noise measurements	42
Table II : Legal noise limits	43
Table III : Measured load cell thrusts; co-rotating air jets	56
Table IV : Augmentations based on measured bare nozzle thrust, co-rotating air jets	57
Table V : Load cell thrust measurements; contra-rotating air jet pairs	58
Table VI : Augmentations based on measured bare nozzle thrusts, contra-rotating air jet pairs	59
Table VII : Augmentation for bare augmentor	64
Table VIII: Contra-rot. VVG pairs; Comparison of pitot and load cell thrust	67
Table IX : Co-rot. AJVGs; Comparison of pitot and load cell thrust, air jet only blowing, varying air jet skew angle	73
Table X : Co-rot. AJVGs; Comparison of pitot and load cell thrust, combined peripheral and air jet blowing	76
Table XI : Contra-rot. AJVG pairs; Comparison of pitot and load cell thrust, air jets blowing only; varying air jet skew angle	78
Table XII : Contra-rot. AJVG pairs; Comparison of pitot and load cell thrusts, combined peripheral and air jet blowing	79
Table XIII: Engineering augmentations, co-rotating air jets	98
Table XIV : Engineering augmentations, contra-rotating air jet pairs	99
Table XV : Measured and theoretical bare nozzle thrust for different air jet driving pressures	100

D) List of Figures:

(the Figures for all the Chapters of this thesis are shown on pages 110 to 161)

- 1.1a) Mattock's proposed rig design.
 - 1.1b) Final design of rig as manufactured.
 - 1.1c) Photographs of the entire assembly.
 - 1.2a)-c) Vane vortex arrangements and notation: co-rotating, contra-rotating and bi-plane.
 - 1.3a)-c) Effective co-rotating vortex pattern.
 - 1.4a)-d) Effective contra-rotating vortex pattern.
 - 1.5a) Co-rotating vortices affecting boundary layer.
 - 1.5b) Contra-rotating vortices affecting boundary layer.
 - 1.6a) Equally spaced contra-rotating vortices.
 - 1.6b) Non-equally spaced contra-rotating vortices.

 - 2.1) Theoretical thrust versus pressure ratio for primary temperature ratios of 1.0 to 4.0.
 - 2.2) Theoretical thrust versus pressure ratio for diffuser efficiencies varying between 1.00 and 0.96 based on total pressure loss between inlet and exit of diffuser.
 - 2.3) Theoretical thrust versus pressure ratio for diffuser efficiencies varying between 1.00 and 0.40 based on static pressure rise between inlet and exit of diffuser.

 - 3.1a) Planform of flat plate cropped delta wing; span = 7.5mm.
 - 3.1b) Planform of flat plate cropped delta wing; span = 12mm.
 - 3.2) Definition of positive and negative skew angle.
 - 3.3) Static load cell calibration curve.
 - 3.4a),b) Pressure transducer calibration curves.
 - 3.4c) Relationship between pressure and transducer output voltage.
 - 3.5) Tare thrust calibration curve.
 - 3.6a),b) Radial and equi-spaced rake distribution grid.
 - 3.7) Measuring losses in dynamic pressure due to yaw angle.

 - 4.1) Thrust versus pressure ratio for the bare augmentor with and without the pitot rake installed.
 - 4.2a)-d) Thrust versus pressure ratio for co-rotating vane vortex generators with angle of incidence between 13 and 16 degrees in 1° increments.
 - 4.3) Augmentation versus skew angle for co-rotating vane vortex generators.
 - 4.4) Augmentation versus skew angle for contra-rotating vane vortex generator pairs.
-

-
- 4.5) Curves of thrust vs skew angle at constant air jet driving pressure ratio of 2.0, co-rotating air jet vortex generators; peripheral pressure ratio varying between 1.0 and 3.0 in 0.5 increments.
 - 4.6) Curves of thrust vs skew angle at constant air jet driving pressure ratio of 4.5, co-rotating air jet vortex generators; varying peripheral pressure ratio.
 - 4.7) Curves of thrust vs skew angle without peripheral blowing, co-rotating air jet vortex generators; air jet driving pressure ratio varying between 2.0 and 4.5.
 - 4.8) Curves of thrust vs skew angle with constant peripheral blowing (pressure ratio = 3.0), co-rotating air jet vortex generators; air jet driving pressure ratio varying between 2.0 and 4.5.
 - 4.9) Curves of augmentation vs skew angle without peripheral blowing, co-rotating air jet vortex generators; air jet driving pressure ratio varying between 2.0 and 4.5.
 - 4.10) Curves of augmentation vs skew angle with constant peripheral blowing (pressure ratio = 2.5), co-rotating air jet vortex generators; air jet driving pressure ratio varying between 2.0 and 4.5.
 - 4.11) Curves of thrust vs skew angle at constant air jet driving pressure ratio of 2.0, contra-rotating air jet vortex generator pairs; peripheral pressure ratio varying between 1.0 and 3.0 in 0.5 increments.
 - 4.12) Curves of thrust vs skew angle at constant air jet driving pressure ratio of 4.5, contra-rotating air jet vortex generators; varying peripheral pressure ratio.
 - 4.13) Curves of thrust vs skew angle without peripheral blowing, contra-rotating air jet vortex generator pairs; air jet driving pressure ratio varying between 2.0 and 4.5.
 - 4.14) Curves of thrust vs skew angle with constant peripheral blowing (pressure ratio = 3.0), contra-rotating air jet vortex generator pairs; air jet driving pressure ratio varying between 2.0 and 4.5.
 - 4.15) Curves of augmentation vs skew angle without peripheral blowing, contra-rotating air jet vortex generator pairs; air jet driving pressure ratio varying between 2.0 and 4.5.
 - 4.16) Curves of augmentation vs skew angle with constant peripheral blowing (pressure ratio = 2.5), contra-rotating air jet vortex generator pairs; air jet driving pressure ratio varying between 2.0 and 4.5.
-

-
- 5.1) Plot of dynamic pressures obtained through pitot rake in exit plane vs rake grid distance for bare augmentor.
 - 5.2) Dynamic pressure contours in exit plane for bare augmentor; driving pressure ratio of peripheral jet = 4.58.
 - 5.3) Plot of dynamic pressures obtained through pitot rake in exit plane vs rake grid distance with co-rotating vane vortex generators.
 - 5.4) Dynamic pressure contours in exit plane with co-rotating vane vortex generators; driving pressure ratio of peripheral jet = 4.30.
 - 5.5) Plot of dynamic pressures obtained through pitot rake in exit plane vs rake grid distance with contra-rotating vane vortex generator pairs.
 - 5.6) Dynamic pressure contours in exit plane with contra-rotating vane vortex generator pairs; driving pressure ratio of peripheral jet = 4.34.
 - 5.7) Dynamic pressure contours with zero skew air jet vortex generator blowing (air jet driving pressure ratio = 2.74); no peripheral jet blowing.
 - 5.8) Dynamic pressure contours with 15° skew co-rotating air jet vortex generator blowing (air jet driving pressure ratio = 2.98); no peripheral jet blowing.
 - 5.9) Dynamic pressure contours with 30° skew co-rotating air jet vortex generator blowing (air jet driving pressure ratio = 2.89); no peripheral jet blowing.
 - 5.10) Dynamic pressure contours with 45° skew co-rotating air jet vortex generator blowing (air jet driving pressure ratio = 2.84); no peripheral jet blowing.
 - 5.11) Dynamic pressure contours with 60° skew co-rotating air jet vortex generator blowing (air jet driving pressure ratio = 3.05); no peripheral jet blowing.
 - 5.12) Dynamic pressure contours with 75° skew co-rotating air jet vortex generator blowing (air jet driving pressure ratio = 3.04); no peripheral jet blowing.
 - 5.13) Normalized dynamic pressure contours with 30° skew co-rotating air jet vortex generator blowing (air jet driving pressure ratio = 2.22); no peripheral jet blowing.
 - 5.14) Normalized dynamic pressure contours with 30° skew co-rotating air jet vortex generator blowing (air jet driving pressure ratio = 2.89); no peripheral jet blowing.
 - 5.15) Normalized dynamic pressure contours with 30° skew co-rotating air jet vortex generator blowing (air jet driving pressure ratio = 3.64); no peripheral jet blowing.
-

-
- 5.16) Normalized dynamic pressure contours with 30° skew co-rotating air jet vortex generator blowing (air jet driving pressure ratio = 4.33); no peripheral jet blowing.
 - 5.17) Dynamic pressure contours for combined air jet and peripheral jet blowing: zero skew air jet vortex generator blowing (air jet driving pressure ratio = 2.72); peripheral jet driving pressure ratio = 2.53.
 - 5.18) Dynamic pressure contours for combined air jet and peripheral jet blowing: 15° skew co-rotating air jet vortex generator blowing (air jet driving pressure ratio = 2.88); peripheral jet driving pressure ratio = 2.50.
 - 5.19) Dynamic pressure contours for combined air jet and peripheral jet blowing: 30° skew co-rotating air jet vortex generator blowing (air jet driving pressure ratio = 2.77); peripheral jet driving pressure ratio = 2.50.
 - 5.20) Dynamic pressure contours for combined air jet and peripheral jet blowing: 45° skew co-rotating air jet vortex generator blowing (air jet driving pressure ratio = 3.08); peripheral jet driving pressure ratio = 2.52.
 - 5.21) Dynamic pressure contours for combined air jet and peripheral jet blowing: 60° skew co-rotating air jet vortex generator blowing (air jet driving pressure ratio = 3.12); peripheral jet driving pressure ratio = 2.53.
 - 5.22) Dynamic pressure contours for combined air jet and peripheral jet blowing: 75° skew co-rotating air jet vortex generator blowing (air jet driving pressure ratio = 3.10); peripheral jet driving pressure ratio = 2.51.

 - 5.23) Dynamic pressure contours with zero skew air jet vortex generator blowing (air jet driving pressure ratio = 3.07); no peripheral jet blowing.
 - 5.24) Dynamic pressure contours with 15° skew contra-rotating air jet vortex generator pairs blowing (air jet driving pressure ratio = 3.18); no peripheral jet blowing.
 - 5.25) Dynamic pressure contours with 30° skew contra-rotating air jet vortex generator pairs blowing (air jet driving pressure ratio = 2.96); no peripheral jet blowing.
 - 5.26) Dynamic pressure contours with 60° skew contra-rotating air jet vortex generator pairs blowing (air jet driving pressure ratio = 3.09); no peripheral jet blowing.
 - 5.27) Normalized dynamic pressure contours with 30° skew contra-rotating air jet vortex generator pairs blowing (air jet driving pressure ratio = 2.37); no peripheral jet blowing.
-

-
- 5.28) Normalized dynamic pressure contours with 30° skew contra-rotating air jet vortex generator pairs blowing (air jet driving pressure ratio = 2.96); no peripheral jet blowing.
 - 5.29) Normalized dynamic pressure contours with 30° skew contra-rotating air jet vortex generator pairs blowing (air jet driving pressure ratio = 3.61); no peripheral jet blowing.
 - 5.30) Normalized dynamic pressure contours with 30° skew contra-rotating air jet vortex generator pairs blowing (air jet driving pressure ratio = 4.14); no peripheral jet blowing.
 - 5.31) Normalized dynamic pressure contours with 30° skew contra-rotating air jet vortex generator pairs blowing (air jet driving pressure ratio = 4.66); no peripheral jet blowing.
 - 5.32) Dynamic pressure contours for combined air jet and peripheral jet blowing: zero skew air jet vortex generator blowing (air jet driving pressure ratio = 3.00); peripheral jet driving pressure ratio = 2.54.
 - 5.33) Dynamic pressure contours for combined air jet and peripheral jet blowing: 15° skew contra-rotating air jet vortex generator pairs blowing (air jet driving pressure ratio = 3.15); peripheral jet driving pressure ratio = 2.54.
 - 5.34) Dynamic pressure contours for combined air jet and peripheral jet blowing: 30° skew contra-rotating air jet vortex generator pairs blowing (air jet driving pressure ratio = 2.83); peripheral jet driving pressure ratio = 2.53.
 - 5.35) Dynamic pressure contours for combined air jet and peripheral jet blowing: 60° skew contra-rotating air jet vortex generator pairs blowing (air jet driving pressure ratio = 2.99); peripheral jet driving pressure ratio = 2.51.
 - 5.36) Sketch of vortices shedding from the edges of an air jet vortex generator set at an angle of 0° skew (i.e. the jet is injected in the axial direction).
-

-
- 6.1a) Vortex pattern on tapered wing with relatively small sweep.
 - 6.1b) Vortex pattern on slender delta wing.
 - 6.2) Development of vortex formation for Mach numbers of 0.6, 0.85 and 0.95 with varying angle of incidence.
 - 6.3) Carpet plot of lift curves for highly-swept low aspect ratio wings as function of M_∞ and C_L .
 - 6.4) Plot of lift coefficient vs incidence α for a slender delta and a swept wing.
 - 6.5) Plot of augmentation vs vane angle of incidence α at a peripheral driving pressure ratio of 5.0. Results for 7.5mm and 12mm vane span are given.
 - 6.6) Plot of augmentation vs diffuser area ratio for co- and contra-rotating vane vortex generators having a vane span of 12mm.
 - 6.7) Theoretical prediction of augmentation with pressure ratio and varying primary inlet to duct area ratios; 100 per cent efficient diffuser; choked secondary inlet and varying diffuser area ratios.
 - 6.8) Comparison of theoretical prediction based on total pressure diffuser efficiency and experimental results.
 - 6.9) Comparison of theoretical prediction for diffuser efficiency based on static pressure rise and experimental results.

E) Acknowledgement:

I wish to thank deeply my personal supervisor, Dr P.A. Lush who on a weekly basis discussed with great consideration all the academic problems that arose in the course of the research activity.

Considerable credit also goes to the academic staff of our department and also the fellow research students in my room who were always there to give some advice or suggestions. Furthermore, I like to thank the departmental technicians, Mr M. Smith, Mr C. Barber and Mr K. Harvey for preparing the practical aspects of this project. It was necessary to re-call Mr J. Wright from retirement to do the initial metal work for which I am extremely grateful.

I also like to thank British Aerospace for the meetings we had during which several interesting points were raised. Finally, I am in great debt to City University for their support providing me with a University research grant and therefore giving me the opportunity to pursue a very exciting and revealing research project.

F) Declaration:

I grant powers of discretion to the University Librarian to allow this thesis to be copied in whole or in part without further reference to me. This permission covers only single copies made for study purposes, subject to normal conditions of acknowledgement.

G) NOTATION:

A	--	area
AJVG	--	air jet vortex generator
AR	--	area ratio or aspect ratio
BLC	--	boundary layer control
C_N	--	normal force coefficient
D	--	distance
M	--	Mach number
PR	--	pressure ratio: p_{01} over p_a
R	--	universal gas constant, radius
Re	--	Reynolds number
T	--	temperature
TR	--	temperature ratio: T_{01} over T_a
U	--	velocity
V	--	velocity
VVG	--	vane vortex generator
b	--	vane span
c	--	vane chord
d	--	distance
h	--	vane vortex generator height
k	--	constant
m	--	mass or inlet to duct area ratio
m	--	mass flow rate
n	--	diffuser inlet to exit area ratio
r	--	normalized radius
x		coordinates
y		
z		
α	--	vane skew angle (w.r.t. axial direction)
β	--	air jet skew angle (w.r.t. axial direction)
γ	--	angle
δ	--	elevation angle of air jets
Φ	--	thrust augmentation ratio
ϕ	--	thrust augmentation
τ	--	ratio of specific heats (for air $\tau = 1.4$)
η	--	efficiency
λ	--	taper ratio
μ	--	viscosity
ν	--	kinematic viscosity
π	--	universal constant

ρ -- density

Suffices:

AJVG,A -- refers to air jet vortex generator
a -- atmospheric condition
e,exit -- exit conditions
o -- total
p,peri -- refers to peripheral jet
r -- root
t -- tip
x -- distance
01 -- total reservoir
1,2,3 -- stations or various notations for distances
 ∞ -- free stream

Superscripts:

* -- choked condition

1.) INTRODUCTION

1.1.) GENERAL:

Longitudinal stability studies for Short Take-Off Vertical Landing aircraft have shown that some sort of Reaction Control System is desirable. This desire led to the idea of a compact thrust augmenting ejector-diffuser located at nose and tail of an aircraft. Since the cross-sectional area at these points is limited, a determining factor for the practicality of such a device is its overall length. The principle of augmentation is achieved as follows: the primary jet introduced via a nozzle mixes with the secondary air flow drawn in by the differential in pressure. The combined flow must then be diffused to allow the pressure to recover to near atmospheric conditions. For a fixed diffuser area ratio, it is an advantage to maximize the diffuser angle, thereby reducing its length. This angle cannot normally exceed about 8 degrees due to separation, but may be increased by the use of a Boundary Layer Control (BLC) technique, such as Vortex Generators (VG's). These devices re-energize the flow near the wall by entraining flow into the boundary layer. Vane vortex generators have become well established for this kind of BLC, but they always carry a drag penalty. The use of air jet vortex generators would probably overcome this problem, rather they would increase the thrust.

This research project was introduced to the author in March of 1989. The theme of the project was that the City University wished to pursue a project which considered the possibility to enhance the bare nozzle thrust of an ejector-diffuser by at least fifty percent. It became clear that preliminary studies had been made and according to these the project proved viable. The intention then was to refine the initial studies and then try to manufacture an ejector meeting the desired requirements.

Studying the literature related to ejector-diffusers showed that the requirement of fifty percent thrust increase on its own was not that hard to obtain, the difficult and previously not attempted part was to make the device as short as possible. The ultimate aim was to have a device with a total length of less than 500mm. The requirements and physical constraints for the full size, i.e. real life application augmentor were:

-
- a) thrust augmentation ≥ 1.5
 - b) total length $< 500\text{mm}$
 - c) overall thrust $> 9000\text{N}$
 - d) supply pressure = 16bar
 - e) temperature of supply air 750K
 - f) injection via a nozzle

Initially it was believed that the thrust augmentation was to be achieved by a boundary layer control (BLC) technique, making possible the use of a short large angle diffuser. The BLC method envisaged was that of air jet vortex generators (AJVG).

1.2.) HISTORICAL DEVELOPMENT:

A preliminary assessment of the general arrangement and layout of the thrust augmentor was made by Mattock ^[1], a former research student working on this project. His proposed device can be seen in Figure 1.1a. The design features were mainly based on research done by the Vought Corporation Advanced Technology Centre ^[2], the Flight Dynamics Research Corporation ^[3] and the National Aeronautics and Space Administration ^[4]. Further relevant material on ejector design is given in references ^[5] and ^[6].

Mattock particularly spent time on the design of the intake, the bell-mouth, which was being used unaltered despite the fact that the final overall design was changed considerably. It was only necessary to scale it to the required dimensions. There seemed to be two ways of increasing the overall performance of a short augmentor, the first to improve the mixing between the primary and secondary flows and the second to improve the efficiency of wide-angle diffusers. The two ways are likely to be additive. Mattock's original design had to be altered for the following reasons. The objective originally set for the current project was to study the possibility of improving the diffuser by using boundary-layer-control (BLC). The first consideration then was that, with high pressure air available, tangential blowing might well be the most effective form of BLC. This could be achieved by diverting some of the primary air away from the central jet. The peripheral wall jet thus formed would itself contribute towards the flow entrainment (ejector effect), to an unknown lesser or greater extent than the debit from that of the central jet. Assessment of any effect of boundary layer control would hence be extremely difficult. It was therefore decided to study first the performance of an ejector formed by the peripheral jet only (which also automatically solves the mixing problem

for the primary nozzle flow) and to try to separate out its relative contribution to entrainment and BLC by using diffusers of different lengths and angles. Vortex generators would also be studied as an auxiliary means of boundary-layer-control. It was envisaged that the optimum thrust augmentor might eventually combine peripheral and central jets. This eventual combination could then also incorporate improvements in the efficiency of the central jet that resulted from work known to be in progress elsewhere, e.g. hyper-mixing nozzles as employed by Miller^[9].

For a time another research student RJ Flynn also assisted in the design work. He was responsible for the design of the peripheral blowing (including the supply of air and all "internal" components), the vortex generators and the bell-mouth. The remainder, the design of the diffuser, the mounting stand, an intermediate mixing section and the instrumentation was the responsibility of the author. The major aims throughout the initial design phase were to simplify the device as much as possible. In Figure 1.1b the layout of the rig as it was manufactured is shown. Furthermore, in Figure 1.1c a photograph of the rig and its location is illustrated.

In Chapter 3 more detail is given of the various phases of the final design required in order that the rig could be manufactured by the workshops and then set up and tested in the high speed laboratory of the Centre for Aeronautics, City University, London.

1.3.) VORTEX FORMATION:

The City University has gained a valuable reputation and insight into the use and function of vortex generators through other theoretical work and experiments carried out in the past. Pearcey^[7] contributed extensively to the enhancement of knowledge and the understanding of vortex formation. A number of experimental verifications carried out on the validity of VG's could be mentioned here, e.g. retardation of separation on aerofoils up to extremely high angles of incidence (35degrees), boundary layer control on an aerofoil set in a supersonic air stream, and so on. The study and understanding of vortex formation is essential to this project because it considers the physics of vortex movement for example.

On the history of vortex generators the literature revealed that the principle of boundary layer control by vortex generators in the form that we now know them was first conceived and formulated by Bruynes and Taylor^[8] of the United Aircraft Corporation in 1947. Boundary layer control is achieved by increased mixing between the external stream and

the boundary layer. It is promoted by vortices trailing in the streamwise direction over the surface, in close proximity to the edge of the boundary layer. Fluid particles from the free stream, being of high momentum, mix and to a certain extent replace the low momentum air close to the surface. The fluid particles move on helical paths into the boundary layer and out again. The exchange of momentum causes a net increase in streamwise momentum within the boundary layer. since this re-energization occurs as a continuous process the natural boundary layer retardation and growth due to skin friction and adverse pressure gradients is reduced. This effect can be exploited in various forms, for example retardation of separation on aerofoils or controlling buffeting on transonic aerofoils.

The simplest form and "original" type of vortex generators are vane vortex generators (VVG). These devices protrude normal from the surface and each one is set at an angle of incidence relative to the free stream in order to produce a single trailing vortex. They are positioned in rows across the surface (the spacing of the individual VVGs is rather important and will be discussed below). There are fundamentally two different arrangements of vortex formation, namely:

- a) co-rotating vortices and
- b) pairs of contra-rotating vortices.

Co-rotating vortices are obtained by setting all the vanes to the same angle of incidence. Usually the vortices are of equal strength, at the same height above the surface and also equi-spaced. Contra-rotating vortices are generated by alternately setting the vanes at positive and negative angles of attack, thereby grouping them as pairs. Again they are usually of equal strength, at the same height above the surface, but equi-spaced in pairs only. A variation of (b) is the bi-plane type where the vanes are set as alternate pairs (Fig. 1.2). Depending on the number of generators employed are other formations possible. Since the number of vortex generators was limited to eight there seemed no point in investigating the bi-plane or any other complex configuration, i.e. the co- and contra-rotating vortex formation were tested exclusively.

In the course of studying vortex formation Pearcey found that to establish an effective co-rotating vortex pattern the spacing of adjacent vortices needed to be kept above a certain minimum value. In Figs. 1.3(b) and 1.3(c) (taken from Pearcey^[7]) effective vortex patterns are shown. One observes strong discrete vortices lying close to the surface but sufficiently spaced apart, such that the low energy air is prevented from being swept back into the surface after it has been

swept out by the adjacent vortex.

This system can be obtained only if the individual vortices have an initial spacing of more than about three times their height. If a smaller spacing than this critical ratio is chosen the vortices tend to dampen one another. They then fail to sweep high momentum air to the surface at any point in the cross-section of the boundary layer (Fig. 1.3(a)). It was found that when this point was clearly understood, the performance of co-rotating generators compared well with that of the contra-rotating system. For certain applications the co-rotating system, in fact, turned out to be superior, for example for boundary layer control over wings at very high angles of incidence. This is due to their nature of staying at fairly constant height above the surface and therefore they are effective over a longer distance. Once the spacing is well above this minimum value, the effectiveness falls only very slowly with further increase provided the individual vortices are strong. Systems with a distance to height ratio of five to six are frequently used successfully in practice.

On the subject of contra-rotating the researchers discovered that the induced velocities are responsible for a substantial change in the vortex path as the vortices move downstream. It became clear how important the determination of the vortex path was to the design of these systems. Furthermore, it was established that the effectiveness in delaying separation maximizes as the boundary layer is kept thin between the vortex pairs, i.e. the low energy air is carried out between the intermediate pairs of vortices. The vortices are effective in delaying separation when they are arranged as shown in Fig 1.4(a) (Pearcey^[7]). This Figure refers to a specific case where all generators were equally spaced and the cross-sectional measurements were taken at 1.6 generator heights downstream of the source. It can be seen that the favourable vortex arrangement breaks down as the spacing was increased as shown in Figs. 1.4(b) to 1.4(d). These Figures also show the effects of the induced velocities, i.e. the vortex centres move closer together in pairs and further away from the surface. Many generator heights downstream the vortices eventually become damped out (Fig. 1.4(d)). They also suggest a degradation in their effectiveness, limited to a distance of about ten generator heights downstream of the source, as the vortices move away from the surface in pairs. All contra-rotating arrangements possess this particular feature, but it can to some extent be controlled in the way the vanes are set up. The failure of the vortices of such a system to follow the surface is also clearly shown in Fig. 1.5(b)^[7], particularly when this is contrasted with Fig. 1.5(a) for co-rotating vortices.

Closer inspection of the contra-rotating system for which the vortex

generators are equally spaced (Fig. 1.6(a) taken from Pearcey^[7]) reveals that the net resultant induced velocity at the centre of any one vortex is initially parallel to the surface. This is precisely the same as for the co-rotating system. The major difference is the fact that when resolving the vectors of the vortices and their respective images they induce velocities in opposite directions for adjacent vortices. This causes them to move closer in pairs as they travel downstream and inevitably produce an induced velocity directed away from the surface.

For contra-rotating systems for which the vortex generators are unequally spaced as shown in Fig. 1.6(b), certain features similar to the ones mentioned above can be seen. To illustrate the vortex paths in two dimensions they are projected on to a plane normal to the stream. This representation can be regarded as a transformation of the three dimensional particle movement to a two dimensional problem. The array of vortices is described by: the spacing between vortex A and vortex B is smaller than between B and C. The individual vortex paths are indicated and can be considered qualitatively by assuming that their general directions are determined by the induced velocities due to the nearest real vortex or vortex image. Three stages are characteristic for the paths. The first stage applies when the distance AB is less than BC. The path is then directed towards the surface. As the vortex moves closer to its image the particles begin to travel parallel to the surface (stage 2). The combination of these two stages lead to the grouping of vortex pairs BC, DE, etc. The net effect of this third stage is a movement away from the surface. It was found that the vortices are most effective for BLC during stage two.

1.4.) PURPOSE AND AIMS OF THIS PROJECT:

The original proposition of having a duct to nozzle area ratio in the range of 15 to 20, and meeting the requirement for a thrust augmentation of 1.5 proved difficult. This was essentially because, at the pressure ratio specified i.e. 16:1, the secondary flow would have become choked thus limiting the thrust on the inlet and hence the augmentation. Calculations of the ejector-diffuser as performed by Mattock using one-dimensional mass, momentum and energy equations revealed that assuming a diffuser efficiency of 100 per cent, an augmentation of 1.5 times the bare nozzle thrust could have been achieved with the following solution: a duct to nozzle area ratio of 38 and a diffuser area ratio of 1.09 for the given pressure ratio. This clearly was not the only solution, combinations of a lesser duct to

nozzle and a greater diffuser area ratio or vice versa were feasible but only if the assumption of a less than 100 per cent efficient diffuser was used. There was no direct proportionality between these two ratios making a simple relationship non-existent.

For diffusers of non-ideal behaviour both the ratios had to be raised. For example, if a diffuser efficiency of 95% was assumed, based on the loss in total pressure between the entry and exit of the diffuser, then one solution was: a duct to nozzle area ratio of 53 and a diffuser area ratio of 1.338. These figures showed that the overall exit to nozzle area ratio rose from 41.4 for the ideal diffuser to 70.9 for the 95% efficient one. Incidentally, the latter overall ratio was very close to the solution when no diffuser at all was installed. This in effect meant that the diffuser needed to be more than 95% efficient to prove its existence.

Translating the results obtained into proper dimensions showed that a very large rig was necessary, which would have been extremely difficult to mount in a University laboratory. Remember that a net thrust of 9000N was desired. Assuming a thrust augmentation ratio of 1.5, this effectively equated to a nozzle of 62.6mm in diameter producing the required 6000 Newtons of bare nozzle thrust at a pressure ratio of 16:1. Inserting the above area ratios gave duct diameters of 388mm and 459mm for the ideal and non-ideal case respectively.

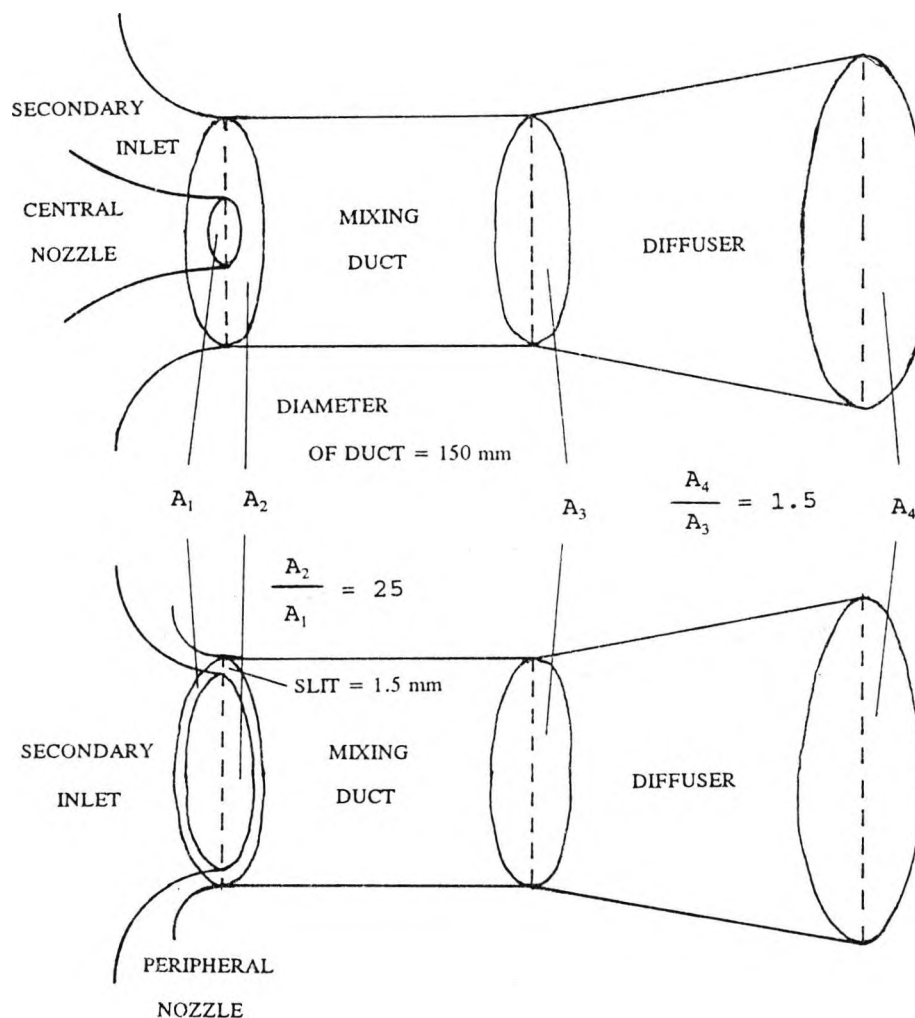
The movement away from relatively small duct to nozzle area ratio (15 - 20), as was the original outline when the project was started, towards higher area ratios resulted in potential problems in ensuring adequate mixing between the primary and the secondary air flows. The problem of mixing suddenly seemed to become the issue of major importance. Various forms of hyper-mixing nozzle designs were studied by Mattock. In the end it was decided that too many problems were asked to be solved simultaneously. This led to the idea that instead of a central nozzle a peripheral one should be employed to raise the mixing shear area. It also made the practice of boundary layer control much easier.

As mentioned above the full scale ejector would have had a huge duct diameter and would have drawn enormous amounts of air from the compressed storage. Consequently the decision was taken that a model with an approximate scale of 1:2.5 should be built. The pressure ratio for the primary was also scaled down in order not to choke the secondary; an upper ceiling for the pressure ratio of just over 6:1 was selected. Using the chosen scale factor caused the duct diameter to lie in between 155mm and 184mm for the above discussed cases.

It was finally decided that the duct should have a diameter of 150mm, but at the same time the duct to nozzle area ratio was decreased and the diffuser area ratio increased (Sketches 1 and 2 below show the

basic layouts and define the various stations of the central and peripheral nozzle ejector). One of the requirements of the rig design became the feasibility study of including a variable duct to nozzle area ratio in the range of 19 to 25. This proved extremely difficult

Sketch 1: Layout with central nozzle



Sketch 2: Layout with peripheral nozzle

due to the circular nozzle arrangement and the idea was therefore dropped. Instead a fixed slit of 1.5mm was manufactured with the provision of increasing the slit continuously up to 3mm by turning more material off the peripheral slot. The slit of 1.5mm translated to an injection area of 700mm², hence giving the required area ratio of just over 25, since the duct area was 17672mm². At the same time the

diffuser was designed such as to have possible area ratios of 1.3, 1.4 and 1.5. The overall area ratios, defined as the exit over injection area, therefore came to 32.8, 35.3 and 37.9 respectively.

Having established these all determining dimensions and ratios the detailed design work started. The other important design limitation were the manufacturing techniques available. The rig had to be designed such that it could be produced by the workshops of the City University. The final rig would then be set up in the high speed laboratory and the feasibility of obtaining the desired augmentation of 1.5 times the bare nozzle thrust would be investigated using the vortex generators.

2.) PRELIMINARY INVESTIGATIONS

2.1.) THEORETICAL MODELLING OF RIG:

From preliminary investigations of the general dimensions and the principle layout of the rig the following important parameters were initially decided:

- i) maximum mass flow rate: 2kg/sec
- ii) max. total pressure within nozzle = 6 bar
- iii) temperature of supply air \approx 288K
- iv) diameter of working section = 150mm
- v) desired thrust augmentation ratio \geq 1.5

Points i) and iii) were determined by the physical limitations and constraints of the primary air, supplied from the reservoir tank. The primary air in the reservoir tank was at ambient atmospheric conditions and there was no provision available to heat the flow, therefore cold flow had to be used. The maximum working section driving pressure (ii) was the scaled down value of the full scale pressure ratio specified in Section 1.1.). The working section diameter was selected on the basis of remaining within the constraint boundaries, as invoked, for example, by the maximum mass flow rate. A net thrust of one and a half times the bare nozzle thrust was desired.

Having these parameters in mind a theoretical basis needed to be established to decide on the peripheral slot size and the diffuser area ratio. Mattock^[1] in conjunction with Lush found equations (2.1), (2.2) and (2.3) below, devised from a control volume approach, to represent the device, as shown in Figure 1.1a (see also Sketch 1 in Section 1.4. for schematic view). These equations were derived from the three one-dimensional conservation equations, namely mass, momentum and energy. Several very important assumptions were made to allow the setting up of these equations:

- a) primary nozzle choked
 - b) complete mixing between primary and secondary flow
 - c) inlet total pressure equal to atmospheric pressure
 - d) secondary inlet flow isentropic
 - e) adiabatic flow throughout device
 - f) exit static pressure equal to atmospheric pressure
 - g) negligible wall friction, no boundary layers
 - h) uniform conditions across any plane
-

The first assumption just implied that a driving pressure greater than the critical pressure needed to be applied in order to choke the primary inlet. If blowing into atmospheric air this meant a pressure greater than $1.89 p_a$ was required. Point b) was largely an assumption which was met by choosing an appropriate mixing length. Assuming an inlet total pressure equal to the local atmospheric pressure was probably quite easily satisfied for the given bell-mouth shape. Points d) to f) were aspects which for simplicity had to be assumed as stated. The seventh assumption clearly was a rather poor one since a boundary layer was certain to develop. For a refined mathematical model this should be included. Fortunately, it was known that for high speed subsonic flow boundary layers grow very slowly, hence their adverse effect was not too grave. Finally the last assumption was rather poor. A velocity profile factor should have been included, as Miller ^[9] did for his one-dimensional mass, momentum and energy equations. This last point probably was the largest shortcoming of the model. If the model would have been the centre of this research all the eight assumptions could and should be introduced as parameters into the equations below.

$$0.335 PR^2 m^2 + \frac{M_2^2 (1-m)^2}{(1+0.2M_2^2)^6} + \frac{PR M_2 m (1-m)}{1.728 (1+0.2M_2^2)^3} \left[\sqrt{TR} + \sqrt{TR^{-1}} \right] =$$

$$(1+0.2M_4^2) M_4^2 n^2 \quad \text{--- (2.1)}$$

$$1.26788 PR + \frac{(1+1.4M_2^2)}{(1+0.2M_2^2)^{7/2}} \left[\frac{1}{m} - 1 \right] =$$

$$\frac{(1+1.4M_3^2)}{m} \left[\frac{M_4}{M_3} \right]^{7/6} \eta^{1/6} n^{7/6} \quad \text{--- (2.2)}$$

$$\frac{M_3}{(1+0.2M_3^2)^3} = \frac{\eta n M_4}{(1+0.2M_4^2)^3} \quad \text{--- [2.3]}$$

$$\text{note: } PR = \frac{P_{01}}{P_a}, \quad TR = \frac{T_{01}}{T_a}, \quad \gamma = 1.4$$

The derivation of these equations can be followed in Appendix IA; the derivation of the accompanying performance terms are given in Appendix IB.

A computer program was written solving equations 1 to 3. This program was initially written by Mattock in BASIC on a BBC and therefore was rather slow due to the large number of iterations involved. Consequently the program was rewritten in Fortran (a listing of this program is given in Ref. [10]). The features of the program can be summarized as:

- step 1: arbitrarily select low subsonic inlet Mach no., say $M_2 = 0.1$
- step 2: inserting this value of M_2 into equa.(2.1) and solving this equation quadratically produces one real solution for diffuser exit Mach no. M_4
- step 3: applying the Newton-Raphson iteration technique to equa.(2.3) produces (to a high accuracy) a solution for diffuser entrance Mach no. M_3
- step 4: all terms in equa.(2.2) are now known and are inserted
- step 5: if equa.(2.2) is not satisfied then the initially chosen value of M_2 is increased by small amount, eg 0.01 or 0.001 for greater accuracy, and the calculations restart from step 2
- step 6: on the condition that equa.(2.2) is satisfied to near proximity, the performance terms are evaluated and then put into an output file for later reference

On executing the program the following six variables were read in from a data file: $m, n, \eta, M_{\text{initial}}, PR, TR$. The term M_{initial} was the Mach number at the throat of the secondary inlet and η was the diffuser efficiency parameter based on the loss in total pressure between the inlet and the exit.

By the time the Fortran Code worked properly the nozzle design was scrapped in favour of a peripheral blowing arrangement. Fortunately, the equations required minor changes only. With the help of the program the optimum area ratios were established. There were two ratios which needed optimizing, namely n and m . Where m was the ratio of peripheral slot area over mixing section duct area and n was defined as the diffuser exit over entry area (where the entry area was clearly the same as the working section and as the parallel walled mixing section duct area). For a working section diameter of 150mm the results of the optimisation suggested diffuser area ratios between 1.3 and 1.5 and the slot sizes between 1.5 and 3 millimetres. These results showed a close relationship between the two ratios as can be expected. Having established these important parameters the detailed component design work began. In Section 3.1.) the various components, e.g. the diffuser and the working section are discussed in more detail.

It should be mentioned at this point that the three conservation equations were modified such as to model the rig in its expanded form, namely including the air jet vortex generators. The jets add extra terms to the mass, the momentum and also the energy equation. The modified equations in their final form are as listed below. The procedure to converge to a numerical solution in the computer program was done the same way as described above.

$$q^2 + 2qr + (qs+rs) \sqrt{TR} + (qs+rs) \sqrt{TR}^{-1} + r^2 + s^2 = (1 + 0.2M_4^2) M_4^2 n^2 \quad \text{--- (2.4)}$$

where:

$$q = PR_p M_{1p} m_p (1 + 0.2M_{1p}^2)^{-3}$$

$$r = PR_A M_{1A} m_A (1 + 0.2M_{1A}^2)^{-3}$$

$$s = M_2 (1 - m_p) (1 + 0.2M_2^2)^{-3}$$

$$\begin{aligned} & PR_p m_p (1 + 0.2M_{1p}^2)^{-3.5} (1 + 1.4M_{1p}^2) \\ & + PR_A m_A \cos\beta \cos\delta (1 + 0.2M_{1A}^2)^{-3.5} (k_A + 1.4M_{1A}^2) \\ & + (1 + 0.2M_2^2)^{-3.5} \left[(1 - m_p) (1 + 1.4M_2^2) - k_A m_A \cos\beta \cos\delta \right] = \\ & (1 + 1.4M_3^2) \left[\frac{M_4}{M_3} \right]^{\frac{7}{6}} \eta^{\frac{1}{6}} n^{\frac{7}{6}} \quad \text{--- (2.5)} \end{aligned}$$

$$\frac{M_3}{(1 + 0.2M_3^2)^3} = \frac{\eta n M_4}{(1 + 0.2M_4^2)^3} \quad \text{--- (2.6)}$$

again:

$$PR = \frac{P_{01}}{P_a}, \quad TR = \frac{T_{01}}{T_a}, \quad \gamma = 1.4$$

The subscripts A and P refer to the air jet nozzle and peripheral nozzle parameters respectively. The angle β is the skew angle and δ is the elevation angle of the jet leaving the vortex generator plug.

Please note the factor k_A in equation 2.5 which can vary between zero and one according to the pressure assumed on the inclined surface of

the air jet VG plug. If the pressure is assumed to be the same as that of the nozzle exit plane then the factor is zero; if the pressure is assumed to be the static pressure of the cross-stream then the factor becomes one. A factor of 0.5 probably represents the true physics of the local fluid flow quite well. Without experimental tests it is impossible to determine this factor any more accurately. It is believed that a closer look at the interaction between the air jet and the cross-stream would pose a major task in its own right, but would yield considerable insight into the expansion of the jet. Using a Schlieren picture would also show if the jet remained attached via an expansion fan or separated at the corner and re-attached at some distance downstream.

This meant that the term including k_A was effectively the pressure thrust contribution from the AJVGs.

2.2.) RESULTS FROM MODEL:

The area of interest was primarily limited to try and satisfy the requirements and remain within the constraint boundaries. This meant that the pressure ratios (PR) to be considered varied from just beyond the critical PR, i.e. 1.89 at standard atmospheric conditions, to about five. The upper limit of a total pressure of six within the primary nozzles was considered to be the scaled down pressure of a real application as pointed out in Chapter 1.1.). The equations were set up to include possible temperature effects, but since the primary air was taken straight from the storage tank the temperature ratio (TR) effectively equated to one, i.e. cold flow was assumed.

The only variables left were therefore the area ratios of:

- a) the primaries relative to the duct, denoted by m , and
- b) the exit over the duct, denoted by n .

If the effects of temperature were to be included in the mathematical model, a clear relationship would have developed. As the temperature ratio increased the augmentation dropped. In Figure 2.1 this behaviour is illustrated. It is interesting to note that the augmentation for the low pressure ratios remained greater than for the higher PRs as the temperature ratio is raised. This must be caused by the fact that the term including the temperature ratio in Equation (2.1) becomes more dominant as the pressure ratio is increased. For a temperature ratio of four the augmentation falls from nearly 100% near the primary choking pressure to about 60% at a pressure ratio of five. Miller^[9] in

his work made a reference to Bevilaqua ^[11], where the author claimed that for real flows, hot gas jets ($TR \approx 3.0$) developed a better degree of mixing than the cold gas ones. This meant a smaller deduction in augmentation than expected, in many cases a drop of between three to four percent only was possible. According to that theory, temperature had hardly detrimental effects.

Returning to the area ratios the following features were determined. As the ratio of m was decreased it became harder to choke the secondary, i.e. greater and greater primary pressure ratios were required to achieve entrainment of large proportions. Since the primary pressure ratio had to be less than five, due to the experimental constraints, this gave a limitation for the choice of secondary area ratio m . The diffuser area ratio n had a similar effect, namely as its ratio was increased the rate of entrainment rose. This implied that a balance had to be found between a large diffuser and small primary inlet or vice versa. The mathematical model clearly allowed both extremes but the limiting factor was the feasibility and practicality of such a system for a real application. The limits of each ratio were illustrated in the original "Feasibility Study" ^[11] by Mattock. The final choice was 0.0396 for m and between 1.3 and 1.5 for n . The variation in n was desirable because for a very efficient diffuser the secondary would have become choked for an area ratio of 1.5. The lower limit avoided this problem altogether.

As was just mentioned the efficiency of the diffusion (η) also made a large contribution to the selection of a desirable ratio n . In Fig. 2.2 the effect of η in the range of a one hundred per cent efficient diffuser to a 96 per cent efficient one in one per cent steps is illustrated. Remember that the efficiency was defined as the loss in total pressure between the inlet of the diffuser and its exit. The graph shows clearly how the secondary choking was delayed to higher primary pressure ratios as the efficiency reduced. A net thrust of 700N and more was obtainable for an ejector with $m_{\text{peri}} = 0.0396$ and $n = 1.5$, i.e. a ratio of $n/m = 37.9$. Note the curve for the bare nozzle thrust crossing the constant efficiency lines. This meant that a 97% and less efficient diffuser would have thrust degradation for low pressure cases and for higher PRs only would augmentation be possible.

The representation with the theoretical bare nozzle thrust crossing the constant efficiency lines was not very encouraging. Somehow a better representation was desired. The original proposition of basing the diffuser efficiency on the total pressure loss between the inlet and the exit of the diffuser was suggested by the ESDU ^[12] data items and was therefore followed. As that representation turned out to be unsatisfactory, the decision was taken to go back to the usual diffuser

efficiency which is founded on the static pressure rise between the inlet and the exit of the diffuser. Fortunately, it proved that there was a direct relationship between the two definitions of diffuser efficiency and therefore the original equations could be maintained and were modified within the computer program as calculations proceeded. In each iteration cycle the modified definition of diffuser efficiency was evaluated. The result of this process can be viewed in Figure 2.3, where thrust is plotted against pressure ratio. The slope of the 100 per cent efficient diffuser is clearly the same as before but the slopes for the less efficient diffuser do not have constant slopes. This is in total contrast to the thrust vs pressure ratio curves which are parallel for the various diffuser efficiencies (Fig. 2.2) when based on total pressure loss. Instead the static pressure rise within the diffuser leads to a 'fan-shaped' distribution, i.e. the slopes become less and less steep as the efficiency is reduced. Suddenly, this modified representation was a very satisfying solution encompassing the theoretical bare nozzle thrust nicely. A diffuser efficiency of minimal size, incidentally, modelled the bare nozzle thrust. This result is far from 70 per cent which can usually be expected from a diffuser. Entrainment of secondary air via the process of good mixing would possibly produce that kind of diffuser efficiency.

Including the modified efficiency (based on static pressure rise) the relationship between Mach No. and pressure was slightly more extensive than for the total pressure definition, as shown by the increased complexity between the two diffuser efficiencies in equation (2.7) below:

$$\eta = \frac{\left(1 + \frac{\gamma-1}{2} M_4^2\right)^{\frac{\gamma}{\gamma-1}}}{\left(1 + \frac{\gamma-1}{2} M_3^2\right)^{\frac{\gamma}{\gamma-1}}} \quad \text{--- (2.7)}$$

$$\eta_{static} \frac{\left(1 + \frac{\gamma-1}{2} M_4^2\right)^{\frac{\gamma}{\gamma-1}}}{\left(1 + \frac{\gamma-1}{2} M_3^2\right)^{\frac{\gamma}{\gamma-1}}} = \eta_{static} + 1.0$$

where η was the diffuser efficiency based on total pressure loss and η_{static} was the diffuser efficiency based on static pressure rise

However, as both efficiencies were closely related it was simpler to use the conservation equations based on the total pressure definition and then modify for the static pressure definition at a later stage in the theoretical determination of the total thrust. In fact the

mathematical model was structured such as to incorporate the static pressure diffuser efficiency definition at the end of each iteration cycle, N.B. one iteration cycle consisted of the initially assumed low inlet Mach no. M_2 plus the sum of the total number of cycles (k) times the incremental change in Mach no. M_2 , i.e.

$$M_{2\text{new}} = M_{2\text{initial}} + k * M_{2\text{increment}}.$$

For the very first iteration where $M_{2\text{new}}$ was equal to $M_{2\text{initial}}$ a 100 per cent efficient diffuser was assumed. This was necessary for the model to work properly. Thereafter the assumed static pressure diffuser efficiency (η_{static}), for example 65 per cent, was inserted into equation (2.2) above and the new equivalent diffuser efficiency based on total pressure loss was used for the next iteration cycle. This continuous process produced the fan-type distribution of theoretical net thrust versus pressure ratio and should therefore be recommended for this kind of work.

3.) EXPERIMENTAL ARRANGEMENTS AND PROCEDURES

3.1.) DESIGN OF EXPERIMENTAL RIG:

As mentioned earlier the design work was divided between RJ Flynn and the author. This thesis incorporates extensive work done by Flynn, who has produced a written account of his part of the work in the Design Study Report No. 2, August 1989 ⁽¹³⁾. The components considered include the main working section (peripheral nozzle), the auxiliary working section (vane and air jet vortex plug mounting), the working section nut, the spacer, the air jet vortex generator plug, the flexible piping, the octagonal supply reservoir and finally the bell-mouth. The complete set of drawings can be viewed in Appendix 10.2, where also all other important components of the augmentor are listed. A discussion of these remaining parts will follow in the next paragraphs.

3.1.1.) DIFFUSER DESIGN:

The idea of a diffuser is to have some controlled means of decelerating very high velocity flow and thereby recovering the low sub-atmospheric static pressure back to atmospheric in a very efficient manner. The emphasis lies on efficiency in order to justify its use. From many previous experiments it was known that diffusers with semi angles of around four degrees work reliably well. This angle was then chosen for the diffuser. It clearly was far from the requirement of having a wide angled diffuser but this requirement had to remain in the background until the apparatus was set up properly and some experience was obtained with a device which was very likely to work. It is anticipated that at a later stage the semi angle will be increased, thereby decreasing the overall length.

The design of the diffuser was such that it had an area ratio of 1.3, 1.4 or 1.5 which simply could be changed by adding another diffuser frustum shape (see Draw. 7 for details). For ease of manufacture the diffuser cone was cut out of a thick-walled tube with a semi angle of 4 degrees. The frustum shapes were added by the means of flanges (the flanges conform to BS4504). The material used was mild steel. During manufacture special care was taken to blend the parallel walled mixing section to the diffuser taper of 4 degrees. Furthermore, the flanges were made such that they met with a minimal gap to avoid any surplus

turbulence levels or initiators for separation bubbles to form.

3.1.2.) MIXING SECTION:

The requirement for a mixing section arose from the fact that the spreading angle for a free wall jet is only around four to six degrees. The direct implication of this would be incomplete mixing on a large scale between the peripheral jet and the secondary air and hence the desired thrust augmentation would certainly not be achieved. The specifications for the length of this section was unfortunately quite unclear because it was not known how the pressure gradients were going to affect the mixing of the flow. The chosen length of 300 mm was rather optimistic taking account of the aforementioned spreading angle. A section at least twice this length would be required to ensure full mixing of the two flows. From the point of view of manufacture the piece was simple. A fairly standard tube was turned to a 150 mm diameter inside bore and then flanges were welded on to this tube. The material used again was mild steel. A perspex tube was proposed but got rejected on the grounds of strength. For this section the same applies to the flanges as for the diffuser above. A wall thickness of 3 mm was calculated to be sufficiently strong to withstand the maximum hoop stresses which were to occur. For practical manufacturing purposes the wall thickness turned out to be much thicker making the combination of the mixing section and the diffuser very heavy. In retrospect it was rather foolish to specify weighty mild steel because these sections needed to be removed regularly in order to set new angles to the VGs. Aluminium as a raw material would have been seriously more expensive but probably would have meant a shorter manufacturing time scale and would have served the operator.

3.1.3.) THE MOUNTING STAND:

A major decision to be made was the way in which the entire device was to be mounted. The exhaust air could either be directed sideways, up or down. The horizontal configuration was rejected immediately because it was difficult to mount and to measure the forces. Blasting downwards would have meant that the arrangement had to sit far off the ground requiring a large frame. If the net thrust was bigger than the weight it also would cause the assembly to take off making the force measurements quite difficult. Hence by systematic exclusion only one final way remained, namely to have the thrust and the weight acting in the same downward direction.

An important parameter to be decided early on was the distance between the intake at the bell-mouth and the floor. This distance needed to be

sufficiently large to minimize flow distortion caused by the presence of the ground. At first a height of 1m was selected. But intuitive feeling dictated a larger height. The whole device was lifted to 1.4 meters. For stability reasons four wooden legs were initially proposed. Their sections needed to be 50 mm squared to carry the maximum load of approximately 250 kgs. This would have meant a blockage of around seven percent based on a frustum representation of the stand. In the end a steel frame sounded more suitable because one could weld it easily together and it required a hollow section of only 20 mm square. The blockage went down to the two percent region. Since the frustum approach did not seem to represent the physics too well a sink image method was adopted. After a short excursion into source methods an appropriate computer program was written, giving the velocities in the x and y direction respectively. The results showed fairly small magnitudes in the transverse y-direction velocities.

In the final design the number of legs was reduced to three since also three load cells were used which then sat nicely on top of each leg eliminating the problem as caused by bending of the top frame mounting support plate (Drawing 40). The thickness of the frame mounting plate was selected to be 9mm in order to make the frame very rigid. The layout of the frame made it very much self supportive.

The rig mounting plate which sat on top of the above described plate required some further thought. The evaluation of its thickness was determined by plate theory, i.e. looking at a plate with a hole in the middle (refs. ^[14], ^[15] and ^[16]). The results from these sources for the required plate dimensions and applied loads suggested a thickness of 8 mm and adding a reasonable safety factor gave a plate thickness of 14 mm.

3.1.4.) WORKING SECTION:

It seems appropriate to explain first the term working section as it is used here. The section referred to is where the primary air was being injected. Also included was the section where the vortex generators were located. In Mattock's design there was primary injection via a central nozzle plus some AJVGs downstream. In the design that was manufactured this had been changed completely, namely two different set-ups were being considered. Firstly, the testing was performed with a peripheral jet on its own. This provided the reference basis for the later configurations to be calibrated against. Then the section with the vortex generators was added. Solid vane vortex generators were tried out first. Two different set-ups were tested: eight co-rotating VG's or four contra-rotating VG pairs.

The vane vortex generators were mounted on 'plugs' which slotted into

the working section mounting. The entire plug could then be adjusted with a purpose-built protractor-type tool. The chosen angle was frozen by tightening the securing nuts. These VVG 'plugs' were later replaced by AJVG 'plugs' which were fed by an additional octagonal reservoir sitting on top of the other one. The reservoir and the working section were joined by flexible piping to facilitate the removal of the plugs. This arrangement produced extensive problems, which will be explained later on. The air jet plugs were also adjusted by a purpose-built tool requiring access to the inside of the working section duct, i.e. making necessary the removal of the diffuser and the mixing section. This special tool consisted of a 'foot' which would slide into the jet slot and a pointer which would be set against a scale ranging from minus fifteen to plus fifteen degrees relative to the vertical. The pointer itself could be adjusted relative to the 'foot' in 45 degree increments. This effectively gave a continuous range of ± 90 degrees relative to the vertical.

3.1.5.) VANE DESIGN:

Previous studies on vane vortex generators by Pearcey^[7] and others have led to a specific vane design. The span of the vane was chosen such that it protruded outside of the primary jet assuming a spreading angle of six degrees for the wall jet. Having in mind that the vanes were approximately 70 mm downstream of the injection slot the primary jet had expanded from 1.5 mm at the nozzle to approx. 7 mm. Consequently the vane span was chosen as 7.5 mm. The chord extended over the entire length of the replaceable 'plugs', i.e. 32 mm. The vane looked like a flat plate cropped delta wing (Fig. 3.1a) having a sweep-back of 60 degrees.

Since the mixing of the primary and secondary flows was not as good as desired for the first set of tests it was decided that a vane with a larger span might move the vortex cores out towards the middle of the working section and hence contribute to enhanced mixing. Incidentally, the span was increased by 50 percent to 12 mm (Fig. 3.1b).

3.1.6.) AIR JET VORTEX GENERATOR DESIGN:

It was mentioned above that the entire rig was built within the workshops of the City University. The delicate air jet vortex generator (AJVG) 'plug' was no exception. The final design (Draw. 20a) was manufactured in two halves. This procedure was necessary because of the manufacturing equipment available. A solid perspex cube of 40 mm³ was milled on a CNC machine such that the required shape was established.

The milling bit was taken to a depth of 10 mm. When joining the two mirror image halves this provided a slot with a width of 20 mm. The jet exit had a rectangular section because Freestone^[17] showed that the vortex strength from such a jet is greater than that of a round jet. The throat of the jet had a section of 4x20 mm and the jet was inclined at an angle of 30 degrees relative to the flat bottom surface of the plug.

A purpose built angle setting tool was manufactured, able to slide neatly into the throat of the AJVG plug. With the help of this tool and a protractor scale, divided into one degree increments, the skew angle of the jet relative to the axial direction of the rig could be set in the range of ± 90 degrees. The disadvantage of this method of setting the skew angle was the fact that the tool needed to be inserted into the delicate throat causing the occasional chipping of the perspex. Fortunately, the ensuing damage was very limited. The benefit on the other hand was that no extra holes needed drilling. These holes otherwise would have been required for a pair of setting tongs to be placed.

In Figure 3.2 a definition is given on how a positive and a negative skew angle was set. This was clearly particularly important for the contra-rotating arrangements.

3.2.) COMMISSIONING OF THE RIG:

3.2.1.) DEAD WEIGHT LOAD CELL CALIBRATION:

Initially, the load cells were calibrated by using static load tests. In order to load the augmentor evenly a simple ancillary device was devised. This device consisted of a wooden board lying on top of the diffuser exit with a hole located centrally. A rope was then passed down the inside of the augmentor fastened to the board at the top. Approximately 20 cm below the bell mouth a hook was attached to the rope. This hook was a standard piece of equipment used to support a number of cast iron weights. Before testing the weights were individually weighed on a weight scale. One by one the weights were then carefully shifted on to the hook and the corresponding voltages as produced by load cells were read off. The load cells work on the principle of the piezo-electric effect; as a load is applied to the cell the crystals become deformed and produce a charge. This charge is then amplified by the charge amplifier and converted to voltages which then can easily be displayed on voltmeters. The relation between the deformation and the charge produced is extremely linear within the operating range of the load cell. Overload seriously distorts the crystal matrix and leads to irreversible faults rendering the elements useless. The calibration curve for the static test is shown in Figure 3.3. It can be seen that the curve is straight as could be expected. Using the correct conversion factors gave the following relationship between the applied load and the output voltage:

$$1 V \equiv 111.47 N \quad \text{--- (3.1)}$$

3.2.2.) PRESSURE TRANSDUCER CALIBRATION:

There were three independent air circuits in which the pressures needed to be recorded. Firstly, the pressure of the compressed air inside the working section feeding the peripheral slot had to be monitored. Secondly, the pressure of the air fed to the individual jets had to be monitored and thirdly when the pitot rake was installed the pitot pressures in the exit plane were measured using a transducer. The transducers used were of the sturdy diaphragm type (DEAN) connected to a set of FYLDE MINI BALANCES and AMPLIFIERS. The effective ranges of two of the three transducers covered 0-100 psi and the third 0-25 psi for monitoring the peripheral jet, the individual air jets and the

pitot pressures respectively. The former transducers were calibrated against standard Budenberg test gauges covering the pressure range:

$$P_0 - P_a = 0 \text{ to } 6 \text{ bar} \quad \text{--- (3.2)}$$

Both the transducers and the test gauges were linked, for calibration purposes only, via a T-junction to a 2m³ large compression tank which is charged up by a two stage electrically driven compressor. The compressor is switched such that it charges from atmospheric pressure (0 psi) to 100 psi above atmospheric, at which point the compressor shuts off automatically. Two sets of readings were taken at the beginning of the testing and at an intermediate stage. The respective curves are given in Fig. 3.4a and 3.4b showing a similar relationship. In the second test the pressure discharge was also monitored but is not recorded explicitly on the graph because only a minute amount of hysteresis existed. A mathematical expression was devised to represent the curve closely. The description of the curve in the first case was:

$$y = 6.195 x^{1.05} \quad \text{--- (3.3)}$$

where x is in Volts

For the second set of results:

$$y = 6.150 x^{1.05} \quad \text{--- (3.4)}$$

was found to be representative. It should be noted that the first expression was used for the first testing period and the other one thereafter. Since the discrepancy between the two is approximately 0.7 percent this error is not considered as too serious.

The pitot pressure transducer was calibrated using an alcohol manometer recording its height and the respective output from the transducer. Applying the simple formula:

$$p = \rho g h \quad \text{--- (3.5)}$$

the static pressures were found. Figure 3.4c shows the relationship between the pressure and the equivalent transducer output voltage.

3.2.3.) TARE THRUST EVALUATION:

It was important to establish the effect of the air supply tubes to the working section reservoir. As a large pressure is applied to a flexible tube it stiffens up and therefore if it is initially bent it will try to straighten. After realising and understanding this phenomenon extreme care was taken to minimize the bending of the tubes. However, while welding together the various pieces of the octagonal reservoir distortion was unavoidable. This meant that the tare thrust had to be

measured. This was done by blocking off the four supply pipes inside the working section using simple blanking plates. The calibration curve is shown in Figure 3.5. The plot shows a linear relation between the pressure applied and the tare thrust obtained. The tare thrust was a fairly small quantity compared to the overall thrust levels measured (less than 3 percent).

3.2.4.) DATA ACQUISITION:

There were two major test blocks, namely the load cell measurements and the pitot rake measurements. As far as the equipment for displaying the data is concerned both cases were straightforward. For either tests two or three digital voltmeter readings needed to be recorded, depending on the arrangement of the rig. When the solid vane vortex generators (VVG) were installed two outputs required recording and with the AJVGs in place this increased to three. For the VVG layout one voltmeter gave the equivalent pressure of the peripheral driving pressure and the other showed the load cell thrust reading or the pitot rake pressure. When the AJVGs were installed the third voltmeter displayed the equivalent pressure of the AJ driving pressure.

The pressure in the exit plane was recorded at 45 discrete points using simple pitot probes. Each of the pitot probes was connected via a silicon tube to a reservoir of large volume compared to the volume of the tubing. While running the rig the reservoir could be isolated by clamping off the silicon tube. The reservoir then acted as pneumatic memory. Each of the 45 reservoirs finally was connected to a port on a scanivalve head.

3.2.5.) PITOT RAKE ASSEMBLY:

In order to achieve fast accumulation of data during the test runs it was decided that a two dimensional rake bed should be used. During testing it turned out that the two dimensional rake also had the invaluable advantage that the flow throughout the exit plane was frozen at one instant, thereby excluding the need for long runs; alternatively one could have obtained a full dynamic pressure picture from several runs but this would have produced a time averaged representation of the flow in the exit plane which was not really desired. The total number of pitot probes (45) was limited by the use of a single D3-type scanivalve which has a maximum of 48 ports. Several ports needed to remain "open" for calibration purposes.

Two feasible solutions emerge. On the one hand since the diffuser exit had a round perimeter a radial rake distribution (Fig. 3.6a) seemed favourable; on the other hand there was the possibility of employing

a straightforward equi-spaced rake (Fig. 3.6b).

As one can see from the Figures it would have proved rather difficult to manufacture and mount the radial assembly but more importantly did the likely non-uniform flow restrain from the use of the axisymmetric grid. A further problem with the radial setup are the elongated areas which particularly the outer pitot probes are representing. The cause for these unsuitably shaped areas arose from the idea of having equal sized areas for the convenience of integrating the local thrust values easily. It should be noted that the areas of the inner ring of pitot tubes have an area weighting of four, i.e. these areas are four times as large as those areas of the outer ring. The area weighting of the ring in the middle is two and the outer ring clearly has a weighting of one. Decreasing the area size towards the perimeter was chosen because it was thought that due to the peripheral arrangement of the primary injection most changes in dynamic pressure would occur in the outer radial area of the exit plane. Clearly, this last problem of weighting disappeared completely for the equi-spaced grid, i.e. no prejudice with respect to changes in dynamic pressure is given, but it introduced a new problem, namely the uncertainty around the diffuser perimeter. Some of the pitot probes covered areas extending beyond the perimeter of the exit plane and other areas did not even extend up to the perimeter. It was anticipated, however, that the respective over- and under-estimates would cancel out to a considerable extent.

It was mentioned above that the distribution of the pitot tubes was on an equal area basis. This method gave a very simple way of determining the overall thrust of the augmentor, namely by doubling the dynamic pressures and multiplying by the local area A_L to give:

$$\text{local thrust} = \rho U^2 A_L \quad \text{--- (3.6)}$$

and then summing up all the local thrusts gave the total thrust. Since the square grid representation was selected, A_L was simply 24 mm squared. A tube spacing of 24 mm was chosen on the grounds of covering the exit area in the most efficient way possible, always having in mind the maximum number of 45 pitot tubes available.

3.2.6.) NOISE TESTS:

Theoretical predictions were done for the determination of the noise levels produced by a free round jet, which for the given physical rig dimensions without any attenuation would be in the region of 150 dB. To be deducted from that value was the attenuation of the pressure waves by the room volume plus the absorption by the walls. The absorption rate of the concrete walls and ceiling is very low, i.e. the pressure waves are simply reflected and therefore produce a high

reverberation level. Theoretical calculations lead to a final pressure level of approximately 135 dB at a distance of 1m away from the rig. A fairly good noise insulator is heavy board (ideally acoustic board) plus a layer of 50 mm thick acoustic foam. The thickness of the foam is determined by the wavelength of the acoustic wave. It is known that the 2000 Hz frequency area causes particular strain to the human ear. It is therefore necessary to absorb this frequency, which equates to a wavelength of about 25 mm. In order to simulate closely the ear, noise meters are weighted around the 2000 Hz mark. The complete acoustic treatment led to a figure of 90 dB, now lying within the allowable noise band for a high speed laboratory. It needs mentioning that the workshops are located next door to the rig and hence special attention to quieten the rig was essential. The proposed acoustic 'booth' can be viewed in Drawing 60, Appendix 10.2.

The noise prediction was found to be a considerable overestimate of the actual noise measured; this is probably due to the fact that the noise estimate was based on a round nozzle rather than a narrow slit as used for the primary injection. The slit causes the frequencies to shift to much higher frequency levels, so highly pitched that they become inaudible to the human ear. With regard to the running of the project this clearly was very good news. The noise tests were performed at a working section pressure ratio of approximately 6.2, i.e. at the uppermost end of the test conditions. The following results were measured:

Room upstairs	80-83 dB
Back room (gangway)	84 dB
Industrial tunnel area	81 dB
Workshops	81 dB
Rig (at 1m distance)	105 dB
Reverberant level (lab.)	97 dB

Table I: Noise measurements

It must be stressed that these values were obtained without any noise reduction in the form of an acoustic screen and therefore were extremely encouraging. They did imply that no further attenuation needed to be considered as long as no excessive time was spent on testing. The period of continuous testing clearly became restricted by the reservoir air available. It turned out that an eight minute run took about half an hour of charging up the reservoir tank. Taking an

average working day did therefore not make possible more than one hour of testing, henceforth the acoustic booth lost its viability, leaving the entire process of testing very straightforward. The acoustic screen also would probably have modified the pressure field slightly, calling for some calibration and correction factors, which would have complicated matters extensively.

The industry standard on noise allows a continuous noise level of 90 dB for an eight hour day. Halving the working hours permits a doubling in noise level, i.e. raising it by three dB. In general this gives the following picture:

90 dB = 8 hrs
93 dB = 4 hrs
96 dB = 2 hrs
99 dB = 1 hr etc.

Table II: Legal noise limits

The table shows that the running of the rig was well within the legal noise boundaries, as the reverberant level measured within the laboratory was 97 dB and the total testing accounted for less than one hour per day.

3.3.) ERROR ASSESSMENT:

For experimental work it is very important to assess the errors incurred by all contributing factors. There are two basic kinds of error which need quantifying separately, namely the systematically and the randomly generated error. The former for example causes a shift without changing the shape of a curve. The latter is rather self explanatory. Listed below are factors contributing towards the systematic error:

3.3.1) Experimental setup

3.3.2) Accuracy of instruments

a) Electrical equipment

b) Pitot probes

c) Force measuring instruments

3.3.3) Loads caused by air supply tubes

3.3.4) Random errors

These factors probably need further explanation.

3.3.1.) EXPERIMENTAL SETUP:

There were various intrinsic problems with the experimental setup. The distance of the rig to the ground has clearly an effect on the way the secondary air is drawn into the bell-mouth. If the distance is too small the air drawn in is unnecessarily accelerated reducing the static pressure excessively and thereby emphasising the ground/rig interaction. This is not an error in itself but gives a less representative case of an independent thrust augmentor. It was believed that the chosen distance was sufficient to give the rig the desired independency.

A further limitation was the location of the rig assembly. This location was determined by the laboratory space available. As can be seen in Drawing 61 the rig was only about two meters away from the corner walls and therefore some distortion to the entrained flow must be expected. To quantify this effect could have been done by using the method of sink images in a three dimensional array. As the sink strength diminishes as a function of one over the distance squared the ground (dist. = 1.4 m) has a larger interaction effect than the walls. The calibration of the load cells posed bigger problems than initially anticipated. One major contribution towards a rather large discrepancy in load readings was caused by pre-loading the cells. Pre-loading was achieved by tightening down the M6 set bolts joining the main plate and

the support frame. The holes for the bolts were unfortunately drilled by hand and therefore were not properly aligned with the vertical axis. This mis-alignment caused some friction on the inside surface of the load cell which in turn caused very inconsistent results; before and after loading with an external load a large offset occurred. This phenomenon became worse as the bolts were tightened but persisted even as the bolts were completely unfastened. Obviously, this situation introduced highly intolerable experimental errors and called for modification.

It proved advantageous once again that the net thrust acted downwards, forcing the load cells to compress. This meant that the top plate just needed to be held in place, i.e. to stop lateral movement for security reasons. Three simple 5 mm diameter metal pins fulfilled this task satisfactorily, eliminating the bolts.

3.3.2.) ACCURACY OF INSTRUMENTS:

One major error was produced by the fact that all electrical devices like transducers needed to be calibrated against certain known quantities like liquid manometers. This process in itself was quite accurate but the changes as inflicted by the time factor could not be taken account of. The test programme span across two years. The transducers were re-calibrated at six month intervals and showed a variance of up to two percent but without specific tendency. The output from the transducers was fed through amplifiers for which the manufacturers calibration curves indicate a repeatability of two percent accuracy. From previous experience with these instruments this level of accuracy can be believed.

The next problem arose from the ancillary equipment to the load cells, the charge amplifier. As the name implies this instrument takes the extremely small changes in charge from the cells and then amplifies these to easily readable levels in the mV range. Since the cells use the piezo-electric effect (i.e. the loads are registered as variations in charge caused by crystal deformation) they do not really work in the static load case. This adaptation is obtained artificially by introducing a very large capacitor into the electrical system. It was found out that a leakage still persisted (about 1 mV per sec.). This discharge rate remained fairly constant for some time until the cells were loaded several times. The charge amplifier then started to overcompensate and henceforth the readings began to increase. However, since this rate of increase was rather small compared to the total output and occurred unpredictably no action to avoid it was taken. An unfortunate consequence of this is that the high pressure tests have a better repeatability than the low pressure ones, because of the

relative magnitudes of the output voltages.

Specific problems with the load cells included the dead weight calibration which was explained earlier. Several tests were performed and always gave linear weight to voltage outputs. The various curves laid more or less parallel within a narrow bandwidth, i.e. an error of less than half a percent was recorded. It could not be established due to which reason these shifts were caused. Possible factors are the relative humidity, the temperature and the atmospheric pressure. The pitot rake measurements had their own set of problems, namely the fact that the pitot tubes were not all perpendicular to the diffuser exit plane. This clearly was a problem related to the production process. A lot of care was taken during the manufacture but 1.5 millimetre diameter brass tubing is easily bent. After the final assembly of the rake arrangement each tube was straightened and it can be assumed that a deviation of less than five degrees was achieved. The loss in pressure as a function of misalignment angle in yaw can be viewed in Figure 3.7. The graph shows that the losses for a total head tube are negligible certainly for angles up to ten degrees. A greater error is caused by the fact that the flow swirls considerably for large angles of skew.

While using the pitot rake configuration further problems arose. The major problem came from the stepping device, known as scanivalve, which connects 48 ports with one pressure transducer. Since the Mach number in the exit plane reached peak levels of up to 0.4 and 0.5 the pitot pressures were accordingly large (several thousand Pascals). Effects of compressibility were considered and the results suggested that a maximum error of four percent for a localized area was not too serious to require corrections. But these high pressures caused leakages from one port to the next. This problem was contained by applying a balance pressure to the scanivalve housing. One problem that still persisted when the motor scanned from a high pressure port to a low pressure port or vice versa was that the values were smeared out slightly because a finite volume of air was carried forward. Fortunately, this does not affect the aggregate results which were used to compare with the load cell measurements. When scanning through the ports a second time showed very similar results to the first scan implying that the 'smearing' effect was quite small. The change was less than two mV compared to a typical value of 500 mV representing an error of less than half of one percent. This effect was so small that it can be considered negligible compared to the random errors which are dealt with below.

3.3.3.) LOADS CAUSED BY AIR SUPPLY TUBES:

The subtitle above already incorporates all the main terms which contribute towards the error. It was known that elastic tubes which have a throughput of highly pressurised air (several bar) try to straighten themselves if they have a certain degree of pre-bending, i.e. some curvature. Due to the manufacturing process of the octagonal reservoir, the eight individual pieces had to be welded together causing some deformation. Consequently, the four connectors did not accurately align with those of the working section connectors. This mis-alignment was rectified as much as possible by using washers to obtain the desired relative positions. The remaining inaccuracy was measured by blanking off the supply tubes within the working section and then applying a range of pressures to the connecting tubes. This calibration gave a certain relationship between pressure ratio (PR) and tare thrust as shown in Fig. 3.5. Since pressurisation of the tubes gave a positive thrust this amount of thrust had to be subtracted later on from the measured values. Fortunately the graph of PR versus thrust was a simple linear curve. The tare thrust amounted to approximately 3.5 percent relative to the bare nozzle thrust and clearly less for the augmented thrust. After the tests with the solid VVGs installed were completed, the second octagonal reservoir was added on top of the other octagonal reservoir (see Fig. 1.1b) to supply air to the air jet vortex generators.

The initially specified design of having connectors welded to the three inch pipe-work, quickly proved highly error prone because there was no simple remedy to adjust the mis-alignment. The degree of distortion of the large reservoir pipe due to the welding process was not properly anticipated. The tare thrust caused by the straightening of the eight individual flexible supply tubes was of the same order as the net thrust measured for the thrust augmentor. This situation clearly was unacceptable. The problem was solved by repositioning each connector individually with the working section reservoir installed on the rig, making this process extremely accurate but also very time consuming. The author acknowledges the fact that this problem should have been thought of in the design phase and dealt with accordingly. Re-calibration showed a similar relationship between the driving pressure ratio and the tare thrust as above, where the lower peripheral nozzle working section was fed only, emphasising the accuracy obtained from this modification.

3.3.4.) RANDOM ERRORS:

When running the rig using the load cells to measure the thrust two digital readings needed to be taken, a) the load cell output and b) the corresponding peripheral slot pressure. Reading two gauges simultaneously proved rather difficult particularly since the digits did sometimes not settle down within a reasonable time period (about two seconds). Experience with the system showed that the errors were fairly small; ± 2 mV compared to an average value of 500 mV which corresponds to an error band of ± 0.4 per cent. This clearly makes the assumption that the values were read off correctly in the first place which of course must be assumed at this point. Potential mistakes could only be rectified once the results were plotted. Due to the fluctuating nature of the measurements any false point was extremely difficult to detect and therefore it must be stated that no provision was made for this shortcoming. Making mistakes while noting down data is clearly another potential source for error and is rather impossible to suppress for a manual data acquisition system. The author nevertheless believes that major care was taken in acquiring the data and thereby reducing the above mentioned mistakes to a very small margin.

As anybody can imagine these problems became even more pronounced when reading off values from three different digital voltmeters, which was necessary for the joint peripheral and individual jet configuration. Despite the aforementioned difficulties with the equipment it was believed that most of the possible errors were looked at and thus eliminated. Due to the nature of the testing facility an experimental error band of ± 0.4 per cent for either the load cell readings and the pressure readings should be allowed for. In addition the error from the pressure transducer calibration curves which came to ± 0.7 per cent as a maximum must be taken account of. Applying the generally applicable formula for calculating the total random error we have: the accumulation of the individual errors are squared then added and then square rooted. This in effect implied that an error band of just less than ± 1.0 per cent should be allowed for.

4.) THRUST MEASUREMENTS

USING LOAD CELLS

This Chapter deals with all the relevant measurements obtained from the load cell tests. Using load cells was the quickest technique to determine the net thrusts. A total of three cells was used, with each cell placed on top of one of the three support legs for rigidity and hence accuracy reasons. The signals from the three cells were combined and then fed through a single charge amplifier. More information could have been extracted if each of the load cells could have had its own charge amplifier, but this was rejected due to financial constraints. Three individual signals would have given an indication of the contribution towards total thrust at three discrete points.

It is important to note at this point that the data presented in this entire Chapter was obtained at a diffuser area ratio of $n = 1.5$. The measured thrusts were all normalized to standard atmospheric conditions of 1013 mbar, except where explicitly otherwise stated.

Furthermore, it must be remembered throughout this section that the parallel walled mixing section was installed for all the tests.

4.0.1.) Determination of bare nozzle thrust:

The bare nozzle thrust (BNT) of the peripheral nozzle was initially evaluated using the theoretical formula for a convergent nozzle flow, taking account of the momentum and pressure thrust. An accurate experimental test programme, by blanking of the secondary inlet and installing static pressure tapings to monitor the base pressure, was thought of but was rejected because of the modifications involved. Furthermore, the uncertainty of its validity was the stronger reason for its rejection. The closest to a bare nozzle thrust test was achieved by removing the mixing section, the diffuser sections and the bell-mouth. Blowing the peripheral jet with a primary pressure ratio of five the thrust for the peripheral nozzle (there was of course still some secondary entrainment!) came to 98.4 percent of the theoretical value. Since this value was within the experimental error band it can be assumed that the theory over-estimated the thrust but that the margin was not too large.

The BNTs with the air jets blowing, as discussed in Section 4.3. below, were determined experimentally by again removing the mixing section, the diffuser and the bell-mouth leaving only the working section with

the ejectors. The total bare nozzle thrust of the eight individual air jets was measured with the jets set to 0°, 15°, 30° and 45° skew angle. Since the respective BNTs reduced according to the cosine function it was deduced that a direct relationship existed between the angle and the bare nozzle thrust, i.e.:

$$BNT \text{ at some skew angle } \beta = \cos(\beta) BNT_0 \quad \text{--- (4.1)}$$

where BNT_0 was the zero degree skew bare nozzle thrust.

Due to the peripheral arrangement of the air jet vortex generators and the elevation of the jets the surface area of the jet shear layers were quite large and therefore entrained excessive amounts of secondary air which in turn clearly produced thrust forces on the support structure. Hence the ensuing augmentations presented are smaller than if based on 'true' bare nozzle thrust.

It must be emphasised that the calculation of 'true' theoretical BNT was difficult for the given shapes of the jets. Even the determination of thrust for a round nozzle of equivalent cross-sectional area poses problems, because of the reasons discussed below, e.g. non-ideal flow parameters. Theoretically there were various possibilities to evaluate bare nozzle thrust:

- a) ideal isentropic convergent-divergent nozzle
- b) ideal convergent nozzle
- c) fully expanded flow equations for convergent nozzle
- d) inclusion of discharge and velocity coefficients
in a), b) and c)

The controlled expansion of a convergent-divergent nozzle does not strictly apply to the air jet vortex generator nozzles because it requires a contoured nozzle. The formula giving the highest thrusts for a given driving pressure is the fully expanded flow equation. Physically the flow was unlikely to attain this condition; the confined space within the mixing section prohibited a full expansion. More realistic was the formula for an ideal convergent nozzle. This formula was used extensively because it seemed to simulate the likely physics of the flow best. If discharge and velocity coefficients were to be included in calculating the BNTs, they would represent losses, reducing the ideal values to actual ones. From previous investigations of nozzles it was known that these losses are fairly small. Any such losses certainly would translate into increased augmentations. Hence if the ideal convergent formula for calculating the bare nozzle thrust is used the corresponding augmentations are conservative.

All the comments on the calculation of the BNT apply to nozzles blowing in the axial direction. What happens as a nozzle is set at some oblique

angle to the axial direction? Literature on this subject of evaluating the thrust for a jet injecting obliquely at supersonic speed into a secondary stream was not available to the author. From the tests with exclusive AJVG blowing it was established that the thrust degraded as a function of cosine of the skew angle. This clearly implied that the transverse velocity and pressure component of the momentum did not contribute towards the axial thrust.

One major assumption was made in determining the combined peripheral and air jet bare nozzle thrust in Section 4.3., namely that the individually measured BNTs simply added to give the total bare nozzle thrust, i.e. the combined BNTs were not explicitly tested. It is probable that the combined thrusts would have given other slightly different results due to the flow interactions of the two streams but it was not thought to justify the time required to determine all the possible combinations considered.

4.1.) BARE AUGMENTOR

There was a requirement for one test series only, and that was to measure the thrust at different pressure ratios (PR). The test procedure adopted was a slow build up in pressure from just beyond choked condition to an approximate pressure ratio of 5.5, raising the pressure in steps of 0.3 to 0.5 bar. As testing experience grew it did prove that the step size was not that critical because a very linear relationship developed between the thrust and the PR. However, larger steps were not used in order to minimize errors. Having a representative number of data points ensured a good curve, revealing any odd point. Using the appropriate calibration factors, as established in Chapter 3, and taking into account the atmospheric conditions and the tare thrust, the millivolt readings were converted to real units (N/m^2).

The results of these tests can be viewed in Fig. 4.1. A least squares fit technique was adopted for the line joining the data points. Two independent data curves are shown in this Figure. The lower curve represents the measurements with the pitot rake installed on top of the diffuser exit plane and the upper one shows the bare augmentor thrust without the rake in place. The discrepancy between the two curves was most likely caused by the drag on the pitot rake, reducing its values by some margin.

When calculating the augmentation ratio (Φ), which was defined as the measured thrust divided by the theoretical peripheral bare nozzle thrust, at different PRs a certain trend was established, namely that

Φ decreased as PR increased. At a pressure ratio of 5.0 the augmentation ratio came to $\Phi = 1.15$. This number implied clearly that a 15 percent augmentation on top of the bare nozzle thrust was already achieved with this simple arrangement. In the third column of Table IV the augmentation ratios are listed for PRs in the range 1.5 to 3 rising in 0.5 increments. The value for a pressure ratio of 1.5 was interpolated from the least squares fit curve and strictly speaking must be considered with some caution because the primary nozzle was not choked. The implication of this condition was that the bare nozzle thrust should have been calculated using a subsonic approach rather than the simplified choked solution.

4.2.) MODIFIED AUGMENTOR WITH VANE VORTEX GENERATORS

The experimental layout and testing technique was similar to the one described in Section 4.1. What did change was the inclusion of the auxiliary working section which housed the steerable vanes. Unfortunately, the rig had to be dismantled considerably in order to alter the angle of incidence of the vanes. The mixing section and the diffuser section needed to be removed. The angle of the vanes was set with the help of an inclinometer. It should be noted for later reference that the vane angle of attack was always relative to the axial direction, i.e. it referred to a fixed frame of reference for simplification rather than to the relative streamwise direction of the flow. Ideally these two systems should coincide but this is obviously quite unlikely due to the non-uniform behaviour of the flow and hence its corresponding streamlines.

For these set of tests all the vanes were set to one particular angle, e.g. 15 or 16 degrees. Their physical locations were approximately two and a half vane chord lengths downstream of the peripheral injection slot.

4.2.1.) CO-ROTATING VORTICES

From Pearcey^[7] it was known that vanes installed on aerofoils perform best when skewed to between 15 and 20 degrees. The test series was directed towards finding the optimum vane angle as quickly as possible, hence a start from the lower value was initiated. The vane angles were then collectively increased in one degree increments, using the technique described above, until a reduction in performance was

observed. Quickly it turned out that the initially chosen angle of 15 degrees was too large to obtain a full picture, hence the angle was reduced in one degree increments down to 12°. The processed values were then plotted and some example plots in the range $\alpha = 13$ to 16 degrees are shown in Fig. 4.2a-d. As for the bare augmentor in Section 4.1 above, least squares fits were applied to the data points. Here again it can be seen that there is a linear relationship between pressure ratio and net thrust. Using the aforementioned plots the respective augmentations were determined. Since the high pressure end gave more accurate results, a comparison at PR = 5.0 is given in Fig. 4.3 (note: the values were interpolated using the mathematical expression obtained from the least squares fit describing the slope of the curve). The maximum augmentation was reached at $\alpha = 16^\circ$. At this angle the performance of the vanes were at their maximum. It should be noted at this point that the tests were repeated with the vanes set to the same angles but in the opposite direction. The obtained results compared well with the first set of results which led to the conclusion that the flow was fairly symmetrical.

4.2.2.) CONTRA-ROTATING VORTICES

These tests were performed with precisely the same layout as those explained just above, but the fundamental difference was the inclusion of contra-rotating VVG pairs instead of the co-rotating VVG's. Any one pair consisted of one vane set at plus x degrees of incidence and one vane set at minus x degrees of incidence, i.e. the vanes were set at $\pm x$ degrees alternately. The magnitude of x was the same for all the vanes. Measurements were taken in one degree increments, this time starting from 12° straight away and ending at 17 degrees incidence. Again an inclinometer was used to set the vane angle just as in Section 4.2.1. A processed collection of the experimental results, showing augmentation ratios at discrete skew angles, can be viewed in Fig. 4.4. The graph reveals that the contra-rotating setup had a fairly wide band of maximum augmentation. Close to thirty percent augmentation were obtainable for the 14 to 16 degree range. The peak was reached at an incidence of 14° for this set of results. It should be realised that if error bands were added to all the test values, the results for the 14 to 16 degree range would all lie within that band. Beyond 16 degrees a definite feature occurred, namely the augmentation dropped off sharply. This occurrence was similar to that of the co-rotating arrangement.

4.3.) MODIFIED AUGMENTOR WITH AIR JET VORTEX GENERATORS:

In order to interpret the accumulated sets of results more easily they were tabulated for various constant pressure ratio conditions. The four tables give values for:

- a) net thrust levels: (Table III, Table V)
- b) augmentation ratios: (Table IV, Table VI)

The air jet PRs are shown horizontally across (values of 2.0, 2.5, 3.0, 3.5, 4.0 and 4.5) and the peripheral PRs are represented along the vertical. The latter pressure ratios are also increased in half a bar increments starting from 1.0 up to 3.0. The limit of three had been selected because above this, the augmentations continued to reduce to a level which could be reached with the simple augmentor, i.e. making the complicated layout involving the two independent jets (peripheral plus individual AJVGs) superfluous. The second column of the tables specifies the skew angle to which the air jet vortex generator 'plugs' were turned. Any one set of results for a constant peripheral pressure ratio consisted of six skew angles for the AJs (0°, 15°, 30°, 45°, 60° and 75°). Skewing the air jets to 90 degrees was considered to be nominally the same as blowing the peripheral jet only, but no explicit measurements were taken for this condition. Justification for that argument was that half the momentum would be diverted towards the secondary inlet and the other half would move down the mixing section in the ordinary way. For the real application, as the peripheral and the individual air jets were superimposed, the normally blown air jets would interact with the peripheral jet and would degenerate or enhance its performance. The degenerating component would be caused by flow interaction between the particles from the air jets and the particles drawn in through the secondary inlet. The enhancing component would be the fact that the air jets would force the particles from the peripheral primary to move towards the central axis of the augmentor and thereby increase the mixing shear area. Summarizing these effects it can be said that for combined peripheral and air jet blowing the air jets act as vortex generators and therefore produce different results as when switched off.

Where a pressure ratio of one is specified for the peripheral or AJVG results, it effectively meant that the one or the other jet was turned off. From Chapter 3.3. it should be remembered that error bands of \pm four percent need to be attached to the individual values.

The thrust augmentations, listed in the second set of tables, were defined as the measured net thrusts divided by their respective measured bare nozzle thrusts (BNT).

THRUST MEASUREMENTS [N]
(co-rotating AJVGs)

AJVG pressure ratio

	ANGLE	1.0	2.0	2.5	3.0	3.5	4.0	4.5	
P e r i p h e r a l p r e s s u r e r a t i o	1.0	0	0	174	221	264	302	335	363
		15		167	211	252	288	322	352
		30		154	188	221	252	281	308
		45		138	169	197	223	246	267
		60		105	132	156	177	195	209
		75		46	56	66	78	90	103
	1.5	0	80	236	281	322	359	391	420
		15		229	273	313	349	380	408
		30		219	252	283	312	340	366
		45		192	223	249	271	289	302
		60		168	192	213	231	245	256
		75		132	145	156	165	171	176
	2.0	0	136	291	336	377	413	444	472
		15		295	336	374	408	438	464
		30		282	312	340	367	393	418
		45		250	277	301	323	342	359
		60		228	248	266	282	296	307
		75		186	196	204	210	216	219
	2.5	0	188	335	382	423	459	489	514
		15		335	384	426	461	489	510
		30		335	364	391	416	441	464
		45		301	330	356	377	396	410
		60		281	298	313	327	338	347
		75		239	246	252	257	261	264
3.0	0	241	384	429	469	504	534	559	
	15		391	437	477	511	538	560	
	30		380	412	442	470	495	517	
	45		350	373	395	415	432	448	
	60		313	329	343	354	364	372	
	75		298	302	305	308	311	314	

Table III: Measured load cell thrusts; co-rotating air jets

AUGMENTATION (based on experimental BNT)
(co-rotating AJVGs)

		AJVG pressure ratio							
	ANGLE	1.0	2.0	2.5	3.0	3.5	4.0	4.5	
P e r i p h e r a l p r e s s u r e r a t i o	1.0		0	1.78	1.70	1.64	1.56	1.50	1.42
			15	1.77	1.70	1.63	1.55	1.48	1.41
			30	1.79	1.69	1.60	1.53	1.46	1.40
			45	2.03	1.88	1.76	1.65	1.56	1.49
			60	2.23	2.10	1.97	1.86	1.74	1.64
			75	1.83	1.71	1.62	1.57	1.56	1.58
	1.5	1.23	0	1.51	1.50	1.48	1.44	1.39	1.33
			15	1.52	1.50	1.47	1.43	1.39	1.33
			30	1.56	1.50	1.44	1.39	1.34	1.30
			45	1.48	1.45	1.41	1.37	1.31	1.25
			60	1.58	1.56	1.53	1.49	1.44	1.38
			75	1.62	1.60	1.58	1.54	1.50	1.46
	2.0	1.22	0	1.39	1.39	1.38	1.34	1.31	1.27
			15	1.44	1.43	1.42	1.39	1.35	1.30
			30	1.44	1.41	1.37	1.34	1.30	1.26
			45	1.40	1.37	1.34	1.30	1.26	1.21
			60	1.43	1.41	1.38	1.35	1.32	1.28
			75	1.39	1.38	1.37	1.34	1.30	1.26
	2.5	1.20	0	1.34	1.35	1.35	1.34	1.31	1.26
			15	1.36	1.37	1.37	1.36	1.32	1.27
			30	1.40	1.37	1.33	1.30	1.27	1.23
			45	1.33	1.32	1.31	1.28	1.25	1.20
			60	1.36	1.33	1.31	1.28	1.25	1.22
			75	1.32	1.31	1.29	1.27	1.24	1.20
3.0	1.19	0	1.30	1.32	1.32	1.30	1.28	1.24	
		15	1.32	1.34	1.34	1.32	1.29	1.25	
		30	1.34	1.32	1.30	1.28	1.26	1.22	
		45	1.25	1.24	1.22	1.20	1.18	1.15	
		60	1.23	1.22	1.20	1.18	1.15	1.11	
		75	1.31	1.29	1.27	1.25	1.22	1.19	

Table IV: Augmentations based on measured bare nozzle thrust, co-rotating air jets

THRUST MEASUREMENTS [N]
(contra-rotating AJ pairs)

AJVG pressure ratio

		ANGLE	1.0	2.0	2.5	3.0	3.5	4.0	4.5
P e r i p h e r a l p r e s s u r e r a t i o	1.0	0	0	174	221	264	302	335	363
		15		168	214	256	292	324	350
		30		146	187	224	256	283	306
		45		117	147	174	198	220	239
		60		75	97	116	134	149	163
		75		29	38	46	54	61	68
	1.5	0	80	236	281	322	359	391	420
		15		233	277	317	353	384	411
		30		212	248	281	311	337	361
		45		186	211	234	255	275	293
		60		149	164	178	191	204	216
		75		101	105	109	113	119	125
	2.0	0	136	291	336	377	413	444	472
		15		289	333	373	408	439	465
		30		268	303	334	362	387	409
		45		241	265	287	307	326	344
		60		208	220	232	244	257	269
		75		162	162	163	165	168	172
	2.5	0	188	335	382	423	459	489	514
		15		339	383	421	455	485	510
		30		329	363	393	420	445	465
		45		297	319	339	358	376	392
		60		257	268	280	291	303	315
		75		215	214	214	215	217	219
3.0	0	241	384	429	469	504	534	559	
	15		389	435	476	510	539	562	
	30		381	415	445	470	492	510	
	45		349	372	392	409	424	437	
	60		323	331	338	346	354	363	
	75		277	271	267	265	264	266	

Table V: Load cell thrust measurements; contra-rotating air jet pairs

AUGMENTATION (based on experimental BNT)
(contra-rotating AJ pairs)

AJVG pressure ratio

	ANGLE	1.0	2.0	2.5	3.0	3.5	4.0	4.5	
P e r i p h e r a l p r e s s u r e r a t i o	1.0		0	1.78	1.70	1.64	1.56	1.50	1.42
			15	1.82	1.75	1.67	1.59	1.51	1.43
			30	1.75	1.69	1.62	1.55	1.48	1.40
			45	1.70	1.62	1.55	1.48	1.41	1.35
			60	1.55	1.50	1.45	1.39	1.34	1.28
			75	1.13	1.12	1.10	1.08	1.06	1.02
	1.5	1.23	0	1.51	1.50	1.48	1.44	1.39	1.33
			15	1.55	1.54	1.51	1.47	1.41	1.35
			30	1.50	1.47	1.44	1.40	1.35	1.30
			45	1.47	1.42	1.37	1.32	1.28	1.23
			60	1.40	1.33	1.28	1.23	1.19	1.16
			75	1.19	1.14	1.09	1.05	1.01	0.99
	2.0	1.22	0	1.39	1.39	1.38	1.35	1.31	1.27
			15	1.44	1.44	1.43	1.41	1.37	1.33
			30	1.40	1.39	1.36	1.33	1.29	1.24
			45	1.37	1.34	1.31	1.27	1.23	1.19
			60	1.30	1.26	1.22	1.18	1.15	1.12
			75	1.19	1.13	1.08	1.03	0.99	0.97
	2.5	1.20	0	1.34	1.35	1.35	1.34	1.31	1.26
			15	1.37	1.38	1.38	1.36	1.32	1.28
			30	1.39	1.38	1.35	1.33	1.29	1.25
			45	1.34	1.31	1.28	1.25	1.22	1.18
			60	1.28	1.24	1.20	1.17	1.14	1.11
			75	1.18	1.12	1.08	1.04	1.00	0.97
3.0	1.19	0	1.30	1.32	1.32	1.30	1.28	1.24	
		15	1.34	1.35	1.35	1.34	1.31	1.27	
		30	1.35	1.34	1.33	1.30	1.26	1.22	
		45	1.31	1.28	1.26	1.23	1.20	1.17	
		60	1.29	1.25	1.21	1.17	1.14	1.10	
		75	1.22	1.15	1.10	1.05	1.02	0.99	

Table VI: Augmentations based on measured bare nozzle thrusts, contra-rotating air jet pairs

4.3.1.) CO-ROTATING VORTICES

An examination of the net thrust table revealed that the values increased from left to right and top to bottom as should be expected since the respective pressure ratios were raised linearly. The thrust produced by the peripheral jet added in a fairly linear manner to the air jet thrust. In Figures 4.5, 4.6 this occurrence is verified graphically, where the thrust is plotted against air jet skew angle for two constant AJ pressure ratios of 2.0 and 4.5 respectively; it can be seen that the thrust increment between the curves was fairly constant. When subtracting a constant value of thrust equal to the initial thrust as produced by the peripheral jet only, a small discrepancy occurred. This discrepancy between the two curves must be caused by the interaction of the two jets. The measured thrusts minus the peripheral thrust gave new net thrust values which were lower than those for the air jets blowing only. This feature was made clearer when looking at the calculations of the augmentation ratios.

Other features of the test results emerged as the thrust was plotted versus skew angle at constant air jet driving pressures. Six curves in the range $PR = 2.0$ to 4.5 , rising in 0.5 increments, are shown in Figs. 4.7 and 4.8. The two extremes of the table were selected to demonstrate two interesting points: looking at the plot where a peripheral PR of 1.0 , i.e. no peripheral blowing, is specified it seems that the curves converge to a point below 0 on the thrust axis for a skew angle of 90 degrees. This actually would be possible if more air travels towards the secondary inlet rather than in the usual streamwise direction. A measurement of this condition would have proven quite difficult due to the precise setting of the air jets required. The second plot with $PR_{peri} = 3.0$ shows a much clearer shortcoming, again for the skew angle $\beta = 90^\circ$ case. The assumption that the air jets did not contribute towards the thrust in any way as they were skewed to 90 degrees seemed to be wrong. When looking at a mathematical model for a jet blowing normal to the freestream flow the momentum contribution towards thrust is certainly zero, but the effect of mixing is being neglected. In this particular example shown in Fig. 4.8 the curves suggest a thrust in the region of $285N$ rather than the $241N$ as obtained for the exclusive peripheral blowing. It meant that the discrepancy of $44N$ was contributed from the air jets in the form of enhanced mixing between the primaries and the secondary, and not from the direct increase in momentum, i.e. this discrepancy in thrust is probably due to the vortex generation. Unfortunately no tests could be performed under these conditions because the noise produced by the air jets was excessive, well beyond the 'normal' noise levels for lesser skew angles.

From the point of view of obtaining maximum augmentation the configuration with the air jets only operating gave the really interesting results, although it must be realised that the net thrust levels were fairly small and therefore not of so much use for real life applications. The table shows that more than one hundred percent improvement on experimental bare nozzle thrust was possible. This was achieved for the condition when the AJ inlet just became choked and the jets were skewed to 60 degrees. In Figure 4.9 one sees how the augmentation curves rose as the skew angle was raised and then fairly suddenly fell off for skew angles beyond 60 to 65 degrees. It should be remembered that all the augmentations were based on experimental thrusts which took account of the degeneration in bare nozzle thrust with the cosine function of the skew angle. This effectively meant that a major component of primary axial streamwise momentum was re-directed. For a real application this probably would prove unacceptable because it is 'expensive' to produce the primary momentum in the first place. As the peripheral jet was blown harder at $PR = 2.5$ (Fig. 4.10) the augmentations obtained fell to more modest values in the region of 20 to 35 percent. The plot suggested a steady decline in augmentation as the skew angle was raised. This decline was probably related to the fact that primary momentum from the air jets was re-directed. The reduction in augmentation did not, however, follow directly the air jet thrust times the cosine of skew angle function. This was due to the different effects on mixing as the AJ plugs were turned. It emerged that for certain combinations of AJ and peripheral jet driving pressure certain optimum angle of skew for the air jets were required, in order to maximize augmentation.

4.3.2.) CONTRA-ROTATING VORTICES

When studying the net thrust table the general trend that the values increase from left to right and top to bottom applies as for the co-rotating arrangement. It was interesting to note how the difference in thrust levels between 0 and 15 degrees skew reduced as the peripheral pressure ratios were increased and even reversed, i.e. the thrust for 15 degrees skew became larger than for 0 degree skew (Fig. 4.11 and Fig. 4.12). This was rather surprising since there was a factor of $\cos 15^\circ$ (roughly 4%) being lost as the jets were skewed. This loss in axial momentum must have been overcompensated by enhanced mixing of the two primary jets and the secondary air because there was no other contribution to which it could be attributed. It was expected that the pressure contour plots would give a better indication of what the cause for this occurrence was.

A rather surprising feature occurred as the air jets were skewed to 75

degrees and the peripheral pressure ratio was raised to 2.5 and more: the interaction of the two flows caused the net thrust to fall initially as the air jets were being blown harder. How was this possible? One explanation was that at this skew angle the flow leaving the AJVG plugs had a large velocity component in the angular direction. This caused flow interactions of the two primaries and thereby reduced the axial kinetic energy at a faster rate than the direct gain from the axial velocity component of the jet itself plus the beneficial effect of forming discrete vortices. It seemed that the enhanced mixing via the vortices still worked since the net thrusts were higher than for the peripheral blowing only assembly. The enhancement was quite marginal though (Fig. 4.14).

Looking at the results for the augmentations the case without peripheral blowing again was the more interesting as the augmentations were rather high. From Fig. 4.15 a steady decline in augmentation can be observed with increasing skew angle. Only initially, starting from no skew, did the augmentations rise and then peaked at about 10 degrees. Beyond 60° the curves started falling off very sharply, probably caused by any two jets from one pair interacting with each other in an adverse fashion, i.e. flow interactions forced reductions in streamwise energy faster than the beneficial effect of forming discrete vortices and hence enhanced mixing. When adding a peripheral jet, blowing at $PR = 2.5$ (Fig. 4.16), the fundamental picture was the same as described above, what did change was a reduction in overall augmentation. For the cases where air jet pressure ratios of 4.0 and greater were applied and the vortex generator 'plugs' were skewed to 75° and more the thrusts measured reduced to a lower value than the bare nozzle thrust, which clearly is an undesirable condition.

5.) THRUST MEASUREMENTS AND PRESSURE DISTRIBUTION USING PITOT RAKE

This Chapter deals with the results for those tests which involved the use of the pitot rake assembly to determine the thrust and more importantly the pressure distribution in the exit plane of the diffuser. After processing the data, contour lines for constant pressure conditions were developed. Some features applying to all the contour plots considered are discussed in Section 5.3.1.

In Section 3.2.5. above the method for evaluating the total thrust, using the pitot rake, of the augmentor was described. It was mentioned that the dynamic pressure for each probe needed to be doubled to give the loading per unit area. Since the pitot probes were positioned in a square arrangement, the distance between any two probes squared represented a unit area. Multiplying the loading and the unit area clearly gave the unit thrust. Assuming that each of the unit thrusts were constant throughout their unit areas, a simple addition of the 45 unit thrusts determined the total thrust. The measurements for the total thrust are presented under the individual headings of 'bare augmentor', 'modified augmentor with vane vortex generators' and so on.

5.1.) BARE AUGMENTOR

At a very early stage in the experimental research programme the dynamic pressures in the exit plane were monitored for the purpose of verification of the load cell measurements. It should be remembered that the bare augmentor was that configuration which had peripheral primary blowing only. Measurements using the pitot rake assembly were obtained at four discrete pressure ratios (2.67, 3.58, 4.58 and 5.74). These pressure ratios were not specifically selected but were meant to represent a good cross-sectional view over the effective range of the augmentor. The maximum pressure ratio in the design phase was selected as 6.0; the lower end was limited by the choked condition of the primary jet, i.e. a pressure ratio of 1.89 and greater was required to guarantee choked condition when injecting into air at atmospheric pressure. Since the static pressure within the augmentor reduced to sub-atmospheric as secondary air was drawn in, a PR less than the

critical sufficed to ensure choked condition. The number of sets of tests was kept to a representative minimum. From the previous load cell tests it became known that there was a linear relationship between the pressure ratio and the net thrust rendering more than four tests excessive.

In the table below the summarized pitot rake results are shown. The column headed Thrust (N.B. these were the summed up local thrusts) lists the experimentally obtained values. The theoretical bare nozzle thrusts (BNT) were calculated for the respective discrete pressure ratios and atmospheric conditions. The augmentation was simply defined as measured thrust over bare nozzle thrust (where the BNT was the theoretical ideal convergent nozzle thrust):

PR	Thrust [N]	theor. BNT [N]	augmentation
2.67	205.9	175.7 ($p_a = 1012\text{mbar}$)	1.172
3.58	308.3	261.2 ($p_a = 1014\text{mbar}$)	1.180
4.58	418.0	354.8 ($p_a = 1014\text{mbar}$)	1.178
5.74	531.5	464.3 ($p_a = 1016\text{mbar}$)	1.145

Table VII: Augmentation for bare augmentor

A closer look at the dynamic pressure plot for PR = 4.58 (Fig. 5.1) revealed several very interesting features. Firstly, the steep gradients towards the edges of the diffuser exit perimeter were noteworthy. These gradients were clearly produced by large differentials in velocity, the velocity distribution was in turn an indication that a peripheral nozzle was being employed. Secondly, it should be noticed that the complete curves look like U-shaped curves offset in the y-direction by some small amount. Taking the PR = 4.58 case as an example the trough went as low as 900 Pa but the peaks rose above 20 kPa. Thirdly, the wide shallow 'bottoms' of the U-shaped curves were immediately apparent. They indicated incomplete mixing between the primary and secondary air of large proportions. This phenomenon became even clearer as the dynamic pressure data was reprocessed to form a constant pressure contour plot (Fig. 5.2) in the x and y direction of the relevant exit plane. The plot revealed several very specific features. The arrows on the perimeter represented the position of the four supply tubes feeding the peripheral reservoir. The ensuing consequence of this arrangement was the formation of the four characteristic 'lobes'. They represented areas of very high dynamic pressure, i.e. the momentum flux was very high in these areas. Ideally the contour lines should be concentric circles, formed by equal

introduction of momentum through the peripheral slot. As the contour lines were, they suggested that the size of the reservoir of the peripheral jet was too small to allow the flow to settle down sufficiently to equalize the pressure within the reservoir. The problem probably could have been contained by choosing a larger number of supply tubes or by increasing the size of the reservoir or of course a combination of both. Despite this short-coming it was decided that a modification would have taken too much time and man-hours to justify it. Instead it was accepted that this was the basis which should be improved. The rather obvious scope for improvement was to transfer momentum to the very low pressure area near the centre of the test plane. The plot also showed that the low pressure area was expanding more to the left, which possibly was caused by a multitude of factors. One was the physical location of the rig with several nearby walls. It was believed that the walls influenced the way in which secondary air was drawn in. The other factor was the air supply to the octagonal reservoir which was fed from a single side only.

This resultant effect of having differentials in pressure within the octagonal reservoir must have been extremely small because its cross-sectional area was huge compared to the cross-sectional areas of the feeder pipes leading to the peripheral reservoir. The octagonal reservoir was large enough to give the flow ample chance to slow down and act as a settling chamber.

5.2.) MODIFIED AUGMENTOR WITH VANE VORTEX GENERATORS

5.2.1.) CO-ROTATING VORTICES

The load cell measurements were just means of determining the best VVG configuration quickly, i.e. to get a picture of the maximum thrust enhancement. They did not, however, give any indication of the actual modification to the flow field within the augmentor. One observation that was immediately deduced from the load cell plots was that mixing between the primary and secondary air must have increased in order to justify the steeper slopes of the thrust vs PR curves (compare Fig. 4.1 and Fig. 4.2c for example). This fact was substantiated when looking at the dynamic pressure plot (Fig. 5.4) taken at the diffuser exit plane near the optimum vane angle of 15 degrees. Measurements again were performed at four pressure ratios as for the bare augmentor, namely 2.81, 3.47, 4.30 and 5.17. For the purpose of comparing a dynamic pressure plot with that of the simple augmentor (Fig. 5.2) the data for a similar pressure ratio was selected. To obtain the same reference pressure ratio was near impossible and hence the next closest set of data had to suffice. At a PR of 4.3 the discrepancy to the pressure ratio for the bare augmentor only amounted to about 6 percent. The difference for the dynamic pressure distribution was quite striking. The 'bottoms' of the U-shaped curves had shifted considerably to larger dynamic pressure values (see Fig. 5.3). Only for the central rake (No.4) did the dynamic pressure dip to less than 2kPa. But at the same time the really high pressure peaks near the injection points have been smeared out. The maximum dynamic pressure measured came to 13 kPa compared to 22 kPa for the bare augmentor. It was deduced that the vanes were a good means of promoting mixing via the mechanism of discrete vortex formation. The vortices caused some localized high momentum air to be redistributed towards the centre due to the process of mixing. This process was responsible for an increase in shear area of the primary jet which meant that the pressure differential between the primary and secondary air was spread over a larger cross-sectional area. Consequently, more air was drawn in through the secondary inlet and hence the inlet thrust on the bell-mouth was increased. At the same time the momentum flux in the exit plane also enhanced giving a considerable net increase in thrust.

5.2.2.) CONTRA-ROTATING VORTICES

Two sets of results were obtained for the contra-rotating VVG configuration, namely at a pressure ratio of 3.12 and 4.34. The tests were performed with the vanes adjusted to 14 degrees, i.e. very close to the optimum angle, as determined by the load cell measurements. Figure 5.5 shows the dynamic pressures measured for the latter pressure ratio. It revealed several important features. The curves for the central rakes (2,3,5,6) had a very particular shape, similar to a rounded M. Also noteworthy were the fairly small changes in pressure compared to the previous dynamic pressure plots for the co-rotating setup and especially the bare augmentor.

The total thrust, which clearly was the sum of local thrusts and which in turn were obtained as explained in Section 3.2.5., came to:

PR	pitot rake thrust	load cell thrust	difference
3.12	269.6N	288.9N	-6.7%
4.34	442.8N	437.5N	1.2%

Table VIII: Contra-rot. VVG pairs; Comparison of pitot and load cell thrust

The pitot rake values compared well with those interpolated from the load cell measurements. The pitot rake thrusts under-read by approximately four percent. Under-reading implied that some of the momentum was failed to be picked up by the rake assembly. This deficiency must have been caused by either missing the high spots and over-emphasising the low pressure areas or by leakage of some of the pressure within the measuring apparatus. As was explained in Section 3.3. dealing with the errors, a lot of care was taken to minimize the errors on the data acquisition system. One assumption was made which strictly was inaccurate, namely using the incompressible Bernoulli's equation to determine the dynamic pressures (N.B. the local thrust per unit area is equal to twice the dynamic pressure). For Mach numbers up to 0.3 this assumption is not bad at all because the difference between the incompressible and fully expanded compressible expression amounts to 0.1 percent only. Even up to a Mach No. of 0.5 is the discrepancy rather small, less than 1%. Since the Mach numbers in the diffuser exit plane did not rise much beyond this value, the aggregate error must be quite small. It was more likely that the reduced pressure measurements were caused by the swirl in the flow initiated by the generation of vortices. Since the vortices had a considerable transverse velocity component a pressure gradient

developed across the exit plane, making the assumption of having static pressure equal to atmospheric throughout invalid.

5.3.) MODIFIED AUGMENTOR WITH AIR JET VORTEX GENERATORS

5.3.1.) GENERAL COMMENTS ON CONTOUR PLOTS:

There are certain features appearing in all the contour plots, Figures 5.7 to 5.41, and should therefore be explained at this point. The solid circle with a radius of 91.8 mm represents the boundary, i.e. the solid wall of the diffuser exit. The eight dashes equi-spaced at 45 degree intervals outside of the circle indicate the positions of the air jet vortex generator (AJVG) injection points.

For simplified reference purposes the following convention will be used for locating certain areas on the contour plots: an imaginary line should be drawn through the centre of the circular exit plane. Where the line intersects the right hand side ($r_{\text{exit}} = R_c$) the datum is assumed. Going around the perimeter in an anti-clockwise sense determines the reference angle, i.e. the top is situated at 90°, the left hand side at 180° and the bottom at 270°. Coming back to the datum closes the circle and is equal to 360°. For further convenience the circle is split into four quadrants; the first being the first 90°, the second being between 90° and 180° and so on.

The air jets will also be numbered in the case an individual jet needs to be specified. Following the above convention of moving around the perimeter in an anti-clockwise sense, No.1 jet is positioned at 22.5°, jet No.2 is located at 67.5°, jet No.3 at 112.5° and the others follow in 45 degree increments.

All contour plots required that the no-slip condition was satisfied at the boundary, i.e. at the perimeter of the plots which represented the wall of the diffuser. This meant that the dynamic pressure at the wall was equal to zero. Away from it a steep dynamic pressure gradient was present. These closely spaced contour lines were not plotted because their individual shapes could not be determined from the pitot probe measurements. It can be assumed, nevertheless, that they were in very close proximity to the boundary. The exit plane was approximately 560mm downstream of the injection points. To make a prediction for the displacement thickness of the boundary layer in the region where the vortices were present would have been exceedingly difficult. It was known that the displacement thickness was very considerably reduced underneath the cores of the vortex sheet, well below the value for a two-dimensional flow over a flat plate, but rose fairly sharply away from the vortex sheet.

If the boundary layer growth in the inlet, the bell-mouth, was considered it became clear that the determination of the displacement thickness using the assumption that laminar flow was present led to:

$$\frac{\delta^*}{x} \approx \frac{1.72}{\sqrt{Re_x}} \quad \text{--- (5.1)}$$

(this is the displacement thickness parameter describing the distance from the surface to the points where the effective modified shape due to the presence of the boundary layer forms)

The displacement thickness on a flat plate of equivalent length as along the surface of the bell-mouth would have grown to less than half a millimetre. Since there existed a favourable pressure gradient along the surface the thickness grew even less than on a flat plate, i.e. the effective duct diameter was reduced by less than a millimetre.

It is important to realise that each pressure contour plot was obtained from two pressure versus distance plots. The orthogonal co-ordinate system (x,y) , and accordingly the respective distances, was chosen such that the axes aligned with the rakes. The centre of the co-ordinate system represented the centre of the diffuser exit plane (this point coincided with pitot probe no. 23). Since the layout of the rakes was on a square grid the tubes were equi-spaced and separated by 24mm. As shown in Section 3.2.5. the 45 pitot tubes were distributed into seven rakes. The outer ones consisted of 5 and the inner ones of 7 probes. When the rig was run pressure readings were recorded at all 45 points of the grid, i.e. at points like $(-72\text{mm}, -24\text{mm})$ or $(48\text{mm}, -48\text{mm})$ as examples. The recorded pressure values were then plotted at constant y -distance values $(-72\text{mm}, -48\text{mm}, -24\text{mm}, 0\text{mm}, 24\text{mm}, 48\text{mm}, 72\text{mm})$ against distance x . The five or seven values of any one rake were then joined by smooth lines, because it was known that there could be no sudden jumps in pressure. This limited amount of data clearly needed to be borne in mind when processing the raw data further. Most of the points on any one rake were joined by curves, which were functions of polynomials of degree four. Several of these representations did not join the points appropriately in some places and were modified by hand using French curves. In order to gain more information the co-ordinate system was then rotated by 90 degrees, i.e. plotting pressure values versus distance y at constant x -distance values. A lot of care was taken to match the pressure values with the correct (x,y) locations. It became clear quickly that the greatest changes occurred towards the perimeter of the plane. Due to the scarcity of information here it had to be concluded that the degree of confidence was rather poor for constant pressure lines lying in between the range:

$0.8 R_c < r_{\text{exit}} < 1.0 R_c$, where r_{exit} is defined as a fraction of the exit plane radius R_c , i.e. $r_{\text{exit}} = 0$ at the centre and $r_{\text{exit}} = R_c$ at the perimeter boundary. This proved very unfortunate because the vortices seemed to have a significant effect in this area, particularly for the co-rotating arrangement. The author, however, believes strongly that special features appeared in that somewhat uncertain area, which were 'real' and will be discussed in the individual sections later. For r_{exit} less than $0.8 R_c$ it was believed that the lines joining the points were accurate to a fairly high degree. The smoothness of the lines joining the points probably did not quite represent the real picture, but it was thought to be a detail of less importance. For most plots the high pressure areas (peaks) and the low pressure areas (troughs) illustrated very nicely. This fact gave a lot of confidence in the understanding of the formation of vortices.

As mentioned above, the pitot measurements were taken at a distance of over half a metre downstream of the injection points. Using the knowledge on vortex formation, as described extensively by Pearcey^[7] it was deduced that the vortices produced by the air jets must have diffused and hence gained in cross-sectional area. This fact signified that despite the large spacing of the probes it was possible to track down the likely positions of the vortices.

5.3.2.) CO-ROTATING VORTICES:

There are two test series which revealed most about the formation of vortices produced by the eight individual AJVG plugs. The particular features and characteristics were demonstrated by looking:

- a) at the change in the shape of the constant contour pressure lines with varying skew angle β at similar air jet (AJ) driving pressures and
- b) at the change in the shape of the constant non-dimensionalised contour pressure lines with fixed skew angle β but with varying air jet driving pressures.

For the former case it was decided that a pressure ratio of 3.0 was desirable as a representative case but it turned out that the actual experimental AJ pressures ranged from a PR of 2.74 to 3.05 which accounted for a change of approx. 11 percent between the minimum and the maximum value. This variation in PR needed to be kept in mind but was not thought to cause excessive distortion for comparison purposes. The pressures in the exit plane were directly related to the AJ driving pressure and therefore have the same relative change as above. The skew

angle was gradually raised in 15 degree steps, including zero degrees (which, strictly viewed, should not be included because the sense of rotation was not co-rotating but formed an important base to make comparison with) up to 60 degrees. The corresponding contour plots are shown in Figs. 5.7 to 5.12. Test results for the 75 degree case (Fig. 5.12) were obtained but these should be considered with great care because of the excessive amount of swirl. The swirling motion had a large transverse velocity component, falsifying the pitot probe readings as mentioned in Section 3.3. "EXPERIMENTAL ERRORS". The readings obtained were wrong due to the flow reversal in the middle of the exit plane, i.e. the pitot probes were pointing the wrong way to get a valid reading. The central area with its flow reversal was analogous to flow past a solid cylinder with the plane of reference at the backward facing side of the cylinder. After some discussion it was decided that this particular distribution of dynamic pressure might have been caused by the phenomenon of vortex breakdown.

Returning to the more relevant contour plots the following statement was true; the dynamic pressure in the middle of the test plane was lower than the average and then increased above the average towards the perimeter up to approximately $r_{\text{exit}} = 0.7$ to $0.85 R_c$ and thereafter started to drop again. In column 3 of Table IX the average dynamic pressure values are listed, which are directly proportional to the pitot rake total thrusts by multiplying them by two and 45 times the unit squares of 24mm^2 and then normalizing it to standard atmospheric conditions.

The values for the load cell thrusts in the fifth column were interpolated from the data curves obtained in Section 4.3.1. above. The last column represents the difference between the pitot rake and the load cell thrust. The values are all negative and therefore imply that the pitot rake assembly failed to 'capture' all the dynamic pressure. For angles up to 45° the difference is quite small, but as the jets are skewed to 60° it has increased to more than 10%. A probable cause for the reduced pitot reading is the swirling motion of the jets.

Angle β	PR_{AJ}	average dynamic pressure (N/m^2)	pitot rake total thrust (N)	load cell total thrust (N)	percentage difference (%)
0°	2.74	4608.1	235.4	241.2	-2.4
15°	2.98	4842.2	247.1	250.0	-1.2
30°	2.89	4172.8	213.4	213.7	-0.1
45°	2.84	3436.5	175.6	188.5	-6.8
60°	3.05	2728.9	140.6	158.0	-11.0

Table IX: Co-rot. AJVGs; Comparison of pitot and load cell thrust, air jet only blowing, varying air jet skew angle

The second series of tests were performed at a fixed skew angle of 30 degrees and the pressure ratios looked at included 2.22, 2.89, 3.64 and 4.33. In order to obtain a simple basis for comparison between the various plots it was necessary to non-dimensionalise the pressure. This was done by dividing each individual pressure by the average, where the average was the sum of the pressures from each port divided by the total number of ports. The other possibility would have been to non-dimensionalise on the driving pressure ratio. The skew angle of 30 degrees was chosen because at this angle the loss in axial momentum amounted to only about 13 percent and it was known that a single discrete vortex was forming (see Ref. ^[7] for details on vortex strength and its formation). Since there was no peripheral blowing for this test series all the primary momentum came from the air jets and therefore the loss in axial momentum was an important factor reducing the axial total thrust.

Considering the low pressure ratio case first, Fig. 5.13, with $PR = 2.22$, showed an unambiguous pressure distribution, that is a low pressure area of less than half the dynamic average in the middle and then increasing pressure towards the edge of the exit plane. For exit radii approximately greater than $0.65 R_c$ the pressure rose to values which were larger than the average. Note the two concentrations of high pressure spots at the left and the right. These were probably a consequence of the high momentum primary co-rotating vortices. They follow the known behaviour that they remain in the spatial vicinity of their origin, i.e. the distance of the vortex core to the solid surface remained fairly constant. A slight movement towards the central axis did occur due to the differential in pressure. Due to the mirror image of the individual vortex a net movement along the circular perimeter

opposing the direction of rotation was present. This movement could not specifically be monitored but is a consequence of the vortex / image pair. By the time the vortices have reached the exit plane, where the measurements have been taken, some interaction and diffusion has happened and therefore the precise structure of the individual vortices cannot be determined. The limited number of probes certainly did not allow this kind of detail to be extracted from the measurements.

In proximity of the perimeter the dynamic pressure dropped off to satisfy the no-slip condition at the wall. As stated in Section 5.3.1. above the level of confidence of joining the constant pressure points was not high for the area where the exit radius was greater than $0.8 R_c$. Approximations which were thought to represent the actual picture were applied. In many cases the plots of pressure versus distance displayed peak pressures close to the edges of the grid and then the pressure fell off right at the edge; N.B. the distance grid was defined by the pitot rake arrangement.

As the pressure was increased, Figs. 5.14 to 5.16, it was noted that the pressure distribution within the exit plane became more balanced. This meant a reduction in the deviation away from the average. For the highest AJ driving pressure ratio of 4.33, the low pressure spots were not much less than 0.75 of the average and the high areas did not rise much beyond 1.25 times the average. The uniform pressure distribution would have been a good 'platform' to start an increase of semi-angle for the diffuser. The plot for the high driving pressure implied that the vortices were reliable in forcing proper mixing between the primary and the secondary air flow. Noteworthy were the formation of low and high pressure spots around the perimeter in an alternating fashion. On the right hand side of the plot the low spots are not that clear but the area in between the high pressure areas are less than average. It was believed that these spots were generated by the vortices which themselves became more pronounced as the driving pressure was increased.

The measurements of case a) above were repeated with the addition of peripheral blowing. It was aimed to have a pressure ratio of 2.5 throughout the test series. During testing the peripheral blowing varied between 2.5 and 2.53 which represented a change of around one percent only. Again it was aimed to test the air jets at a pressure ratio of 3.0 but it actually varied between 2.72 and 3.12. This range was rather large because it proved quite difficult to control the two control valves, regulating the supply pressure to the two primaries. Since these control mechanisms were simple mechanical ball valves, the degree of control was quite limited. Care was taken to regulate the peripheral air supply close to the requirement and then try to match

the air jet supply pressure. Opening or closing one valve immediately influenced the mass flow rate of the other supply because both were fed from the same reservoir. With more experience on the system one probably could have achieved a narrower pressure band, but this would have caused a much extended testing programme.

Looking at the contour plots, Figs. 5.17 to 5.22, revealed very similar behaviours to the cases without peripheral blowing. The lowest dynamic pressures were measured in the centre for all angles of skew and then increasing pressures towards the perimeter were recorded, extending to approximately $r_{\text{exit}} = 0.85 R_e$. For larger exit radii the dynamic pressures started reducing. It was concluded that the transfer of momentum towards the centre was not promoted strongly by the vortices. The cause for this behaviour must lie with the formation of co-rotating vortices, which, as discussed earlier, remain close to their spatial origin as they travel downstream.

Particularly when the jets were skewed to 15° did the pressure contour lines form near perfect concentric circles and this despite of the imperfections of the supply system. This led to the conclusion that the vortices formed were very stable and therefore established the well ordered pattern. For angles up to 60 degrees was it especially noteworthy to observe the pattern of fairly clear concentric circles. From Freestone's ^[16] measurements on vortex strength it was known that the strength parameter maximizes at around 60 degrees. Despite the strong vortices it was not possible to identify the eight individual vortices on the plot. It can be assumed fairly safely that the vortices have interacted with each other by the time they reached the reference plane.

In Table X below there is a list of the average dynamic pressures, which are important to indicate the areas below and above the average. In order to obtain high augmentations it proved essential to get equal dynamic pressures throughout the exit plane, i.e. ideal mixing.

Angle β	PR _{AJ}	PR _{pe}	average dynamic pressure (N/m ²)	pitot rake total T (N)	load cell total T (N)	percent diff.
0°	2.72	2.53	7774.2	396.8	400.0	-0.8
15°	2.88	2.50	7848.7	400.2	416.6	-3.9
30°	2.77	2.50	6965.1	365.2	378.4	-3.5
45°	3.08	2.52	6912.4	358.3	359.2	-0.2
60°	3.12	2.53	6226.0	320.9	316.8	1.3
75°	3.10	2.51	4666.9	241.7	253.1	-4.5

Table X: Co-rot. AJVGs; Comparison of pitot and load cell thrust, combined peripheral and air jet blowing varying air jet skew angle

The load cell thrusts were again determined from Table III above, interpolating for the required air jet PRs assuming a pressure ratio of 2.5 for the peripheral nozzle. The discrepancy of one per cent for the peripheral jet was thought small enough to make this interpolation process valid.

A comparison of the pitot and load cell thrusts again showed very good agreement, a measure of which is illustrated in the seventh column. It clearly seems that the swirling motion of the air jets are damped by the peripheral jet, therefore giving good agreement even for the 75° case. Due to the addition of the peripheral jet the average dynamic pressures are considerably higher than for those cases where the air jets were blowing on their own. At a skew angle of 15 degrees the average dynamic pressure nearly reached 8 kPa. As the air jets were skewed to large angles the loss in axial momentum rose markedly with the average pressure at 75° reducing to the region of 1/2 of the no-skew arrangement. One particular feature developed looking at the various skew angle settings, namely that for $r_{exit} \leq 0.6 R_c$ the dynamic pressure is less than average and for most of the area $r_{exit} > 0.6 R_c$ it is larger than average.

5.3.3.) CONTRA-ROTATING VORTICES:

As for the co-rotating vortex data immediately above the same basic combinations of pressure ratio and skew angle were selected, i.e. the same testing arrangements as explained in items 5.3.2a) and b) were used. The cases with constant air jet driving pressure ratio of 3.0 were performed at four skew angle settings: 0°, 15°, 30° and 60°. From

the measurements taken above it was known that for the 75 degree case the interaction of the individual jets was rather adverse and therefore not worthwhile investigating. The 45 degree case on the other hand was not thought to represent a special unknown feature. One more remark about the 0° skew angle setting; again this strictly speaking should not be included for this specific set of results, although it was known that a jet with the given cross-sectional area would form two discrete vortices from each end of the slot. These two vortices were turning in opposite directions. In Figure 5.36 the likely flow leaving the air jet vortex generator slot is sketched. From measurements by other researchers in this field using a Conrad yaw-meter a flow behaviour as illustrated was observed. It was also established that the two vortices produced were rather weak. The net effect was, if the individual vortex strength was sufficiently strong, a teaming up of one vortex from one side of the air jet plug with the vortex of the other edge of the AJ plug to form a pair. Hence when the air jets were blowing without any skew they fell into the category of forming twice the number of contra-rotating vortex pairs compared to the tests where the jets were skewed. The zero degree setting was repeated to give a comparison to a previously investigated case. Consequently, some insight and understanding of the instability of the vortices and hence the pressure distribution in the exit plane was obtained.

The contour plots corresponding to the four skew angles are presented in Figures 5.23 to 5.26. Looking at these Figures one feature immediately became obvious; as the jets were skewed the dynamic pressure around the centre became high. This implied that there was suddenly a powerful mechanism to transfer momentum from the peripheral layout of the jets towards the axial centre. It was known that contra-rotating vortices have a tendency to move closer in pairs and then move away from the surface but it was not anticipated to occur to such a strong degree. These results were greeted with extreme satisfaction, but at the same time required thorough investigation. For the 15° case (Fig. 5.24) the uniform dynamic pressure distribution was particularly noteworthy, as $\frac{3}{4}$ of the exit area was covered by the average pressure contour line, represented by the 5 kPa curve. Four closed areas in near proximity to the perimeter, where the pressure is less than average, seemed to have developed at 90 degree intervals. The fourth area which is probably located at around 45 degrees in the reference system was not explicitly picked up by the pitot measurements but is anticipated to be there.

As the jets were skewed to 30 degrees the individual vortex strengths increased enormously hence producing the clear picture shown in Figure 5.25. The four low dynamic pressure areas are now easily detected again at 90° intervals.

In Table XI additional information on the average dynamic pressures recorded in the reference plane and the thrusts measured are listed.

Angle β	PR_{AJ}	average dynamic pressure (N/m ²)	pitot rake total thrust (N)	load cell total thrust (N)	percentage difference (%)
0°	3.07	5046.0	259.0	269.3	-3.6
15°	3.18	4902.4	252.0	269.3	-6.4
30°	2.96	4014.9	206.3	220.8	-6.6
60°	3.09	2268.6	116.7	119.6	-2.4

Table XI: Contra-rot. AJVG pairs; Comparison of pitot and load cell thrust, air jets blowing only;
varying air jet skew angle

Further experimental tests were performed looking at non-dimensional pressure contour lines for the case of varying air jet driving pressure ratios but constant angles of skew β . The skew angle was set to 30 degrees at the beginning of the test series and then remained unaltered throughout. This particular angle was selected rather arbitrarily, the idea was to show and give an understanding on how the AJ pressure ratio affected the vortex formation and hence the pressure distribution in the exit plane. Five tests were performed to see what the effect of driving pressure was. The pressure ratios considered included 2.37, 2.96, 3.61, 4.14 and 4.66. The corresponding contour plots are presented in Figures 5.27 to 5.31. Beginning from the low pressure end the contour pattern was extremely clear, namely a fairly large high pressure spot in the middle and four discrete low pressure areas interspaced at 90 degree intervals. The centres of the low pressure areas were at large exit radii, roughly $r_{exit} = 0.9 R_c$, i.e. very close to the perimeter. As the pressure ratio was increased these features still persisted but the strength of the vortices was so great that the vortex pairs started to interact in the centre degenerating some of the axial momentum. For the largest pressure ratio plot (4.66) it seemed that high momentum 'bubbles' separated from the core and moved towards the perimeter in between the low pressure spots.

Similar to the test series performed for the co-rotating setup was the change in skew angle at constant air jet PR and including peripheral blowing repeated. The contour plots for these tests are shown in Figures 5.32 to 5.35. Some additional information is given in Table XII. Again the peripheral pressure ratio was kept fairly constant

at 2.5 varying by just over one per cent only. The air jet pressure ratio ranged from 2.83 to 3.15 which represented a variation of \pm five per cent around the target pressure ratio of 3.0.

Angle β	PR_{AJ}	PR_{pe}	average dynamic pressure (N/m^2)	pitot rake total T (N)	load cell total T (N)	percent diff. (%)
0°	3.00	2.54	8154.2	419.4	423.0	-0.9
15°	3.15	2.54	7914.2	410.3	432.1	-5.0
30°	2.83	2.53	7295.6	374.9	383.1	-2.1
60°	2.99	2.51	5563.7	286.7	279.5	2.6

Table XII: Contra-rot. AJVG pairs; Comparison of pitot and load cell thrusts, combined peripheral and air jet blowing

6.) COMPARISON OF VARIOUS CONFIGURATIONS

6.1.) Comments on vane vortex generators:

The formation of vortices was a central feature of this piece of research. A partial inclusion of the likely vortex pattern as found by other research teams is therefore included. Küchemann ^[18] suggested that there are planforms which produce acceptable and stable arrangements of non-planar vortex sheets. Without specifying the Reynolds No. explicitly he mentioned the applicability of vortex formation on wings in sub- and supersonic streams. The vortices are established by forcing a leading edge separation, using an aerodynamically sharp leading edge, near the root of a wing. The effective vortex pattern are as illustrated in Figs. 6.1a and 6.1b (taken from Küchemann), where the former refers to a tapered wing with relatively small sweep and the later to a slender delta wing. The vanes used during the testing of the rig performance were a combination of a tapered and a slender delta type wing.

The classical ESDU ^[19] references gave a more detailed approach to the investigation of vortex formation in the transonic speed regime. This reference also dealt to some extent with the calculation of the normal force and of the drag related to lift. The data in the transonic regime was particularly useful because the vanes were operated at this speed. In Figure 6.2, taken from Hall and Rogers ^[20], a crude illustration of the development of the vortex formation for Mach numbers of 0.6, 0.85 and 0.95 can be observed as the angle of attack was raised. The aspect ratio for the wing considered was higher than for the vanes but the principal mechanism was similar. Hall and Rogers also developed a carpet plot representing the lift curves for highly-swept low aspect ratio wing as function of M_∞ and C_L , shown in Fig. 6.3.

Another ESDU ^[21] reference was consulted in order to determine the lift curve slope of the vanes. Several parameters were determined by the choice of the vane planform. One vital assumption also had to be made to evaluate an estimate for the slope, namely that the vanes operated in a flow regime of a Mach number of 0.8. This figure for the Mach no. was estimated, using jet theory as described by Abramovich ^[22], by considering the distance between the peripheral injection and the position of the vanes. If the suggested core region of 12 peripheral slot widths was assumed and knowing that the vanes were

located about 45 slot widths downstream of the injection point, at which point the local Mach number has fallen to approximately 50 per cent of the fully expanded Mach number. This effectively meant that the peripheral jet was driven with a pressure ratio of just over four in order to obtain a Mach no. of 0.8 near the vanes. Without Schlieren pictures taken near the injection point it was impossible, qualitatively at least, to make a prediction of how the flow behaved as it left the slot. For pressure ratios higher than the critical, shock cells were likely to form, modifying the flow to an unknown extent. However, the following relationships emerged making some unconsolidated assumptions, with:

taper ratio $\lambda = 0.594$, aspect ratio $AR = 0.588$

assume $M_\infty = 0.8 \Rightarrow \beta AR = 0.353$, where $\beta = \text{SQRT}(1 - M_\infty^2)$

from the carpet plot for the normal force curve slope it was interpolated using the geometric and flow parameters:

$$\frac{1}{AR} \left[\frac{dC_N}{d\alpha} \right] = 1.99 \text{ (rad}^{-1}\text{)}$$

$$\text{or} \quad \frac{dC_N}{d\alpha} = 0.02063 \text{ (degree}^{-1}\text{)} \quad \text{--- (6.1)}$$

From equation (6.1) it became clear that the normal force curve slope was rather small for a cropped delta type wing operating in a high speed environment.

Since the major component of lift for highly swept cropped delta wings was contributed by the formation of vortices on the upper side of the wing, the lifting surface became insensitive to the conventional stall characteristics of an aerofoil. Researchers have found that the normal force curve slope for delta wings extended fairly linearly up to incidences of 40 degrees and more. In Küchemann's book a Figure, which was taken from Earnshaw and Lawford, shows the lift coefficient versus incidence α for a slender delta wing. This Figure (6.4) also illustrates the lift coefficient for a swept wing. It is noteworthy that the conventional swept wing reaches a maximum lift at an incidence of 20 degrees less than that for the slender wing. The explanation for this behaviour must lie in the three-dimensionality of the vortices forming along the leading edge of the slender wing. The interaction of the vortices with the free stream causes extensive mixing which allows the wing to sustain greater adverse pressure gradients.

Having established this general behaviour for slender wings the question that arose was why the augmentation peaked at a low incidence of around 16 degrees (Figs. 4.3 and 4.4) for the co- and contra-rotating vanes. The answer must be related to the phenomenon

accompanying the generation of lift, namely the corresponding drag penalty of the vanes. There were two main components of drag, the profile and the induced drag.

Another ESDU ^[23] data item was consulted in order to establish the drag associated with the vane vortex generators. From that reference the following lift-dependent drag factor was extracted:

$$C_{D_{\text{vortex}}} = \frac{1 + \delta}{\pi AR} C_L^2$$

where $1 + \delta$ is known as the lift-dependent drag factor and turned out to be equal to 1.002 for the given vane wing shape. The total drag of the vanes was the given lift-dependent drag (induced drag) plus the lift independent drag, i.e. C_{D_0} .

It was believed that the ratio of lift to drag must maximize at an incidence of 16 degrees. This also translated as the best ratio of vortex strength to drag penalty. For greater vane angles the mixing might still be increased but the drag rises more rapidly. The combination of the profile and induced drag overshadow the beneficial mixing effect. The minima (Figs. 4.3 and 4.4) at 14° possibly were caused by local separation bubbles which re-attached.

6.2.) Co-rotating versus Contra-rotating:

6.2.1.) Vane vortex generators:

There was a very important addition to the previous co- and contra-rotating data acquired (Section 4.2.1. and 4.2.2.), namely the adoption of larger span vanes, as described in Section 3.1.5. of this thesis. The data is not explicitly plotted anywhere but is assembled in one combined plot. Particular features of the different size vanes are commented upon below.

The summary of the augmentation performance data at a pressure ratio of 5.0 is shown in Figure 6.5. It should be noted that the data points were interpolated from the load cell plots, using a best fit linear curve, i.e. a least squares fit. The augmentation ratio for the bare nozzle thrust is unity because it forms the reference against which all ratios are evaluated. Next, the augmentation for the basic ejector diffuser arrangement without any flow modification is shown. Its value comes to approximately 15 percent above the bare nozzle thrust. Then the plot shows the cluster of data obtained for the co-rotating and contra-rotating VVG configurations. To make the plot easier to interpret both the 7.5mm and 12mm vane data is represented. For

clarification only four readings near the maxima are shown for any one configuration. A general trend can be observed, namely as the vane span was increased the augmentation remained similar in magnitude but the position of the peak shifted to a lower angle of attack. This is somewhat surprising because it can be deduced from vortex theory that to the first approximation the vortex strength is proportional to the vane chord and independent of the vane span. However, the increased span does extend further into the flow field and thereby changes the position of the trailing vortex. It can be argued that for larger span vanes the mixing is improved because the vortices are nearer to the central axis of the nozzle but this is offset by the increased drag because of the greater area. This demonstrates the conflicting effects of beneficial vortex induced mixing and adverse drag. Both increase with increasing angle of incidence but at different rates. The vortex induced mixing is a linear function with incidence and the drag rises as a function of incidence squared. The net effect has a maximum at some incidence α . Now, as the span is increased the curves for the vortex induced mixing and the drag will have steeper slopes and therefore the maximum will occur at a lower α . As the incidence is raised the drag penalty becomes dominant, i.e. the performance of the augmentor reduces after having reached a peak. To determine this peak position proved to be difficult to evaluate with the test means available. It may be argued that the peaks are not even that important, but the mean thrust augmentation levels within a certain angle of incidence range are the really determining factor. It is believed that due to the inaccuracy, produced by experimental errors, of the test method the data points have fair sized error bands of approximately ± 1 per cent. It would require many more tests to check repeatability and therefore allow higher accuracy.

Figure 6.5 shows clearly that an augmentation of thirty percent is possible with the full length diffuser and VVG's installed. A lot of doubt was associated with the feasibility of such a layout. As far as was known there had not yet been any approach towards augmentors using VVG's. Having this fact in mind the enhancement so far obtained was extremely encouraging. A further novelty was the inclusion of air jet vortex generators instead of vane vortex generators. It was known that these devices also produce vortices of different strength by arranging them in certain ways. At the same time it was anticipated that they increase the augmentation by more efficient mixing, and considerably reducing the adverse drag penalty. The air jets also produce drag but it was believed that their magnitude was smaller than that produced by the solid vanes. Certainly the loss due to form drag was eliminated by using AJVGs. A thorough investigation and comparison of the vane and air jet VGs is given later on.

The augmentations obtained could probably be increased using VVG's, but it was doubted that more than 35% was realistic with the present rig. However, there were still several parameters which could be optimized:

- a) nozzle over inlet area ratio m
- b) diffuser area ratio n
- c) injection angle of the primary air
- d) distance from nozzle to vortex generators
- e) axial length of various components
- f) improve uniformity of injection through primary nozzle
- g) vane vortex generator shape and size

Some of the parameters stated here would have required extensive modifications to the rig, but what certainly could have been exploited was a change of the vortex generator shape and size. If the project had been limited to using solid vanes this clearly would have been of very high priority. The VVG's were however a preliminary stage, used as a comparative data base to the future tests with air jet vortex generators installed.

Looking again at the dynamic pressure plots (Figs. 5.1, 5.3 and 5.5) a simpler comparison between the various configurations can be made by reprocessing the data to form constant pressure contour plots. These are given in Figures 5.2, 5.4 and 5.6 corresponding to the bare augmentor, the co-rotating setup and the contra-rotating configuration respectively. It should be remembered that the contour plots with the vanes installed were obtained near their respective optimum angles. Another important fact that should be noted is that the curves joining the rather scarce data points were by no means unique. Nevertheless it was thought that the representation up to 70 per cent of the exit radius was very good, only towards the perimeter did the confidence reduce. The contour plots were representations looking upstream on to the diffuser exit plane.

The contour plot for the basic augmentor can probably most easily be explained. If the injection of the primary air would be perfect the constant pressure lines would be concentric circles. The real image, however, was entirely different; the four 'lobes' were a consequence of the non-uniform pressure within the primary nozzle reservoir. This must have been caused by the fact that the cross-sectional area was too small to expand and hence to slow down the flow sufficiently, i.e. near the air supply tubes the driving pressure was greater than elsewhere. This condition could have been remedied by increasing the reservoir size but that would have meant a considerable modification to the rig nozzle causing serious delay. Doubling the supply tubes would have been another possibility to minimize the problem but was rejected for the

same reason as before.

Considering the bare augmentor contour plot (Fig. 5.2) in more detail a very limited amount of mixing between the primary and secondary air was observed, implying that the mixing section was too short. The insufficient mixing was deduced from the large differences in pressure between the outer and the central area. The high dynamic pressures within the outer area band implied poor momentum transfer from the peripheral wall jet towards the central axis. If it would not have been so labour intensive to manufacture a longer section, it could have proven very interesting to find the maximum performance of the simple peripheral ejector nozzle arrangement. This could then be judged against the data obtained by, for example, Miller^[9] at Bath University or those results established at the National Aeronautics and Space Administration^[4] or the USAF Institute of Technology^[6] research institutes.

When comparing the constant pressure plot for the co-rotating with the bare augmentor it became immediately apparent that the low dynamic pressure area (e.g. 4 kPa curve) had reduced considerably. This fact was a clear indication that the mixing between the primary and secondary flow had been enhanced. It probably can be deduced that, with co-rotating vortices present, the smaller the central low pressure area the greater the net thrust of the device. Furthermore, the basic structure with the four high pressure areas was still present. What had changed was a shift of those areas towards the centre of the diffuser exit. The explanation for this lay in the formation of the co-rotating vortices. From past investigations on vortices it was established that the leading edge roll-up and the tip vortex combine as the air stream flowed across the vane. As the combined vortex travels along in the streamwise direction it remains at the same distance from the boundary as where it originates because there is no net force causing any shift away from the surface. This occurrence can be proven by vortex theory as for example was done by Milne-Thomson^[23].

The vortices cause high axial momentum primary air to move away from the surface and then scoop lesser axial momentum secondary air back into the primary flow. This continuous process forced a momentum transfer in a radial direction. The vortices were displaced circumferentially by the velocities induced by the images which were located on the other side of the boundary at a slightly larger distance than the vortex cores. For the present arrangement where the vortices were located inside a circular boundary the product of the distance from the centre to the vortex core (X_1) times the distance from the centre to the core of the image (X_2) is equal to R squared, i.e.

$$X_1 * X_2 = R^2,$$

where R is the distance from the centre to the boundary. This

effectively meant that if the distance between the vortex core and the boundary was small compared to R then the distances of the vortex core and the image core to the boundary were nearly equal. As a vortex core would potentially move towards the middle the image would shoot off to infinity. When resolving the induced velocities into components showed a net lateral movement in the direction of the vortex core roll-up at the surface, i.e. for the present case in Figure 5.4 in a clockwise sense. This means that vortices travel in the opposite direction when compared to mechanical wheels. With the understanding of this concept the position of the high pressure spots became rather clearer.

Considering the contra-rotating configuration in the same light as discussed just above, i.e. looking again at the vortices and their images, the position of the high pressure areas again can be justified. Two vortices whose cores turn away from the solid surface form one pair. The circumferential position of the high pressure areas coincided with the mid-position between two VVG pairs. This was as expected because the net effect of the induced velocities was the introduction of a substantial component directed towards the centre of the diffuser. The pressure plot suggested that any two of the trailing vortices closest to the high pressure points have moved closer together and towards the centre under their own mutually induced velocities as they travelled along in the streamwise direction. For an extensive investigation into the flow pattern in the exit plane a yaw meter like a Conrad tube could be used. The contra-rotating constant pressure lines have the most uniform distribution of pressure of the three contour plots. This suggested that this configuration gave the most thorough mixing between the primary and the secondary flow. The two kPa contour has disappeared completely and the 4 kPa curve has receded to a fairly small central area. Since the vortex cores of any one pair moved towards the axial centre the redistribution of high momentum was more thorough than for the single co-rotating vortices, hence the better overall performance of the contra-rotating set-up.

Finally, different diffuser area ratios were tested. In Figure 6.6 the results for an area ratio of 1.0, 1.3, 1.4 and 1.5 for the co- and contra-rotating case are shown. Unfortunately, the contra-rotating configuration was not tested at the optimum angle hence the lower values of augmentations for that case. The plot conveyed that the diffuser did work quite well. The shape of the curves suggested an asymptotic approach to a maximum value, which would probably occur for a somewhat higher area ratio than 1.5. After this maximum the augmentation would start decreasing because the diffuser drag would increase faster than the beneficial enhanced mixing.

A last word about the calculation of the augmentation ratios. The peripheral bare nozzle thrust was evaluated using the theoretical

formula for a convergent nozzle flow, taking account of the momentum and pressure thrust. An experimental testing, by blanking of the secondary inlet and installing static pressure tappings to monitor the base pressure, was thought of but was rejected because of the modifications involved. Furthermore, the uncertainty of its validity was the stronger reason for its rejection. The closest to a bare nozzle thrust test was achieved by removing the mixing section, the diffuser sections and the bell-mouth. At a primary pressure ratio of five the thrust for the peripheral nozzle (there was of course still some secondary entrainment) came to 98.4 percent of the theoretical value. Since this value was within the error band it can be assumed that the theory over-estimated the thrust but that the margin was not too large.

6.2.2.) Air jet vortex generators:

The overall picture with the air jets installed became more complicated than that for the vane vortex generators. This was mainly due to the extra momentum introduced via the air jets. There were two major arrangements which can conveniently be separated, namely the air jets blowing only and the combination of peripheral and air jet blowing. The former set-up can be regarded as a replacement peripheral jet immediately combined with a vortex generating facility. The latter was a repetition of an augmentor having a peripheral primary jet with the addition of vortex forming devices. The fact that the vortex forming devices were jets carrying some momentum in their own right clearly made matters more complex.

Starting from the direct comparison of co- and contra-rotating AJVGs without peripheral blowing using load cell measurements, Figures 4.9 and 4.15 illustrating augmentations for the two arrangements have to be looked at (In order to avoid any confusion at a later stage it should be noted that the term 'augmentation' as used here will be called 'scientific augmentation' in Section 6.4. The reason for changing the terminology will also be explained in that Section). Using the measured bare nozzle thrust, N.B. this was the thrust developed with the air jets blowing only, i.e. removing all the inlet and downstream sections, the augmentation ratios were established. A rather surprising discovery was made as the co-rotating jets were skewed to approximately 65 degrees. The augmentations reached higher levels, throughout the AJ driving pressure regime considered, than for the no skew case. This feature must have been caused by extensive mixing of the primary jet and the secondary air drawn in. From Freestone^[16] it was known that an air jet leaving a rectangular shaped nozzle produces the maximum vortex strength if skewed to around 60 degrees. It therefore

was deduced that these vortex cores generated the largest free shear layers in a three-dimensional field forcing a rapid convergence of axial momentum between the primary and the secondary air flow and hence enhanced mixing.

As the testing with the air jets went on it became more and more obvious that the jets could be used as aerodynamic devices to stir up the primary flow and thereby increase the mixing in a confined space as was present inside this augmentor. This in effect meant that the original proposal to use them as boundary layer control devices was revised and introduced another dimension. Air jets have been applied in other areas before, e.g. control of supersonic shock wave buffeting, but to the authors knowledge not as a means to produce exclusive primary momentum with the provision to augment the primary thrust. It can be and was argued that to use the jets as primary thrust generating devices is not that sensible because the jets need to be skewed to produce their maximum vortex strengths and the penalty for developing vortices is a definite reduction in available primary axial momentum. This led to an alternative path of thinking and will be discussed in Section 6.3.

Returning to Figs. 4.9 and 4.15 the augmentation plot for the contra-rotating arrangement showed a considerably different behaviour compared to the co-rotating one. The augmentations peak at around 10 degrees and fall off fairly steadily up to 50 degrees. Thereafter the curves started to drop away very quickly. They certainly suggested an augmentation of less than unity for the 90° skew case, which was somewhat surprising because the net thrust and the bare nozzle thrust both should be converging to zero. One possible explanation was the way in which the bare nozzle thrust had been measured. It was realised that the cosine relationship between the zero skew bare nozzle thrust and the skewed BNT was determined experimentally using the co-rotating arrangement. It was not repeated for the contra-rotating set-up, which might have produced different results due to the primary jet interactions. Since the testing of this condition was not possible at this stage of the project it needs to be realised that the results for the contra-rotating cases with large degrees of skew need to be interpreted with some caution. For skew angles less than 45° the interactions of the jets were of small magnitude because the opportunity for the jets to interact strongly occurred downstream of the parallel-walled working section, within which the air jets were mounted.

6.3.) Vane versus air jet vortex generators:

6.3.1.) General features using model and load cells:

One all important question that demanded an answer was how the air jets would compare with the solid vanes.

The determination of the augmentation ratios for the augmentor with the vanes included was fairly straight forward, N.B. the augmentations were obtained by dividing the measured total thrust by the measured or theoretical bare nozzle thrust (for the peripheral blowing only it was established that the experimentally measured BNT could be taken as equal to the theoretical ideal convergent BNT). The bare nozzle thrust was the thrust produced by the peripheral jet only for the vane tests but for the air jet vortex generator tests there were two possible combinations of BNT. First, the AJVGs could be blown on their own giving air jet bare nozzle thrust only or, secondly, primary air could be injected simultaneously through the air jets and through the peripheral slot.

From Section 4.1. and again from 5.1. we know that the bare augmentor generated an augmentation of around 19 per cent at a pressure ratio of 3.0. As the pressure ratio was increased the augmentation fell to approximately 15 per cent at a PR of 5.0. This reduction was not so surprising because from the theoretical simulation it was known that a universal feature appeared, namely as the pressure ratio rose the augmentation fell. This fact was easily proven theoretically using a physically modelled representation of the assembly. Assuming that the secondary inlet was choked, i.e. the uppermost ceiling for the augmentation, and a diffuser efficiency of 100 per cent the following expression resulted:

$$\Phi = \frac{0.81 M_e (1 + 0.2 M_e^2)^3}{(1.2679 PR - 1) m} \quad \text{--- (6.2)}$$

where:

$$M_e^2 = 5 \left[(PR m + (1 - m))^{\frac{2}{7}} - 1 \right]$$

m = primary inlet over duct area ratio

In equation (6.2) the diffuser area ratio (n) is a function of the exit Mach number. Plotting maximum augmentation ratio versus pressure ratio showed the behaviour of falling Φ with PR well (see Fig. 6.7). The ratio of m = 0.04 closely represented one of the parameters of the rig. The graph shows that an augmentation ratio of about 3.3 at a pressure ratio of 2.0 reduced to about 1.5 at a pressure ratio of 10.0.

For a real life application it was clearly impossible to choke the secondary for the condition when m was equal to 0.04 ($n = 2.5$) and the pressure ratio was as low as 2.0. The plot also reveals that with increasing inlet to duct area ratio (m) the respective maximum augmentations decreased.

The above results assumed a clearly unrealistic 100 per cent thorough mixing of the primary and the secondary air streams, i.e. uniform conditions across the diffuser exit plane were assumed. The primary flow is allowed to spread at its natural rate and mixes at the free shear layer due to turbulent eddies with the secondary air flow. All the axial momentum is conserved, i.e. the friction forces on the wall are neglected. During the process of mixing some of the mechanical energy is dissipated by the turbulence and appeared as heat. Physically it was clear that large free shear layer areas and turbulence were necessary to have any chance of rapid mixing. The differentials in static pressure between the primary and the secondary air flows were of course very beneficial. For this particular rig it meant a large proportion of total thrust was obtained from the bell-mouth.

The mixing of two streams is largely controlled by viscous interaction. In this case the fast speed primary air (the fully expanded Mach numbers for the jets are greater than unity for a pressure ratio greater than the critical PR) must mix with the low speed secondary air drawn in through the bell-mouth. From physical constraint considerations (a short augmentor was desired) it was necessary to obtain quick mixing between the two flows. The static pressure at the point of primary injection was largely controlled by the driving pressure ratio of the jets and the resulting degree of mixing, i.e. as the mixing increased the greater amount of secondary air was drawn in and the smaller the static pressure became. Two static pressure tappings in between the air jet injection slots recorded the pressure and showed static pressures of less than atmospheric but not near half the atmospheric pressure which would be reached as an upper limit when the secondary air stream was choked. The question that arose was how could it be possible to enhance mixing between the two flows. It was known that the peripheral jet behaved like a wall jet, i.e. the natural spreading semi-angle was not greater than approximately four degrees. This implied a fairly long cylindrically shaped mixing section, much longer than the one used for testing. The small spreading angle is a measure of the scale of turbulence acting at the shear layers. A rise in the mean level of turbulence was clearly the way forward to achieve better mixing. Associated with a higher level of turbulence as generated by the vanes for example was a loss in axial momentum due to drag forces. It was therefore extremely important to balance the beneficial enhancement due to mixing and the loss in axial momentum.

A convenient basis for simple comparison was the bare augmentor. This arrangement which consisted of the bell-mouth, the peripheral blowing, the parallel-walled mixing section and the diffuser produced a net thrust 19 per cent higher than the measured axial bare nozzle thrust at a pressure ratio of 3.0. The particular features of this layout were the large dynamic pressure differentials across the diffuser exit plane as monitored by the pitot rake measurements (illustrated in Figure 5.1). Close to the perimeter and especially near the four primary air feeder injection points the dynamic pressures were very high and then dropped off rapidly towards the central axis reaching nearly zero, i.e. nearly no axial flow was present at this central area.

The improvement due to co- and contra-rotating vortices caused by the solid vanes was considerable. At the respective optimum angles the net thrust measured came to 32% more than the measured bare nozzle thrust at the same pressure ratio of 3.0. The improvement of 32% was close to twice the benefit of the bare augmentor. This discovery led to the conclusion that the vortices 'stir up' the primary injected air, thereby increase the flow interaction and hence enhance the mixing between the two streams. The formation of the vortices was clearly caused by the vanes acting as aerofoil sections having fairly large angles of attack, therefore producing leading edge and tip vortices of considerable strength. The penalty for this formation were losses in axial momentum due to the associated drag of the cropped delta aerofoil sections. As the incidence of the wing sections was increased the drag rose accordingly. The induced drag was the major component of drag as the incidence was set to that angle where the optimum enhancement was reached, i.e. 16° for the co-rotating and 14° for the contra-rotating setup with the 7.5mm span vanes. The lift dependant drag rose as a function of the lift coefficient squared; the same as for conventional aerofoil sections.

The augmentation ratio of 1.32 was unfortunately still well below the desired target of a net thrust of 50 per cent on top of the bare nozzle thrust. From the pitot rake measurements it became quickly obvious that the mixing was still far from being good, represented by the large central area of low dynamic pressures. If a way could be found to fill that area it would mean more thorough mixing and hence a higher augmented bare nozzle thrust. For the contra-rotating VVG layout (Figure 5.6) a clear movement of the vortex pairs towards the centre can be observed. If stronger individual vortices could be produced they would move even more quickly towards the middle due to the increased induced velocities of them and their images. Against this grouping of high pressure areas was the establishment of lower pressure areas in between, i.e. the high momentum from the peripheral jet was concentrated into four individual areas without spreading evenly.

Directly comparable with the vane results were those tests where the air jets were blown on their own without the peripheral jet. The comparison was valid because the combined cross-sectional area of the eight air jets was similar to that of the peripheral slot, i.e. the mass flow rate through the two primaries was of similar size for equal driving pressures. The net cross-sectional area of the air jets was approximately 10% less than the peripheral slot. Another important parameter was the determination of the axial thrust which consisted of pressure and momentum thrust. For the peripheral jet this was simple because both components were directed axially. But for the air jets this was different, since the air jets were not injected in the axial direction a modified determination of thrust had to be established. This was done by measuring the bare nozzle thrust of the air jets in the way described in Section 4.0.1. Closest to axial air jet flow was the situation when the jets were not skewed. At a pressure ratio of 3.0 a net thrust of 1.64 times the measured bare nozzle thrust was recorded. If the net thrust would be based on the possible theoretical axial momentum that could be obtained with the given mass flow rate a thrust of 1.44 times the theoretical bare nozzle thrust was attained. This was clearly a major improvement on the vane vortex generated augmented flow.

6.3.2.) Concentrating on pitot rake results:

In Figures 5.7 and 5.23 basically the same flow conditions are shown, the exclusive difference being the slightly varying driving pressure ratio of 2.74 and 3.07. Between the two tests the angles were reset and therefore may differ according to the margin of accuracy possible with the setting tool. These two Figures are quite similar to the contra-rotating vane pressure contour plot. The main difference is the more evenly distributed dynamic pressure in the region between 50 per cent of the exit radius and the boundary. Furthermore the clear structure of four high pressure spots as for the vane plot was not repeated. Instead eight such high dynamic pressure areas should have developed because of the formation of eight individual vortex pairs from each of the air jet slots. It is probable that the weaker eight vortex pairs were not altogether stable, i.e. moved around to some extent and interacted with each other. The instability can also be observed when comparing the two contour plots (Figs. 5.7 and 5.23). As stated before these two representations of the dynamic pressure in the exit plane should be very similar but at a first look they do seem very different, N.B. these two representations were instantaneous snap-shots as indeed all the other dynamic pressure contour plots were. The major similarities are the low pressure central area and the high pressure

spots at a radial distance of approximately $0.8 R_c$. The distribution of these high pressure spots was, however, not well defined. This behaviour led to the conclusion that the vortex pairs were influenced by internal and external flow fluctuations. Internal fluctuations were caused by changes in the supply pressure and the external flow fluctuations were those produced by dynamic changes away and outside of the rig, e.g. the secondary air stream was modified by strong air movements in the laboratory. Since large quantities of secondary air were drawn in through the bell-mouth, which were clearly drawn in from the laboratory and therefore produced a sub-atmospheric pressure level, these large masses of air had to be recirculated. In a confined space as the laboratory posed this process of recirculation modified the flow into the secondary inlet and therefore the overall flow pattern in the exit plane. However, due to the contraction ratio of the bell-mouth inlet were the effects of the outside disturbances largely damped out.

The contra-rotating vortex pairs produced by the air jets were not that strong. This can be deduced from the contour lines especially since the dynamic pressures in the middle were still fairly low, i.e. the net induced velocities pointing towards the centre were relatively small in magnitude. An implication of this situation was a reduced transfer of high axial momentum air from the perimeter towards the middle. The peripheral arrangement of high dynamic pressure in the region of 60 to 90 per cent of the exit radius R_c seemed to suggest that the air jets attached to the wall despite the fact that the jets were elevated by 30 degrees. If the flow remained attached after leaving the slot or if it re-attached downstream can only be verified if a detailed local investigation could be initiated. Due to time constraints this was not possible nor really feasible with the present rig. As stated before would an investigation at the point of injection of the air jets be very revealing.

When skewing the air jets very serious differences between the distribution of dynamic pressure due to the co- and contra-rotating vortex formation emerged. The highest dynamic pressure areas for the co-rotating cases remained grouped around 25 per cent of the radial exit distance inside of the perimeter towards the centre as for the no skew cases. This behaviour proved valid for skew angles up to 45 degrees. For greater angles it seemed that the highest pressure spots moved to very close proximity of the perimeter. As stated above the 75° skew case should be considered with some caution because of the flow reversals in the central area. The formation of clear concentric dynamic pressure contour lines suggested that the induced velocities of the vortices and their images were the determining forces causing

the primary flow to swirl around the circumference of the boundary, namely the mixing and diffuser wall.

A question arising from all these measurements was where did the vortex core form for the co-rotating setup. From Milne-Thomson's^[24] theoretical considerations it was known that the induced velocities of the relevant adjoining vortices and images acted such as to produce a movement in the circumferential direction but no movement at all in the radial direction, i.e. the vortices remain on a path equi-distant to the boundary. For the parallel-walled mixing section this effectively meant that the vortices were travelling along the wall in the downstream direction without altering their distance from the wall. As the vortices continued into the diffuser it is reasonable to assume that they followed the streamlines, i.e. they move away from the wall at the same rate, as the ratio of their distance from the wall to the total radial distance, as the wall semi-angle opens up. Using this result by Milne-Thomson led to the following ideas. The vortices were formed by the high momentum primary air from the jets which then engulfed and rolled-up the secondary air stream. If one considers this process as continuous it can lead to two possible solutions for the mechanism of transporting high momentum air towards the centre. First it can be said that the jets themselves are the carrier of the momentum or the second solution is that the vortices are located in between the wall and the high pressure areas feeding high momentum air continuously to those locations. This again is a subject which only really can be solved by doing pitot-static flow measurements close to the point of injection of the primary air and downstream. It clearly would be interesting to initiate a new project looking at this particular area paying special attention to simulate the flow speeds of the primary air stream and the secondary air stream. With the present application the primary jets were injected at speeds of three to five times the secondary free stream velocity. For perfect mixing the differential in velocities quickly would converge to unity.

Above, it was stated that the co- and the contra-rotating cases produced totally different pressure contour lines. Picking up that point was rather important because it emphasised and illustrated the different vortex mechanisms. Skewing the jets to 15 degrees and more as contra-rotating pairs (Figs. 5.24 to 5.26) seemed to generate induced velocities large enough to carry the high momentum primary air towards the centre. The contour lines suggested such a considerable transfer of momentum from the boundary to the middle, especially for the 30° case, that a lower dynamic pressure area was left behind. This phenomenon led to the thought that the induced velocities of the vortex pairs can be too strong for the purpose they intend to fulfil, namely to transfer momentum in the radial direction. For the 30° skew case the

interaction of the high momentum air in the middle caused a deterioration in augmentation. Another factor contributing towards a reduction in net thrust was the loss in axial primary momentum due to skew. Based on theoretical axial bare nozzle thrust the augmentation ratio fell to 1.23. With skew angles larger than 30 degrees the losses in axial momentum became the determining factor establishing augmentation ratios again based on theoretical axial BNT of less than 1.0. This condition was, obviously from the point of view of optimizing the augmentation ratios, highly undesirable. From scientific considerations the formation of vortex pairs with strong radially induced velocities can be very beneficial particularly when combined with peripheral blowing. In Figure 5.34 showing the contour lines for the combined peripheral and air jet blowing with the jets skewed to 30 degrees the strength of the induced velocities is established because the highest dynamic pressures are again recorded in the centre. The vortex forming mechanism seemed to produce such strong induced velocities that high momentum 'bubbles' separated from the central core and moved towards the boundary which was suggested by the plot in the form of the four oval shaped spots. The unusual feature was the clear separation of the bubbles. A very strong phenomenon must have caused this clear-cut distribution of dynamic pressure. Comparing this plot with that one where no peripheral blowing was present (Fig. 5.31) showed astonishing similarities. The distribution of the high and low pressure areas is nearly equal. The major difference was in the higher dynamic pressures for the case with peripheral blowing, the reason being the enlarged injected amount of primary momentum. This led to the conclusion that despite the fact that the peripheral jet and the air jets were blown at very similar pressure ratios did the formation of the vortex pairs determine the distribution of the dynamic pressure.

For the 15° skew case with both the peripheral and air jets blowing (Fig. 5.33) it can be seen that the strength of the induced velocities was not sufficiently large to transfer the momentum further to the middle. Having said this, the plot gave indications that the spread of the high dynamic pressure areas had started when comparing with the no skew case. The lowest contour line of 2 kPa certainly had receded to a minimal size. First appearances of low pressure areas near the boundary were occurring, filling in the areas which the centrally moving vortices left behind.

From the point of uniformness the dynamic pressure contours with the jets skewed to 60 degrees gave a particularly good distribution. Again the higher dynamic pressures were recorded in the centre but very limited differentials in dynamic pressure existed across the exit plane. The average dynamic pressure was 5.56 kPa which could be

expected because it lay in between the 5 and 6 kPa contours since these two dynamic pressure contours were covering most of the reference area. Slightly higher pressures were monitored in the middle and slightly lower ones close to the boundary.

Blowing the contra-rotating air jet vortex generator pairs and the peripheral jet together produced not so encouraging results as far as augmentation was concerned. If one assumed that the air jets were driven at a constant pressure ratio of 3.0 and the peripheral jet was driven at a PR of 2.5 then the augmentations came to 1.26, 1.26, 1.18 and 0.83 for the 0, 15, 30 and 60 degree setting respectively. The basis for the calculation of the augmentations were the addition of the two theoretical axial bare nozzle thrusts of the air jets and the peripheral jet. If the augmentations were to be based on the measured bare nozzle thrusts this would have led to the following results: augmentations of 1.35, 1.38, 1.35 and 1.20 for the same angle settings as above. These fairly large differences in augmentation as caused by the various definitions of bare nozzle thrust will be discussed more thoroughly in Section 6.4.

6.4.) Thrust augmentation; scientific versus engineering:

The definition and the evaluation of scientific and engineering thrust augmentation generated some extensive discussion within the aerodynamic community of our university. There were two major streams on how to define augmentation.

The term scientific augmentation was used to describe the ratio of measured thrust over measured bare nozzle thrust (BNT), where the BNT was determined by removing the bell-mouth, the parallel walled mixing section and the diffuser as mentioned in Chapter 4.3. It was found that the measured bare nozzle thrust reduced as the cosine function of the angle of skew as stated in equation (4.1). The fact that the primary air through the air jets was blown in with some elevation angle relative to the axial direction and hence losing some axial momentum was also automatically taken into account. The air jet bare nozzle thrusts were established using the load cells exclusively and are illustrated in the second column of Table XV for varying AJ pressure ratios.

The term engineering on the other hand was an augmentation based on the theoretical determination of convergent bare nozzle thrust without the inclusion of any discharge or velocity coefficients nor any effects of skew and elevation angle. This probably needs to be explained further. For the peripheral slot the calculation of the bare nozzle thrust was the simple theoretical solution for a convergent nozzle, adding the pressure and the momentum thrust acting on and through the injection cross-sectional area. Some of the aerodynamic specialists argued that this same procedure should also be adopted to calculate the air jet BNT. The justification for this procedure lay in the fact that a 'real' application has a fixed quantity of compressed air available which could be used to generate an amount of axial bare nozzle thrust. If the jet is modified in any way, e.g. skewed or elevated, then, they argue, this should generate more BNT than the original amount to make it worthwhile. There was clearly some considerable virtue in this approach and therefore in Table XIII (co-rotating AJVGs) and Table XIV (contra-rotating AJVGs) the true engineering thrust augmentations are shown. It should be noted that for combined peripheral and air jet blowing the BNTs of the two nozzles were calculated separately and then simply added.

Since the BNT used for the peripheral nozzle was the same as the theoretically determined thrust, the air jets were responsible for the modification between the scientific and the engineering thrust augmentations. In Table XV the results for the scientific and the engineering BNTs and the differences between them are shown. Six

AUGMENTATION (based on theoretical BNT)
(co-rotating AJVGs)

AJVG pressure ratio

	ANGLE	1.0	2.0	2.5	3.0	3.5	4.0	4.5	
Peripheral pressure ratio	1.0	0		1.72	1.57	1.44	1.34	1.25	1.19
		15		1.64	1.49	1.37	1.27	1.19	1.13
		30		1.50	1.34	1.21	1.10	1.03	1.00
		45		1.38	1.22	1.09	0.99	0.92	0.88
		60		1.06	0.96	0.87	0.79	0.73	0.69
		75		0.45	0.40	0.37	0.34	0.33	0.33
	1.5	0	1.23	1.48	1.40	1.32	1.26	1.19	1.13
		15		1.45	1.37	1.30	1.23	1.17	1.12
		30		1.38	1.27	1.17	1.09	1.02	0.98
		45		1.18	1.09	1.01	0.93	0.86	0.80
		60		1.04	0.95	0.87	0.80	0.75	0.70
		75		0.83	0.73	0.65	0.58	0.52	0.49
	2.0	0	1.22	1.36	1.32	1.27	1.21	1.15	1.10
		15		1.40	1.34	1.28	1.22	1.17	1.12
		30		1.33	1.24	1.17	1.10	1.04	1.00
		45		1.19	1.10	1.02	0.96	0.90	0.85
		60		1.06	0.97	0.89	0.82	0.76	0.71
		75		0.88	0.79	0.70	0.63	0.57	0.52
	2.5	0	1.20	1.34	1.30	1.26	1.21	1.17	1.12
		15		1.32	1.30	1.26	1.22	1.17	1.11
		30		1.31	1.23	1.15	1.09	1.03	0.99
		45		1.17	1.10	1.04	0.98	0.93	0.87
		60		1.08	0.99	0.91	0.85	0.79	0.75
		75		0.94	0.84	0.75	0.68	0.62	0.57
3.0	0	1.19	1.30	1.27	1.23	1.19	1.15	1.10	
	15		1.30	1.27	1.24	1.20	1.16	1.10	
	30		1.26	1.20	1.15	1.10	1.05	1.01	
	45		1.12	1.06	1.00	0.95	0.90	0.85	
	60		1.02	0.95	0.88	0.82	0.77	0.72	
	75		0.99	0.89	0.80	0.73	0.67	0.62	

Table XIII: Engineering augmentations, co-rotating air jets

AUGMENTATION (based on theoretical BNT)
(contra-rotating AJ pairs)

AJVG pressure ratio

	ANGLE	1.0	2.0	2.5	3.0	3.5	4.0	4.5	
P e r i p h e r a l p r e s s u r e r a t i o	1.0	0		1.72	1.57	1.44	1.34	1.25	1.19
		15		1.68	1.54	1.41	1.30	1.22	1.15
		30		1.45	1.33	1.23	1.14	1.07	1.00
		45		1.15	1.04	0.96	0.88	0.83	0.79
		60		0.74	0.68	0.63	0.59	0.55	0.53
		75		0.28	0.26	0.25	0.24	0.23	0.22
	1.5	0	1.23	1.48	1.40	1.32	1.26	1.19	1.13
		15	1.23	1.48	1.40	1.32	1.25	1.18	1.12
		30	1.23	1.34	1.25	1.17	1.10	1.04	0.99
		45	1.23	1.17	1.06	0.97	0.90	0.85	0.81
		60	1.23	0.93	0.82	0.73	0.66	0.62	0.59
		75	1.23	0.63	0.52	0.44	0.39	0.35	0.34
	2.0	0	1.22	1.36	1.32	1.27	1.21	1.15	1.10
		15	1.22	1.39	1.34	1.29	1.24	1.18	1.12
		30	1.22	1.29	1.22	1.15	1.09	1.04	0.99
		45	1.22	1.17	1.07	1.00	0.93	0.87	0.83
		60	1.22	0.97	0.87	0.79	0.72	0.66	0.63
		75	1.22	0.75	0.64	0.55	0.48	0.44	0.41
	2.5	0	1.20	1.34	1.30	1.26	1.21	1.17	1.12
		15	1.20	1.34	1.30	1.26	1.21	1.16	1.11
		30	1.20	1.30	1.24	1.18	1.12	1.07	1.02
		45	1.20	1.17	1.09	1.01	0.95	0.90	0.86
		60	1.20	1.01	0.91	0.83	0.76	0.71	0.67
		75	1.20	0.83	0.72	0.63	0.55	0.50	0.48
3.0	0	1.19	1.30	1.27	1.23	1.19	1.15	1.10	
	15	1.19	1.30	1.29	1.26	1.22	1.17	1.11	
	30	1.19	1.28	1.23	1.17	1.12	1.07	1.02	
	45	1.19	1.17	1.10	1.03	0.97	0.92	0.87	
	60	1.19	1.06	0.97	0.89	0.82	0.76	0.72	
	75	1.19	0.91	0.79	0.69	0.62	0.56	0.53	

Table XIV: Engineering augmentations, contra-rotating air jet pairs

different pressure ratios driving the air jets were looked at; from just beyond choked condition up to $PR = 4.5$ in increments of 0.5. The measured bare nozzle thrusts were interpolated from least squares fits. As established above was there again a linear relationship between the thrust and the pressure ratio.

The third column illustrates the theoretical 'engineering' BNT, i.e. the ideal convergent bare nozzle thrust. The fifth column represents the 'theoretical scientific' BNT, which includes the degradation according to the cosine function of the elevation angle. It was argued that this factor should be included for the determination of the theoretical scientific bare nozzle thrust caused by a reduction in axial momentum.

PR_{AJ}	measured BNT (N)	theor. BNT (N)	measured over theor. BNT (%)	mod theor. BNT including $\cos(\text{elev.})$	measured over mod theor. BNT (%)
2.0	95.4	100.7	94.7	87.2 N	109.4
2.5	130.7	142.3	91.8	123.2 N	106.1
3.0	161.6	183.9	87.9	159.3 N	101.4
3.5	190.9	225.5	84.7	195.3 N	97.7
4.0	221.2	267.1	82.8	231.3 N	95.6
4.5	255.5	308.7	82.8	267.3 N	95.6

Table XV: Measured and theoretical bare nozzle thrust for different air jet driving pressures

The fourth column shows that the measured bare nozzle thrust underestimated the theoretical convergent nozzle thrust by 5 per cent near the critical PR and by 17% at the higher PR of 4.5. This deficit can be attributed to the deterioration in axial momentum caused by the elevation of the jet leaving the vortex generator plug and therefore was incorporated in calculating the modified theoretical BNTs. Again taking ratios of measured to theoretical bare nozzle thrust showed a greater measured than theoretical BNT for the low PR cases. It is believed that the Coanda effect helped the flow around the sharp exit and therefore reduced the redirection in axial momentum. As the pressure ratio was increased the measured thrust again fell to below the theoretical value. This was attributed to the development of a separation bubble and the associated change in pressure thrust on the inclined surface of the vortex plug. It needs to be emphasized that an investigation of this particular area would be very beneficial but

would require some in depth research in its own right. Unfortunately, the time limitation did not allow for this kind of thorough diversion.

In addition to the definition of the engineering and scientific thrust augmentation above, there was another possibility to look at augmentation. Augmentation as it was used until now described the ratio of two thrusts. For the engineering and scientific definitions a bare nozzle thrust formed the frame of reference. The other possibility was to use the mathematical model, as developed in Chapter 2, assume a diffuser efficiency of 100% and then compare the experimentally measured thrust with that ideal thrust. This clearly lead straight away to efficiencies of less than 100% and was therefore not comparable with the other definitions of augmentation. However, this definition would show positively how inefficient the diffuser worked during testing. The efficiency of the diffuser in the mathematical model was originally based on the loss in total pressure between the inlet and the exit of the diffuser. A comparison of the theoretical results, using this definition of efficiency, with the experimental results showed rather poor agreement. It seemed that the experimental curve crossed over various theoretical curves as illustrated in Figure 6.8. This occurrence lead to the idea that the diffuser efficiency should therefore be based on the static pressure rise between the inlet and the exit. In Figure 6.9 it can be seen that this particular definition of efficiency produced the required 'fan', i.e. the curves were closely spaced at the lower pressure end and then spread as the pressure ratio increased. The fan was generated by the mathematical relationship that even a low diffuser efficiency (e.g. 50 per cent) based on static pressure rise produced fairly high diffuser efficiencies based on total pressure loss for low pressure ratios, i.e. near choking. However, as the pressure ratio was increased more and more, up to the limit where the secondary became choked, low static efficiencies also resulted in fairly low total pressure efficiencies.

For the 100% efficient diffuser the secondary inlet became choked for an approximate PR of 4.4. As the efficiency was reduced the choking of the secondary inlet occurred at much higher pressure ratios. The diffuser efficiency effectively was the parameter that controlled the Mach number in the exit plane and therefore the total thrust of the augmentor. For subsonic flow leaving the diffuser it was known that the static pressure in the exit plane was essentially very close to atmospheric because no real pressure gradient could exist across the free surface. From Bernoulli we know that the total pressure is the combination of the static and the dynamic pressure. Since the static pressure was equal to the atmospheric pressure in the diffuser exit plane the net thrust was purely momentum thrust. If a diffuser

efficiency based on total pressure was assumed and assuming a certain static pressure and Mach No. at the inlet to the diffuser, determined by the upstream conditions, it easily followed that the exit Mach number was forced to go down as the diffuser became less efficient. Including the modified efficiency (based on static pressure rise) the same feature applied but the relationship between Mach No. and pressure was slightly more extensive, which was given in equation (2.7), where the increased complexity between the two diffuser efficiencies was shown.

7.) CONCLUSIONS

The development of the theoretical model for ejector flow using the three conservation equations was an important step in understanding the fundamental flow behaviour. It provided a first insight on how parameters like pressure ratio, temperature ratio, inlet area ratio, diffuser area ratio and diffuser efficiency influenced the net thrust levels. The initial choice of defining the diffuser efficiency as the loss in total pressure between inlet and exit of the diffuser, as suggested by the ESDU data items, was shown to be inadequate and was therefore modified. Basing the diffuser efficiency on the static pressure rise instead resulted in a very satisfying agreement between the theory and the experimental data. It was found that the theoretical peripheral bare nozzle thrust, i.e. thrust augmentation ratio is equal to 1.0, corresponded to a highly inefficient diffuser using this modified definition of efficiency based on static pressure rise.

Measurements of the peripheral bare nozzle thrust showed that the theoretical results were in good agreement with the experimentally obtained results. These measurements were performed by testing the jet on its own, i.e. removing all the up- and downstream sections. A similar test was repeated for the eight air jet vortex generator slots. The combined bare nozzle thrust from the eight slots was fairly close to the theoretical bare nozzle thrust for a nozzle of equivalent cross-sectional area near the critical pressure ratio but worsened as the pressure ratio was increased. This divergence was thought to be caused by the elevation of the air jets relative to the axial direction, altering the pressure thrust on the inclined surface of the vortex generator plug. Furthermore, skewing the co-rotating air jets to some angle reduced the bare nozzle thrust by a factor equal to the cosine of that angle. The theoretical bare nozzle thrust was calculated using the momentum and pressure thrust of a convergent nozzle.

Measurements of the bare augmentor, which consisted of the bell-mouth, peripheral jet, the parallel-walled mixing section and the diffuser having an area ratio of 1.5, produced an augmentation ratio of 1.19 at a pressure ratio of 3.0. This result effectively means a 19 per cent increase in the pure peripheral bare nozzle thrust and corresponds to a static diffuser efficiency of approximately 33 per cent assuming the mathematical model. The efficiency of 33 per cent was still very low for a good diffuser. The cause was thought to be due to the inadequate mixing length provided for the primary and secondary flows to mix naturally, N.B. the spreading angle of a wall jet on a flat plate

amounts to three to five degrees only. It was therefore believed that a longer mixing section would have given the opportunity for more thorough mixing and hence enhanced augmentation ratios. As one of the requirements of the assembly was to reduce the overall length another mechanism had to be found to increase mixing.

As the results from the measurements using the vane vortex generators of cropped delta wing shape were processed it was found that for certain angles of incidence greater augmentation ratios than for the bare augmentor were possible. Both the co- and contra-rotating vortex arrangements generated augmentations of similar maximum magnitude, in the region of 30 per cent, although it must be noted that these maxima were reached at slightly different angles. The co-rotating vortices had their maximum effect at an angle of incidence of 16 degrees and the contra-rotating vanes required two degrees less to perform best. These augmentation ratios of 1.3 corresponded to a static diffuser efficiency of approximately 60 per cent which now compared with a fairly well performing diffuser. Any improvement on this value would become rather difficult to achieve, but further enhanced mixing of the two streams might lead to an increased augmentation ratio. The dynamic pressure plots suggested that there were still rather large regions near the central axis which had fairly low values of velocity. This led to the conclusion that if somehow these areas could be made more uniform before the flow entered the diffuser the desired effect of increasing the augmentation might well be obtained.

The dynamic pressure plots taken near the maximum vane vortex 'effectiveness', despite the rather large spacing of the pitot probes, showed the difference between the co- and the contra-rotating vortex patterns well. The co-rotating vortices remained in close proximity to their originally generated location in the radial direction, but were known to move along in the circumferential direction. This latter behaviour was difficult to monitor because measurements were taken at one station only, namely in the exit plane. If measurements at various stations closer to the vortex generators could be made, the circumferential velocity caused by the vortex/image interaction could be determined from the angle at which the vortex travelled relative to the undisturbed streamwise direction. The contra-rotating vortices on the other hand showed that the vortex/image interaction caused the respective pairs to join and move towards the central axis due to the influence of the induced velocities. Returning to the augmentation ratios, determined above for these two different vane vortex generator lay-outs, which were of similar magnitude probably implied that the surface areas of the shear layers at the edge of the free jet mixing zone, responsible for enhanced mixing, were nearly equal.

The results from the air jet vortex generator blowing were rather more complex than those results obtained for the vane vortex generators. This increased degree of complexity was caused by the fact that additional mass and hence momentum was injected. In order to simplify the matter somewhat the results were split into two considerations:

- a) air jet vortex generator blowing on its own
- b) combined air jet vortex generator and peripheral blowing.

It turned out that the exclusive air jet vortex generator blowing could most easily be compared with the vane results, the reason being that the jet nozzle areas of the peripheral and the eight individual air jets were of similar size, i.e. 700 and 640 mm² respectively. This clearly translated to the injection of similar amounts of mass for equal pressure ratios. The major difference between the air jets and the peripheral blowing was that the air jets were elevated by 30 degrees and also could be skewed but the peripheral jet on the other hand always exhausted in the axial direction. This problem was resolved by defining two independent augmentation ratios, namely the 'scientific' and the 'engineering' ratio. The 'scientific' augmentation ratio took into account the reduction in axial momentum due to elevation and skew angle in evaluating the bare nozzle thrust and the 'engineering' augmentation ratio was calculated as the measured thrust divided by the theoretical bare nozzle thrust assuming the momentum to be directed axially, using the definition for an ideal convergent nozzle. The former 'scientific' definition clearly produced larger augmentation ratios for the given angles of the air jet vortex generators.

One important feature which developed very quickly was that the augmentation ratios strongly depended on the driving pressure within the air jets. For low pressure ratios (≈ 2) the augmentation ratios were rather large but reduced rapidly with increasing pressure ratio. The augmentation ratios for the 'engineering' bare nozzle thrust definition resulted in 1.72 and 1.19 for a pressure ratio of 2.0 and 4.5 respectively with the air jets set to a skew angle of 0 degrees. As the skew angle of the air jets was increased the co-rotating vortices performed much better than the contra-rotating ones. The augmentation ratios fell below one, i.e. the measured thrust became less than the axial bare nozzle thrust, when the air jets were skewed to 60 degrees and more. For practical applications that clearly would be an area to be avoided.

The augmentation ratio of 1.19 at a pressure ratio of 4.5 was smaller than that for the vane vortex generators which led to the conclusion that the air jets perform well for small pressure ratios but as the

pressure ratio was increased the loss in pressure and momentum thrust due to the air jets being elevated was becoming too great. It should be noted that the maximum augmentation for the 'scientific' definition was reached at around 60 degrees of skew for the co-rotating setting (1.64 for a driving pressure of 4.5), which coincided with the expected angle necessary for the maximum vortex strength to develop.

Combining the peripheral and air jet blowing generated 'engineering' augmentation ratios similar to those for the vane vortex generators for certain conditions of driving pressure and skew angle. In general it was noted that the air jets needed to be set to fairly small angles of skew and blown lightly to get maximum augmentations. With increased air jet blowing and increased skew angle the net thrust reduced faster than the enhanced mixing capability of the vortices. For skew angles up to about 45 degrees the co- and contra-rotating vortices produced very similar augmentations, although the dynamic pressure plots showed that the net pressure pattern was rather different. The main similarity seemed to be the fact that the vortices could be used to advantageous effect to increase the surface areas of the shear layers at the edge of the jet mixing zone and thereby increase the mixing between the fast primary air and the slow entrained secondary air. The dynamic contour plots with the contra-rotating pairs demonstrated really well how the induced velocities between the vortex and its image forced the high momentum air, injected peripherally, to move towards the central axis. It is believed that this condition would be perfectly suited to increase the diffuser semi angle (the ultimate aim of this project!) and still obtain a good distribution of dynamic pressure within the exit plane.

Summarizing all the above stated results the author came to the following conclusions; the improvement in thrust augmentation employing vane vortex generators should be judged as very encouraging because these devices are rather easily incorporated and seem to work well throughout the driving pressure regime considered for practical work, i.e. the vanes are thought to be highly promising in a real application, as a Reaction Control System would be. It must be stated, however, that the aim of a 50 per cent enhancement in thrust was a long way off.

High hopes were then pinned on the employment of air jet vortex generators in order to achieve further major improvements in thrust augmentation. These hopes were very quickly shattered because there was a fundamental problem associated with the air jet vortex generators and that was the opposing effect of vortex strength and thrust. The maximum vortex strength is obtained at around 60 degrees of skew, but at this angle the net axial thrust has reduced to cosine 60° times the no skew

axial thrust. This meant that a good vortex strength, i.e. large jet mixing area, was obtained in return for a considerable loss in axial thrust.

For a real application the 'engineering' thrust augmentation definition was clearly the correct choice for reference purposes. The results showed a large dependence on primary jet driving pressure. As the pressure ratios rose to useful levels (e.g. 4.5) the 'engineering' augmentations fell to well below those obtained with the vane vortex generators installed. This occurrence was a major setback and somewhat disappointing, as it was believed that the air jets would overcome the adverse drag penalty associated with the vanes and would therefore always generate better thrust levels. The biggest improvement in augmentation with the air jets were noticed through the fact that these air jets effectively acted as slotted jets, whereby a considerable increase in the net jet mixing area and hence enhanced augmentation was achieved. This observation was deduced by comparing the 'bare augmentor' and the exclusive air jet blowing.

It is suggested that some future work should include an investigation into the jet flow near the air jet injection nozzle. The way in which the flow expands and possibly contracts at supersonic speeds after passing the throat could to some extent modify the shape of the air jet 'plug'. In particular to monitor the pressure on the inclined surface downstream of the throat for different nozzle reservoir pressures would be very revealing. At present only some fairly rough estimates can be made about the pressure in this area. Further experimental studies of the air jet elevation angle would potentially optimize the augmentation ratios for varying driving pressures.

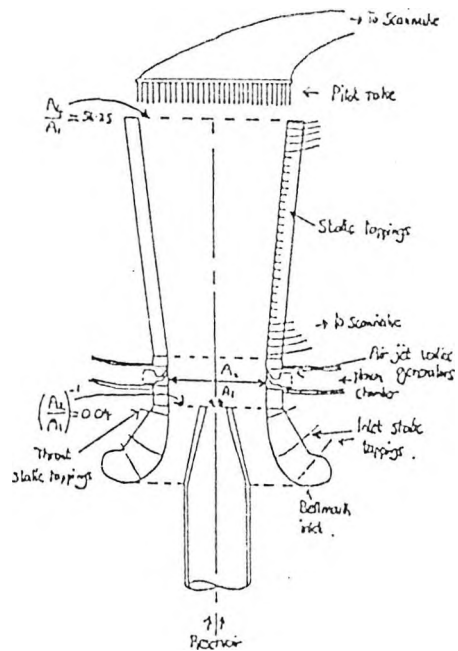
8.) REFERENCES

- 1.) Mattock D.J.: 'Air jet vortex generators in compact thrust augmentors', The City University, London, England, Feasibility Study, Progress Report 1, TF 02/89/01, January 1989
- 2.) O'Donnel, R.M. and Squyers, R.A.: 'V-STOL ejector short diffuser study', Vought Corporation Advanced Technology Centre Inc., Dallas, Texas, USA, AD-A042 319, June 1976
- 3.) Alperin, M. and Wu, J.: 'A jet diffuser-ejector for a V/STOL fighter', Flight Dynamics Research Centre, Van Nuys, California, USA, AD-A124 264, June 1982
- 4.) Alperin, M. et al.: 'Jet diffuser-ejector attached nozzle design', National Aeronautics and Space Administration, NASA-CR-152 361, N81-19412, May 1980
- 5.) Proceedings; Ejector workshop for aerospace application held at Bergamo Centre: 'Ejector nozzle development', Dayton, Ohio, USA, AD-A124 264, June 1982
- 6.) Uhvad, G.C.: 'Experimental investigation of circular thrust augmenting ejectors', USAF Institute of Technology, Wright-Patterson AFB, Ohio, USA, AFIT/GAE/AA/86M-3, December 1985
- 7.) Pearcey H.H.: 'Shock-induced boundary layer separation and its prevention by design and boundary layer control', Vol.2, edited by Lachmann G.V., Pergamon Press, 1961
- 8.) Bruynes H.: 'Fluid Mixing Device', U.S. Patent 2558816, 1951, and also Taylor H.D., United Aircraft Research Department, 'Summary Report on Vortex Generators', Ref. R-05280-9, 1950
- 9.) Miller P. and Seel M.W.R.: 'The application of high pressure ejectors to reaction control systems', Aeronautical Journal, November 1991
- 10.) Beyer U.: 'Use of vane vortex generators in a thrust augmenting ejector', The City University, London, England, MEA/AERO Report No. 174, January 1991
- 11.) Bevilaqua P.M.: 'Advances in ejector thrust augmentation', SAE paper 872322, 1987

-
- 12.) ESDU data item 84029: 'Ejectors and jet pumps: Design and performance for compressible air flow.'
December 1984
 - 13.) Flynn R.J.: 'Air jet vortex generators in compact thrust augmentors.', The City University, London, Design Study Report No. 2, August 1989
 - 14.) Panc, V.: 'Theories of elastic plates', 2nd edition, Chapter 26, p. 535 ff., Noordhoff International Publishing, 1975
 - 15.) Timoshenko and Woinowsky-Krieger: 'Theory of plates and shells', 2nd edition, Chapter 3, p. 51 ff., McGraw-Hill Book Company, 1959
 - 16.) Ugural, A.C.: 'Stresses in plates and shells', p. 27 ff., McGraw-Hill Book Company, New York, 1981
 - 17.) Freestone M.M.: 'Preliminary tests at low speed on vorticity produced by air jet vortex generators.', The City University, London, RM 85/1, 1985
 - 18.) Küchemann, D.: 'The aerodynamic design of aircraft', Pergamon International Library, 1978
 - 19.) ESDU International: 'Transonic Aerodynamics', Volume 3, Item No. 90008, 1990.
 - 20.) Hall I.M., Rogers E.W.E: 'The flow pattern on a tapered swept back wing at Mach numbers between 0.6 and 1.6' ARC R&M 3271, 1960.
 - 21.) ESDU International : 'Normal force and pitching moment of low aspect ratio cropped-delta wings up to high angles of attack at supersonic speeds', Volume 2d, Item no. 90013, 1990.
 - 22.) Abramovich G.N.: 'The theory of turbulent jets.' Technical editing by Leon H. Schindel, The M.I.T. Press, 1963
 - 23.) ESDU data item 74035: 'Subsonic lift-dependent drag due to the trailing vortex wake for wings without camber or twist.'
October 1974
 - 24.) Milne-Thomson, L.M.: 'Theoretical Hydrodynamics', 5th edition, Macmillan, 1968
-

9.) FIGURES

a)



b)

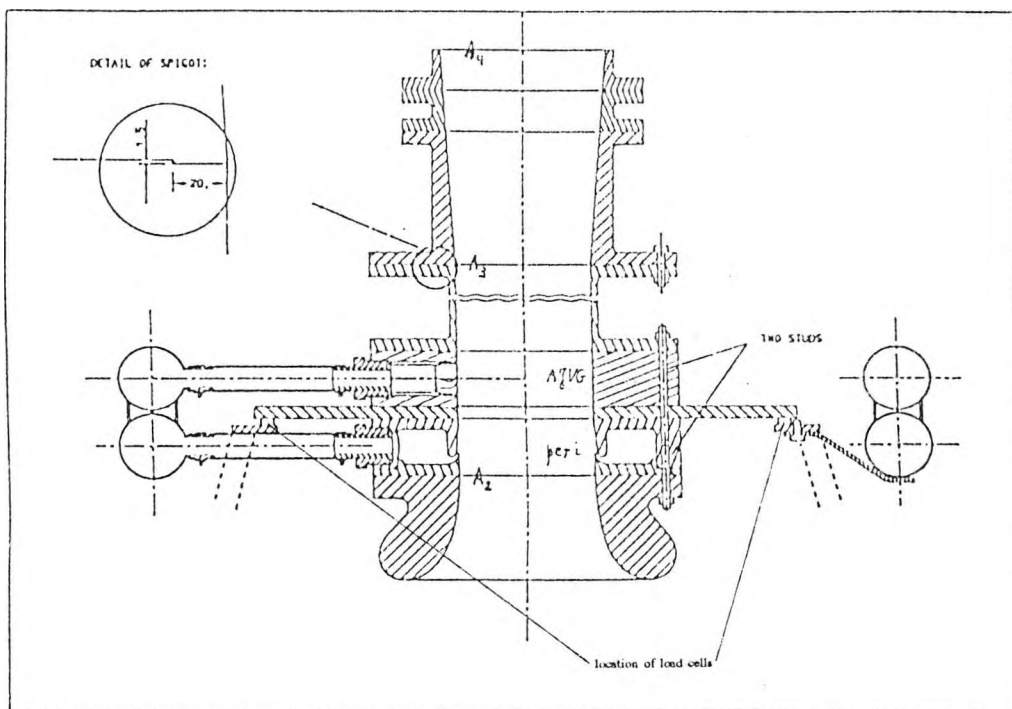


Fig. 1.1a) Mattcock's original proposed rig design.

Fig. 1.1b) Final design and notation of rig as manufactured.

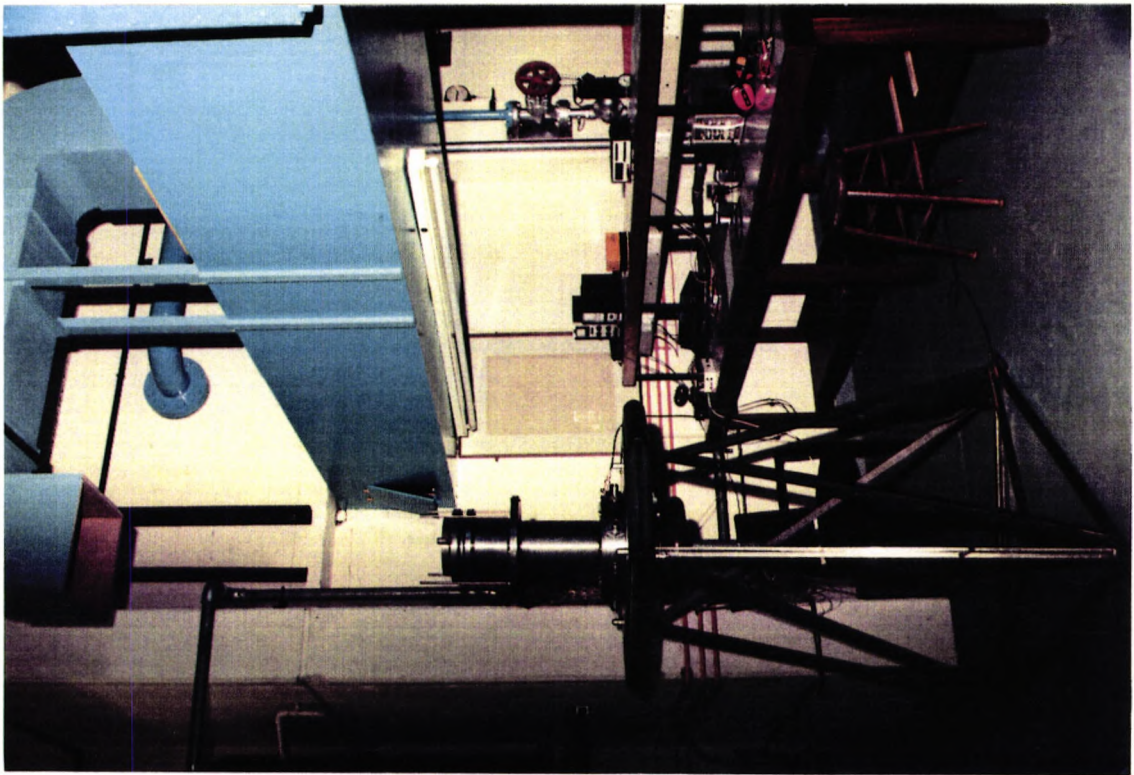
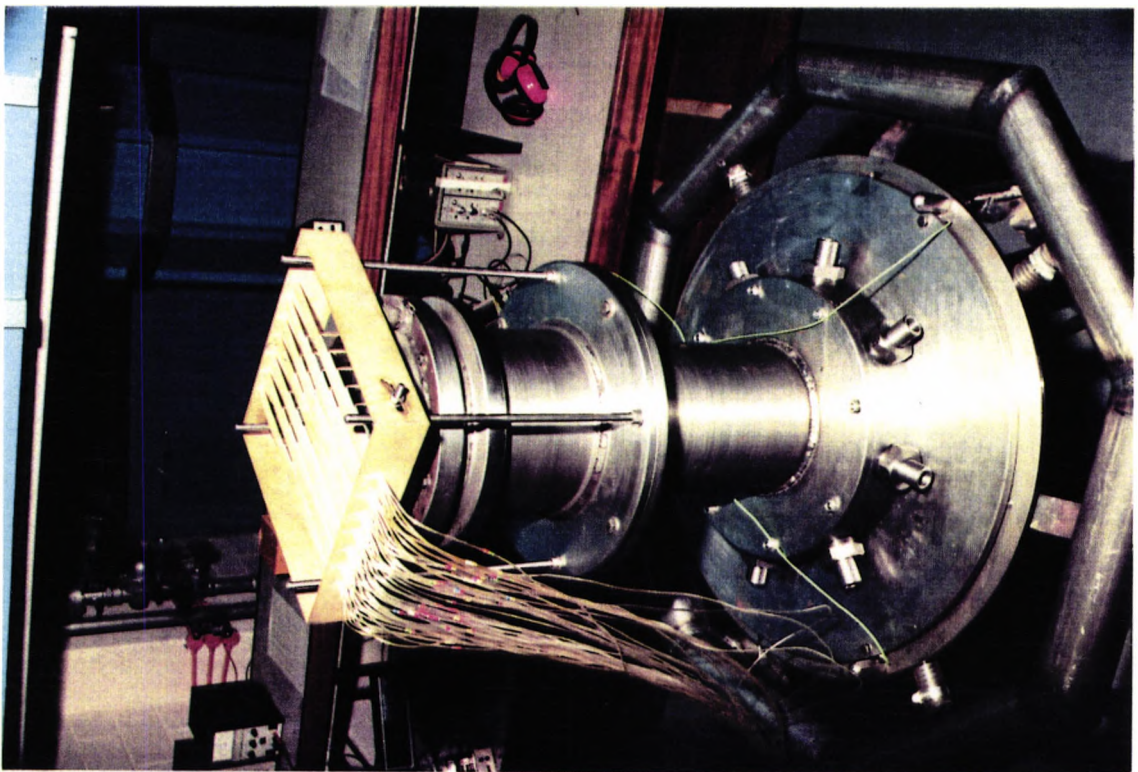
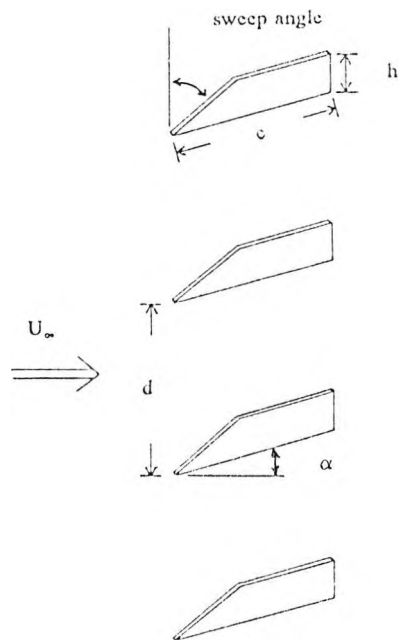


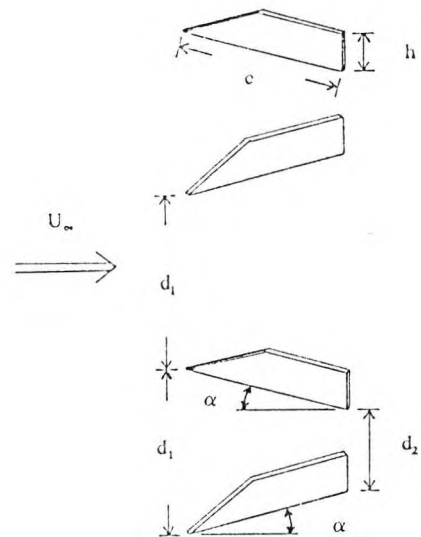
Fig. 1.1c) Photographs of experimental rig.



a) Co-rotating vane vortex generator arrangement:



b) Contra-rotating vane vortex generator arrangement:



c) Bi-plane vane vortex generator arrangement:

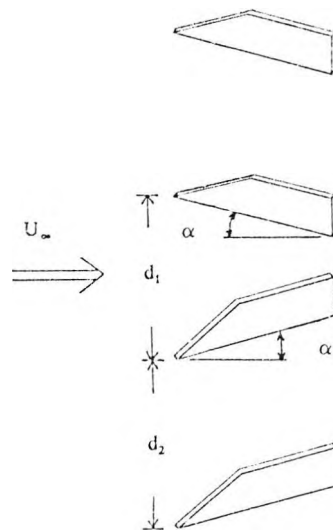
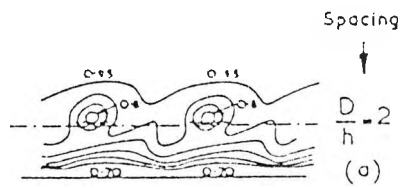
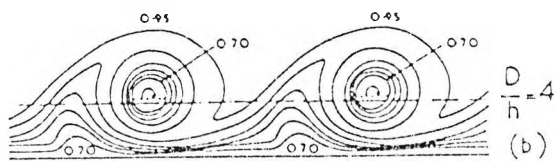


Fig. 1.2a) - c) Vane vortex arrangements and notation: co-rotating contra-rotating and bi-plane.

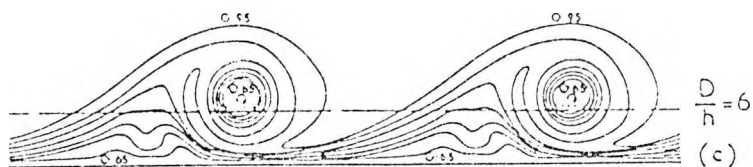
a)



b)



c)



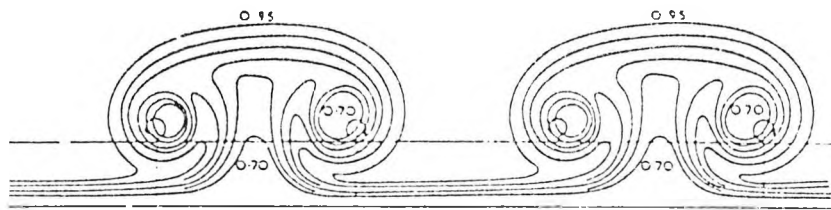
— CONTOURS OF $\sqrt{\frac{H-p_{z0}}{H_x-p_x}}$

----- PROJECTION OF
GENERATOR TIP
(displaced sideways)

----- $\sqrt{\frac{H-p_{z0}}{H_x-p_x}} = 0.95$ in absence
of generators.

Fig. 1.3a) - c) Contours of pitot pressure for co-rotating vortices for different spacing ratios (at a fixed distance downstream of generators on a flat plate).
- taken from Pearcey -

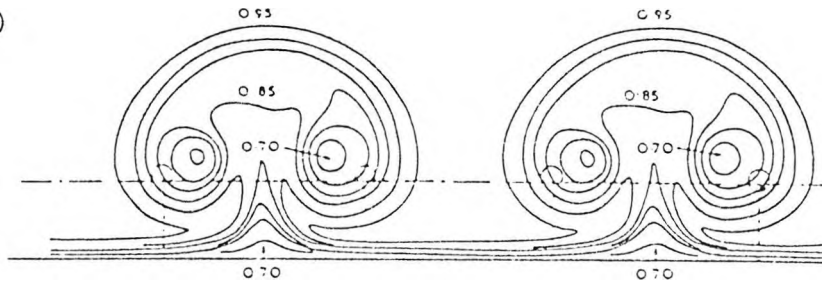
a)

Distance
downstream

$$\frac{x}{D} = 1.6$$

(a)

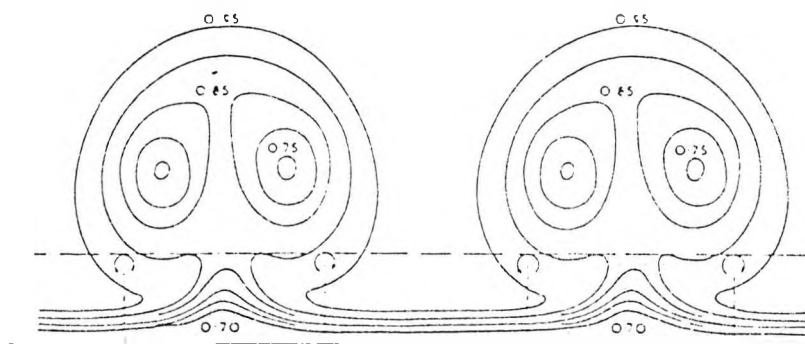
b)



$$\frac{x}{D} = 3.2$$

(b)

c)



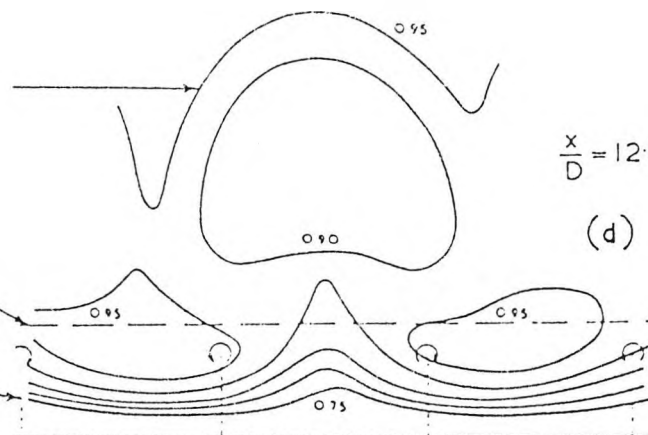
$$\frac{x}{D} = 6.4$$

(c)

d) CONTOURS OF $\sqrt{\frac{H - p_{00}}{H_{00} - p_{00}}}$

$$\sqrt{\frac{H - p_{00}}{H_{00} - p_{00}}} = 0.95$$

in absence of generators

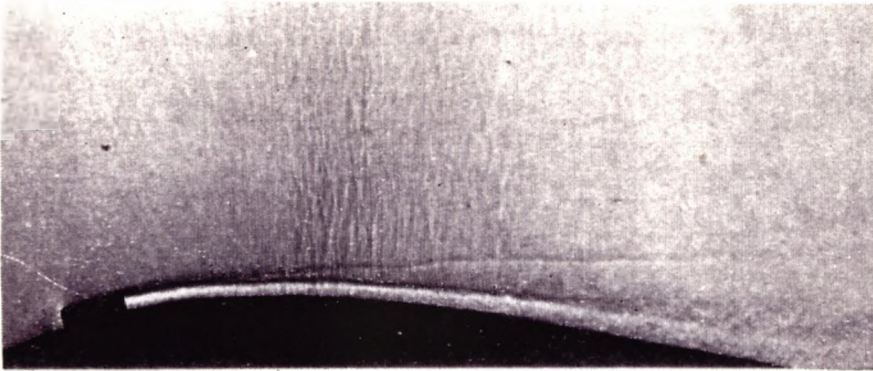
PROJECTION OF
GENERATOR AXIS

$$\frac{x}{D} = 12.8$$

(d)

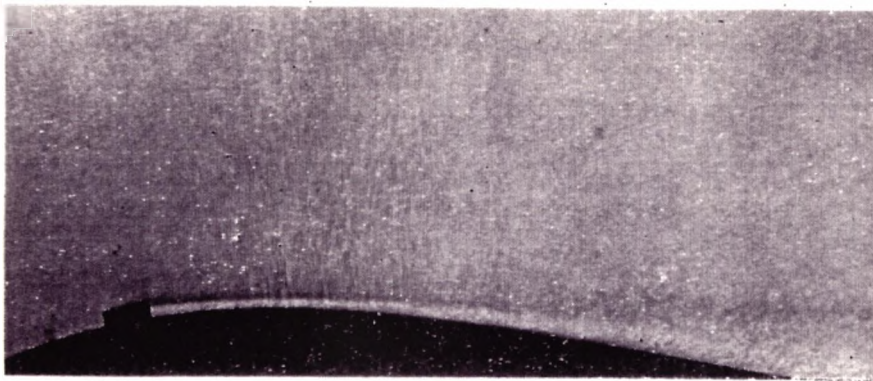
Fig. 1.4a) - d) Contours of pitot pressure for contra-rotating vortices that are initially equally spaced. (Variation of vortex pattern with distance downstream.) - taken from Pearcey -

a)



(a)
Co-rotating

b)



(b)
Counter-rotating
 $D/d = 4$

Fig. 1.5) Vortex paths projected in plane parallel to stream;
 $M_\infty = 0.7$ (velocity now falling over rear of surface).
- taken from Pearcey -
a) Effect of co-rotating vortices on boundary layer.
b) Effect of contra-rotating vortex pairs on boundary layer.

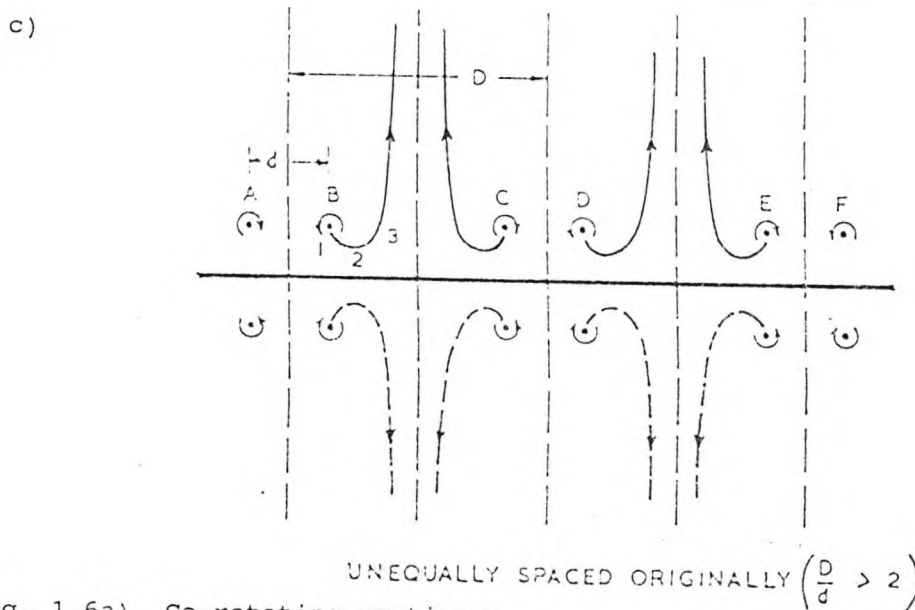
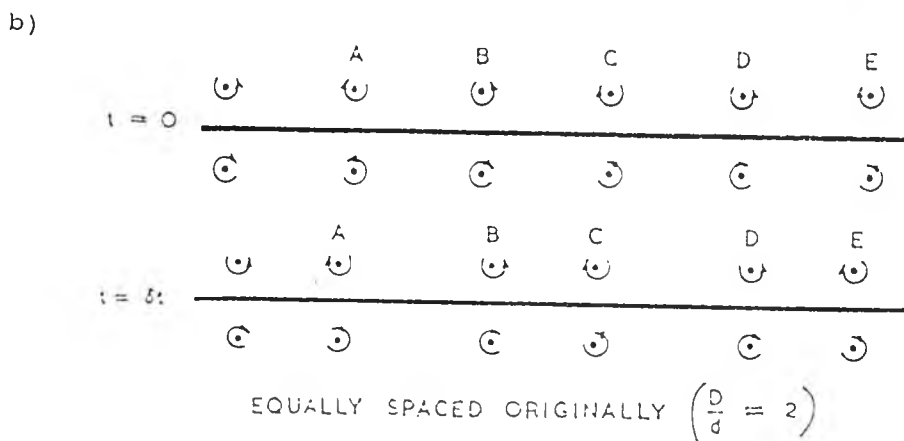
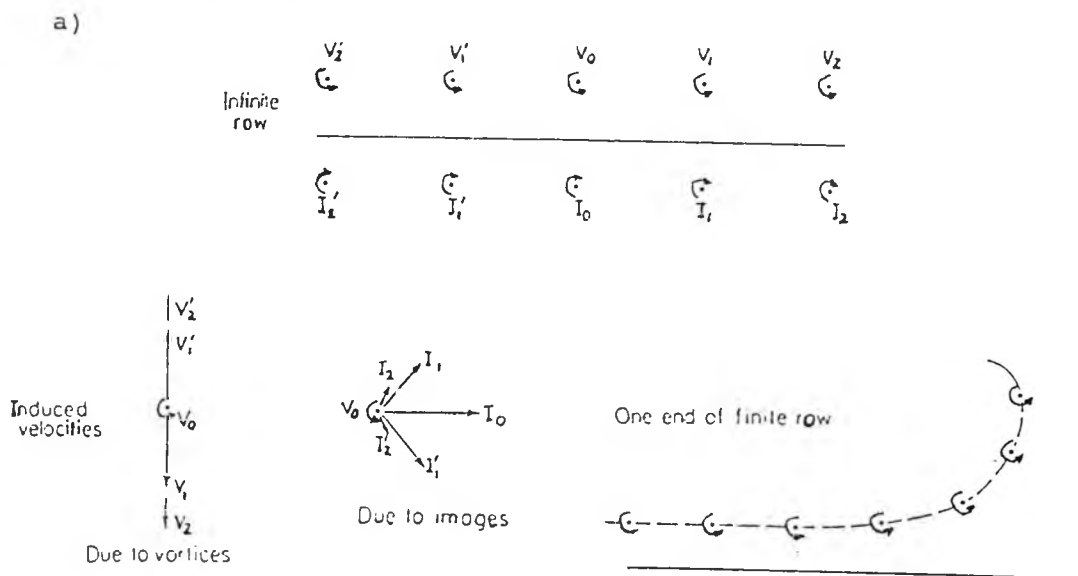
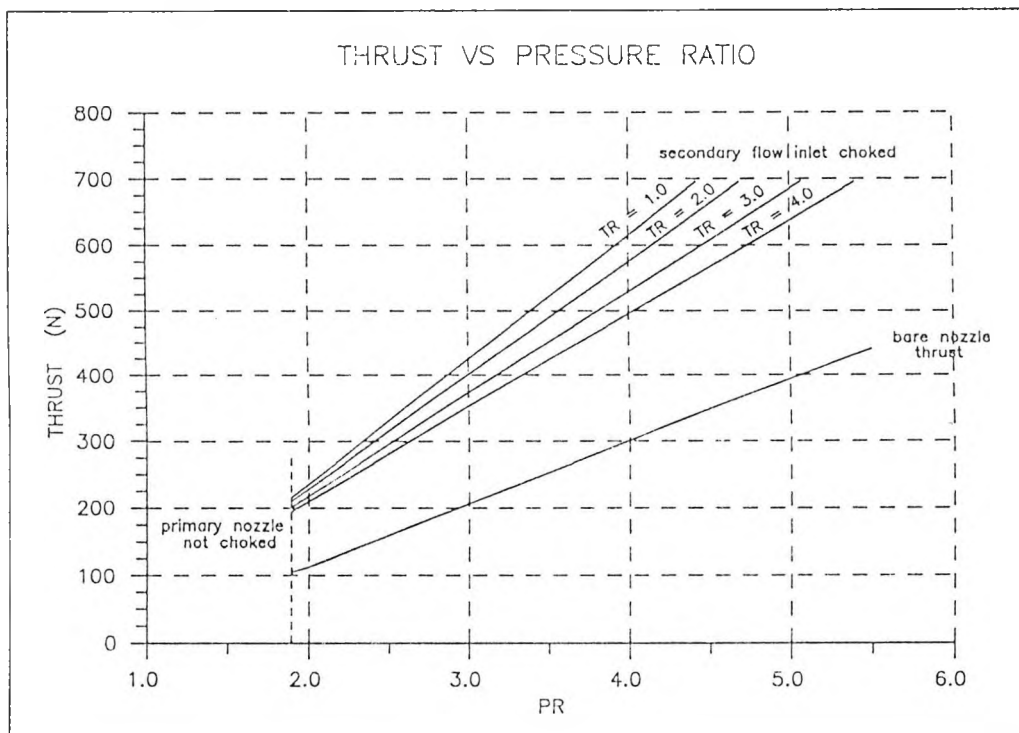
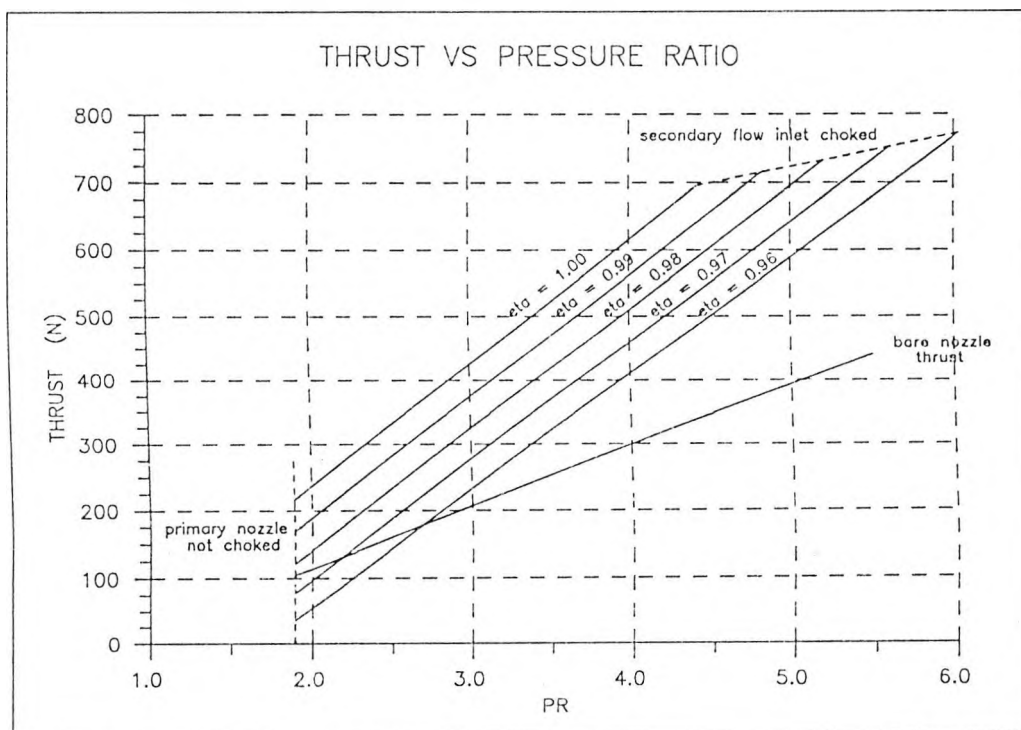


Fig. 1.6a) Co-rotating vortices.
 Fig. 1.6b) Contra-rotating vortices: equally spaced originally.
 Fig. 1.6c) Contra-rotating vortices: unequally spaced originally.
 - all Figures taken from Pearcey -



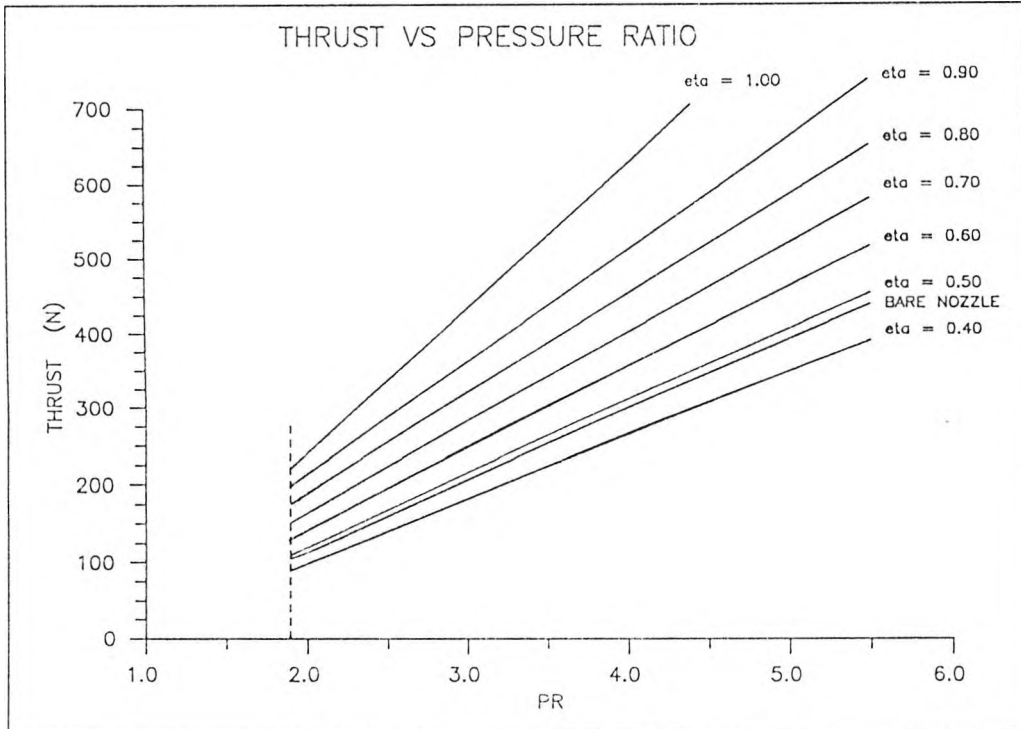
16 Oct 1991

Fig. 2.1 Theoretical prediction of thrust vs pressure ratio with the temperature ratio ranging between 1.0 and 4.0 and a 100 per cent efficient diffuser.



5 Oct 1991

Fig. 2.2 Theoretical prediction of thrust vs pressure ratio with the diffuser efficiency based on total pressure loss and a temperature ratio of 1.0.



28 April 1992

Fig. 2.3 Theoretical prediction of thrust vs pressure ratio with the diffuser efficiency based on static pressure rise and a temperature ratio of 1.0.

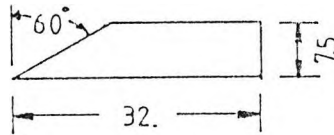


Fig. 3.1a Planform of flat plate cropped delta wing; span = 7.5mm.

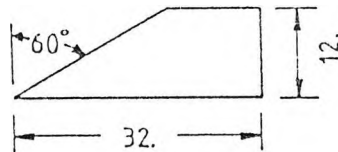


Fig. 3.1b Planform of flat plate cropped delta wing; span = 12mm.

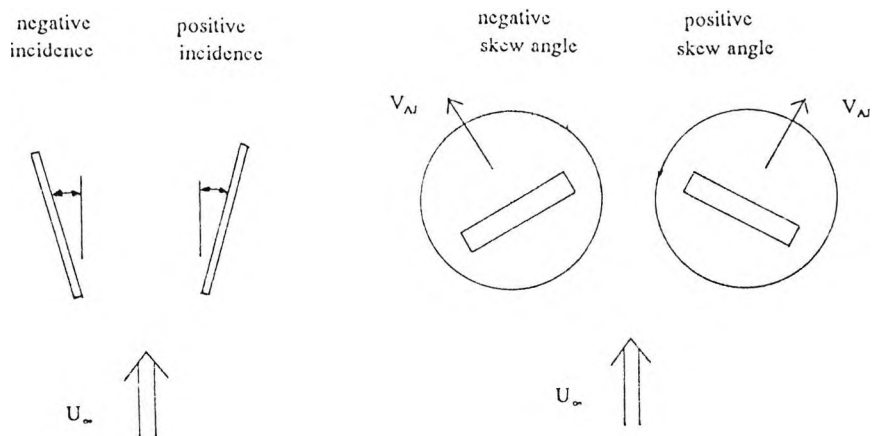
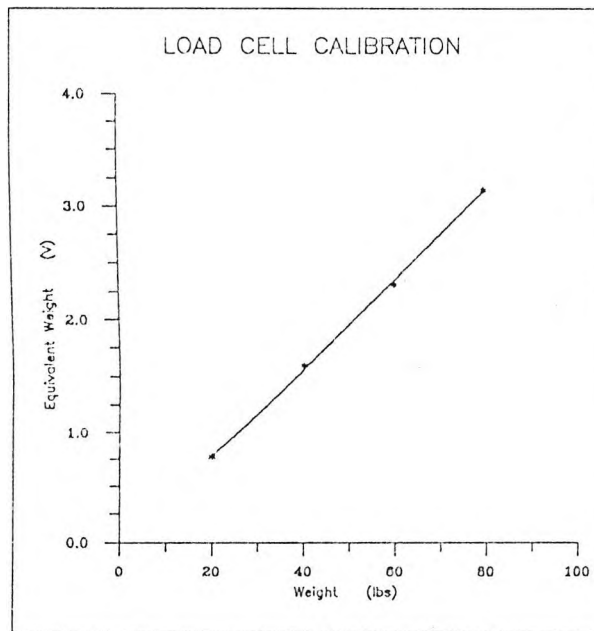


Fig. 3.2 Definition of positive and negative skew angle.



6 Nov 1990

Fig. 3.3 Static load cell calibration curve.

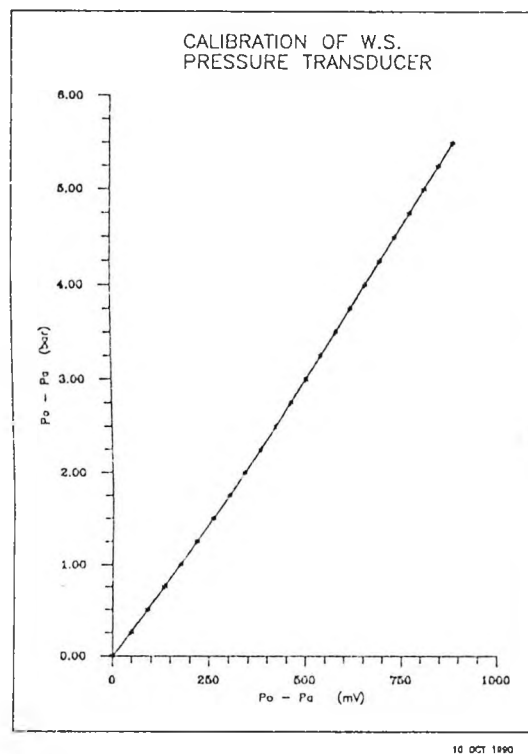
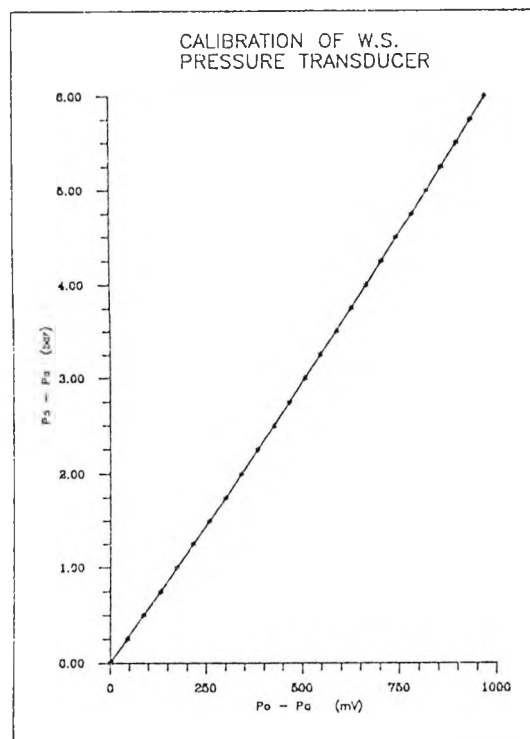
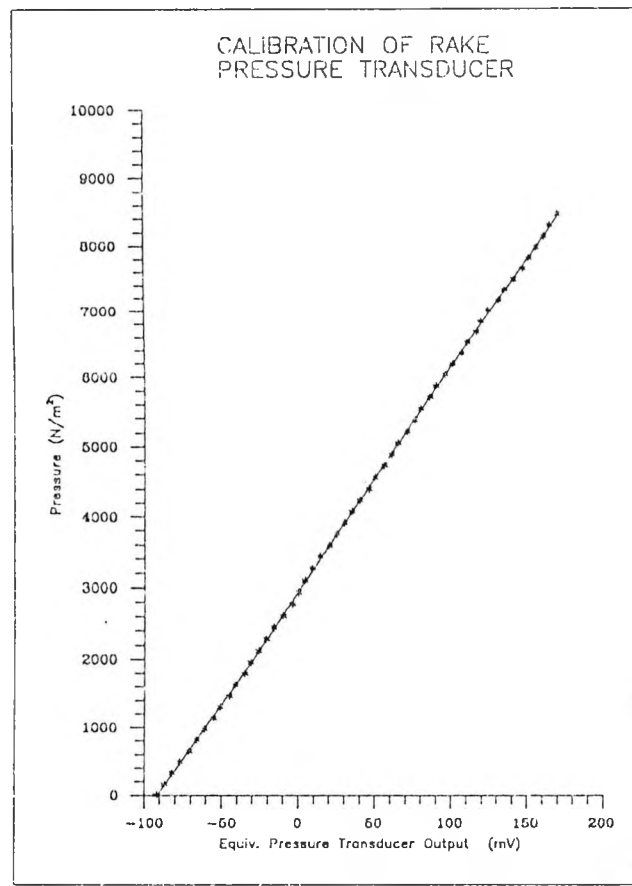
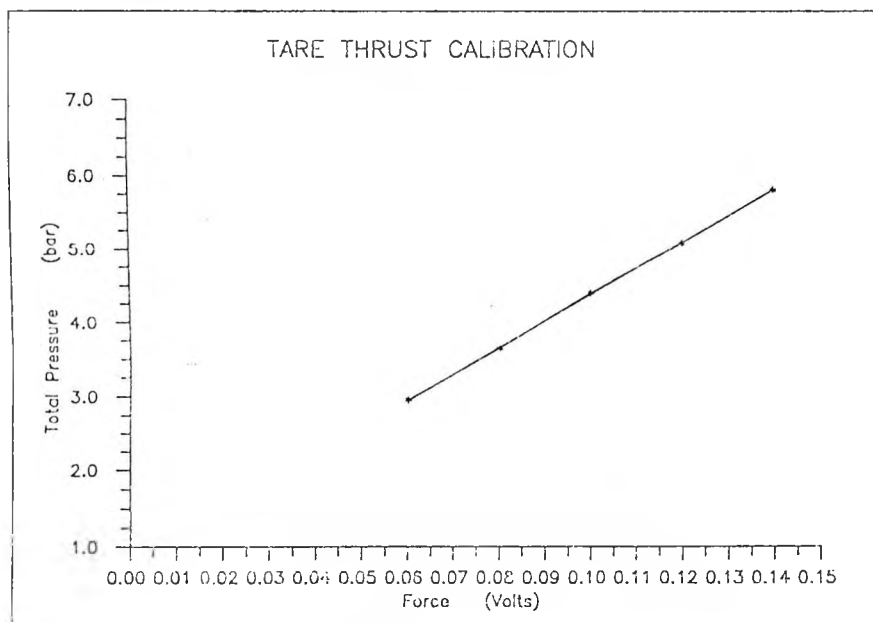


Fig. 3.4a and 3.4b Pressure transducer calibration curves.



10 OCT 1990

Fig. 3.4c Relationship between pressure and transducer output voltage.



5 Nov 1990

Fig. 3.5 Tare thrust calibration curve.

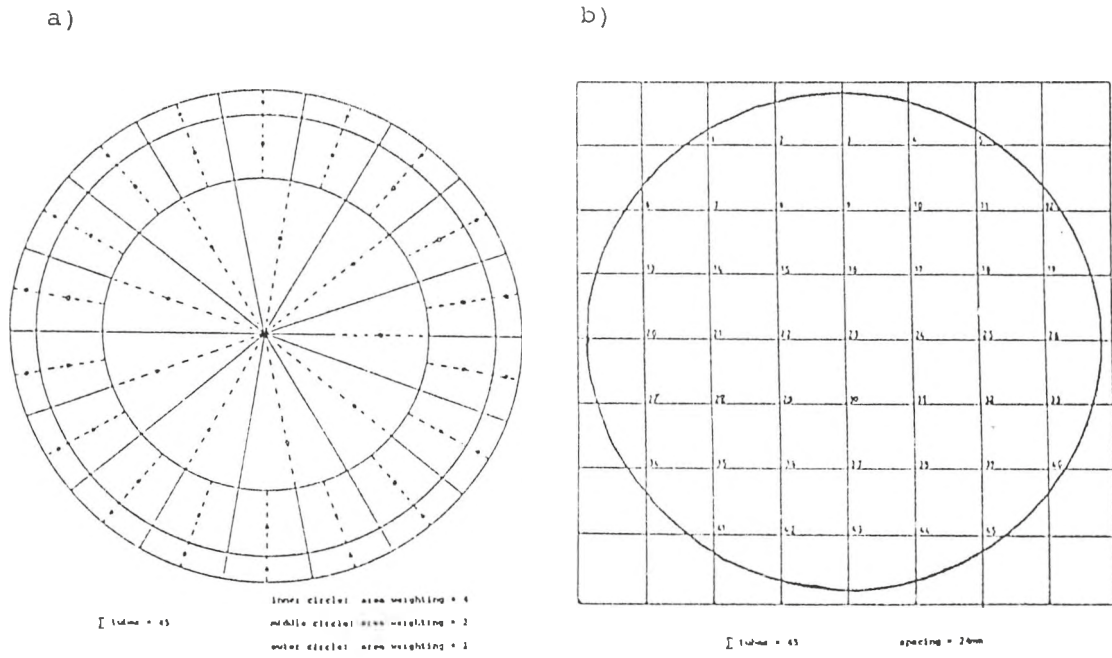


Fig. 3.6a and 3.6b Radial and equi-spaced rake distribution grid.

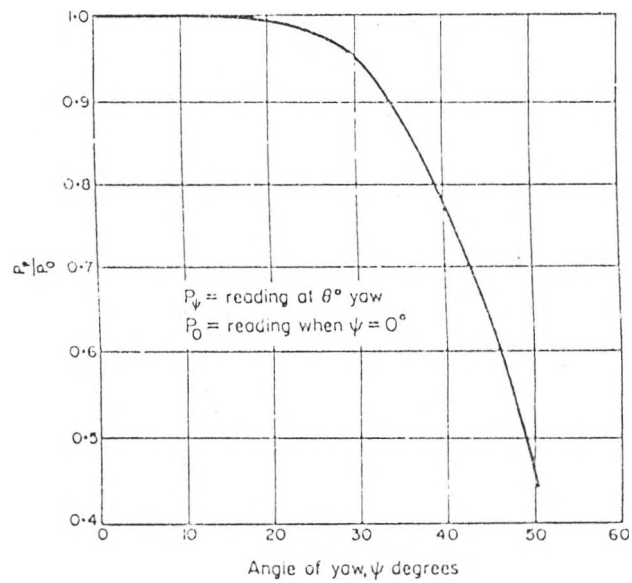
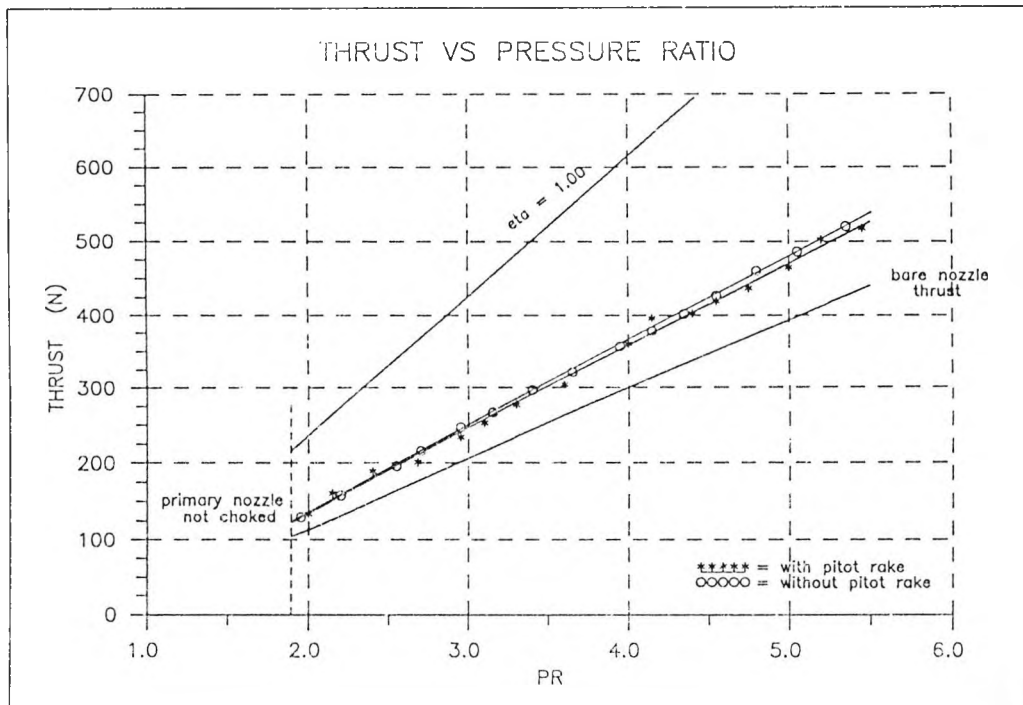
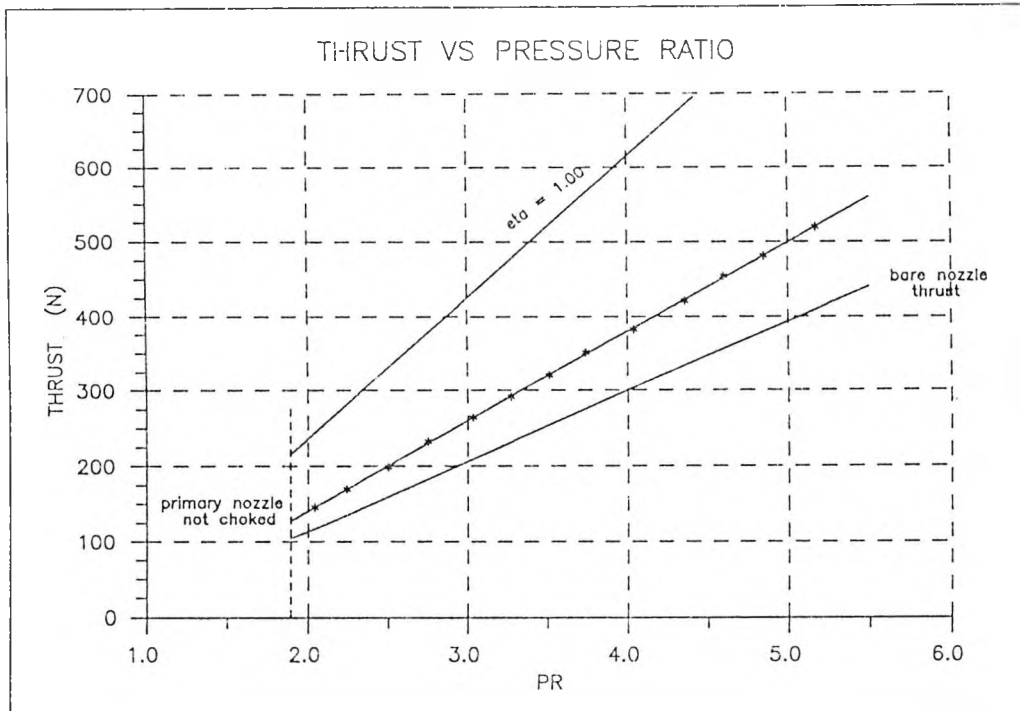


Fig. 3.7 Measuring losses in dynamic pressure due to yaw angle.



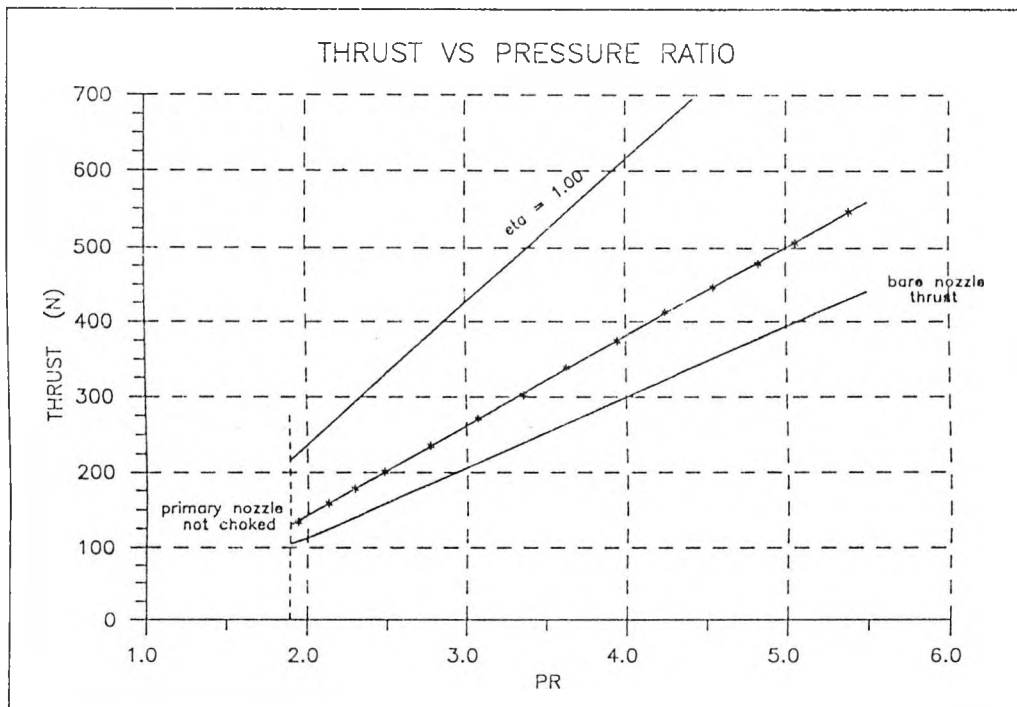
11 Oct 1990

Fig. 4.1 Plot of thrust vs pressure ratio for bare augmentor with and without the pitot rake installed.



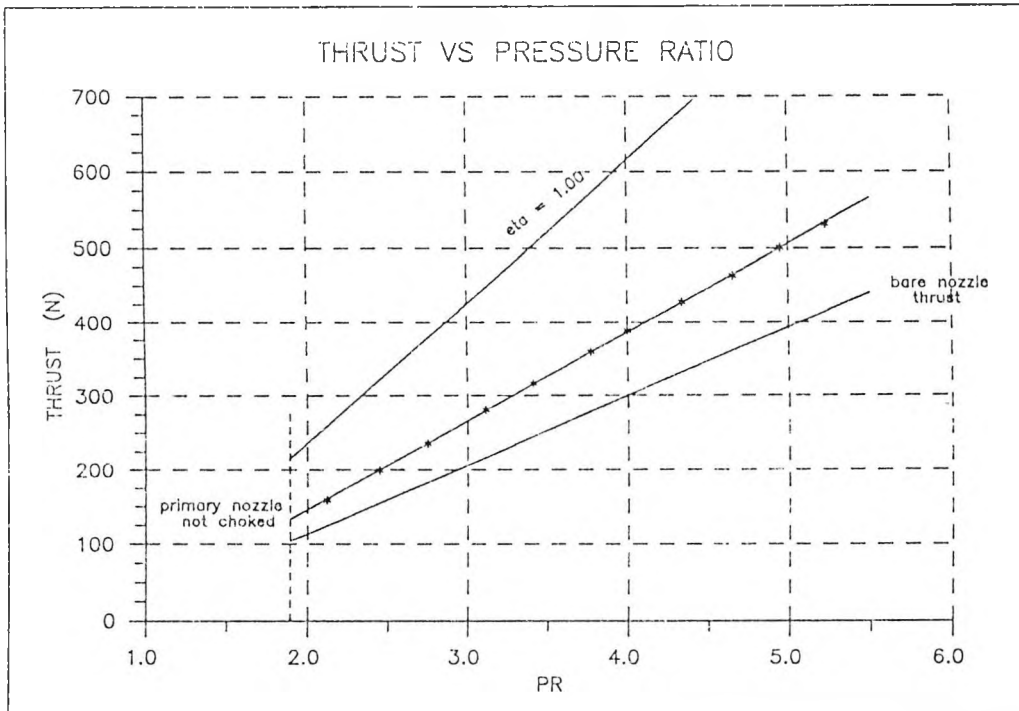
5 June 1990

Fig. 4.2a Thrust vs pressure ratio with co-rotating vane vortex generators and vane angle of incidence = 13°



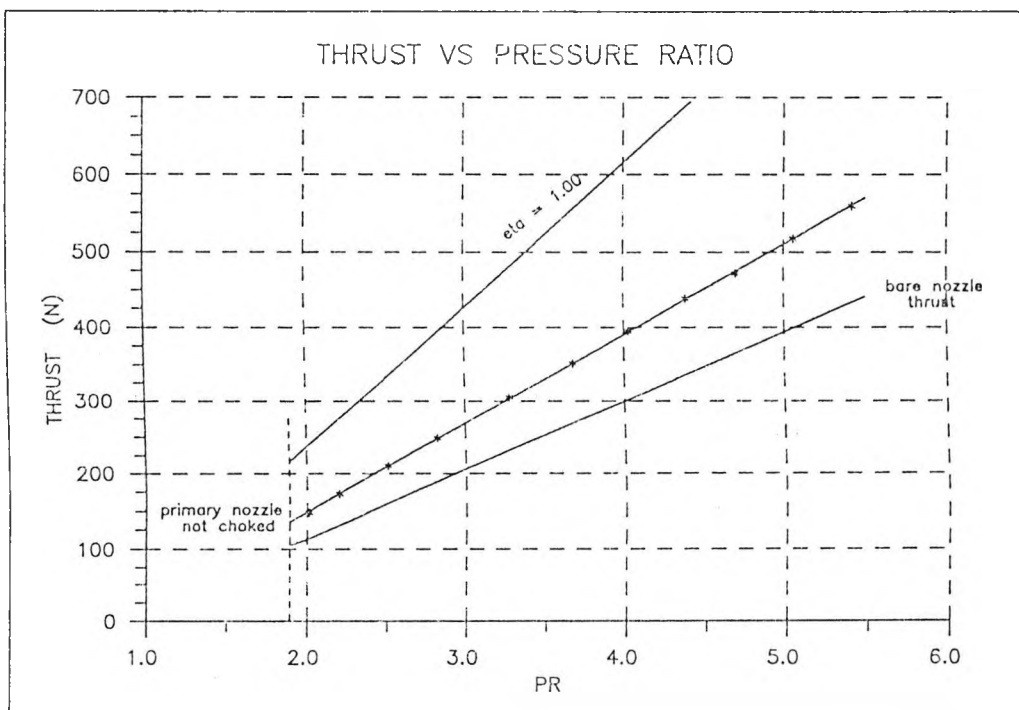
5 June 1990

Fig. 4.2b Thrust vs pressure ratio with co-rotating vane vortex generators and vane angle of incidence = 14°



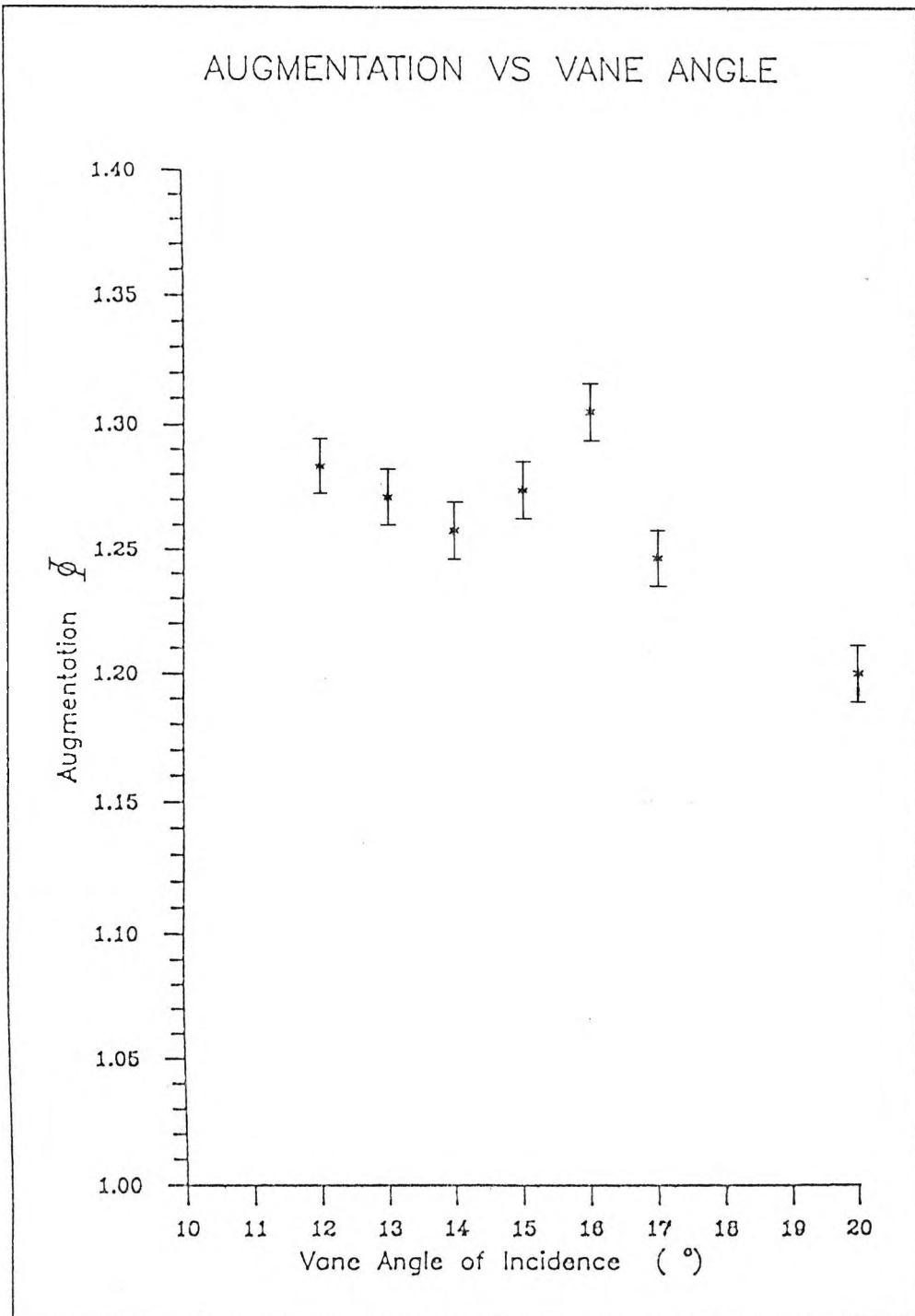
5 June 1990

Fig. 4.2c Thrust vs pressure ratio with co-rotating vane vortex generators and vane angle of incidence = 15°



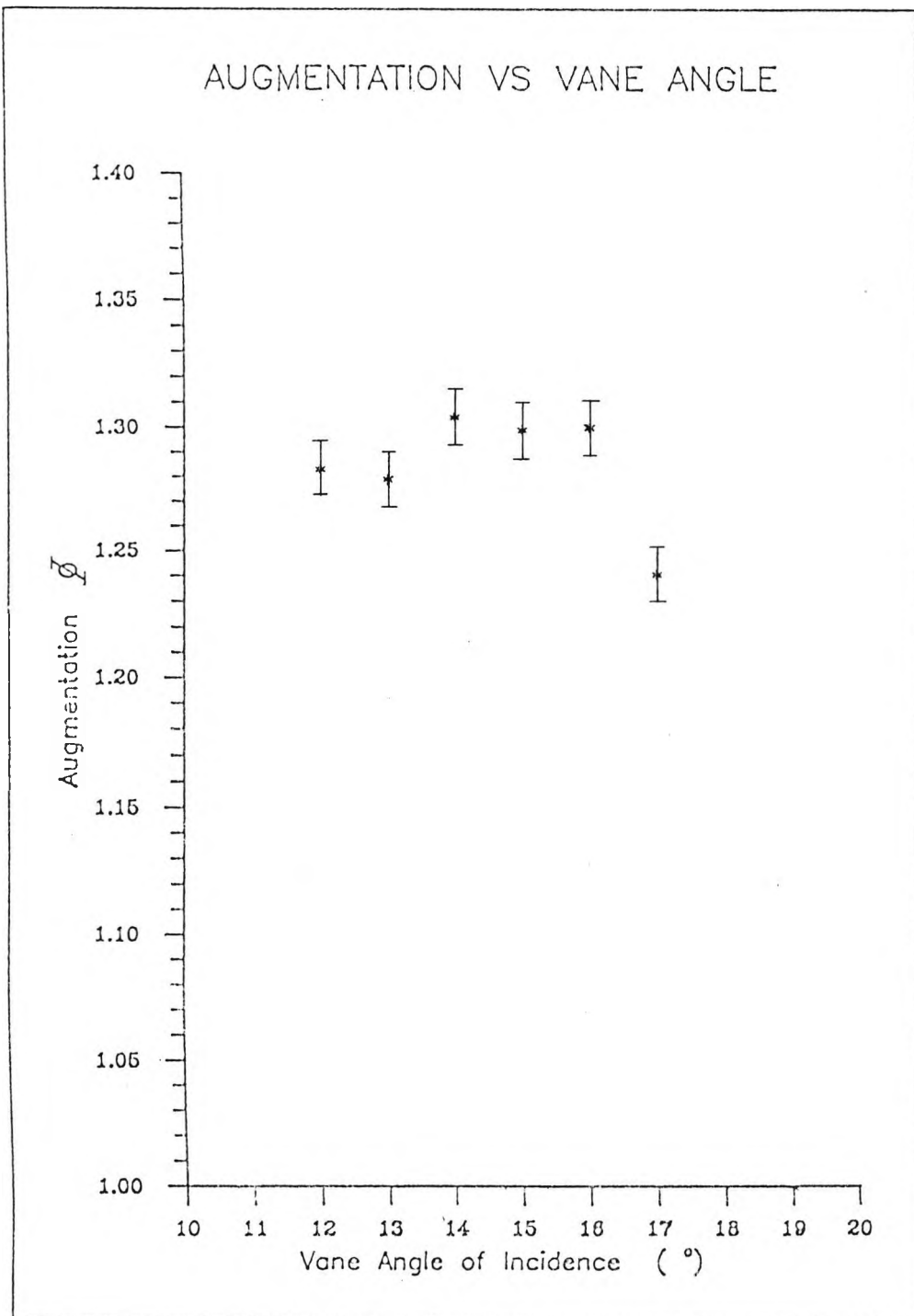
5 June 1990

Fig. 4.2d Thrust vs pressure ratio with co-rotating vane vortex generators and vane angle of incidence = 16°



2 NOV 1990

Fig. 4.3 Plot of augmentation vs vane angle of incidence for modified augmentor including co-rotating vane vortex generators.



2 NOV 1990

Fig. 4.4 Plot of augmentation vs vane angle of incidence for modified augmentor including contra-rotating vane vortex generator pairs.

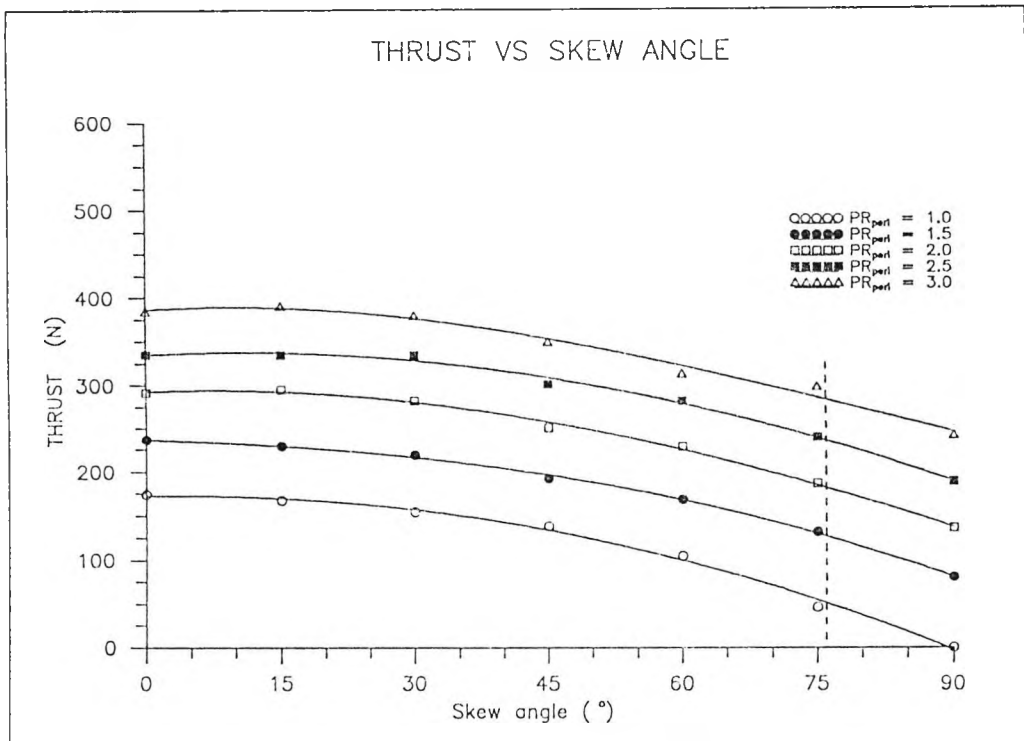


Fig. 4.5 Co-rot. AJVGs: Thrust versus skew angle, varying PR_{peri}
constant $PR_{AVG} = 2.0$

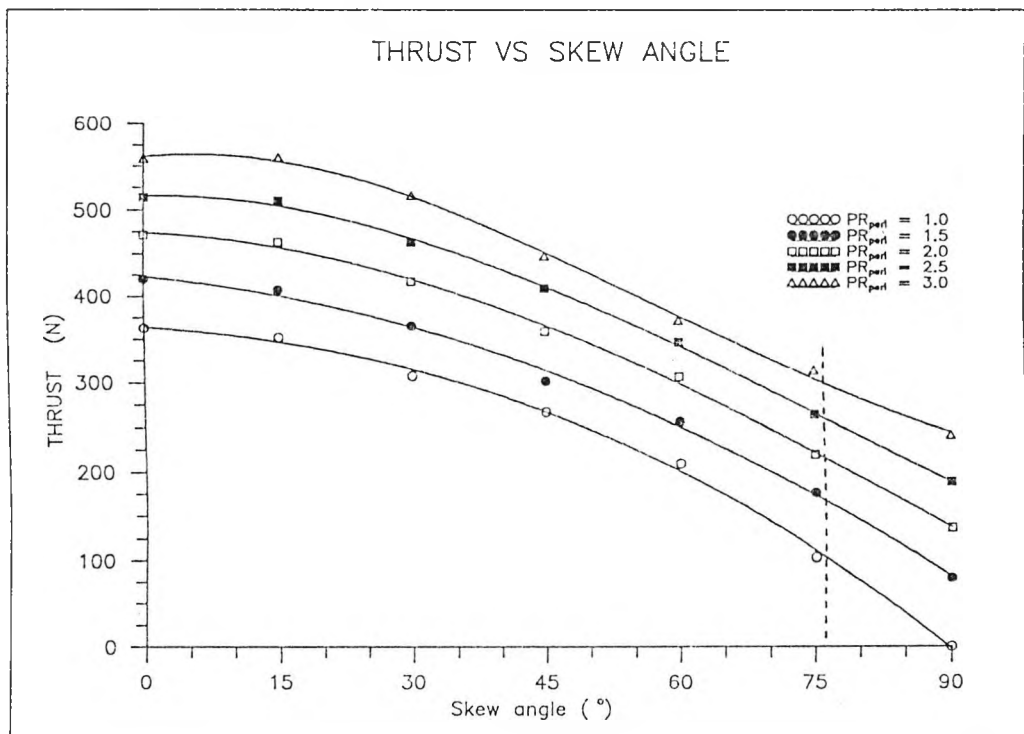
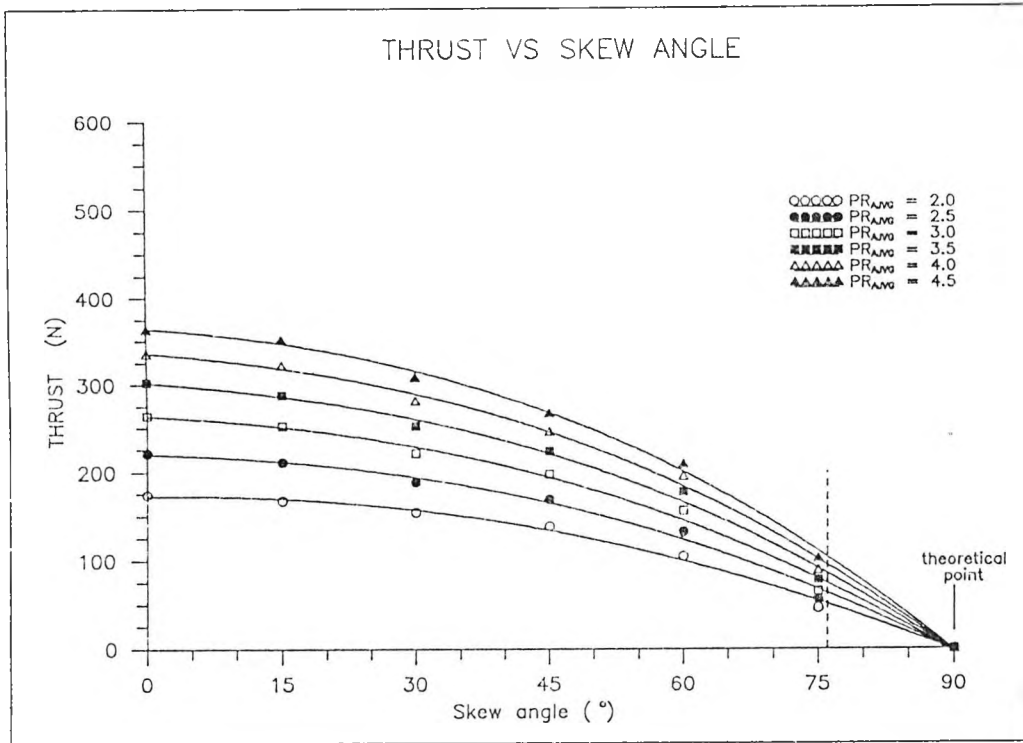
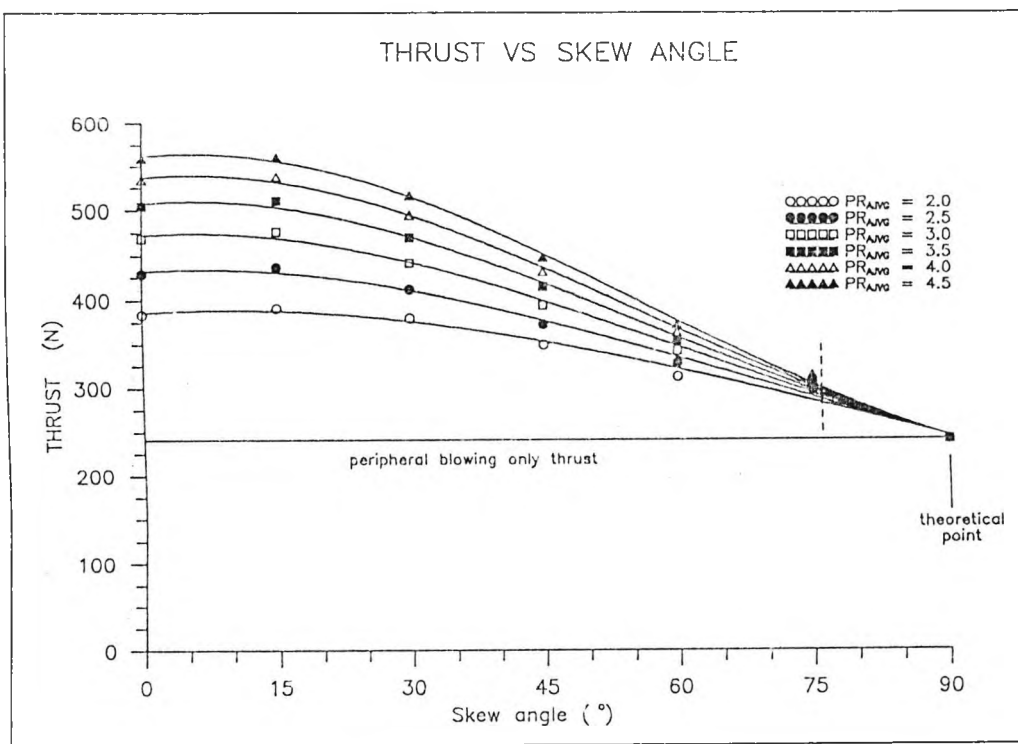


Fig. 4.6 Co-rot. AJVGs: Thrust versus skew angle, varying PR_{peri}
constant $PR_{AVG} = 4.5$



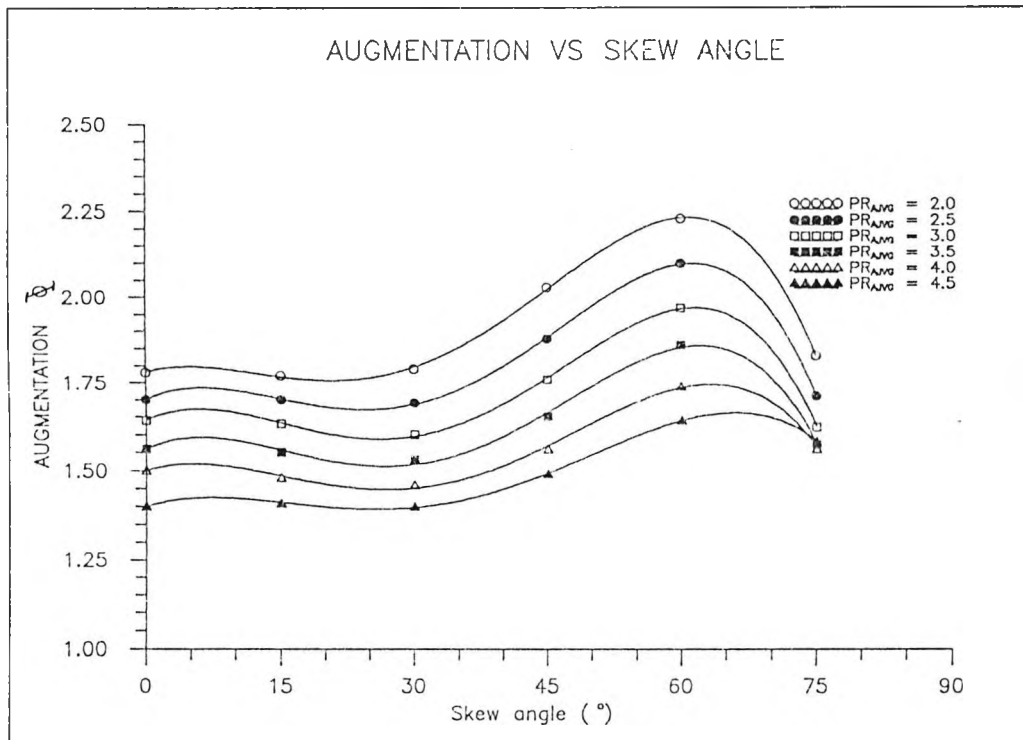
8 Jun 1991

Fig. 4.7 Co-rot. AJVGs: Thrust versus skew angle, varying PR_{AVG} no peripheral blowing



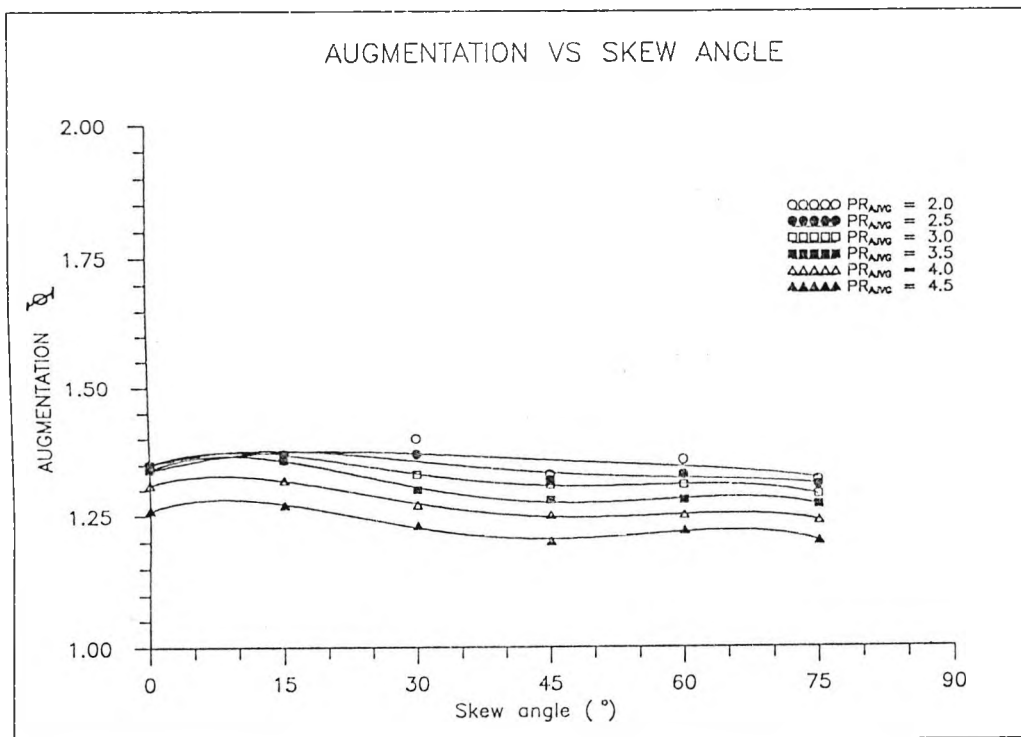
8 Jun 1991

Fig. 4.8 Co-rot. AJVGs: Thrust versus skew angle, varying PR_{AVG} constant $PR_{peri} = 3.0$



26 Jun 1991

Fig. 4.9 Co-rot. AJVGs: Augmentation versus skew angle, varying PR_{AVG} , no peripheral blowing



26 Jun 1991

Fig. 4.10 Co-rot. AJVGs: Augmentation versus skew angle, varying PR_{AVG} , constant $PR_{peri} = 2.5$

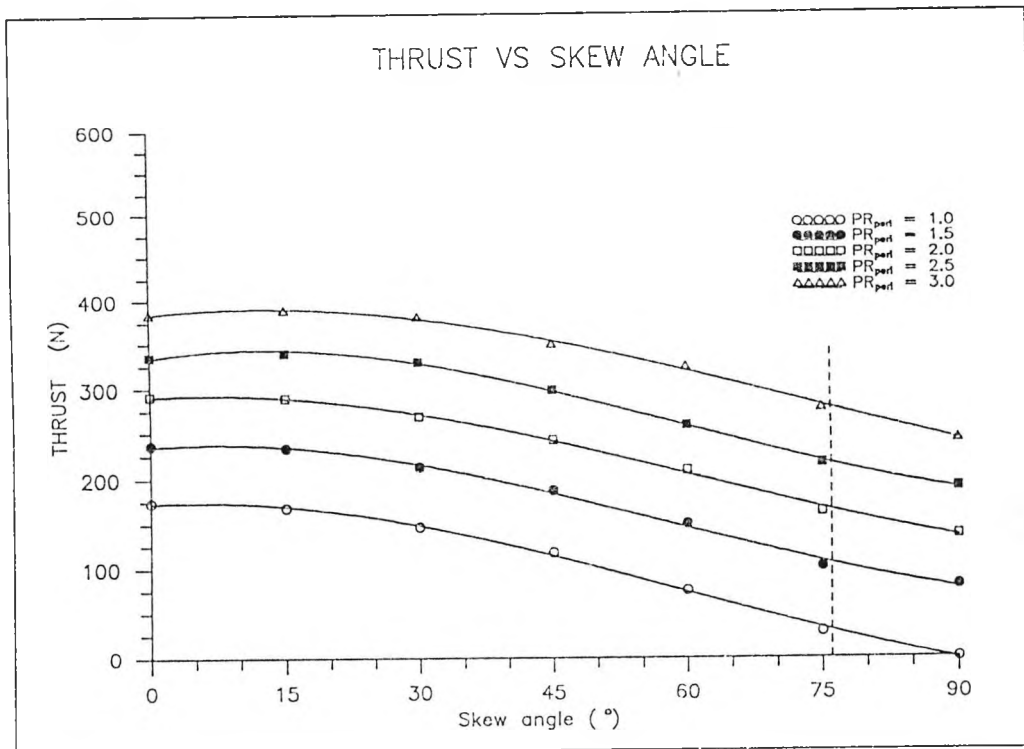


Fig. 4.11 Contra-rot. AJVG pairs: Thrust versus skew angle, varying PR_{peri} , constant $PR_{AVG} = 2.0$

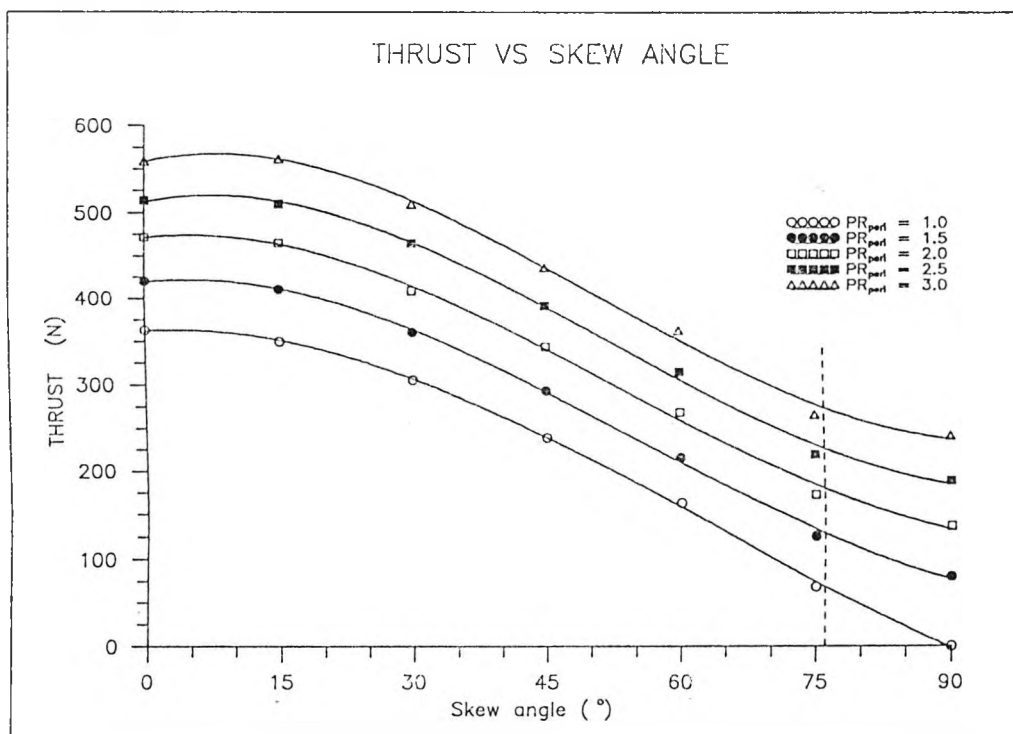
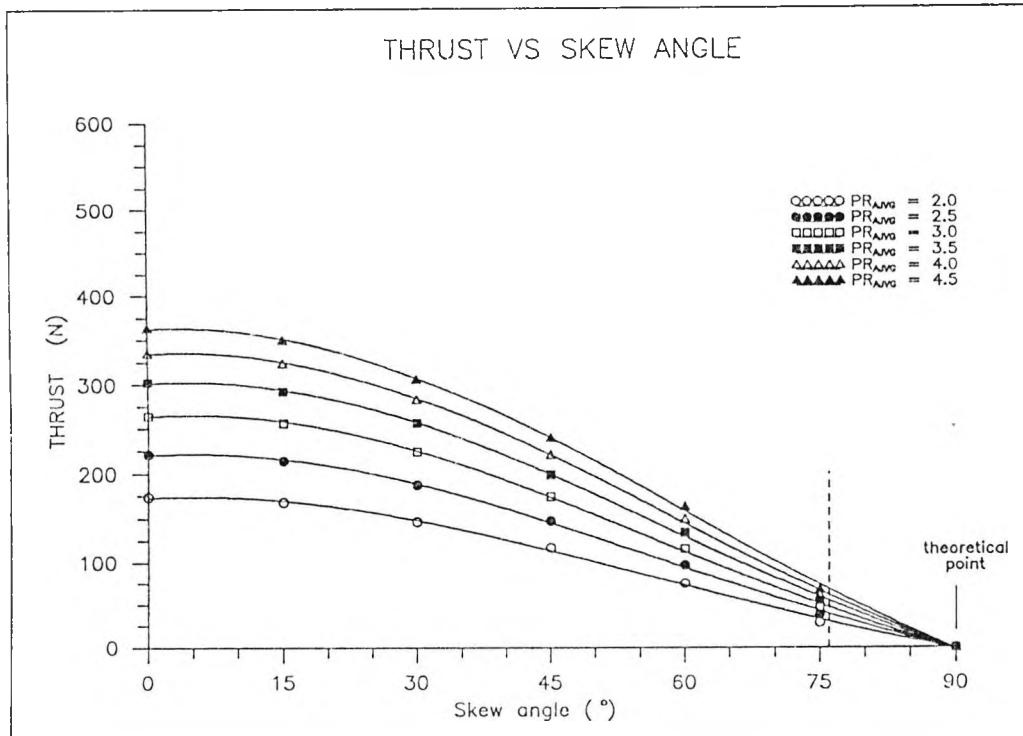
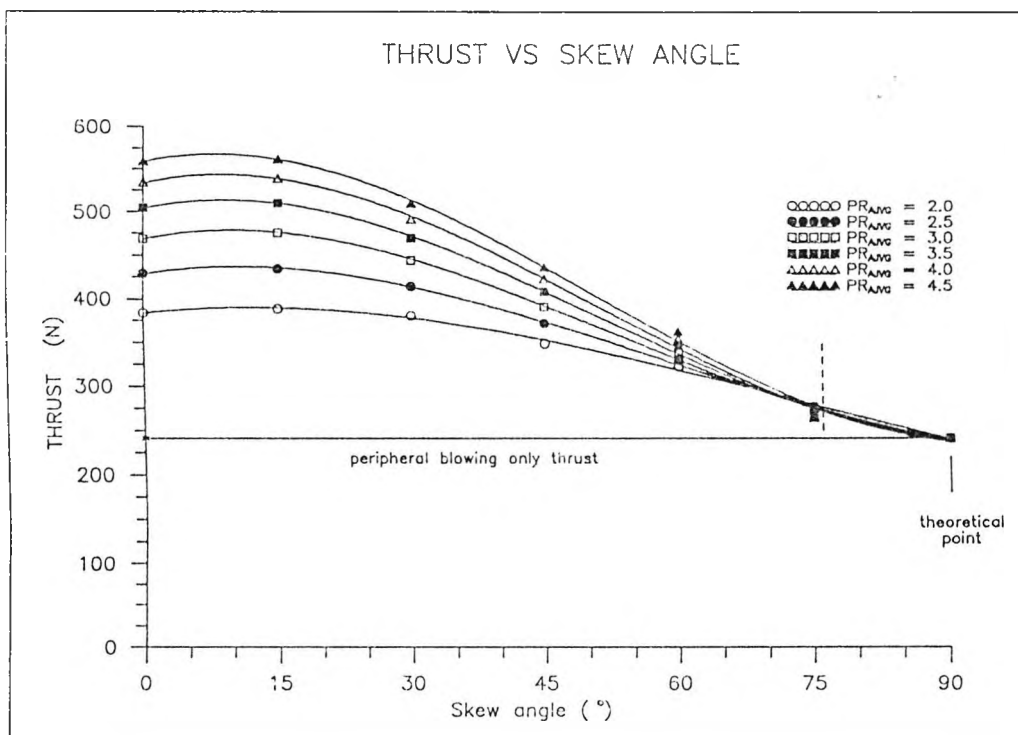


Fig. 4.12 Contra-rot. AJVG pairs: Thrust versus skew angle, varying PR_{peri} , constant $PR_{AVG} = 4.5$



25 Jun 1991

Fig. 4.13 Contra-rot. AJVG pairs: Thrust versus skew angle, varying PR_{AVG} , no peripheral blowing



25 Jun 1991

Fig. 4.14 Contra-rot. AJVG pairs: Thrust versus skew angle, varying PR_{AVG} , constant $PR_{peri} = 3.0$

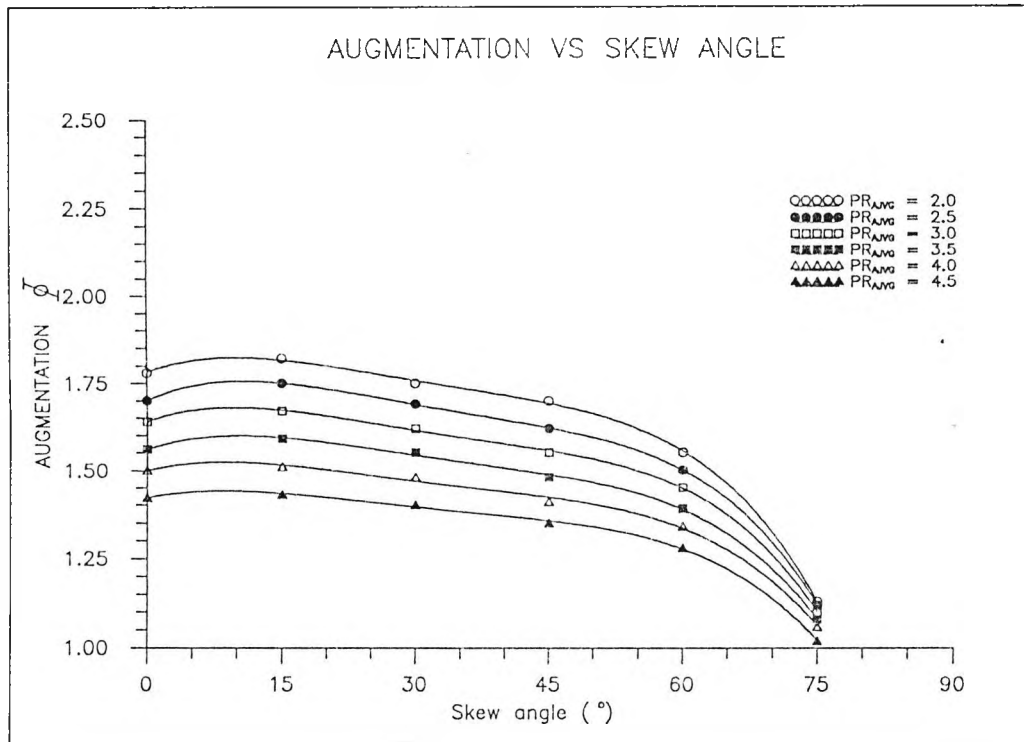


Fig. 4.15 Contra-rot. AJVG pairs: Augmentation versus skew angle, varying PR_{AJVG} , no periph. blowing

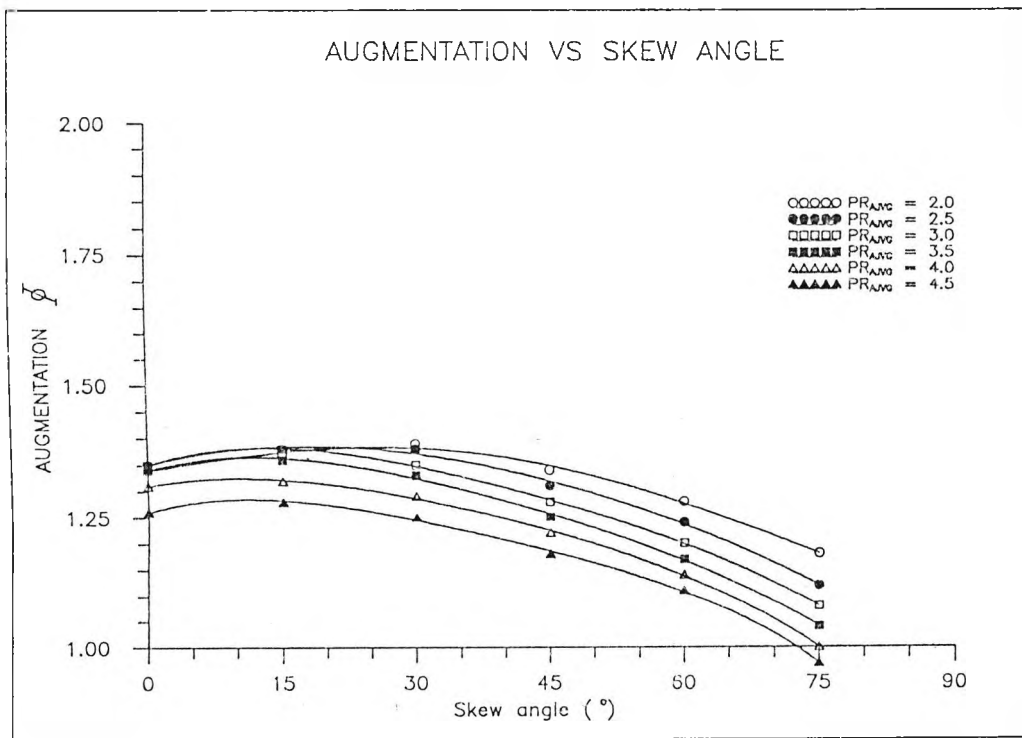
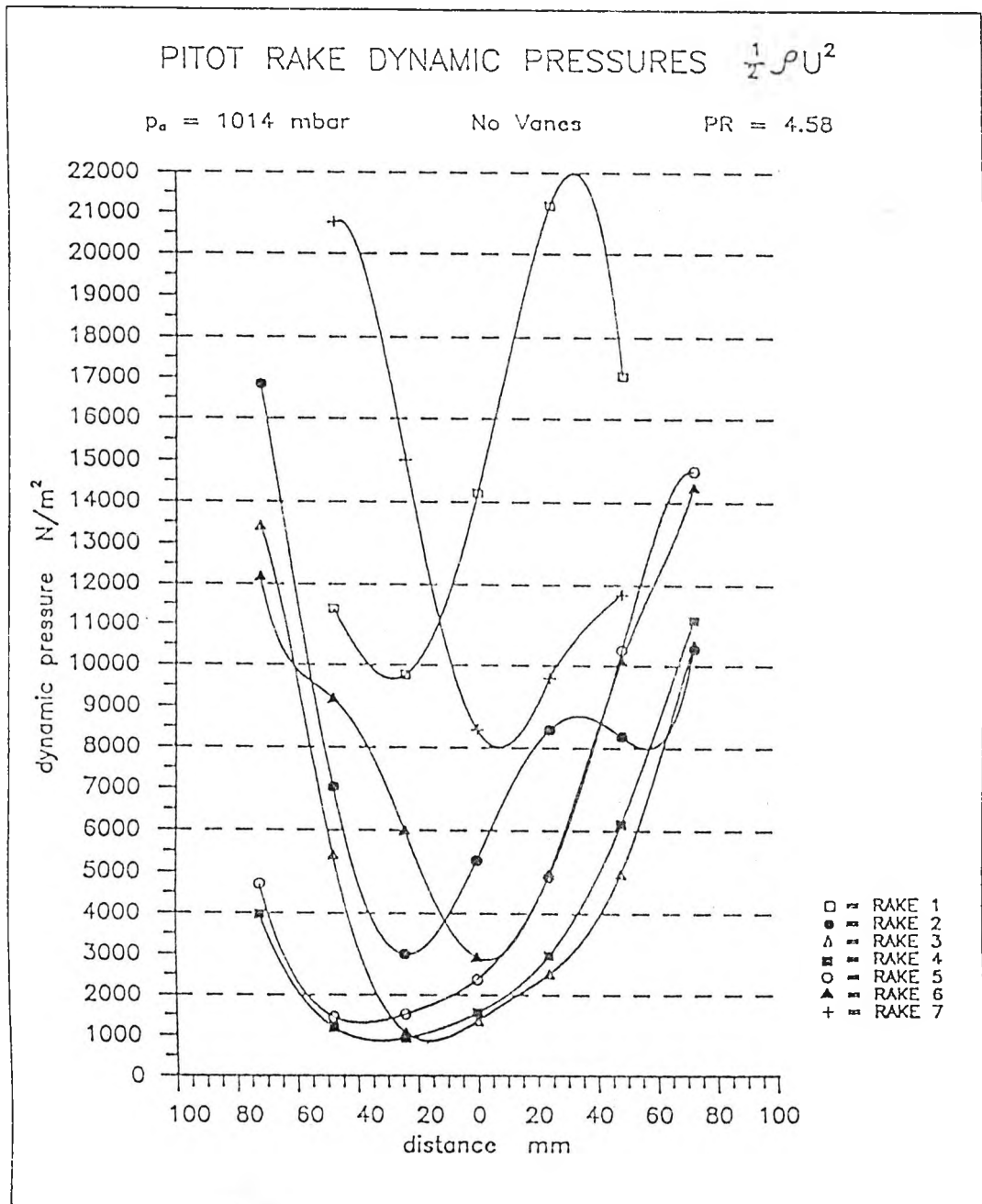


Fig. 4.16 Contra-rot. AJVG pairs: Augmentation versus skew angle, varying PR_{AJVG} , constant $PR_{peri} = 2.5$



20 OCT 1990

Fig. 5.1 Plot of dynamic pressures obtained through pitot rake in exit plane vs rake grid distance for bare augmentor.

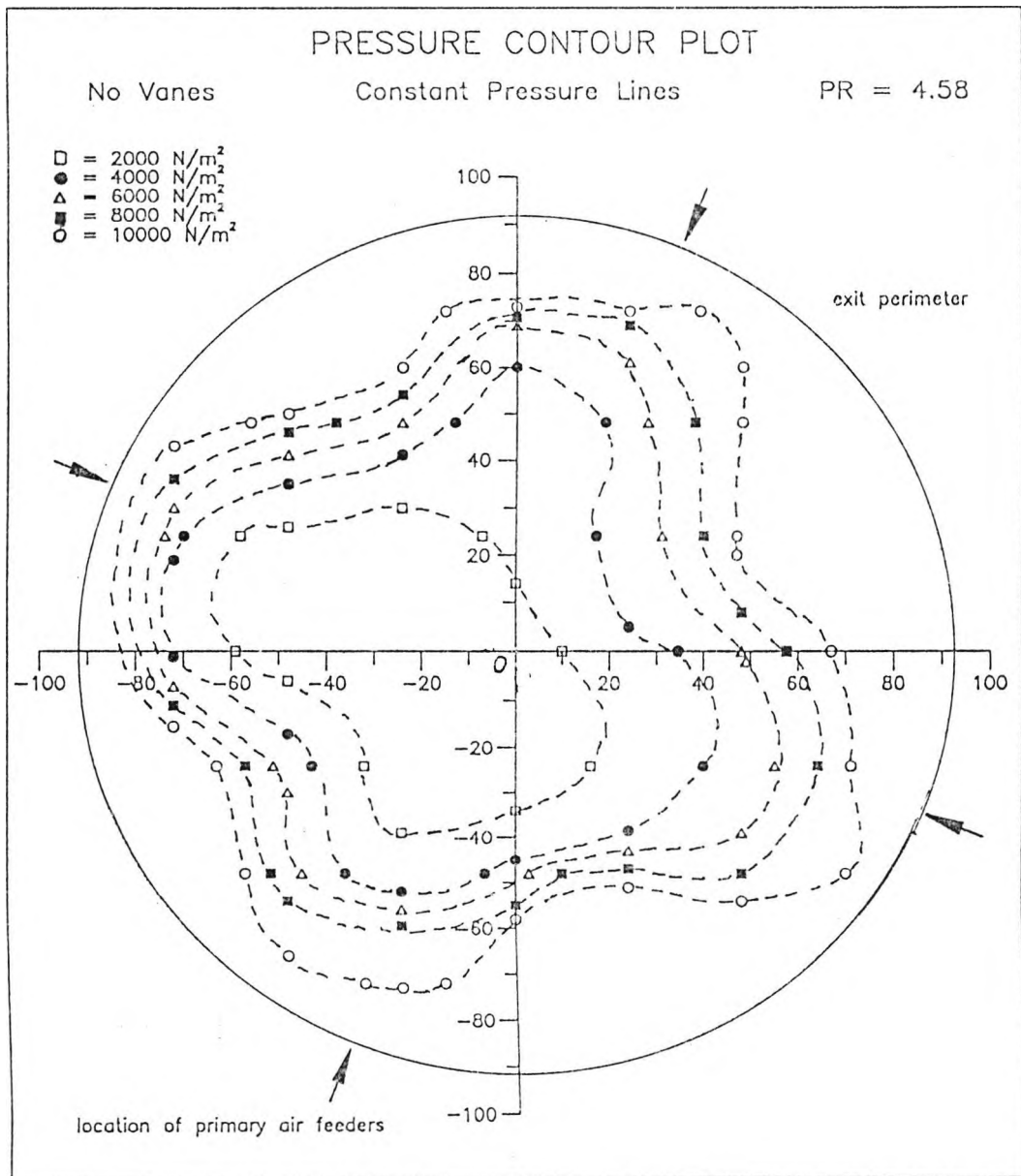


Fig. 5.2 Dynamic pressure contours in exit plane for bare augmentor; driving pressure ratio of peripheral jet = 4.58.

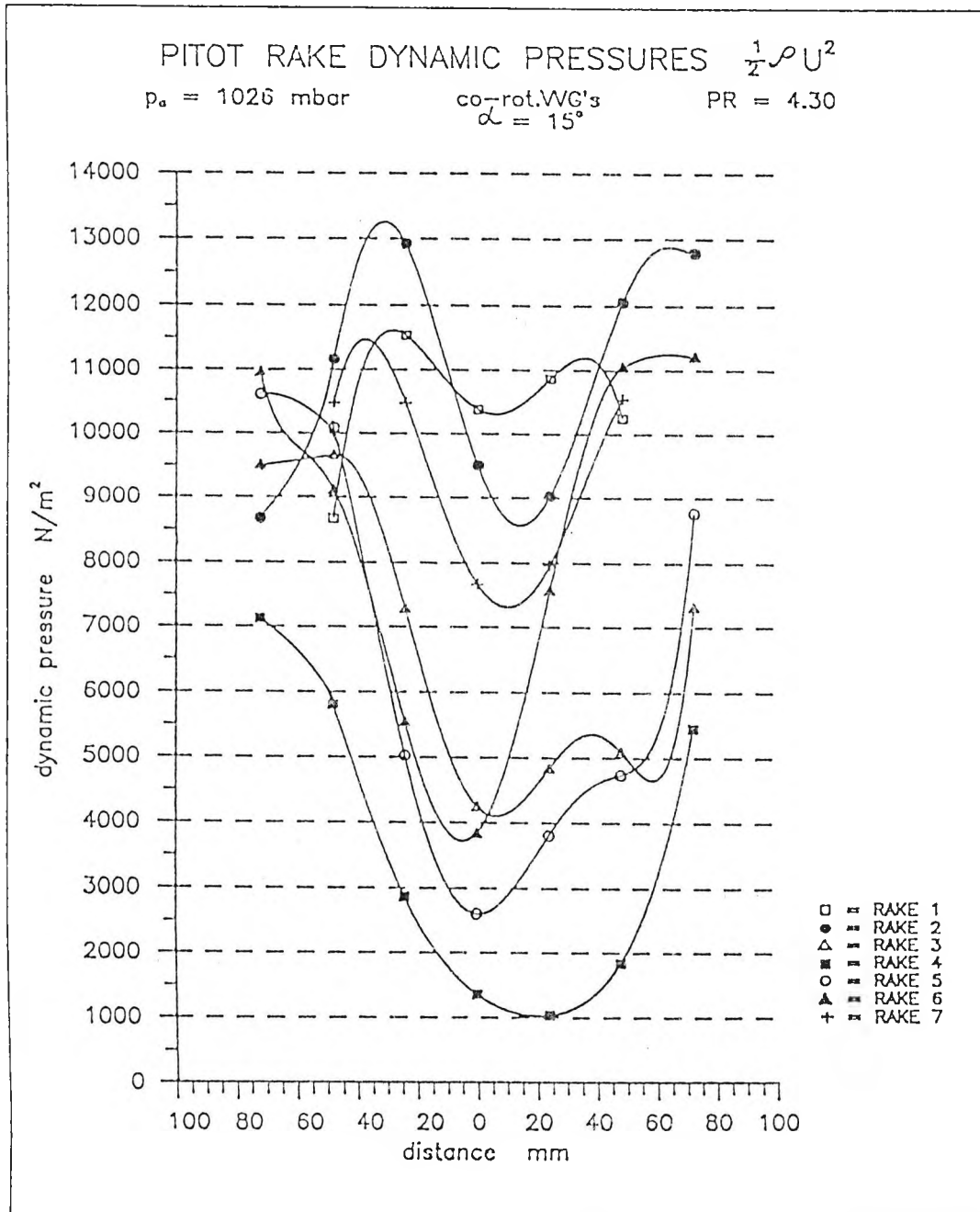


Fig. 5.3 Plot of dynamic pressures obtained through pitot rake in exit plane vs rake grid distance with co-rotating vane vortex generators.

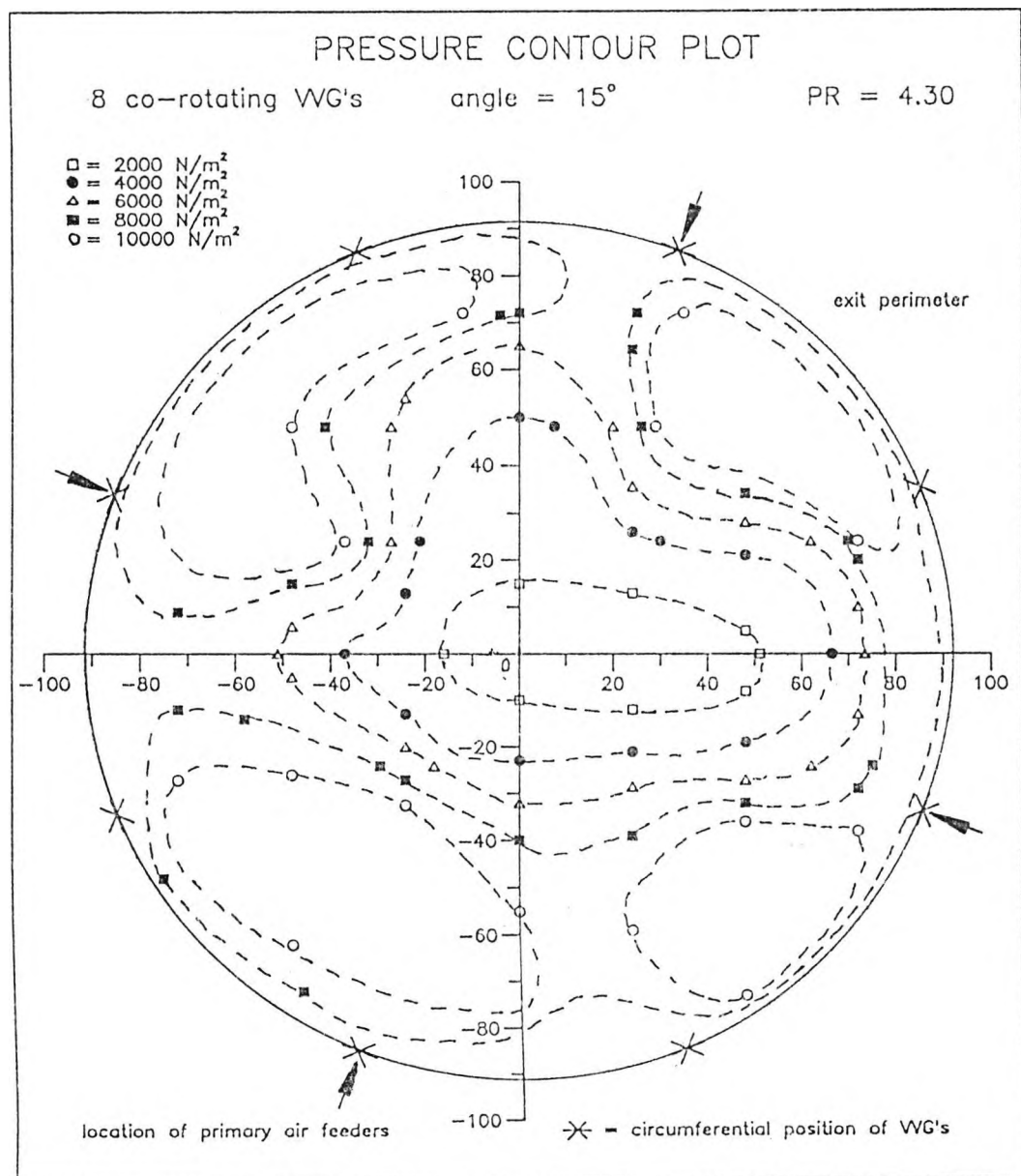


Fig. 5.4 Dynamic pressure contours in exit plane with co-rotating vane vortex generators; driving pressure ratio of peripheral jet = 4.30.

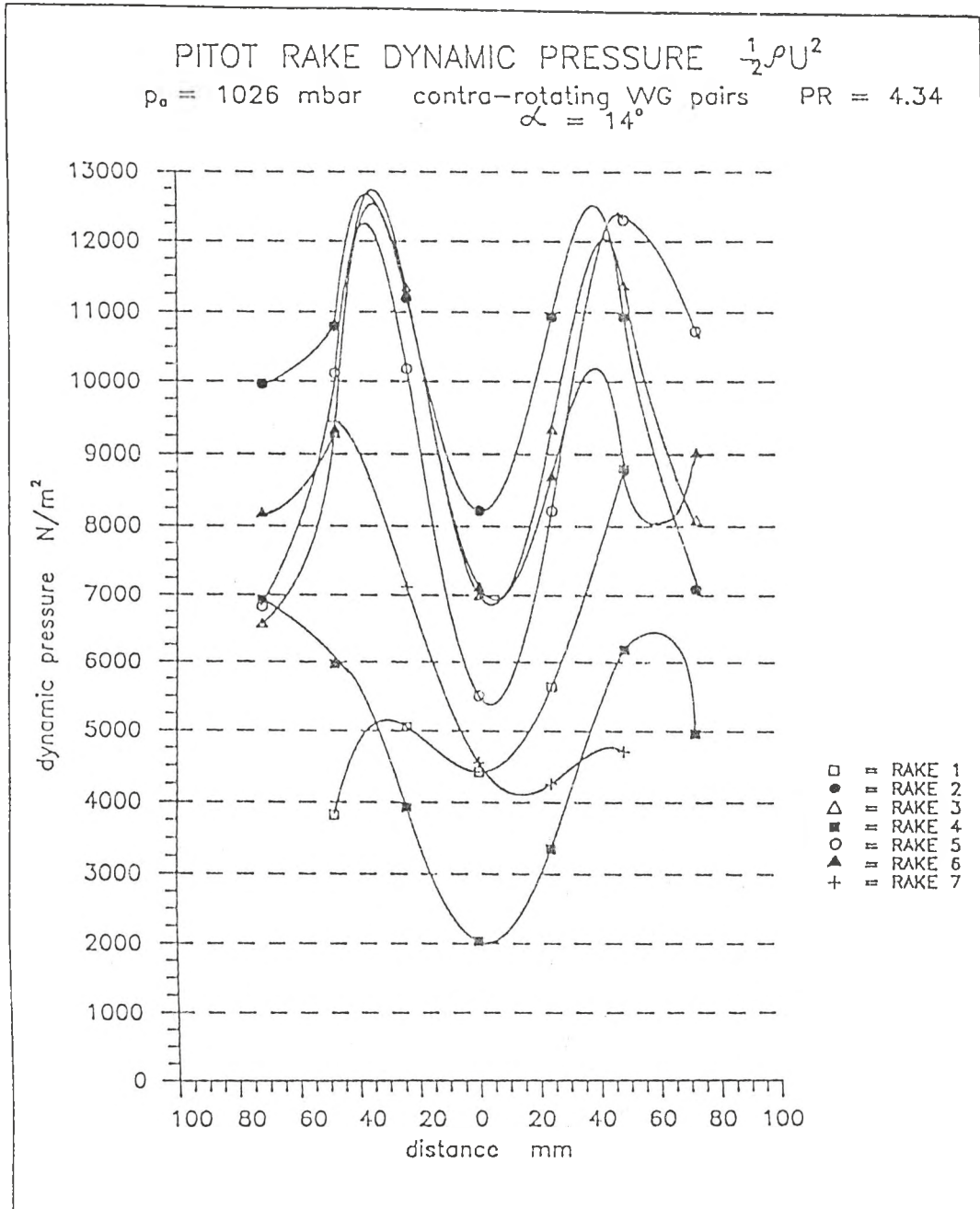


Fig. 5.5 Plot of dynamic pressures obtained through pitot rake in exit plane vs rake grid pairs distance with contra-rotating vane vortex generator pairs.

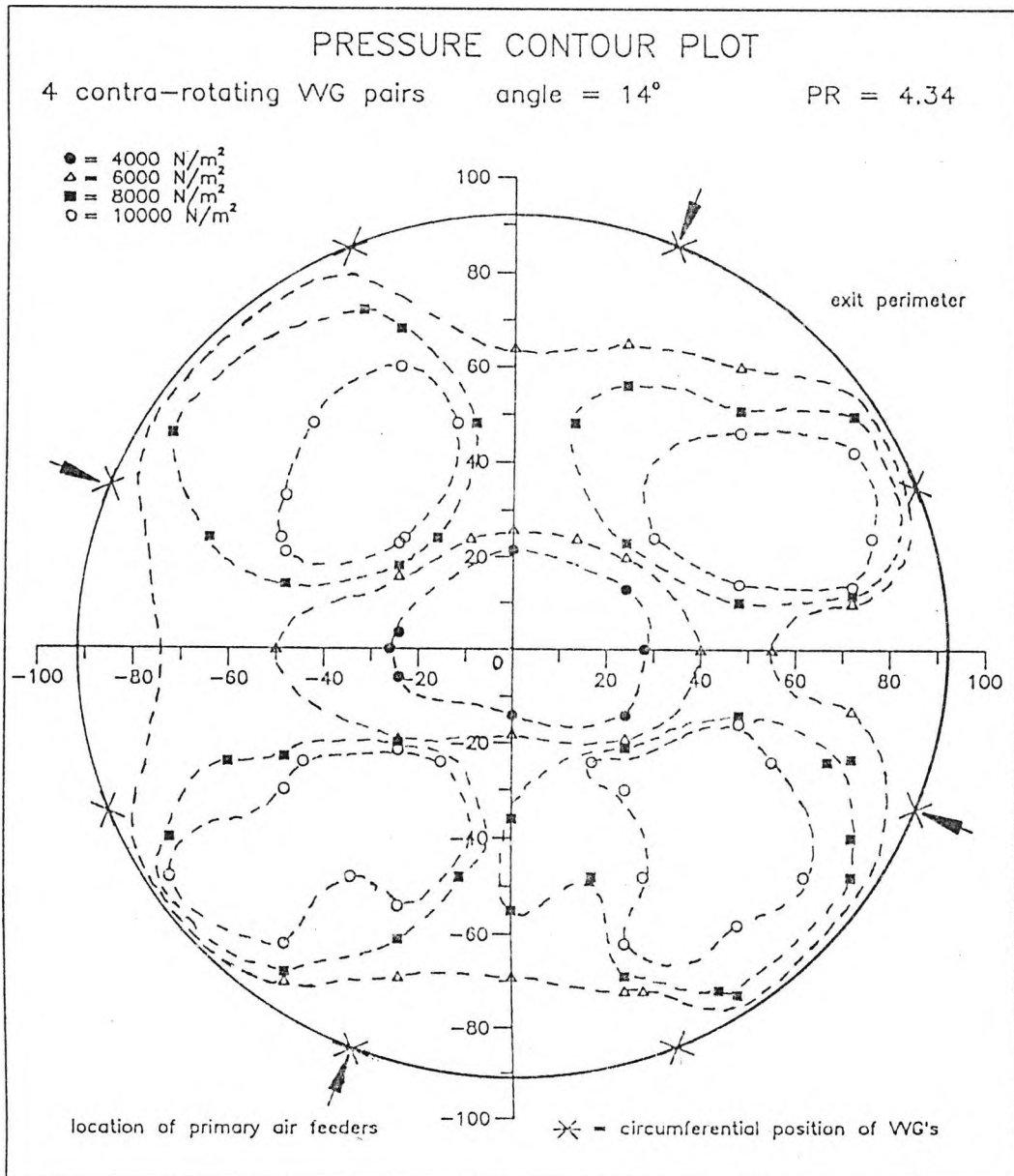
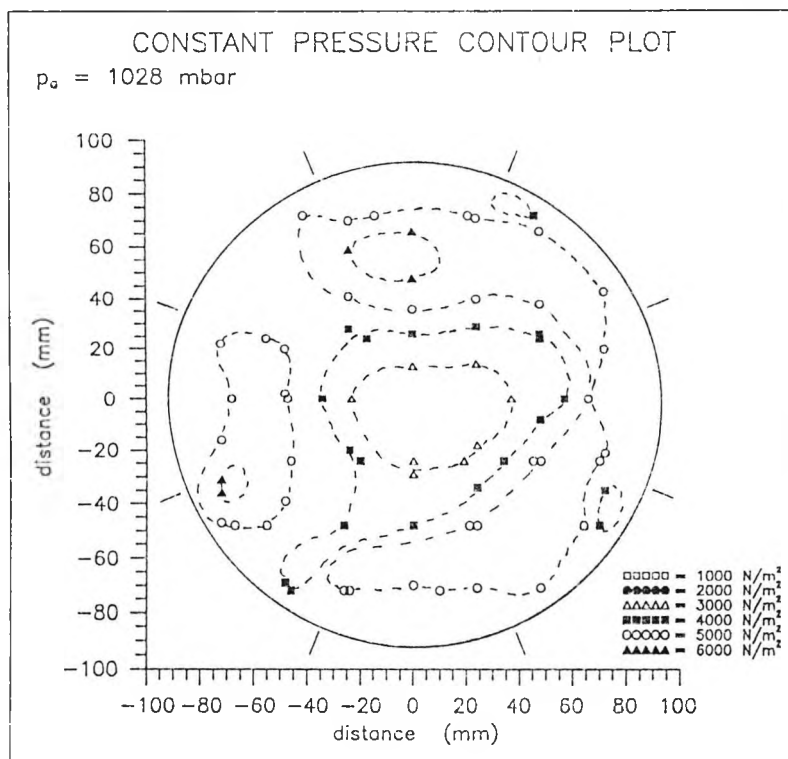
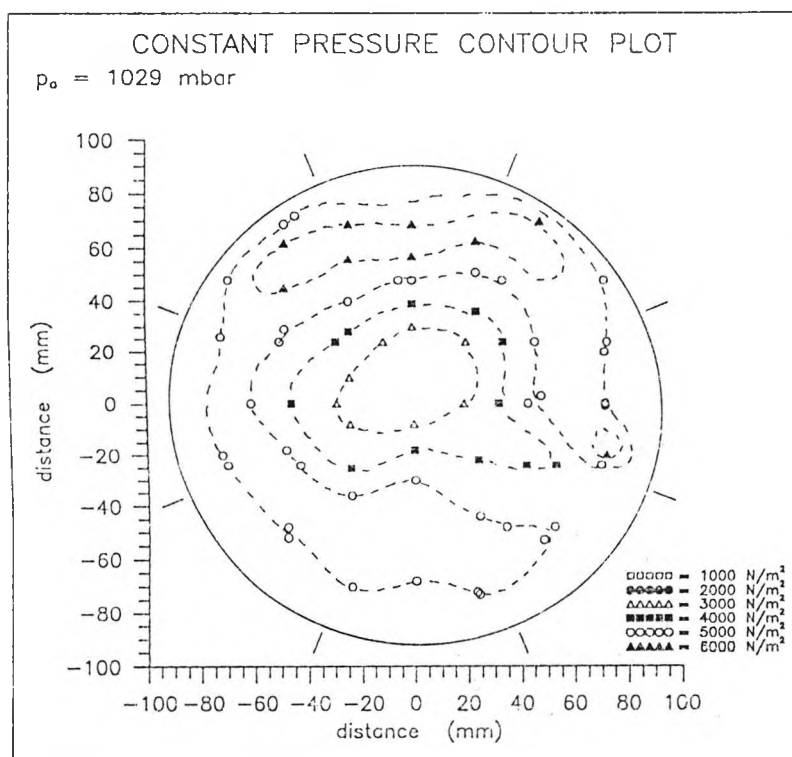


Fig. 5.6 Dynamic pressure contours in exit plane with contra-rotating vane vortex generator pairs; driving pressure ratio of peripheral jet = 4.34.



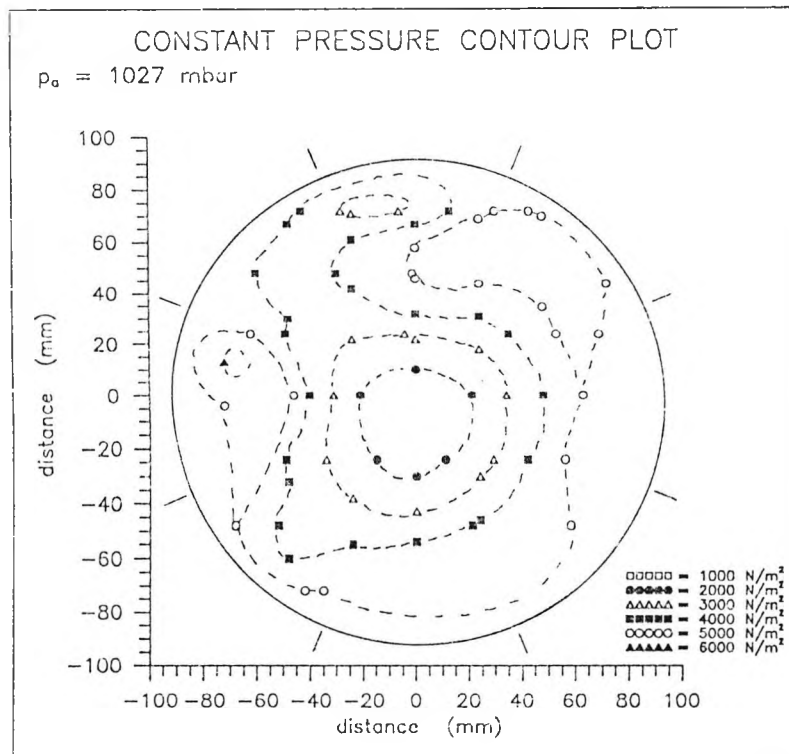
24 Sep. 1991

Fig. 5.7 No skew AJ blowing: Constant pressure contour plot, $\beta = 0^\circ$, $PR_{AVG} = 2.74$, no peripheral blowing



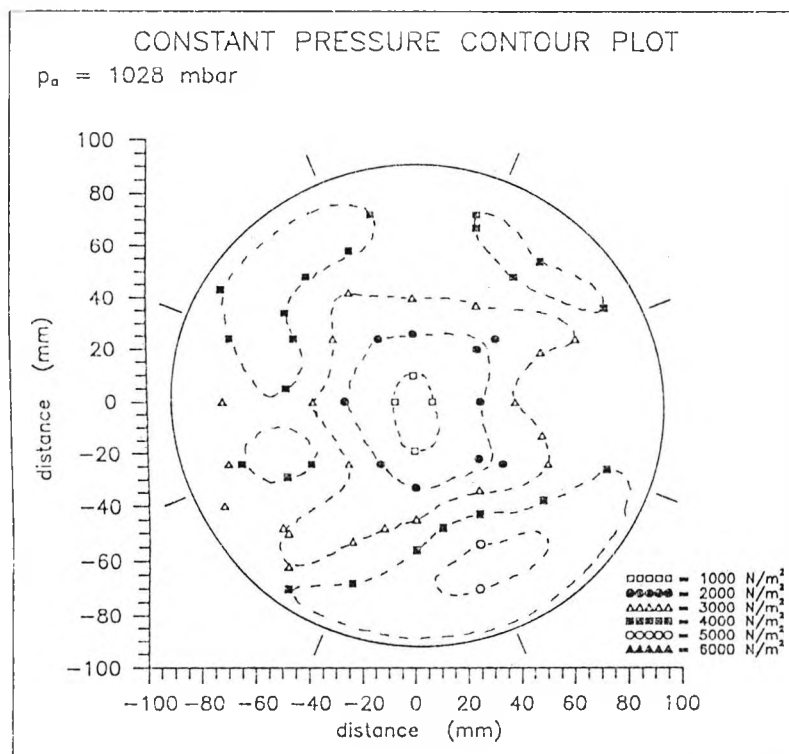
24 Sep. 1991

Fig. 5.8 Co-rotating AJVGs: Constant pressure contour plot, $\beta = 15^\circ$, $PR_{AVG} = 2.98$, no peripheral blowing



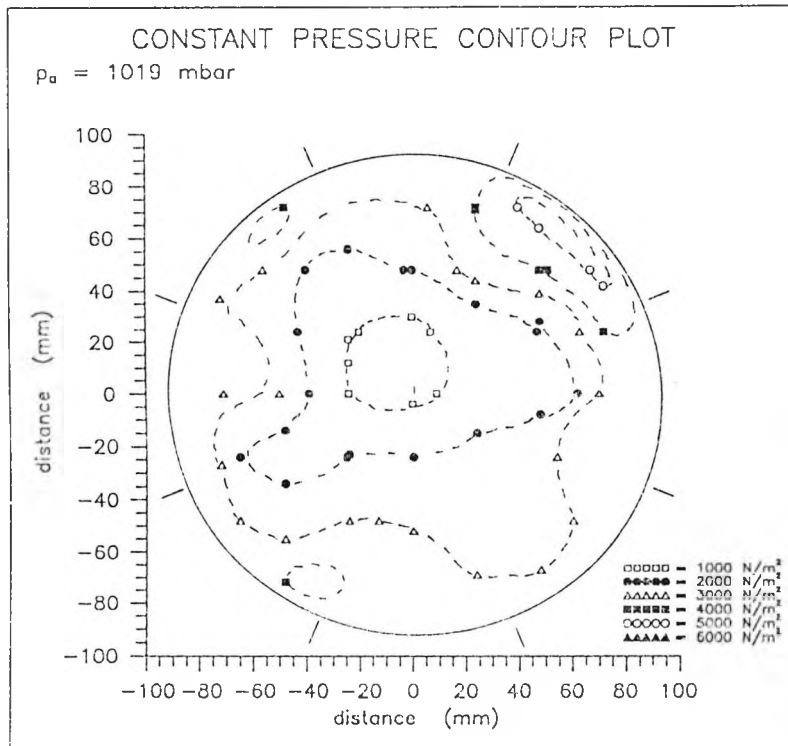
24 Sep. 1991

Fig. 5.9 Co-rotating AJVGs: Constant pressure contour plot, $\beta = 30^\circ$, $PR_{AJVG} = 2.89$, no peripheral blowing



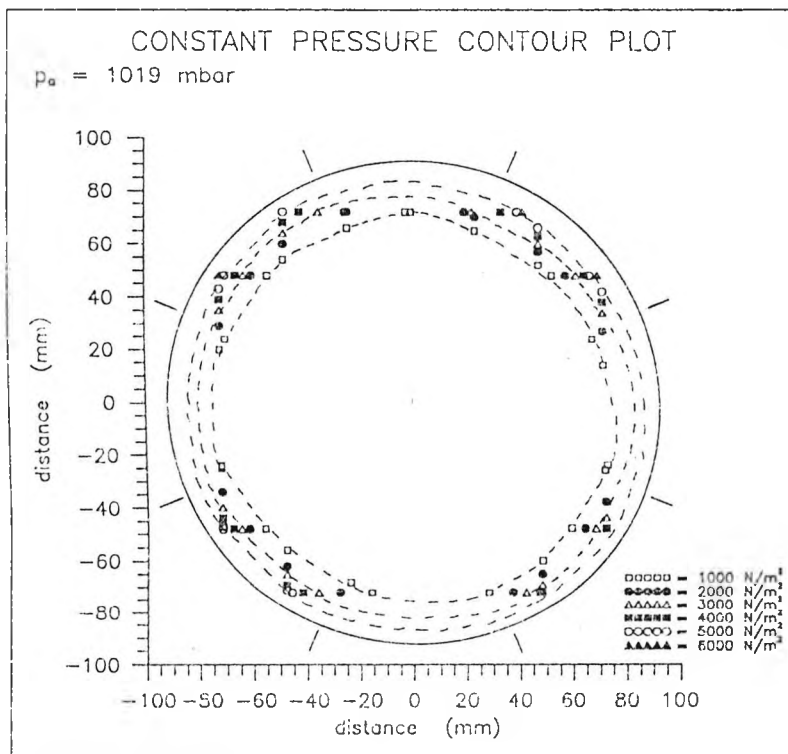
24 Sep. 1991

Fig. 5.10 Co-rotating AJVGs: Constant pressure contour plot, $\beta = 45^\circ$, $PR_{AJVG} = 2.84$, no peripheral blowing



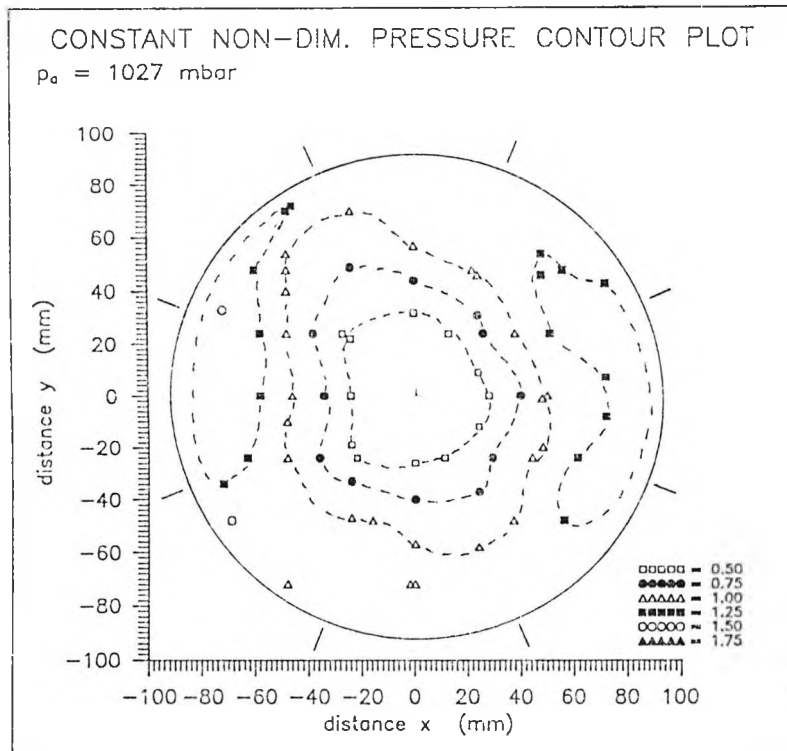
24 Sep. 1991

Fig. 5.11 Co-rotating AJVGs: Constant pressure contour plot, $\beta = 60^\circ$, $PR_{AVG} = 3.05$, no peripheral blowing



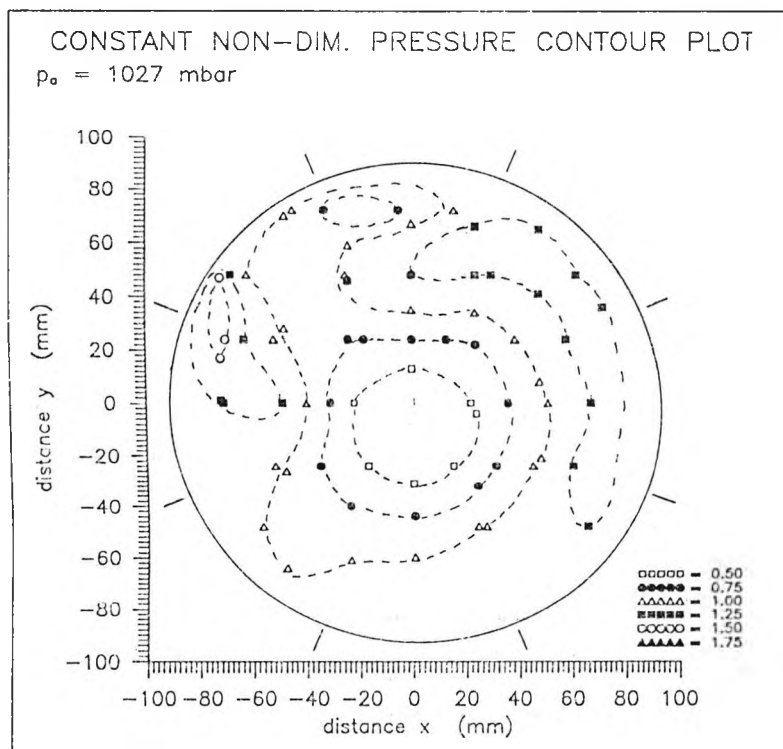
24 Sep. 1991

Fig. 5.12 Co-rotating AJVGs: Constant pressure contour plot, $\beta = 75^\circ$, $PR_{AVG} = 3.04$, no peripheral blowing



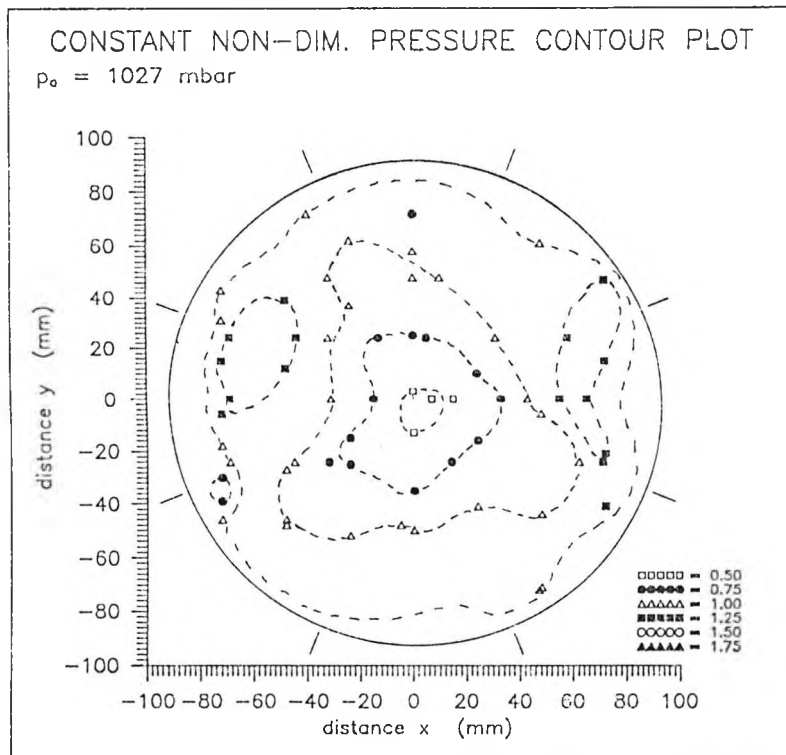
1 Nov. 1991

Fig. 5.13 Co-rotating AJVGs: Constant pressure contour plot,
 $\beta = 30^\circ$, $PR_{AVG} = 2.22$, no peripheral blowing



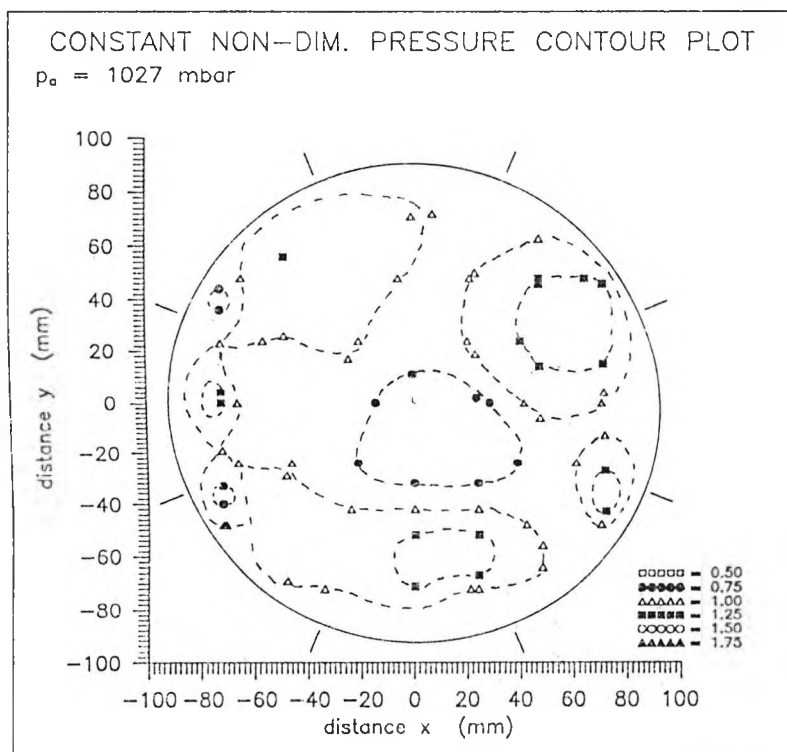
1 Nov. 1991

Fig. 5.14 Co-rotating AJVGs: Constant pressure contour plot,
 $\beta = 30^\circ$, $PR_{AVG} = 2.89$, no peripheral blowing



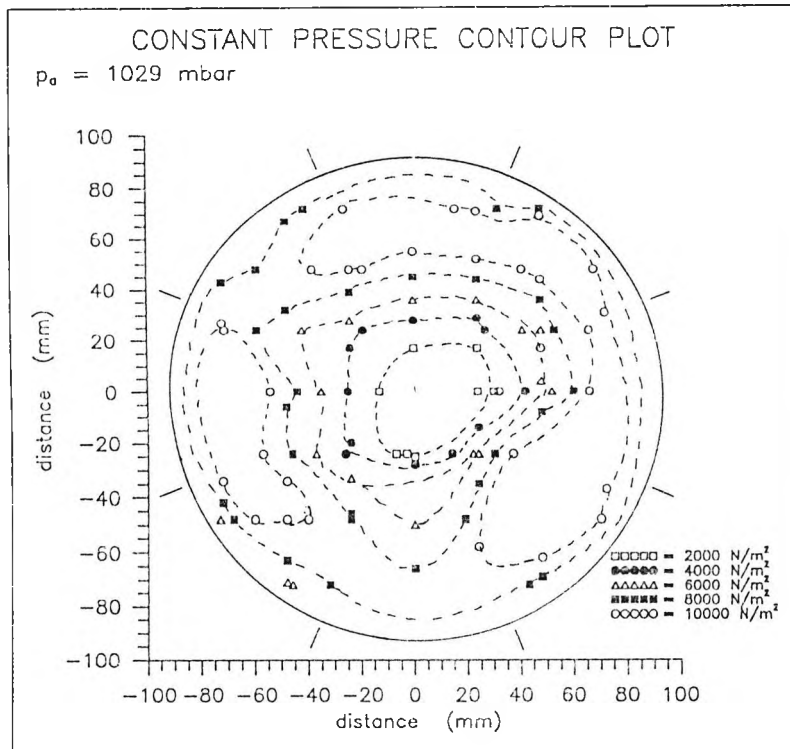
1 Nov. 1991

Fig. 5.15 Co-rotating AJVGs: Constant pressure contour plot,
 $\beta = 30^\circ$, $PR_{AJVG} = 3.64$, no peripheral blowing



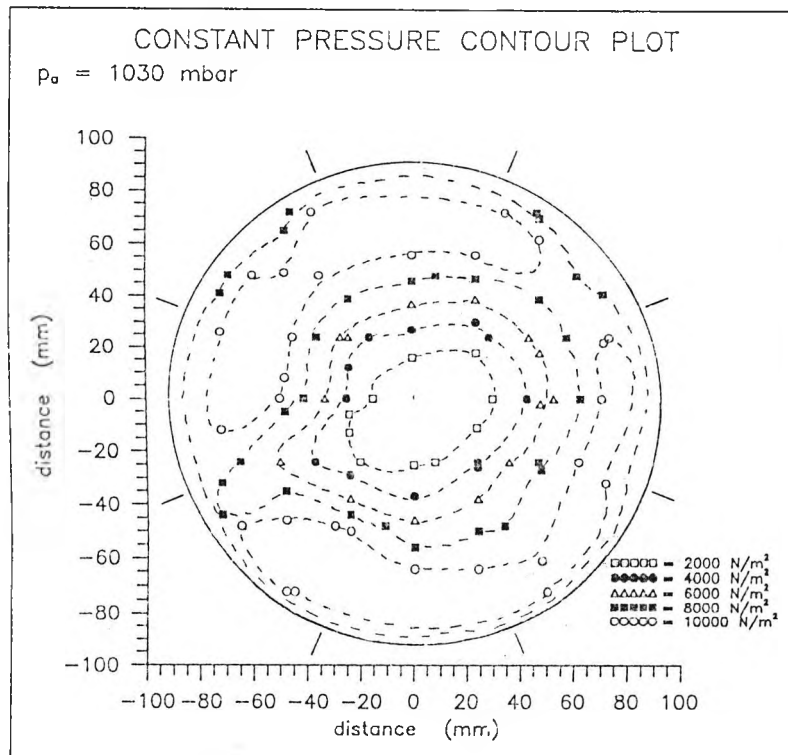
1 Nov. 1991

Fig. 5.16 Co-rotating AJVGs: Constant pressure contour plot,
 $\beta = 30^\circ$, $PR_{AJVG} = 4.53$, no peripheral blowing



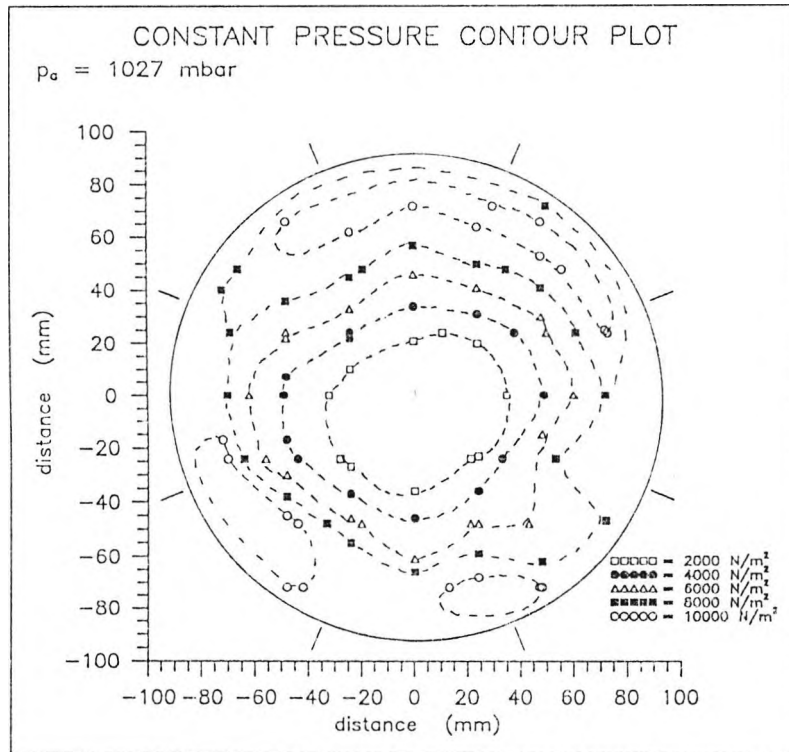
12 Sep. 1991

Fig. 5.17 No skew AJ blowing: Constant pressure contour plot,
 $\beta = 0^\circ$, $PR_{AJVG} = 2.72$, $PR_{peri} = 2.53$



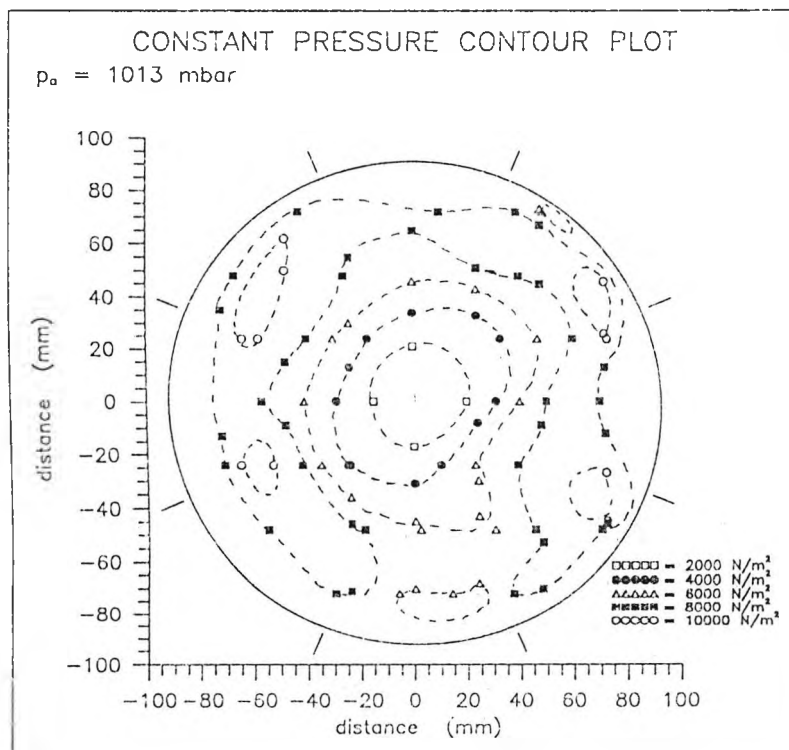
16 Sep. 1991

Fig. 5.18 Co-rotating AJVGs: Constant pressure contour plot,
 $\beta = 15^\circ$, $PR_{AJVG} = 2.88$, $PR_{peri} = 2.50$



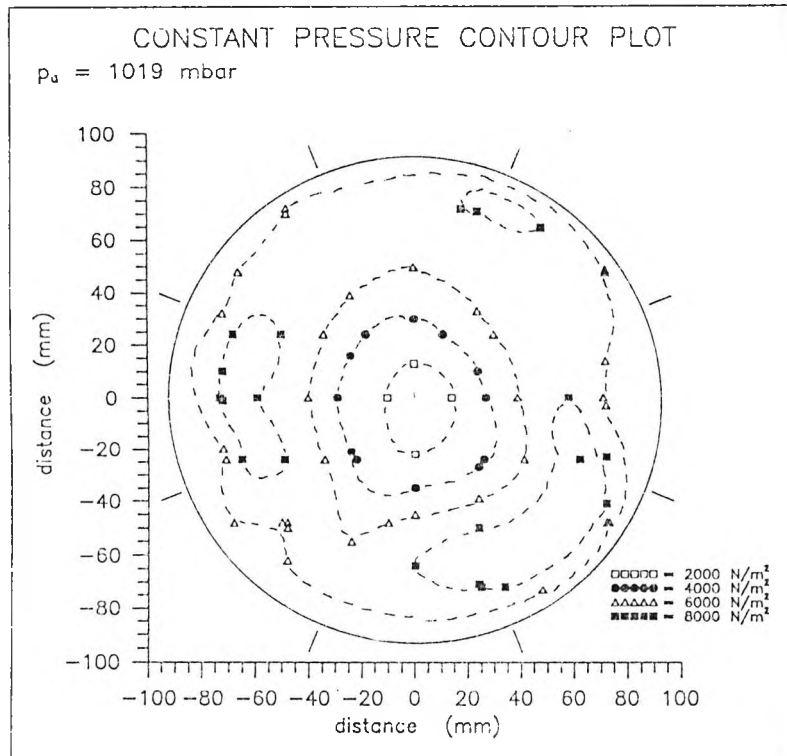
17 Sep. 1991

Fig. 5.19 Co-rotating AJVGs: Constant pressure contour plot,
 $\beta = 30^\circ$, $PR_{AJVG} = 2.77$, $PR_{peri} = 2.50$



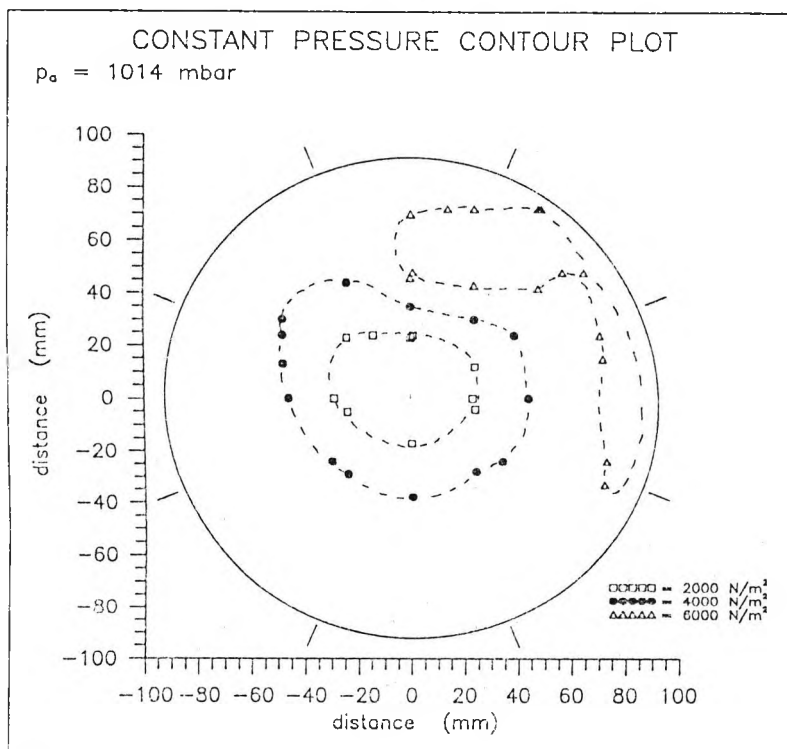
17 Sep. 1991

Fig. 5.20 Co-rotating AJVGs: Constant pressure contour plot,
 $\beta = 45^\circ$, $PR_{AJVG} = 3.08$, $PR_{peri} = 2.52$



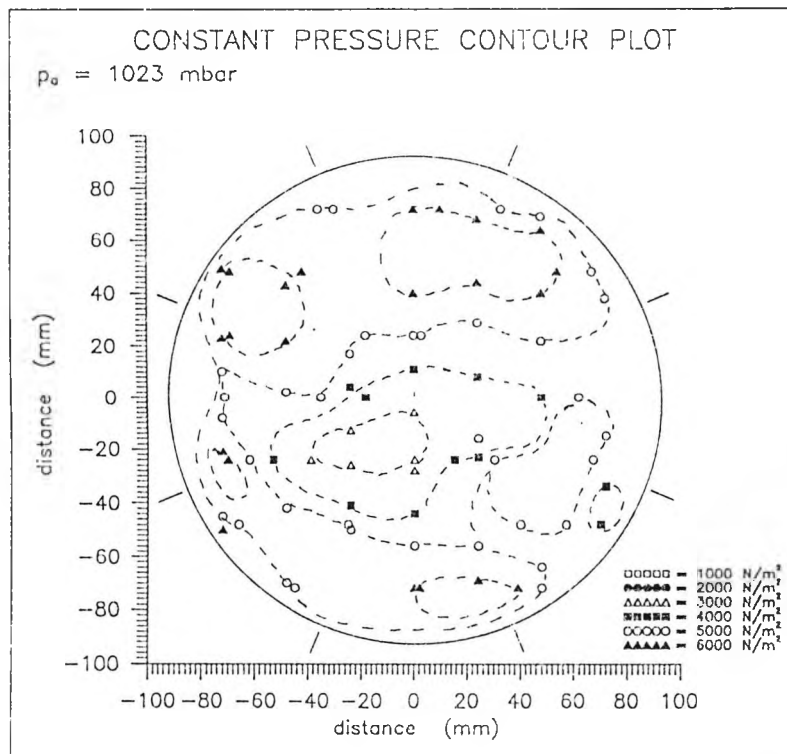
18 Sep. 1991

Fig. 5.21 Co-rotating AJVGs: Constant pressure contour plot,
 $\beta = 60^\circ$, $PR_{AVG} = 3.12$, $PR_{peri} = 2.53$



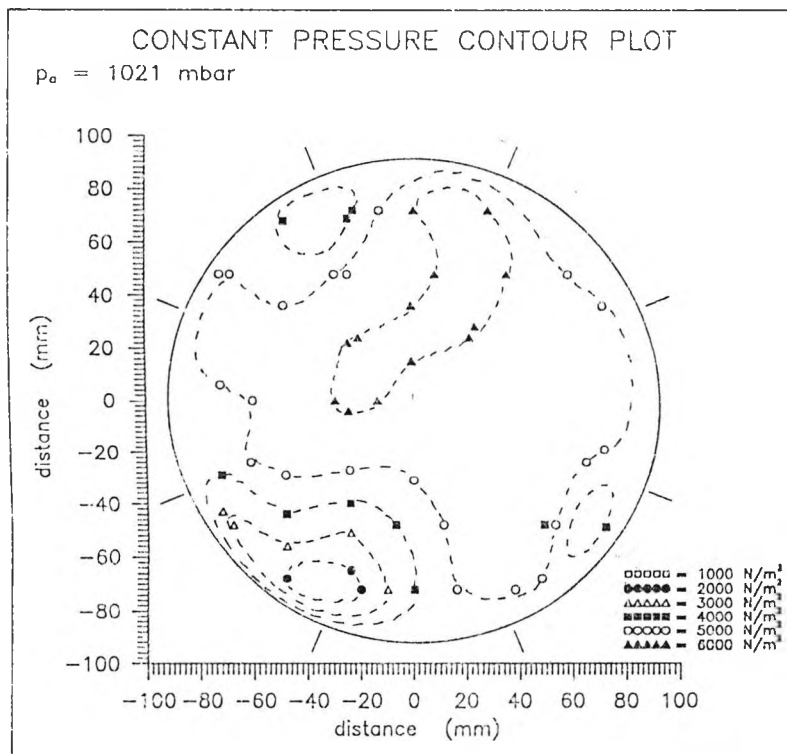
18 Sep. 1991

Fig. 5.22 Co-rotating AJVGs: Constant pressure contour plot,
 $\beta = 75^\circ$, $PR_{AVG} = 3.10$, $PR_{peri} = 2.51$



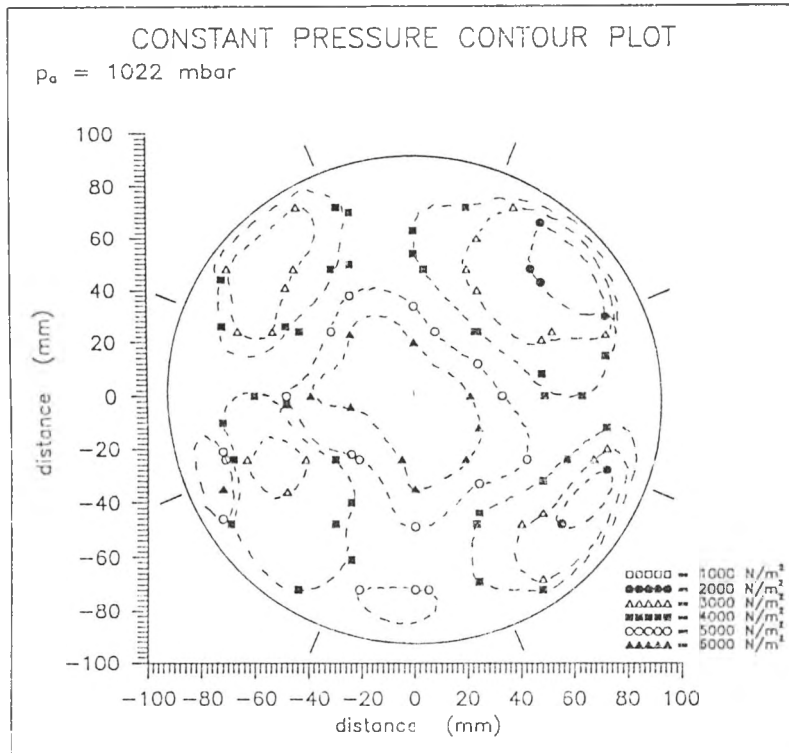
30 Sep. 1991

Fig. 5.23 No skew AJ blowing: Constant pressure contour plot, $\beta = 0^\circ$, $PR_{AVG} = 3.07$, no peripheral blowing



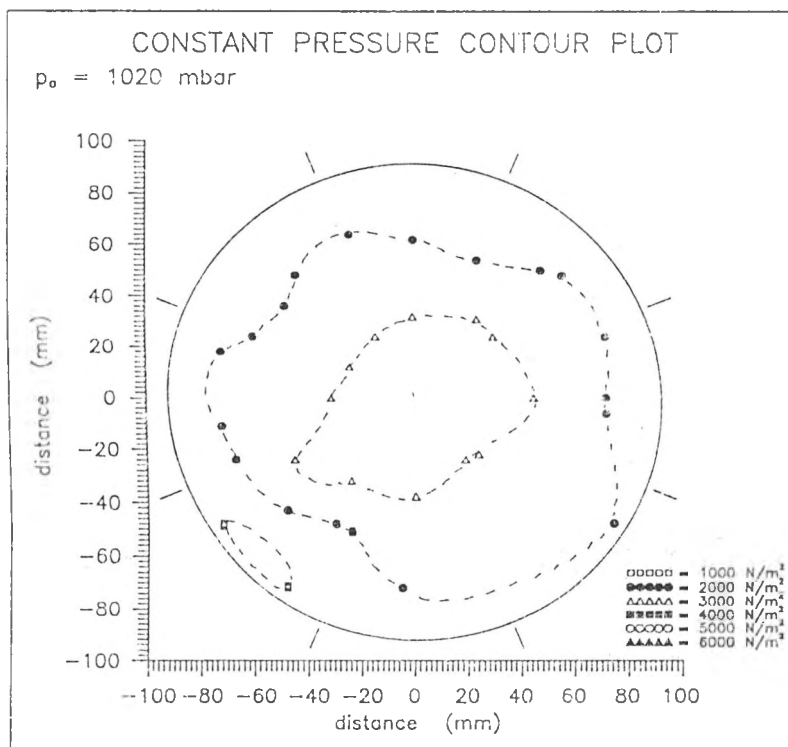
30 Sep. 1991

Fig. 5.24 Contra-rotating AJ pairs: Constant pressure contour plot, $\beta = 15^\circ$, $PR_{AVG} = 3.18$, no peripheral blowing



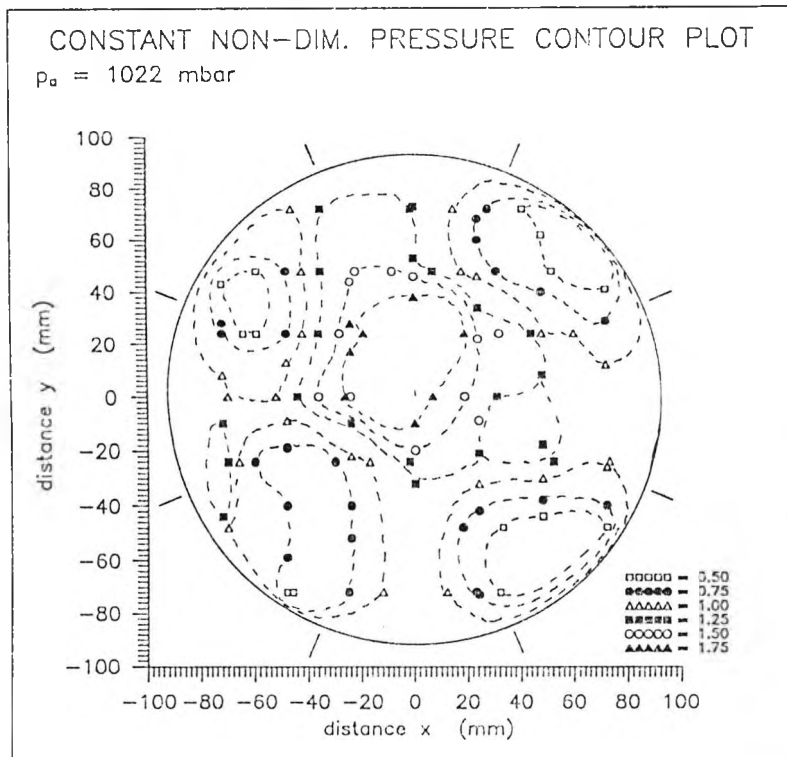
30 Sep. 1991

Fig. 5.25 Contra-rotating AJ pairs: Constant pressure contour plot, $\beta = 30^\circ$, $PR_{AVG} = 2.96$, no peripheral blowing



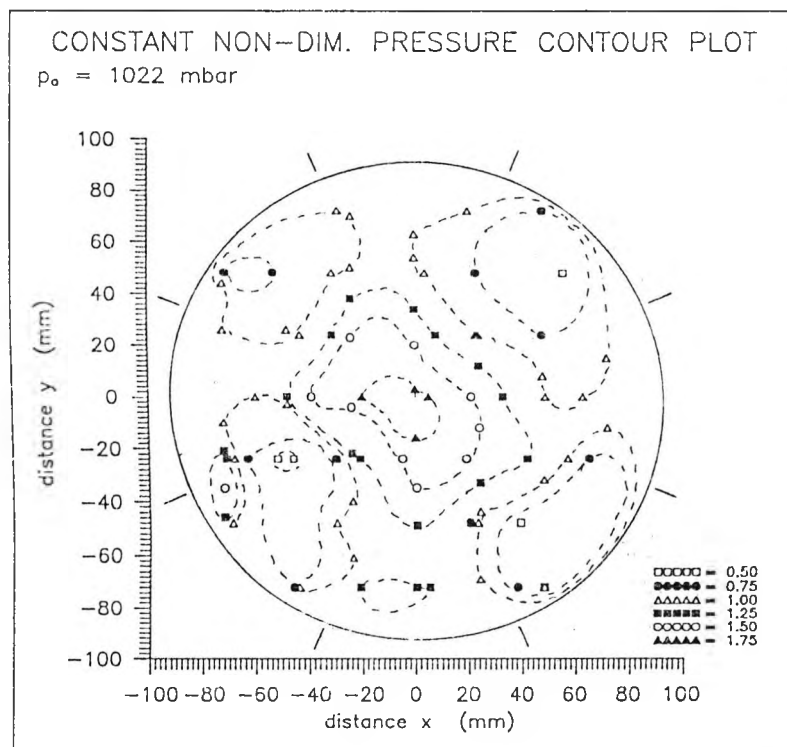
30 Sep. 1991

Fig. 5.26 Contra-rotating AJ pairs: Constant pressure contour plot, $\beta = 60^\circ$, $PR_{AVG} = 3.09$, no peripheral blowing



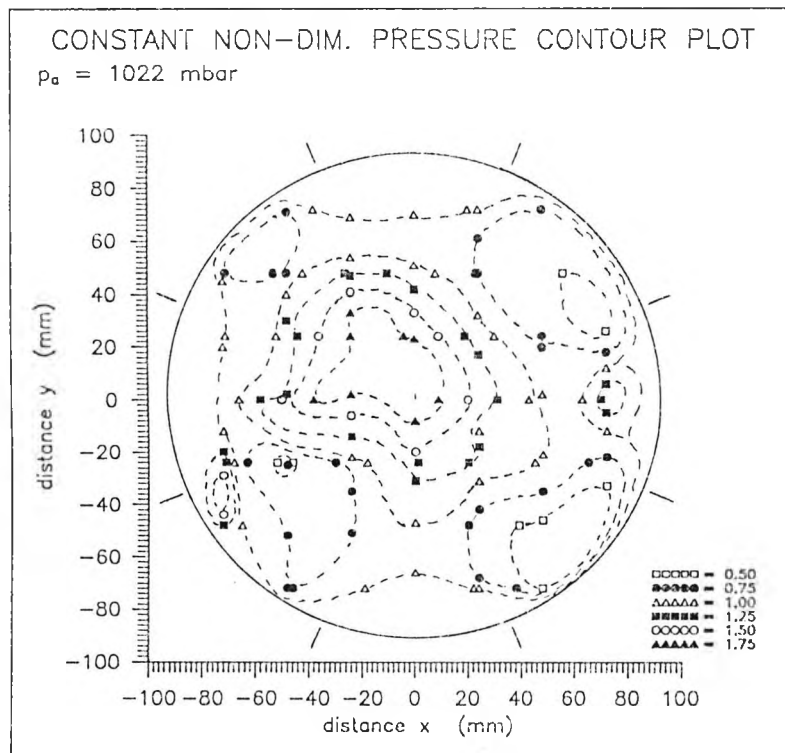
11 Oct. 1991

Fig. 5.27 Contra-rotating AJ pairs: Constant pressure contour plot, $\beta = 30^\circ$, $PR_{AVG} = 2.37$, no peripheral blowing



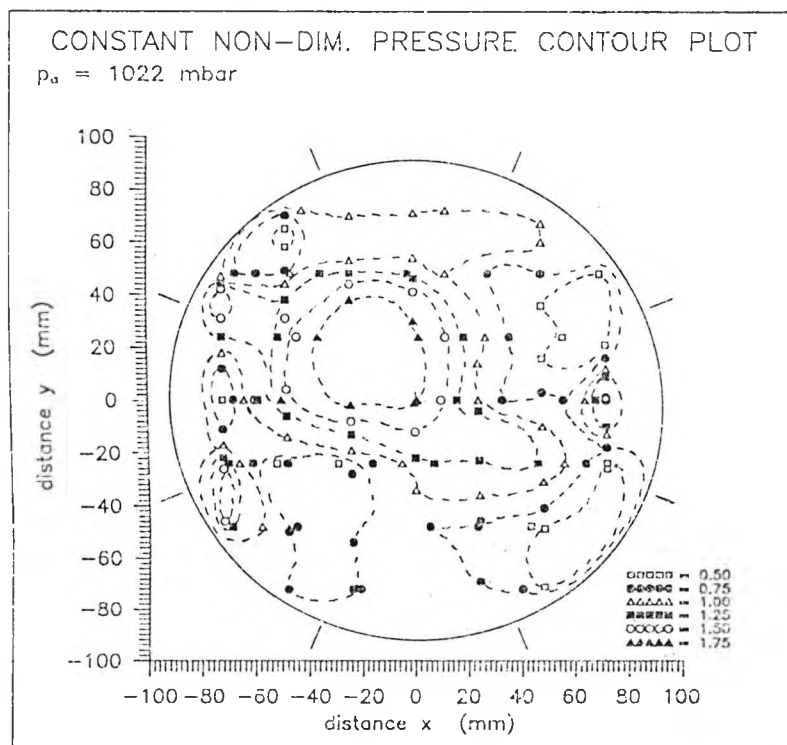
11 Oct. 1991

Fig. 5.28 Contra-rotating AJ pairs: Constant pressure contour plot, $\beta = 30^\circ$, $PR_{AVG} = 2.96$, no peripheral blowing



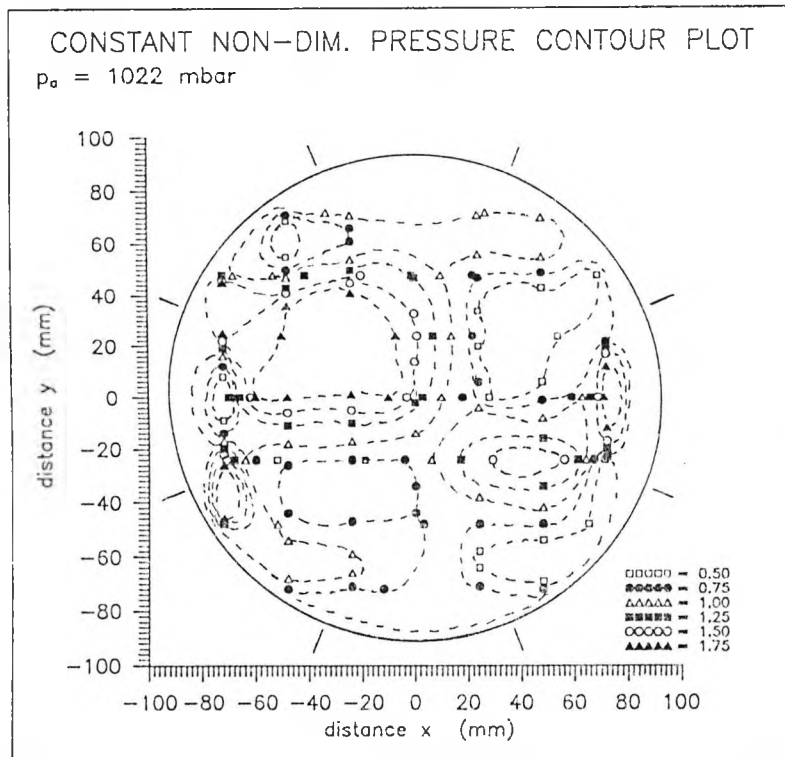
14 Oct. 1991

Fig. 5.29 Contra-rotating AJ pairs: Constant pressure contour plot,
 $\beta = 30^\circ$, $PR_{AVG} = 3.61$, no peripheral blowing



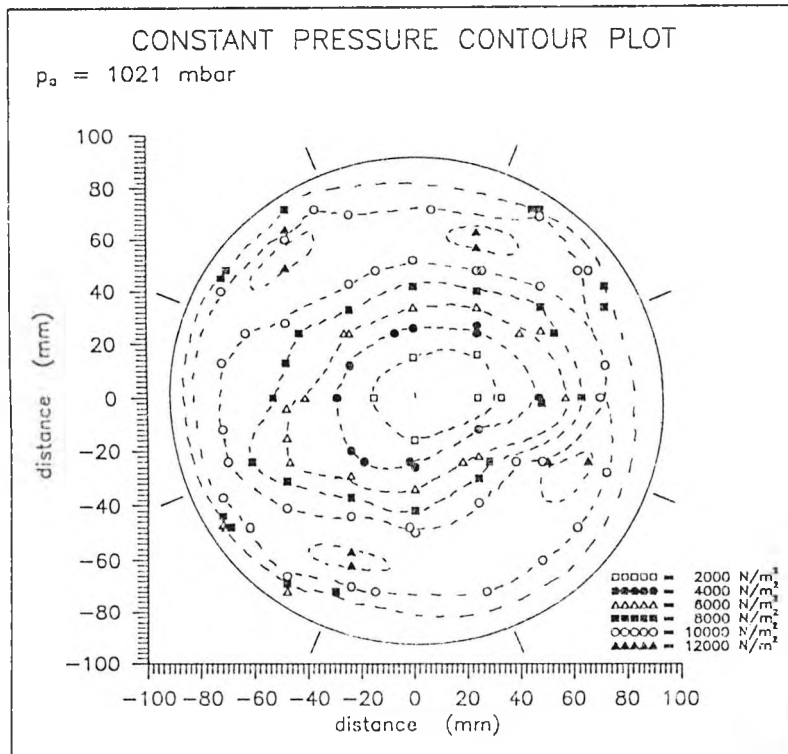
11 Oct. 1991

Fig. 5.30 Contra-rotating AJ pairs: Constant pressure contour plot,
 $\beta = 30^\circ$, $PR_{AVG} = 4.14$, no peripheral blowing



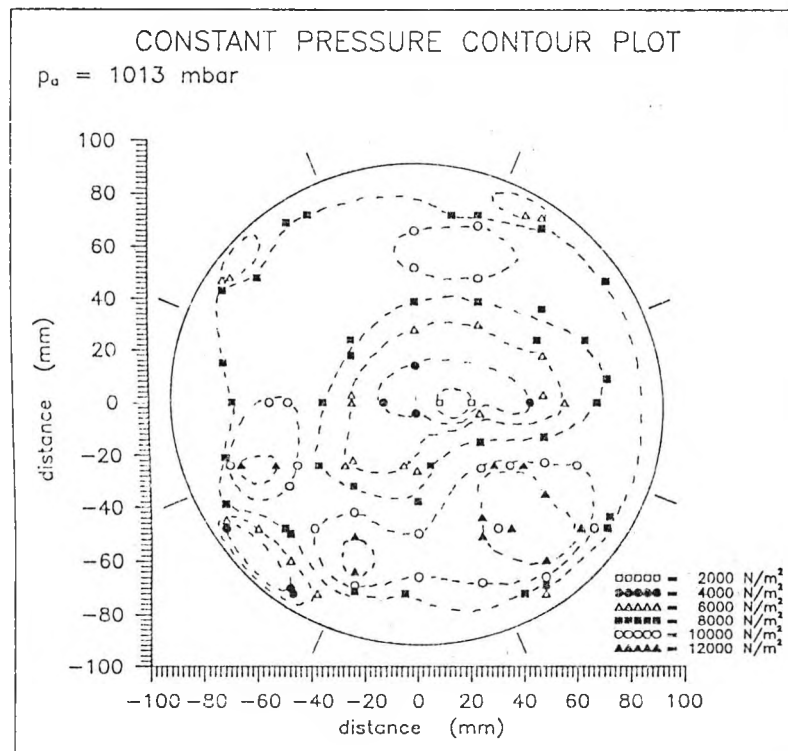
14 Oct. 1991

Fig. 5.31 Contra-rotating AJ pairs: Constant pressure contour plot, $\beta = 30^\circ$, $PR_{AVG} = 4.66$, no peripheral blowing



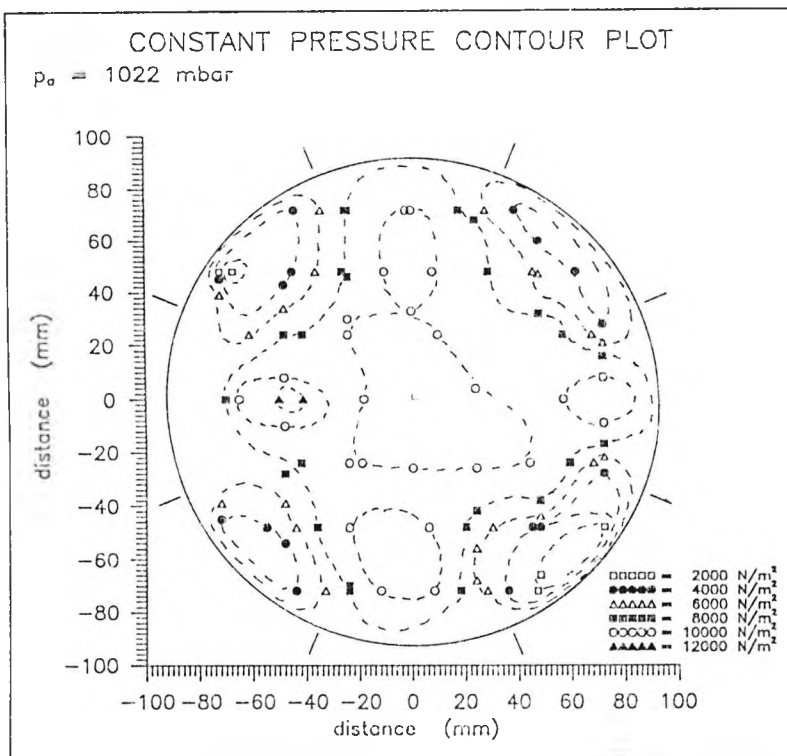
4 Oct. 1991

Fig. 5.32 No skew AJ blowing: Constant pressure contour plot,
 $\beta = 0^\circ$, $PR_{AVG} = 3.00$, $PR_{peri} = 2.54$



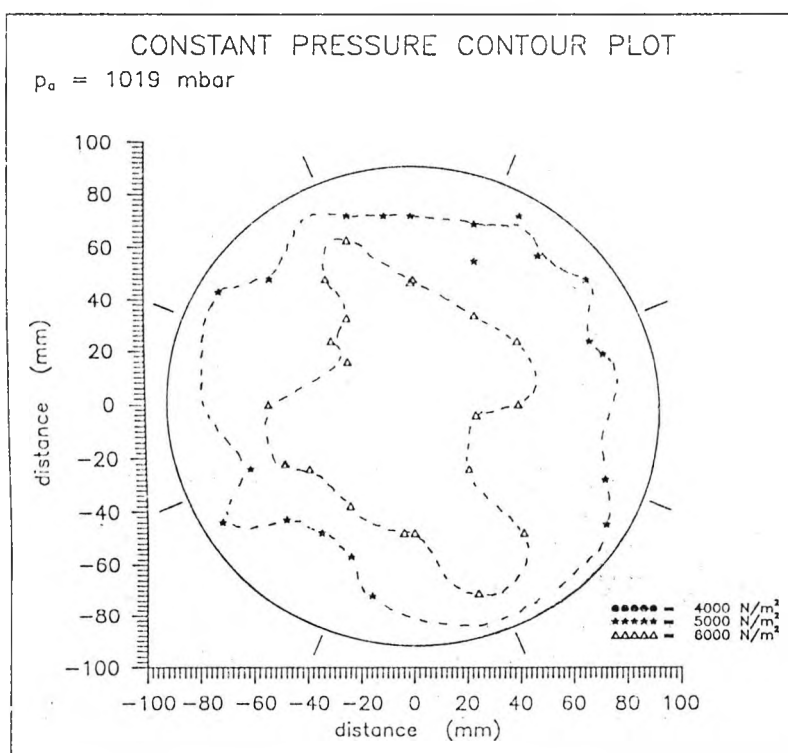
4 Oct. 1991

Fig. 5.33 Contra-rotating AJ pairs: Constant pressure contour plot,
 $\beta = 15^\circ$, $PR_{AVG} = 3.15$, $PR_{peri} = 2.54$



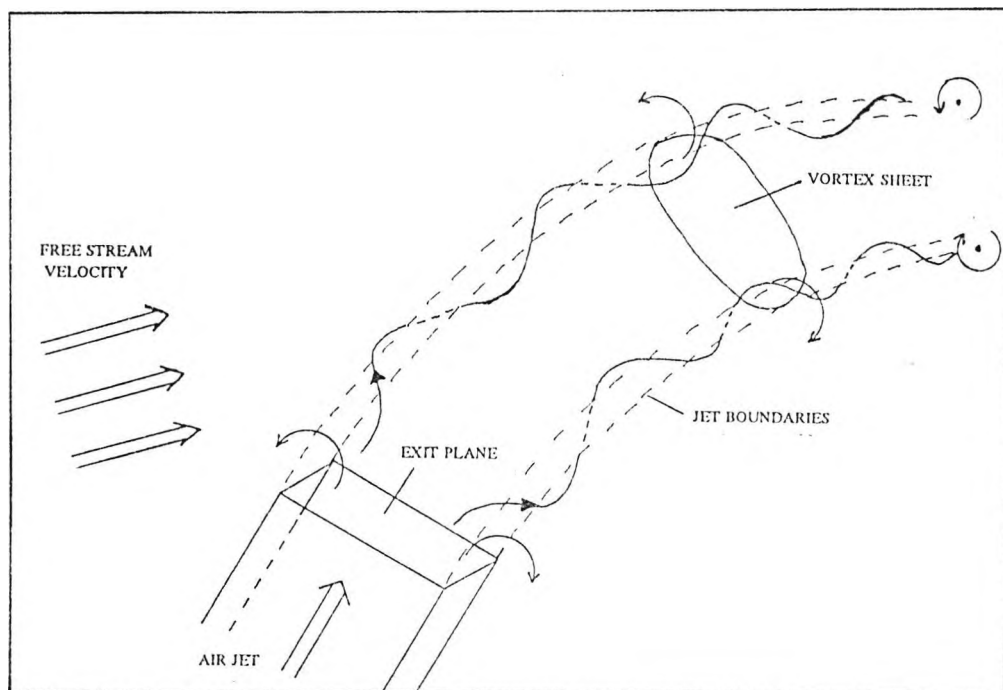
4 Oct. 1991

Fig. 5.34 Contra-rotating AJ pairs: Constant pressure contour plot,
 $\beta = 30^\circ$, $PR_{AVG} = 2.83$, $PR_{peri} = 2.53$

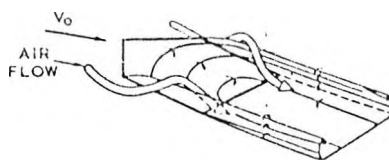


7 Oct. 1991

Fig. 5.35 Contra-rotating AJ pairs: Constant pressure contour plot,
 $\beta = 60^\circ$, $PR_{AVG} = 2.99$, $PR_{peri} = 2.51$

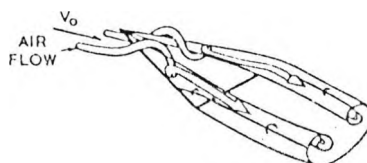


- 5.36) Sketch of vortices shedding from the edges of an air jet vortex generator set at an angle of 0° skew (i.e. the jet is injected in the axial direction).



a TAPERED WING WITH TIP
VORTEX SHEETS

Fig. 6.1a Vortex pattern on tapered wing with relatively small sweep (from Küchemann).



b SLENDER DELTA WING WITH SPIRAL
LEADING-EDGE VORTEX SHEETS

Fig. 6.1b Vortex pattern on slender delta wing.

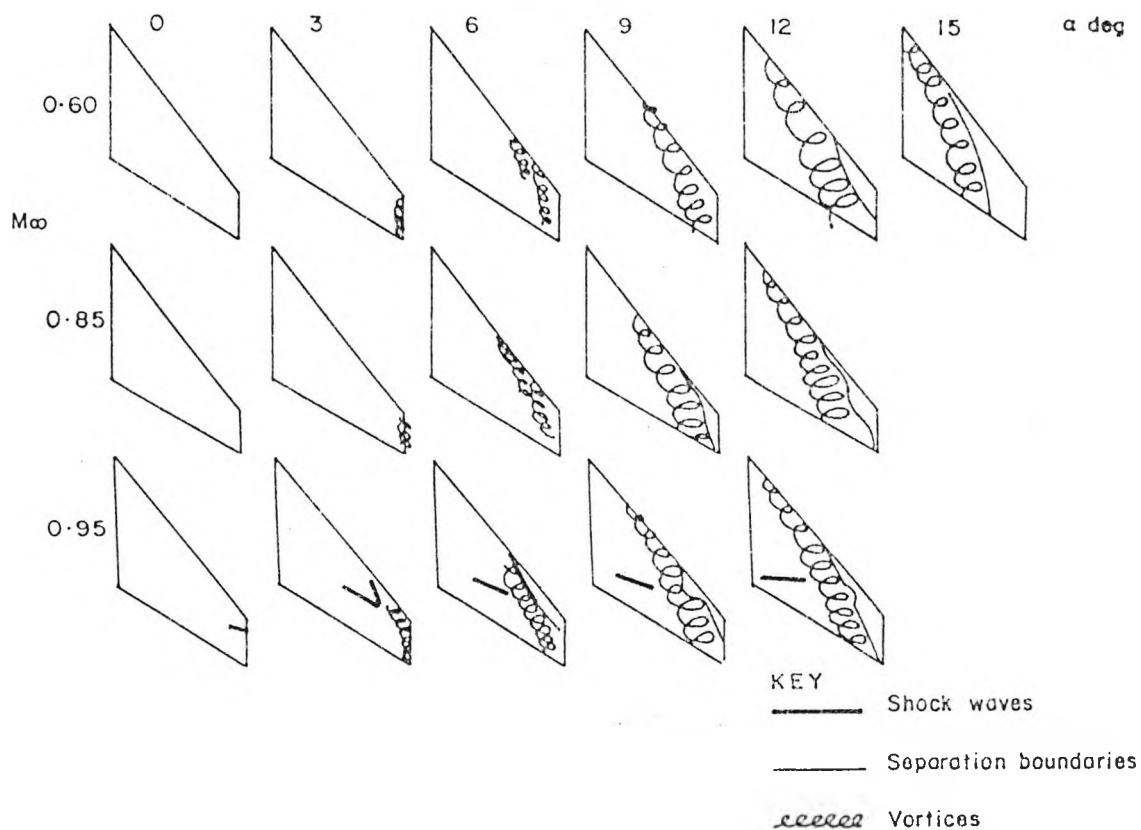


Fig. 6.2 Development of vortex formation for Mach numbers of 0.6, 0.85 and 0.95 with varying angle of incidence on a highly-swept wing of low aspect ratio (from ESDU 90008).

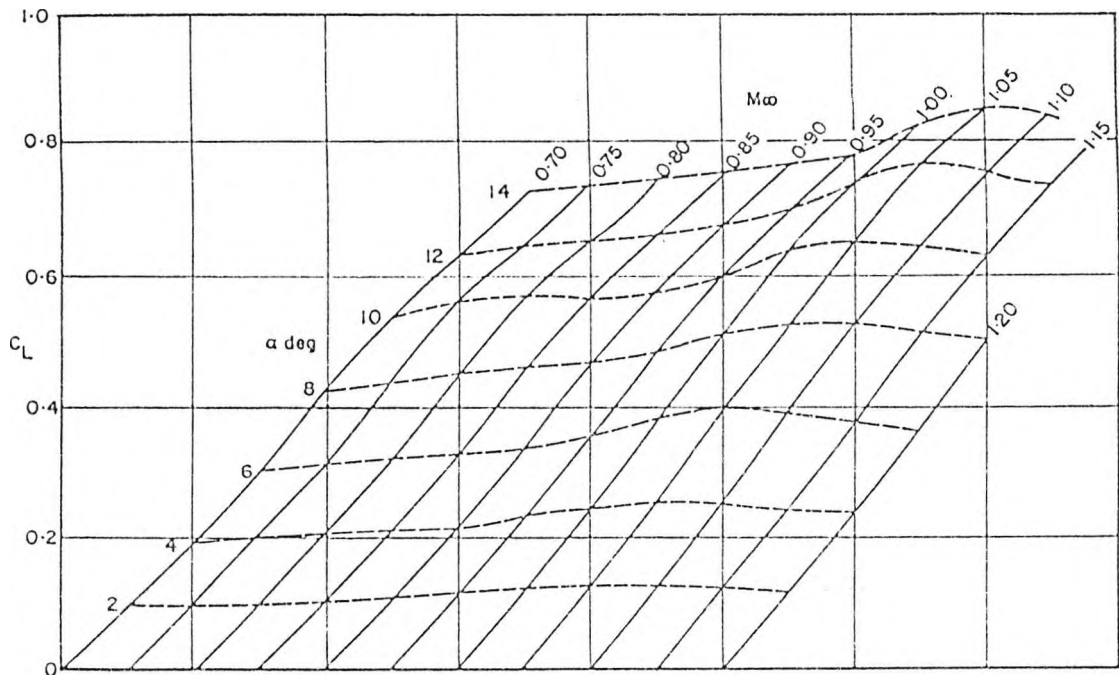


Fig. 6.3 Carpet plot of lift curves for highly-swept low aspect ratio wings as function of M_∞ and C_L .
- taken from Hall and Rogers -

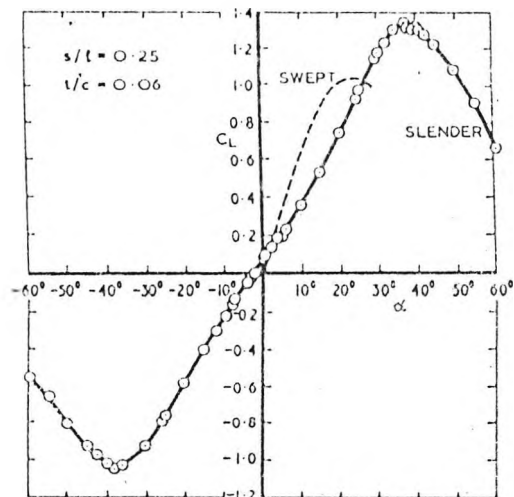
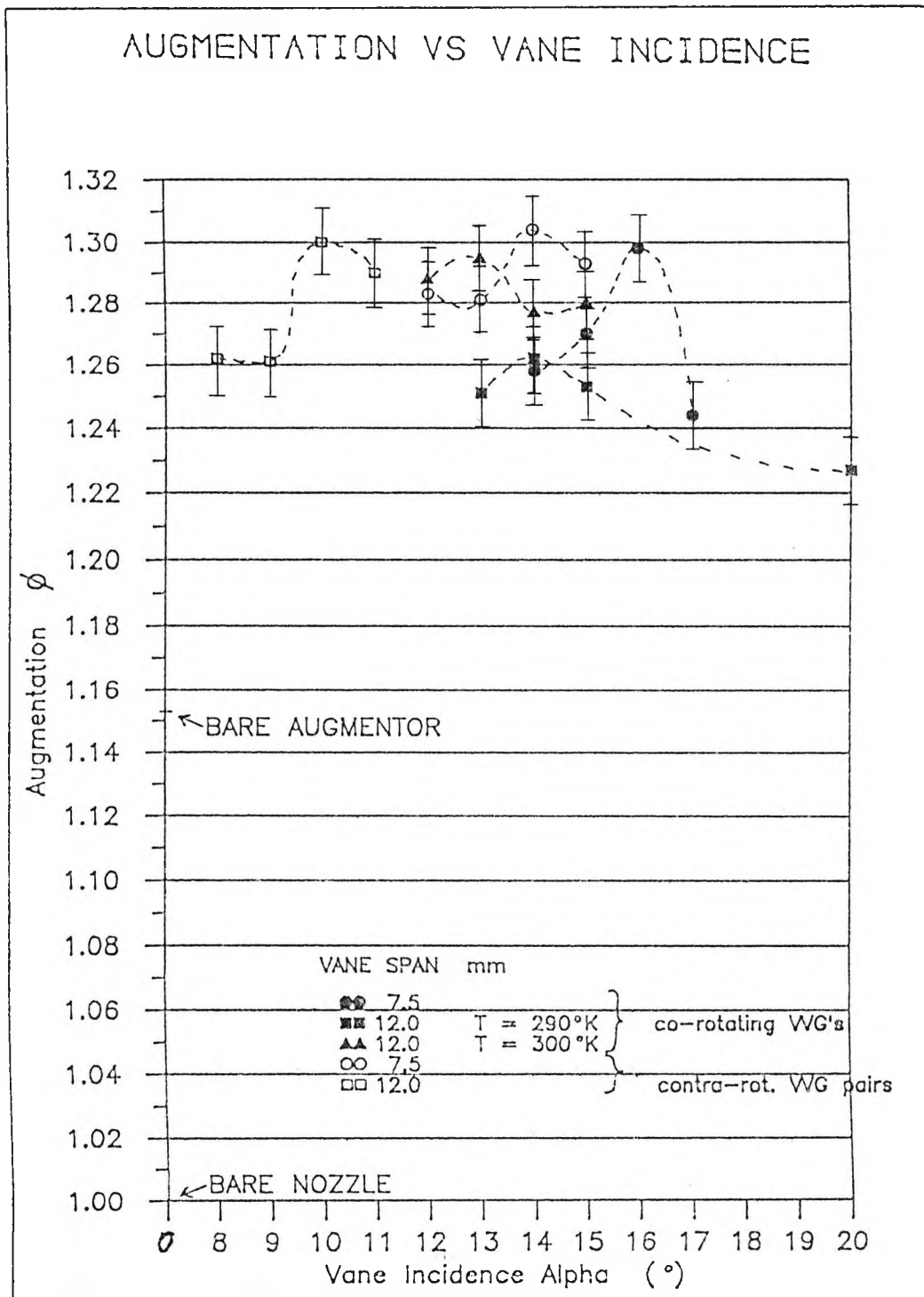
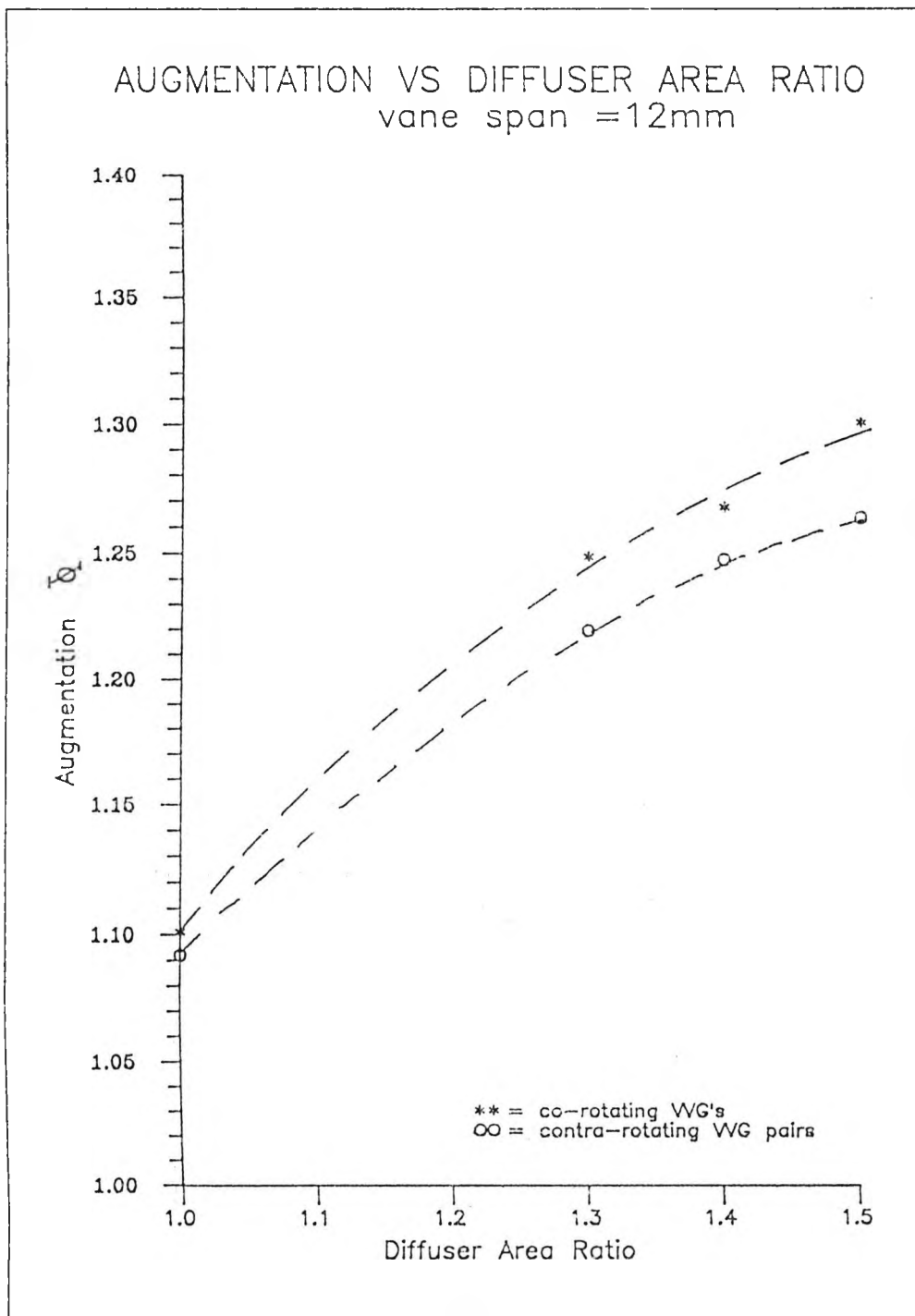


Fig. 6.4 Plot of lift coefficient vs incidence α for a slender delta and a swept wing (after Earnshaw and Lawford).



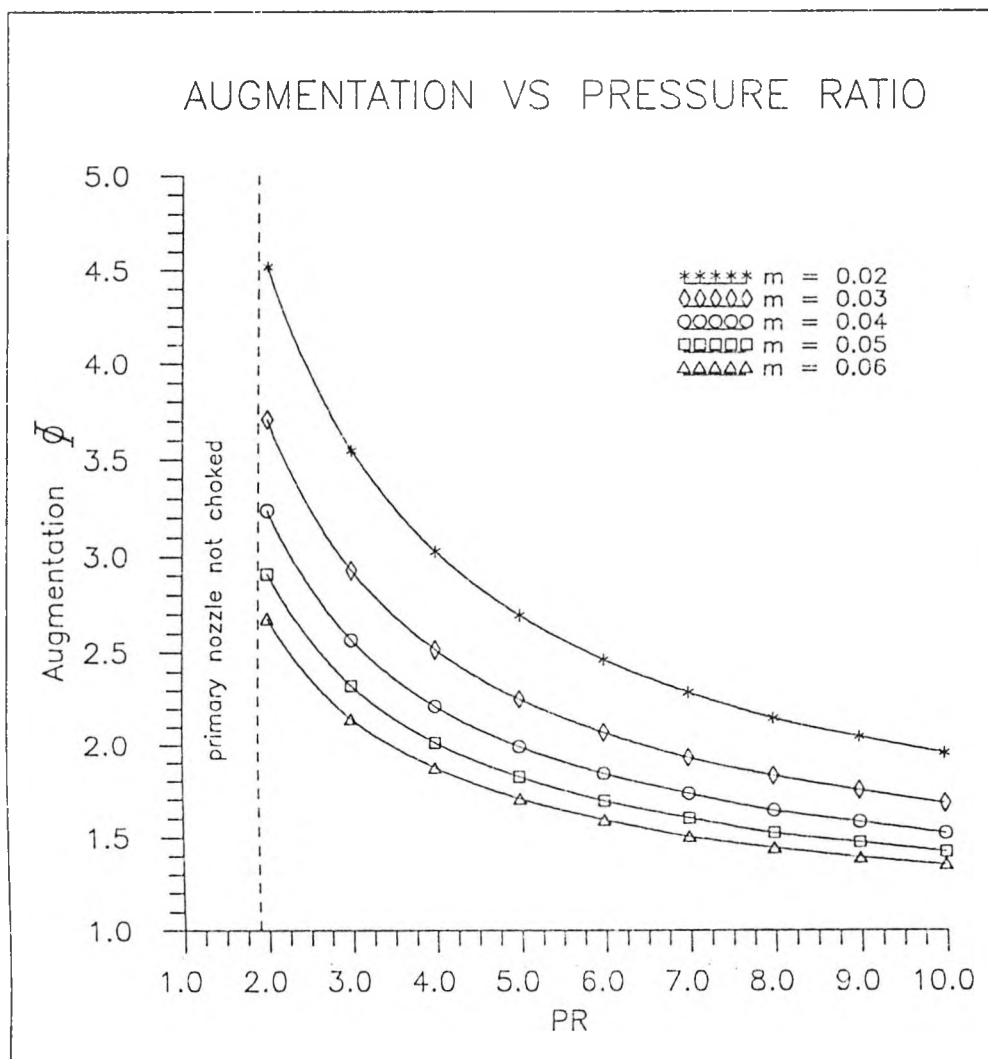
11 OCT 1990

Fig. 6.5 Plot of augmentation vs vane angle of incidence α at a peripheral driving pressure ratio of 5.0. Results for 7.5mm and 12mm vane span are given.



2 NOV 1990

Fig. 6.6 Plot of augmentation vs diffuser area ratio for co- and contra-rotating vane vortex generators having a vane span of 12mm.



25 May 1992

Fig. 6.7 Plot of theoretical maximum augmentation with primary pressure ratio and varying primary inlet to duct area ratios (m); 100 per cent efficient diffuser; choked secondary inlet and varying diffuser area ratios (n).

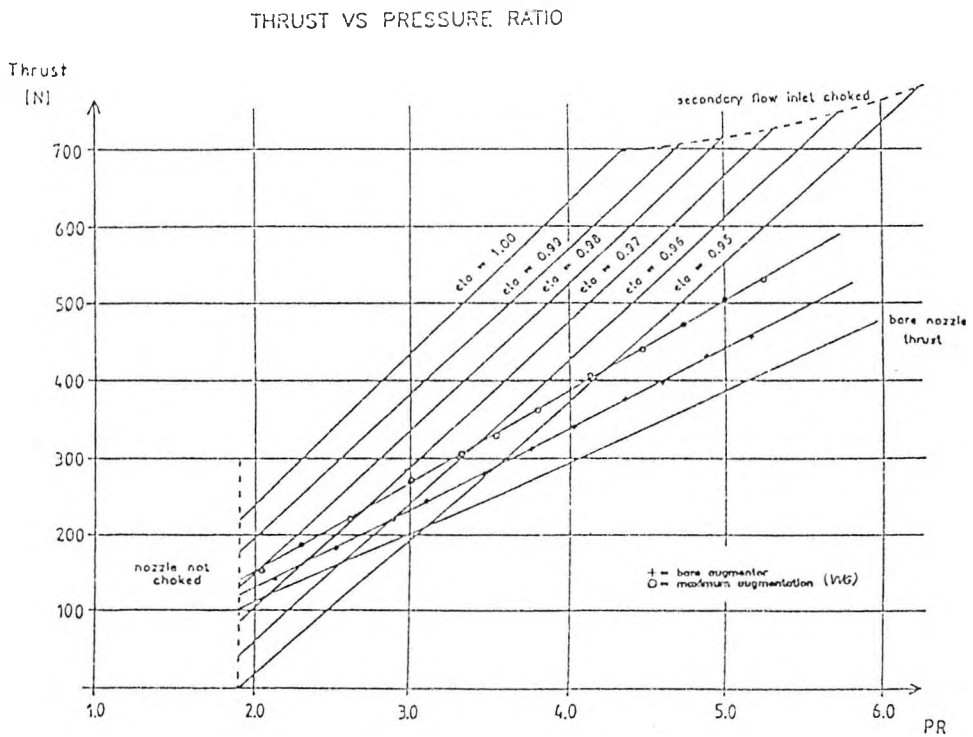
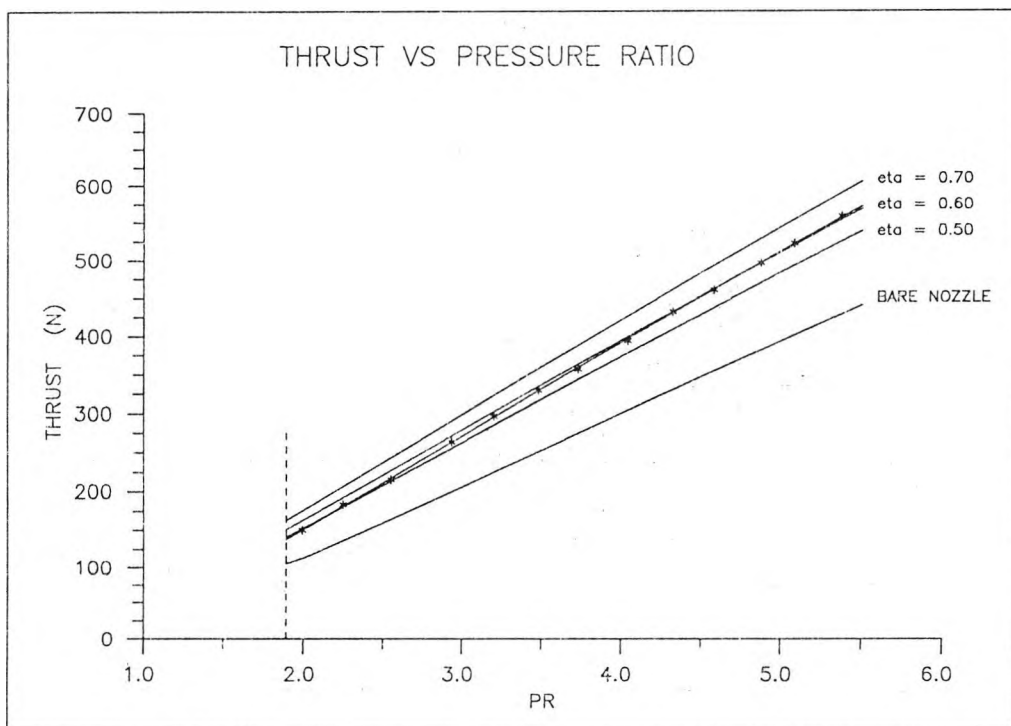


Fig. 6.8 Comparison of theoretical prediction based on total pressure diffuser efficiency and experimental results.



4 Feb 1991

Fig. 6.9 Comparison of theoretical prediction for diffuser efficiency based on static pressure rise and experimental results (co-rotating vane vortex generators set to 15°).

10.) APPENDICES:

10.1.1.) Appendix IA

10.1.2.) Appendix IB

10.1.3.) Appendix IC

10.2.) Appendix II; Drawings

It should be noted that the original drawings have been reduced using a photocopier and therefore the shown scale factors do not represent the correct scaling.

10.1.1.) APPENDIX IA:

Derivation of the equations describing the physics of the flow through the thrust augmentor:

Conservation equations:

i) mass:

$$\dot{m}_1 + \dot{m}_2 = \dot{m}_3 = \dot{m}_4 \quad \text{--- (1)}$$

ii) momentum:

$$(p_1 + \rho_1 U_1^2) A_1 + (p_2 + \rho_2 U_2^2) (A_2 - A_1) = (p_3 + \rho_3 U_3^2) A_3 \quad \text{--- (2)}$$

iii) energy:

$$\dot{m}_1 C_p T_{01} + \dot{m}_2 C_p T_{02} = \dot{m}_3 C_p T_{03} = \dot{m}_4 C_p T_{04} \quad \text{--- (3)}$$

also:

$$\dot{m} = \rho U A \quad \text{--- (a)}$$

where:

$$\rho U = M P \left[\frac{\gamma}{RT} \right]^{\frac{1}{2}} \quad \text{--- (b)}$$

$$\frac{T_0}{T} = \left(1 + \frac{\gamma-1}{2} M^2 \right) \quad \text{--- (c)}$$

and for isentropic flow we have:

$$\frac{P_0}{P} = \left(1 + \frac{\gamma-1}{2} M^2 \right)^{\frac{\gamma}{\gamma-1}} \quad \text{--- (d)}$$

Use mass equation (1) and (a):

$$\rho_1 U_1 A_1 + \rho_2 U_2 (A_2 - A_1) = \rho_3 U_3 A_3 = \rho_4 U_4 A_4 \quad \text{--- (4)}$$

use (b):

$$M_1 P_1 \left[\frac{\gamma}{RT_1} \right]^{\frac{1}{2}} A_1 + M_2 P_2 \left[\frac{\gamma}{RT_2} \right]^{\frac{1}{2}} (A_2 - A_1) = M_3 P_3 \left[\frac{\gamma}{RT_3} \right]^{\frac{1}{2}} A_3$$

multiplying through by $\left[\frac{R}{\gamma} \right]^{\frac{1}{2}} \frac{1}{A_2}$ gives:

$$\frac{M_1 P_1}{\sqrt{T_1}} \frac{A_1}{A_2} + \frac{M_2 P_2}{\sqrt{T_2}} \left[1 - \frac{A_1}{A_2} \right] = \frac{M_3 P_3}{\sqrt{T_3}} \frac{A_3}{A_2} = \frac{M_4 P_4}{\sqrt{T_4}} \frac{A_4}{A_2}$$

now put: $\frac{A_1}{A_2} = m$ and $\frac{A_4}{A_2} = \frac{A_4}{A_3} = n$; note: $\frac{A_3}{A_2} = 1$

$$\frac{M_1 P_1}{\sqrt{T_1}} m + \frac{M_2 P_2}{\sqrt{T_2}} (1-m) = \frac{M_3 P_3}{\sqrt{T_3}} = \frac{M_4 P_4}{\sqrt{T_4}} n \quad \text{--- (5)}$$

from (c) we have:

$$\sqrt{T} = \frac{\sqrt{T_0}}{\left[1 + \frac{\gamma-1}{2} M^2\right]^{\frac{1}{2}}}$$

from (d) we have:

$$\sqrt{P} = \frac{\sqrt{P_0}}{\left[1 + \frac{\gamma-1}{2} M^2\right]^{\frac{\gamma}{2(\gamma-1)}}}$$

using these expressions in equation (5) yields:

since the primary flow is assumed to be choked we have $M_1 = 1$

$$\frac{P_{01} \left[\frac{1+\gamma}{2}\right]^{\frac{1}{2}}}{\sqrt{T_{01}} \left[\frac{1+\gamma}{2}\right]^{\frac{\gamma}{\gamma-1}}} m + \frac{P_{02} \left[1 + \frac{\gamma-1}{2} M_2^2\right]^{\frac{1}{2}}}{\sqrt{T_{02}} \left[1 + \frac{\gamma-1}{2} M_2^2\right]^{\frac{\gamma}{\gamma-1}}} M_2 (1-m) =$$

$$\frac{P_{04} \left[1 + \frac{\gamma-1}{2} M_4^2\right]^{\frac{1}{2}}}{\sqrt{T_{04}} \left[1 + \frac{\gamma-1}{2} M_4^2\right]^{\frac{\gamma}{\gamma-1}}} n M_4$$

it follows that:

$$\frac{P_{01}}{\sqrt{T_{01}}} \frac{m}{\left[\frac{1+\gamma}{2}\right]^{\frac{\gamma+1}{2(\gamma-1)}}} + \frac{P_{02}}{\sqrt{T_{02}}} \frac{M_2 (1-m)}{\left[1 + \frac{\gamma-1}{2} M_2^2\right]^{\frac{\gamma+1}{2(\gamma-1)}}} =$$

$$\frac{P_{04}}{\sqrt{T_{04}}} \frac{M_4 n}{\left[1 + \frac{\gamma-1}{2} M_4^2\right]^{\frac{\gamma+1}{2(\gamma-1)}}} \quad \text{--- (6)}$$

Use momentum equation (2) and divide through by A_1 :

remember $\frac{A_1}{A_2} = \frac{A_1}{A_3} = m$

$$(p_1 + \rho_1 U_1^2) + (p_2 + \rho_2 U_2^2) \left(\frac{1}{m} - 1\right) = (p_3 + \rho_3 U_3^2) \frac{1}{m}$$

insert substitution from (b) and multiply through by m :

$$(p_1 + U_1 M_1 p_1 \left[\frac{\gamma}{RT_1}\right]^{\frac{1}{2}}) m + (p_2 + U_2 M_2 p_2 \left[\frac{\gamma}{RT_2}\right]^{\frac{1}{2}}) (1-m) = (p_3 + U_3 M_3 p_3 \left[\frac{\gamma}{RT_3}\right]^{\frac{1}{2}})$$

using $U = Ma = M(\gamma RT)^{\frac{1}{2}}$ leads to:

$$p_1 (1+\gamma) m + p_2 (1+\gamma M_2^2) (1-m) = p_3 (1+\gamma M_3^2) \quad \text{--- (7)}$$

Using energy equation (3) and dividing by C_p gives:

$$\dot{m}_1 T_{01} + \dot{m}_2 T_{02} = \dot{m}_4 T_{04}$$

Applying the terms for the mass flow rate (a) and (b) yields:

$$p_{01} T_{01}^{\frac{1}{2}} m \left[\frac{1+\gamma}{2}\right]^{-\frac{\gamma+1}{2(\gamma+1)}} + p_{02} T_{02}^{\frac{1}{2}} M_2 (1-m) \left[1 + \frac{\gamma-1}{2} M_2^2\right]^{-\frac{\gamma+1}{2(\gamma+1)}} = p_{04} T_{04}^{\frac{1}{2}} M_4 n \left[1 + \frac{\gamma-1}{2} M_4^2\right]^{-\frac{\gamma+1}{2(\gamma-1)}} \quad \text{--- (8)}$$

using static pressure p_4 rather than total pressure p_{04} at the exit leads to:

$$\rightarrow \text{RHS is equal to: } p_4 T_{04}^{\frac{1}{2}} M_4 n \left[1 + \frac{\gamma-1}{2} M_4^2\right]^{\frac{1}{2}} \quad \text{--- (8a)}$$

$$\text{or } p_{01} T_{01}^{\frac{1}{2}} q + p_{02} T_{02}^{\frac{1}{2}} M_2 r = p_4 T_{04}^{\frac{1}{2}} M_4 s \quad \text{--- (8b)}$$

$$\text{and } p_{01} T_{01}^{-\frac{1}{2}} q + p_{02} T_{02}^{-\frac{1}{2}} M_2 r = p_4 T_{04}^{-\frac{1}{2}} M_4 s \quad \text{--- (6a)}$$

where:

$$q = m \left[\frac{\gamma+1}{2}\right]^{-\frac{\gamma+1}{2(\gamma-1)}} \quad \text{--- (12)}$$

$$r = (1-m) \left[1 + \frac{\gamma-1}{2} M_2^2 \right]^{-\frac{\gamma+1}{2(\gamma-1)}}$$

$$s = n \left[1 + \frac{\gamma-1}{2} M_4^2 \right]^{\frac{1}{2}}$$

solving for $T_{04}^{\frac{1}{2}}$ in (8b) leads to:

$$T_{04}^{\frac{1}{2}} = \frac{p_{01} T_{01}^{\frac{1}{2}} Q}{p_4 M_4 S} + \frac{p_{02} T_{02}^{\frac{1}{2}} M_2 R}{p_4 M_4 S} \quad \text{--- (8c)}$$

substituting (8c) into (6b) leads to:

$$\frac{p_{01}}{T_{01}^{\frac{1}{2}}} Q + \frac{p_{02}}{T_{02}^{\frac{1}{2}}} M_2 R = \frac{p_4^2 S^2 M_4^2}{p_{01} T_{01}^{\frac{1}{2}} Q + p_{02} T_{02}^{\frac{1}{2}} M_2 R}$$

or

$$p_{01}^2 Q^2 + \frac{p_{01} p_{02} T_{02}^{\frac{1}{2}} M_2 Q R}{T_{01}^{\frac{1}{2}}} + \frac{p_{01} p_{02} T_{01}^{\frac{1}{2}} M_2 Q R}{T_{02}^{\frac{1}{2}}} + p_{02}^2 M_2^2 R^2 = p_4^2 S^2 M_4^2$$

dividing by p_{02}^2 and noting that $p_{02} = p_a$ we get:

$$\frac{p_{01}^2}{p_a^2} Q^2 + \frac{p_{01}}{p_a} M_2 Q R \left[\left[\frac{T_{02}}{T_{01}} \right]^{\frac{1}{2}} + \left[\frac{T_{01}}{T_{02}} \right]^{\frac{1}{2}} \right] + M_2^2 R^2 = \frac{p_4^2}{p_a^2} M_4^2 S^2 \quad \text{--- (9)}$$

Definition of diffuser efficiency η :

$$p_{04} = \eta p_{03}$$

remember that:

$$\frac{p_0}{p} = \left[1 + \frac{\gamma-1}{2} M^2 \right]^{\frac{\gamma}{\gamma-1}}$$

$$\therefore p_4 \left[1 + \frac{\gamma-1}{2} M_4^2 \right]^{\frac{\gamma}{\gamma-1}} = \eta p_3 \left[1 + \frac{\gamma-1}{2} M_3^2 \right]^{\frac{\gamma}{\gamma-1}} \quad \text{--- (10)}$$

from equation (5) we know that:

$$\frac{p_3}{T_3^{\frac{1}{2}}} M_3 A_3 = \frac{p_4}{T_4^{\frac{1}{2}}} M_4 A_4 \quad \text{--- (11)}$$

or

$$\frac{p_3}{p_4} = \left[\frac{T_3}{T_4} \right]^{\frac{1}{2}} \frac{M_4}{M_3} n$$

$$\frac{P_3}{P_4} = \left[\frac{T_3}{T_{04}} \right]^{\frac{1}{2}} \left[\frac{T_{04}}{T_4} \right]^{\frac{1}{2}} \frac{M_4}{M_3} n \quad \text{--- (11a)}$$

combining (10) and (11a) and using (c) yields:

$$\frac{\left[1 + \frac{\gamma-1}{2} M_4^2 \right]^{\frac{\gamma}{\gamma-1}} \left[1 + \frac{\gamma-1}{2} M_4^2 \right]^{-\frac{1}{2}}}{\eta n M_4} = \frac{\left[1 + \frac{\gamma-1}{2} M_3^2 \right]^{\frac{\gamma}{\gamma-1}} \left[1 + \frac{\gamma-1}{2} M_3^2 \right]^{-\frac{1}{2}}}{M_3}$$

$$\rightarrow \frac{M_3}{\left[1 + \frac{\gamma-1}{2} M_3^2 \right]^{\frac{\gamma+1}{2(\gamma-1)}}} = \frac{\eta n M_4}{\left[1 + \frac{\gamma-1}{2} M_4^2 \right]^{\frac{\gamma+1}{2(\gamma-1)}}} \quad \text{--- (12)}$$

Finally, using the adiabatic pressure equation (d), in conjunction with the momentum equation (7) the last required equation is found:

$$\frac{P_{01} (1+\gamma) m}{P_a \left[1 + \frac{\gamma-1}{2} M_3^2 \right]^{\frac{\gamma}{\gamma-1}}} + \frac{(1 + \gamma M_2^2) (1-m)}{\left[1 + \frac{\gamma-1}{2} M_2^2 \right]^{\frac{\gamma}{\gamma-1}}} = \frac{(1 + \gamma M_3^2)}{\eta} \frac{\left[1 + \frac{\gamma-1}{2} M_4^2 \right]^{\frac{\gamma}{\gamma-1}}}{\left[1 + \frac{\gamma-1}{2} M_3^2 \right]^{\frac{\gamma}{\gamma-1}}}$$

combining this equation with equation (12) gives:

$$\frac{P_{01} (1+\gamma) m}{P_a \left[1 + \frac{\gamma-1}{2} M_3^2 \right]^{\frac{\gamma}{\gamma-1}}} + \frac{(1 + \gamma M_2^2) (1-m)}{\left[1 + \frac{\gamma-1}{2} M_2^2 \right]^{\frac{\gamma}{\gamma-1}}} = (1 + \gamma M_3^2) \left[\frac{M_4}{M_3} \right]^{\frac{7}{6}} \eta^{\frac{1}{6}} n^{\frac{7}{6}} \quad \text{--- (13)}$$

Inserting the value of 1.4 for γ and renaming:

$\frac{P_{01}}{P_a} = PR$, $\frac{T_{01}}{T_a} = TR$ where $T_{02} = T_a$ results in the three

required equations:

$$0.335 PR^2 m^2 + \frac{M_2^2 (1-m)^2}{(1 + 0.2 M_2^2)^6} + \frac{PR M_2 m (1-m)}{1.728 (1 + 0.2 M_2^2)^3} \left[TR^{-\frac{1}{2}} + TR^{\frac{1}{2}} \right] =$$

$$(1 + 0.2 M_4^2) M_4^2 n^2 \quad \text{--- (A)}$$

$$1.2679 PR m + \frac{(1 + 1.4 M_2^2) (1-m)}{(1 + 0.2 M_2^2)^{\frac{7}{2}}} = (1 + 1.4 M_3^2) \left[\frac{M_4}{M_3} \right]^{\frac{7}{6}} \eta^{\frac{1}{6}} n^{\frac{7}{6}} \quad \text{--- (B)}$$

$$\frac{M_3}{(1 + 0.2 M_3^2)^3} = \frac{\eta n M_4}{(1 + 0.2 M_4^2)^3} \quad \text{--- (C)}$$

10.1.2.) APPENDIX IB:

DERIVATION OF PERFORMANCE TERMS:

The main performance terms which are required are as follows:

- a) thrust of bare nozzle thrust
- b) thrust augmentation ratio
- c) inlet to nozzle thrust ratio
- d) mass augmentation ratio (MAR)
- e) diffuser exit temperature
- f) change in entropy

Using the following standard equations, the above term will be put into a more suitable form for use within the program:

$$\rho U^2 = \gamma p M^2 \quad \text{--- (a)}$$

$$p_0 = p \left[1 + \frac{\gamma-1}{2} M^2 \right]^{\frac{\gamma}{\gamma-1}} \quad \text{--- (b)}$$

$$\rho a = p \left[\frac{\gamma}{RT} \right]^{\frac{1}{2}} \quad \text{--- (c)}$$

- a) Thrust of bare nozzle:

the bare nozzle thrust $F(1)$ is given by:

$$F(1) = (p_1^* + \rho_1^* U_1^{*2} - p_a) A_1 \quad \text{--- (1)}$$

which, from equation (a) becomes:

$$F(1) = (p_1^* (1+\gamma) - p_a) A_1 \quad \text{--- (2)}$$

- b) Thrust augmentation ratio:

The thrust augmentation ratio is defined as the ratio of total thrust over bare nozzle thrust. The total thrust $F(4)$ is given by:

$$F(4) = \rho_4 U_4^2 A_4 \quad \text{--- (3)}$$

which, using equation (a) becomes:

$$F(4) = \gamma P_4 M_4^2 A_4 \quad \text{--- (4)}$$

hence, the thrust augmentation ratio is:

$$\Phi = \frac{F(4)}{F(1)} = \frac{\gamma P_4 M_4^2 A_4}{(P_1^* (1+\gamma) - P_a) A_1} \quad \text{--- (5)}$$

since $\frac{A_4}{A_1} = \frac{n}{m}$ and by inserting $\gamma = 1.4$:

$$\Phi = \frac{1.4 M_4^2 n}{\left[2.4 \frac{P_1^*}{P_5} - 1 \right] m} \quad \text{--- (6)}$$

c) Inlet to nozzle thrust ratio:

The thrust on the inlet, $F(2)$ is given by:

$$F(2) = (P_2 - P_a + \rho_2 U_2^2) (A_2 - A_1) \quad \text{--- (7)}$$

from equations (a) and (2):

$$\frac{F(2)}{F(1)} = \frac{(P_2 (1 + \gamma M_2^2) - P_a) (A_2 - A_1)}{(P_1^* (1+\gamma) - P_a) A_1} \quad \text{--- (8)}$$

by using equation (b) since $p_{02} = p_a$, and with $\gamma = 1.4$:

$$\frac{F(2)}{F(1)} = \frac{\left[\frac{1 + 1.4 M_2^2}{(1 + 0.2 M_2^2)^{\frac{7}{2}}} - 1 \right]}{\left[2.4 \frac{P_1^*}{P_a} - 1 \right]} \left[\frac{1}{m} - 1 \right] \quad \text{--- (9)}$$

d) Mass augmentation ratio (MAR), Ψ :

The MAR is defined as the ratio of entrained mass flow rate divided by the nozzle mass flow rate. The mass flow rate is given by:

$$\dot{m}_1 = \rho_1^* U_1^* A_1 \quad \text{--- (10)}$$

$$\left(\text{where } \rho_1^* = \frac{\rho_{00}}{\left[\frac{\gamma+1}{2} \right]^{\frac{1}{\gamma-1}}} \quad \text{and } U_1^* = a_1^* = (\gamma R T_1^*)^{\frac{1}{2}}, \quad T_1^* = \frac{T_{00}}{1.2} \right)$$

the entrained mass flow rate is:

$$\dot{m}_2 = \rho_2 U_2 (A_2 - A_1) \quad \text{--- (11)}$$

from equation (b) and (c):

$$\Psi = \frac{\dot{m}_2}{\dot{m}_1} = \frac{\rho_a a_a M_2 \left[\frac{1}{m} - 1 \right]}{\rho_1^* U_1^* \left[1 + \frac{\gamma-1}{2} M_2^2 \right]^{\frac{\gamma}{\gamma-1}}} \quad \text{--- (12)}$$

e) Diffuser exit temperature:

Multiplying the mass equation derived in Appendix IA (equation (6)) by $T_a^{1/2}/\rho_a$ and rearranging produces:

$$T_a = T_a \left[\frac{M_4 n}{\frac{P_{01}}{P_a} TR^{-\frac{1}{2}} \frac{m}{1.2^3} + \frac{M_2 (1-m)}{(1 + 0.2 M_2^2)^3}} \right]^2 \quad \text{--- (13)}$$

f) Change in entropy:

The datum entropy was selected to correspond with the entrained inlet, i.e. position 2, therefore $S_2 = 0$. The change in entropy is given by:

$$dS = \dot{m}_4 S_4 - \dot{m}_1 S_1 \quad \text{--- (14)}$$

where, from equation (5) in Appendix IA we get:

$$\dot{m}_1 = p_1^* A_1 \left[\frac{\gamma}{RT_1^*} \right]^{\frac{1}{2}}$$

and

$$\dot{m}_4 = p_4 M_4 A_4 \left[\frac{\gamma}{RT_4} \right]^{\frac{1}{2}}$$

the two entropy terms are:

$$S_1 = C_v \ln \frac{\left[\frac{T_{01}}{T_a} \right]^\gamma}{\left[\frac{p_{01}}{p_a} \right]^{\gamma-1}} \quad \text{--- (15)}$$

and

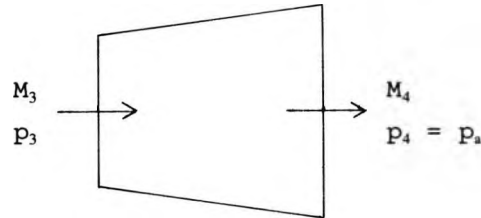
$$S_4 = C_v \ln \eta \left[\frac{T_4}{T_a} \right]^\gamma \quad \text{--- (16)}$$

hence,

$$\frac{dS}{A_1} = C_v \left[\frac{\gamma}{R} \right]^{\frac{1}{2}} \left[\frac{p_4 M_4}{T_4^{\frac{1}{2}}} \frac{n}{m} \ln \left[\eta \left[\frac{T_4}{T_a} \right]^\gamma \right] - \frac{p_1^*}{T_1^*^{\frac{1}{2}}} \ln \left[\frac{\left[\frac{T_{01}}{T_a} \right]^\gamma}{\left[\frac{p_{01}}{p_a} \right]^{\gamma-1}} \right] \right] \quad \text{--- (17)}$$

10.1.3.) APPENDIX IC:

DERIVATION OF RELATIONSHIP BETWEEN TOTAL PRESSURE AND
STATIC PRESSURE DIFFUSER EFFICIENCY:



define:

$$\eta_{stat} = \frac{(P_4 - P_3)_{actual}}{(P_4 - P_3)_{ideal}} \quad \text{--- (IC.1)}$$

or:

$$\eta_{stat} = \frac{\left(1 - \frac{P_3}{P_4}\right)_{actual}}{\left(1 - \frac{P_3}{P_4}\right)_{ideal}} \quad \text{--- (IC.2)}$$

for a diffuser without any losses:

$$P_{03} = P_{04} \quad \text{--- (IC.3)}$$

$$P_3 \left[1 + \frac{\gamma-1}{2} M_3^2\right]^{\frac{\gamma}{\gamma-1}} = P_4 \left[1 + \frac{\gamma-1}{2} M_4^2\right]^{\frac{\gamma}{\gamma-1}} \quad \text{--- (IC.4)}$$

or:

$$\frac{P_3}{P_4} = \frac{\left[1 + \frac{\gamma-1}{2} M_4^2\right]^{\frac{\gamma}{\gamma-1}}}{\left[1 + \frac{\gamma-1}{2} M_3^2\right]^{\frac{\gamma}{\gamma-1}}} \quad \text{--- (IC.5)}$$

it follows that:

$$\eta_{stat} = \frac{\left[1 - \frac{P_3}{P_4}\right]_{actual}}{\left[1 - \frac{\left[1 + \frac{\gamma-1}{2} M_4^2\right]^{\frac{\gamma}{\gamma-1}}}{\left[1 + \frac{\gamma-1}{2} M_3^2\right]^{\frac{\gamma}{\gamma-1}}}\right]} \quad \text{--- (IC.6)}$$

rearranging this equation leads to:

$$\left[\frac{P_3}{P_4} \right]_{actual} = \eta_{stat} \frac{\left[1 + \frac{\gamma-1}{2} M_4^2 \right]^{\frac{\gamma}{\gamma-1}}}{\left[1 + \frac{\gamma-1}{2} M_3^2 \right]^{\frac{\gamma}{\gamma-1}}} - \eta_{stat} + 1 \quad \text{--- (IC.7)}$$

actual total pressure loss between inlet and exit of diffuser is given by:

$$P_{04} = \eta_o P_{03} \quad \text{--- (IC.8)}$$

or:

$$\frac{1}{\eta_o} = \frac{P_{03}}{P_{04}} = \left[\frac{P_3}{P_4} \right]_{actual} \frac{\left[1 + \frac{\gamma-1}{2} M_3^2 \right]^{\frac{\gamma}{\gamma-1}}}{\left[1 + \frac{\gamma-1}{2} M_4^2 \right]^{\frac{\gamma}{\gamma-1}}} \quad \text{--- (IC.9)}$$

inserting this equation into equation --- (7) above leads to:

$$\frac{1}{\eta_o} = \frac{\eta_{stat} \frac{\left[1 + \frac{\gamma-1}{2} M_4^2 \right]^{\frac{\gamma}{\gamma-1}}}{\left[1 + \frac{\gamma-1}{2} M_3^2 \right]^{\frac{\gamma}{\gamma-1}}} - \eta_{stat} + 1}{\frac{\left[1 + \frac{\gamma-1}{2} M_4^2 \right]^{\frac{\gamma}{\gamma-1}}}{\left[1 + \frac{\gamma-1}{2} M_3^2 \right]^{\frac{\gamma}{\gamma-1}}}} \quad \text{--- (IC.10)}$$

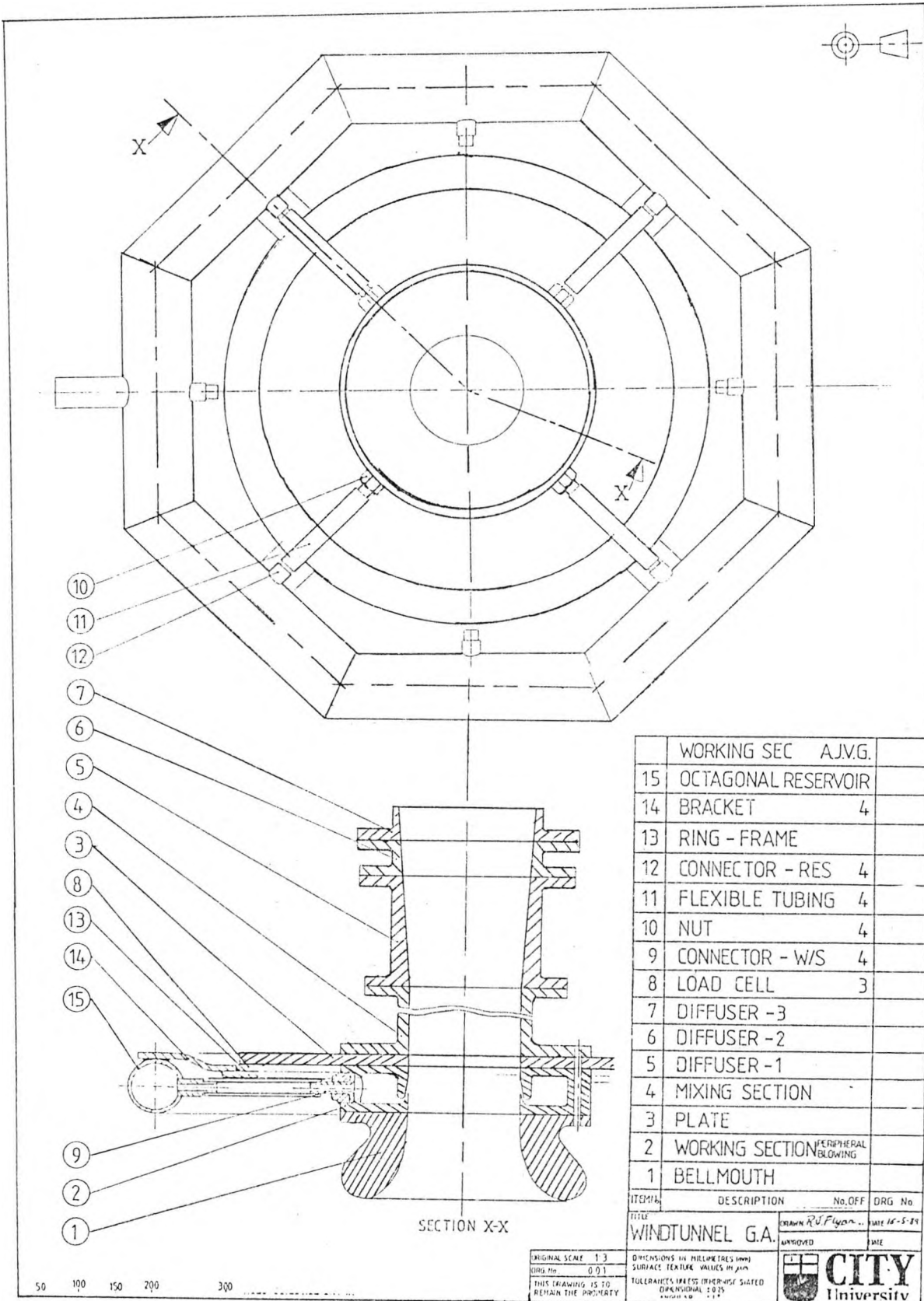
or clearly:

$$\eta_o = \frac{\frac{\left[1 + \frac{\gamma-1}{2} M_4^2 \right]^{\frac{\gamma}{\gamma-1}}}{\left[1 + \frac{\gamma-1}{2} M_3^2 \right]^{\frac{\gamma}{\gamma-1}}}}{\eta_{stat} \frac{\left[1 + \frac{\gamma-1}{2} M_4^2 \right]^{\frac{\gamma}{\gamma-1}}}{\left[1 + \frac{\gamma-1}{2} M_3^2 \right]^{\frac{\gamma}{\gamma-1}}} - \eta_{stat} + 1} \quad \text{--- (IC.11)}$$

10.2.) APPENDIX II:

List of drawings:

	page
001 General arrangement of rig	176
001a General arrangement of rig	177
001b Air jet vortex generator general arrangement	178
002 Bell-mouth	179
003c O-ring corner detail	180
005 Mixing section	181
006 Diffuser (frontal view)	182
007 Diffuser (side view)	183
010 Connector	184
011 Locking nut	185
016 Octagonal reservoir	186
017 Working section (vane and air jet mounting)	187
019 Spacer	188
020 Air jet vortex generator plug	189
020a Modified air jet vortex generator plug	190
021 Vane vortex generator plug	191
040 Main stand	192
050 Pitot rake assembly (plan view)	193
051 Pitot rake assembly (side view)	194
060 Acoustic booth	195
061 General layout of rig	196

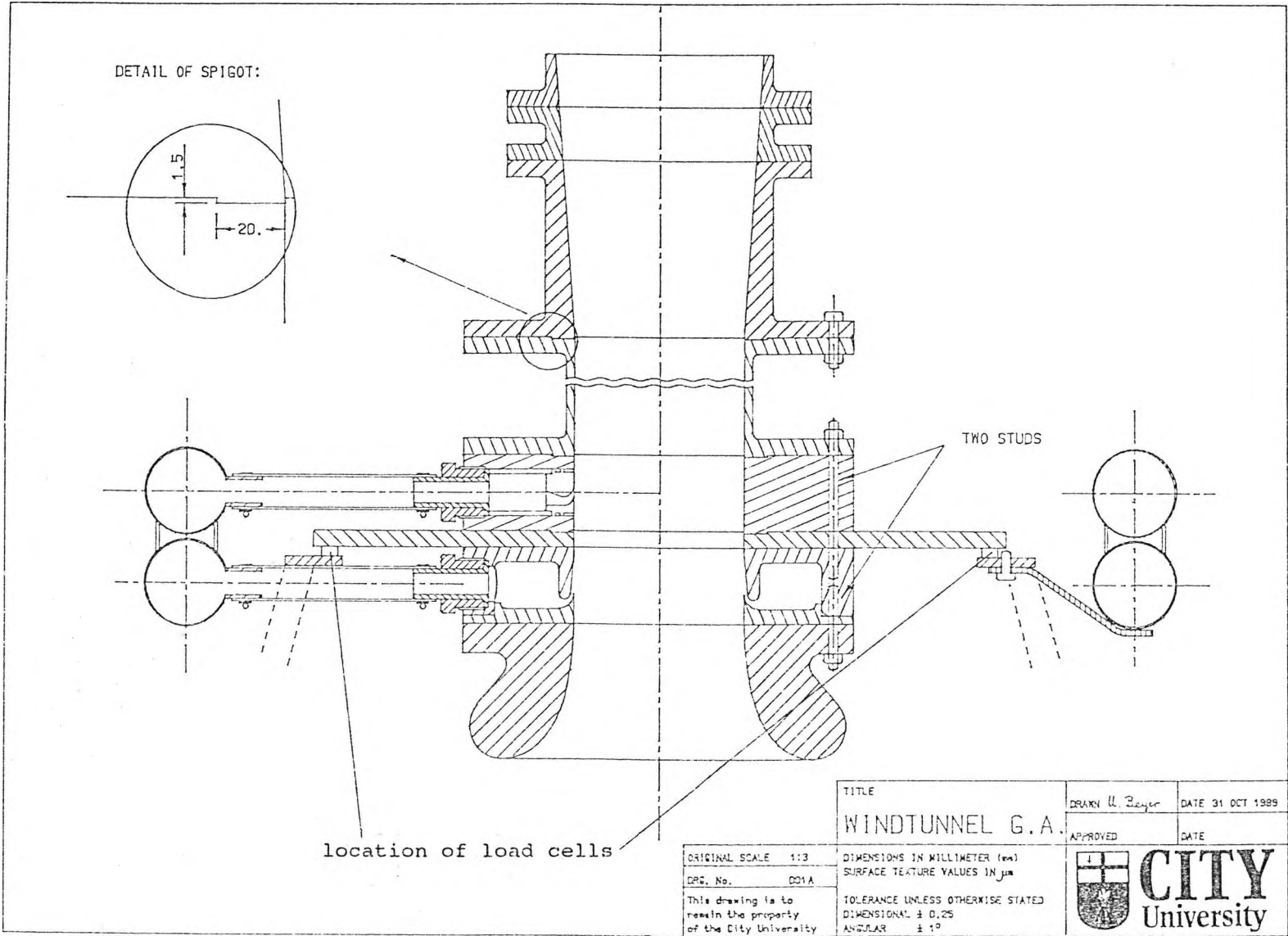


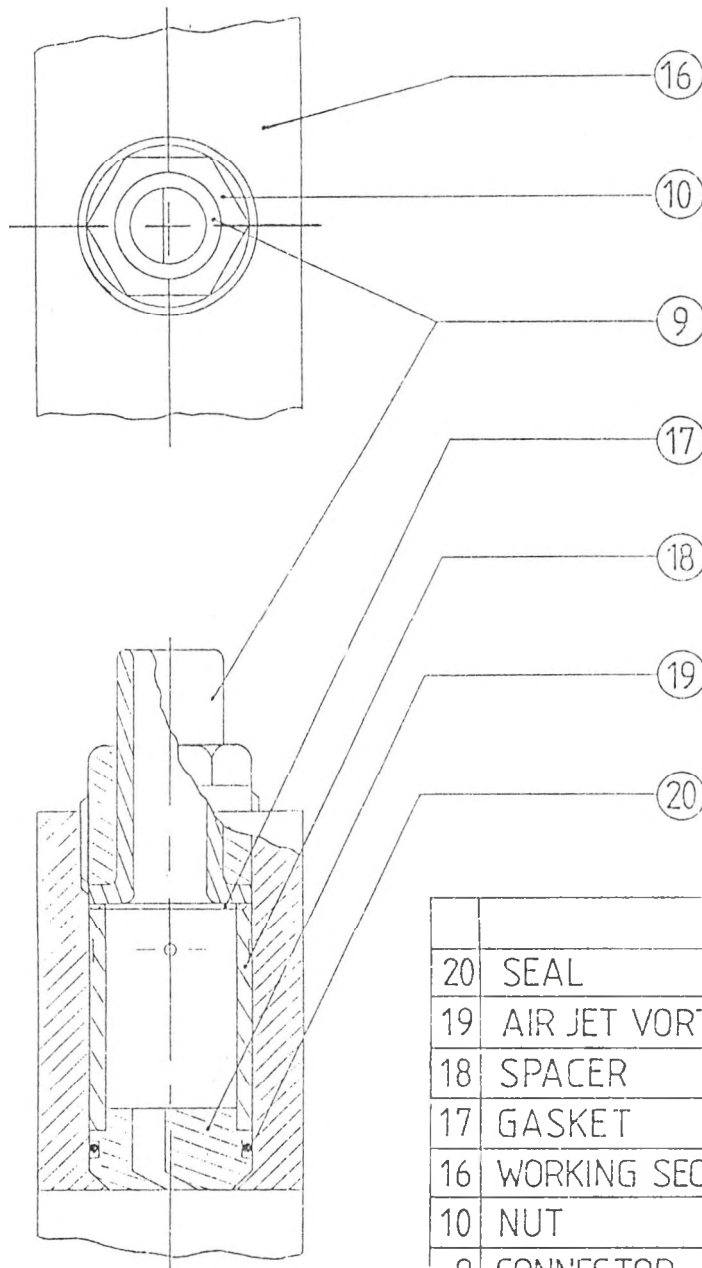
ITEM	DESCRIPTION	No. OFF	DRG No
	WORKING SEC	A.J.V.G.	
15	OCTAGONAL RESERVOIR		
14	BRACKET	4	
13	RING - FRAME		
12	CONNECTOR - RES	4	
11	FLEXIBLE TUBING	4	
10	NUT	4	
9	CONNECTOR - W/S	4	
8	LOAD CELL	3	
7	DIFFUSER - 3		
6	DIFFUSER - 2		
5	DIFFUSER - 1		
4	MIXING SECTION		
3	PLATE		
2	WORKING SECTION <small>PERIPHERAL BLOWING</small>		
1	BELLMOUTH		

WINDTUNNEL G.A.		DATE 10-5-89
APPROVED	DATE	
CITY University		

ORIGINAL SCALE 1:3
 DRG No 001
 DIMENSIONS IN MILLIMETRES (mm)
 SURFACE TEXTURE VALUES IN µm
 TOLERANCES UNLESS OTHERWISE SPECIFIED
 DIMENSIONAL ± 0.25

50 100 150 200 300





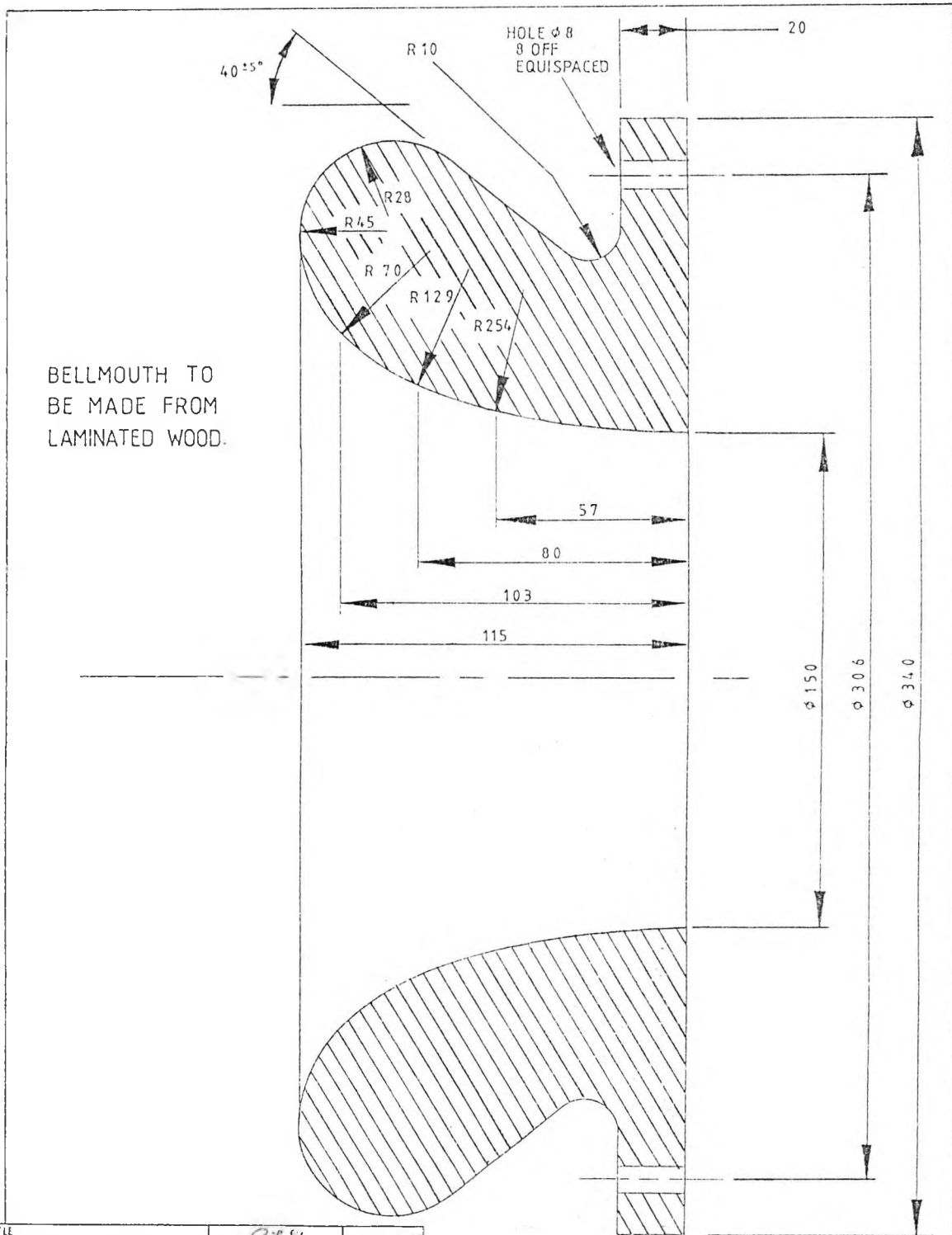
20	SEAL	16	
19	AIR JET VORTEX GEN.	8	
18	SPACER	8	
17	GASKET	16	
16	WORKING SEC. A.J.V.G.	1	
10	NUT	8	
9	CONNECTOR - W/S	8	
ITEM No.	DESCRIPTION.	No. OFF	ORG No.

TITLE: A.J.V.G. GEN' ARR
 DRAWN: R.J. Plym...
 DATE: 12 July 19...
 APPROVED: _____
 DATE: _____

ORIGINAL SCALE: 1:1
 ORG. No. 001b
 THIS DRAWING IS TO REMAIN THE PROPERTY OF TIR. CITY UNIVERSITY

DIMENSIONS IN MILLIMETRES (mm)
 SURFACE TEXTURE VALUES R1, R2
 TOLERANCES UNLESS OTHERWISE STATED
 DIMENSIONAL ± 0.25
 ANGULAR ± 1°



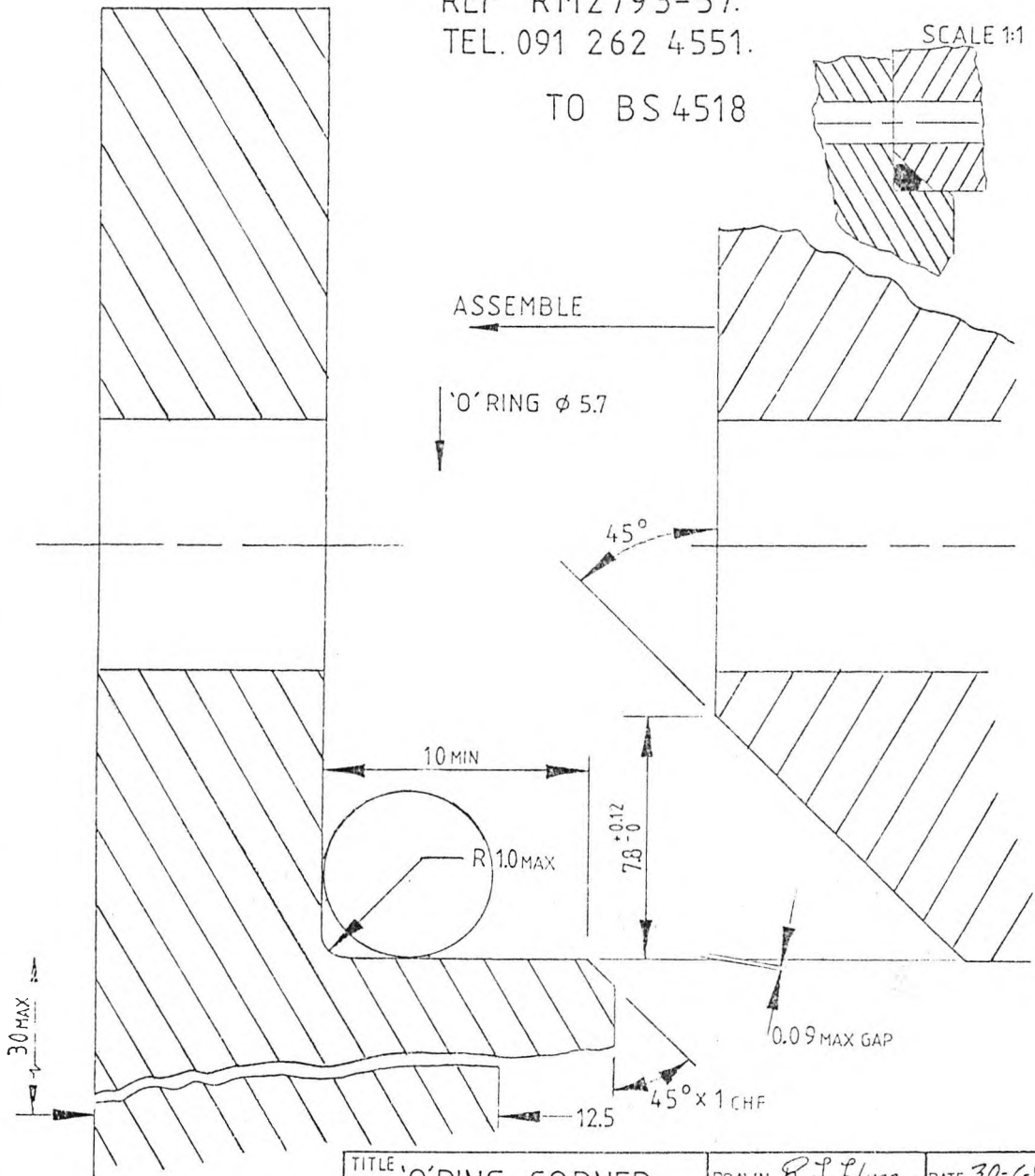


TITLE BELLMOUTH	DRAWN <i>R.J. Flynn</i>	DATE <i>27 Feb 88</i>
	APPROVED	DATE
DIMENSIONS IN MILLIMETRES (mm) SURFACE TEXTURE VALUES IN µm	 CITY University	
TOLERANCES UNLESS OTHERWISE STATED DIMENSIONAL ± 0.25 ANGULAR ± 1°	DRG No. 002 THIS DRAWING IS TO REMAIN THE PROPERTY OF THE CITY UNIVERSITY	

'O' RING TO BE SUPPLIED FROM
 GEORGE ANGUS + CO. LTD. FSD.
 REF RM2793-57.
 TEL. 091 262 4551.

TO BS 4518

SCALE 1:1



DO NOT SCALE.

ORIGINAL SCALE 6 : 1
 DRG.No. 003c
 THIS DRAWING IS TO
 REMAIN THE PROPERTY
 OF THE CITY UNIVERSITY

TITLE 'O' RING CORNER
 DETAIL 2nd ALT

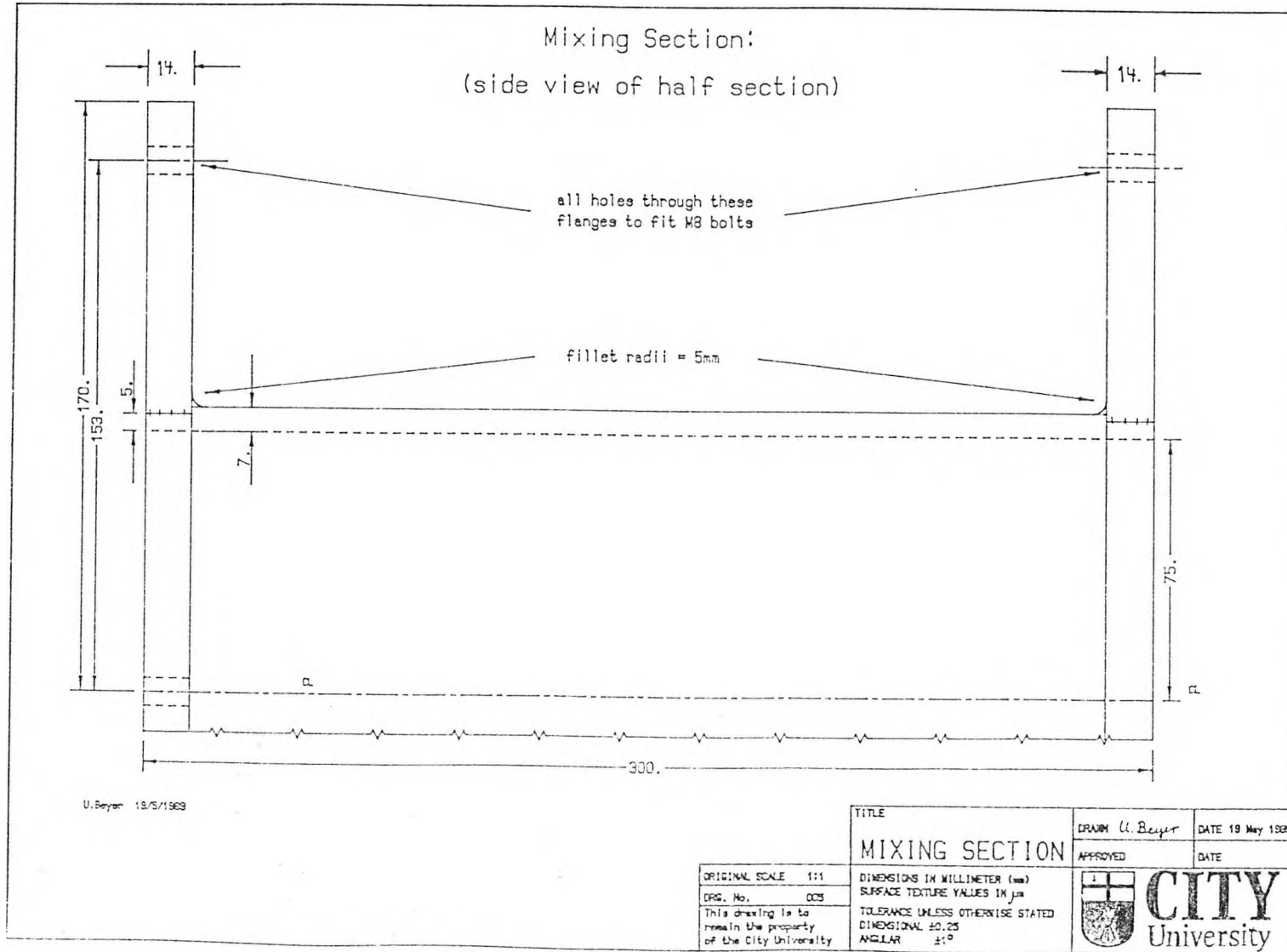
DIMENSIONS IN MILLIMETRES (mm)
 SURFACE TEXTURE VALUES IN μm
 TOLERANCES UNLESS OTHERWISE STATED
 DIMENSIONAL ± 0.25
 ANGULAR $\pm 1^\circ$

DRAWN *R. J. Flynn* DATE 30-6-89

APPROVED DATE

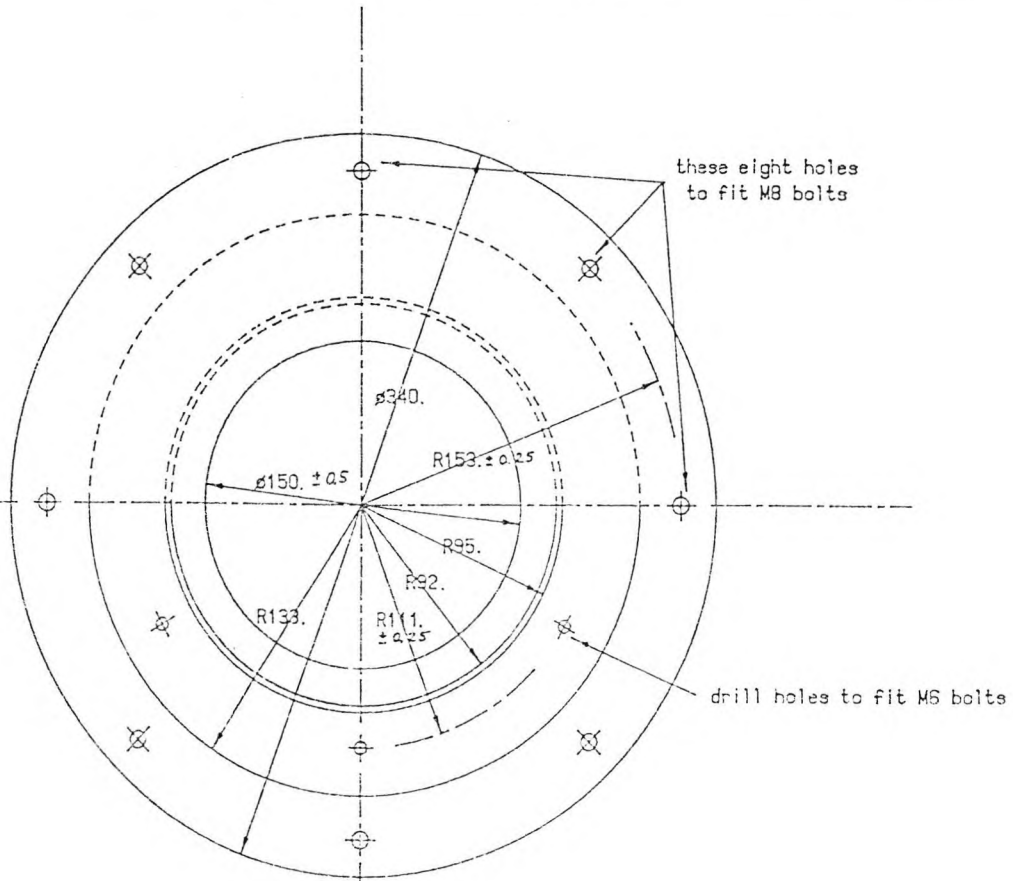


CITY
 University



DIFFUSER:
(front view)

(back view)



SCALE 1:2

U. Beyer 12/5/1989

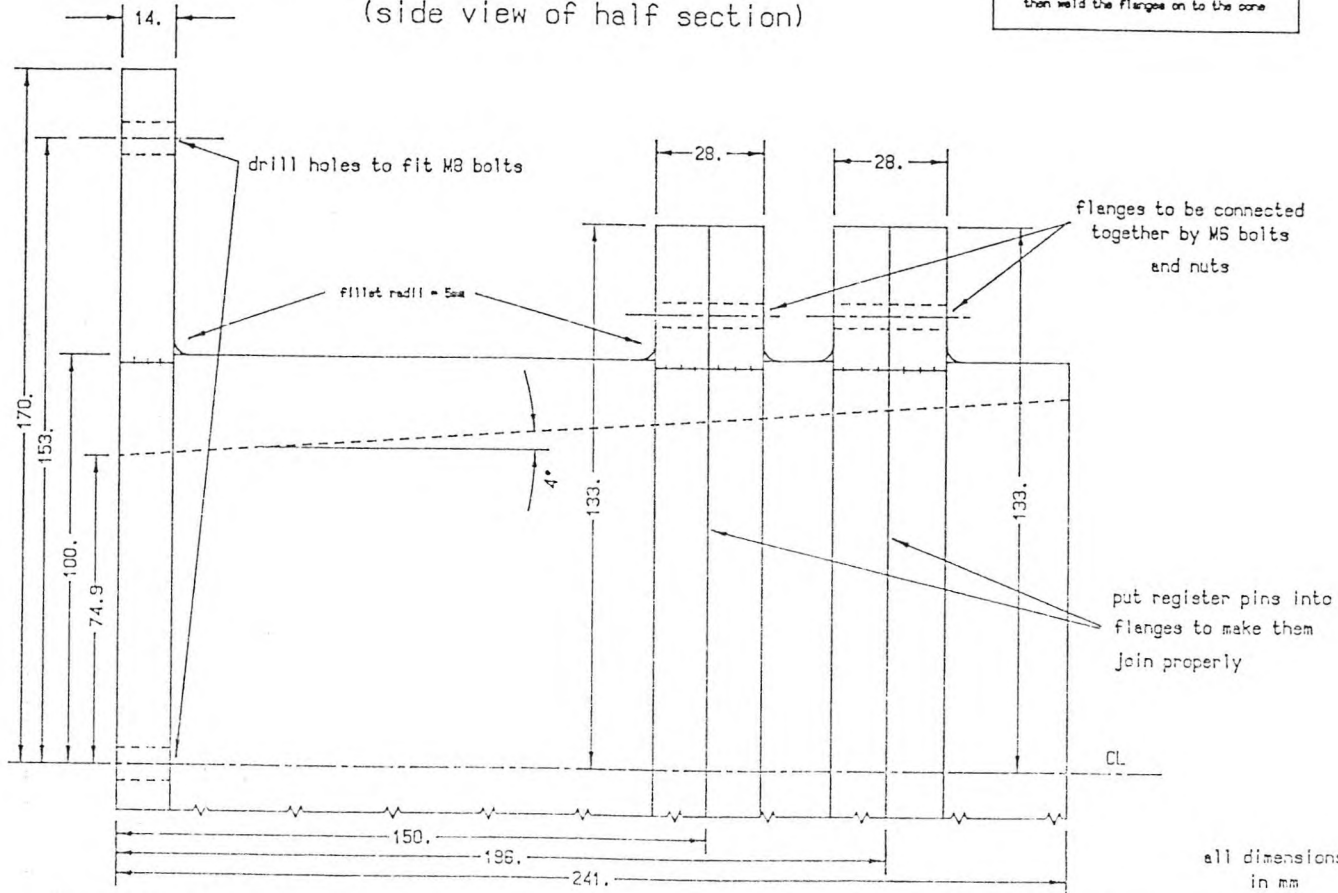
TITLE DIFFUSER (FRONTAL VIEW)		DRAWN U. Beyer	DATE 15 May 1989
APPROVED		DATE	
ORIGINAL SCALE 1:2	DIMENSIONS IN MILLIMETER (mm)		
ENG. No. 006	SURFACE TEXTURE VALUES IN μ m		
This drawing is to remain the property of the City University	TOLERANCE UNLESS OTHERWISE STATED		
	DIMENSIONAL ± 0.25		
	ANGULAR $\pm 1^\circ$		
		 CITY University	

Inspector

DIFFUSER:

(side view of half section)

cone shape to be manufactured out of thick-walled tube then weld the flanges on to the cone

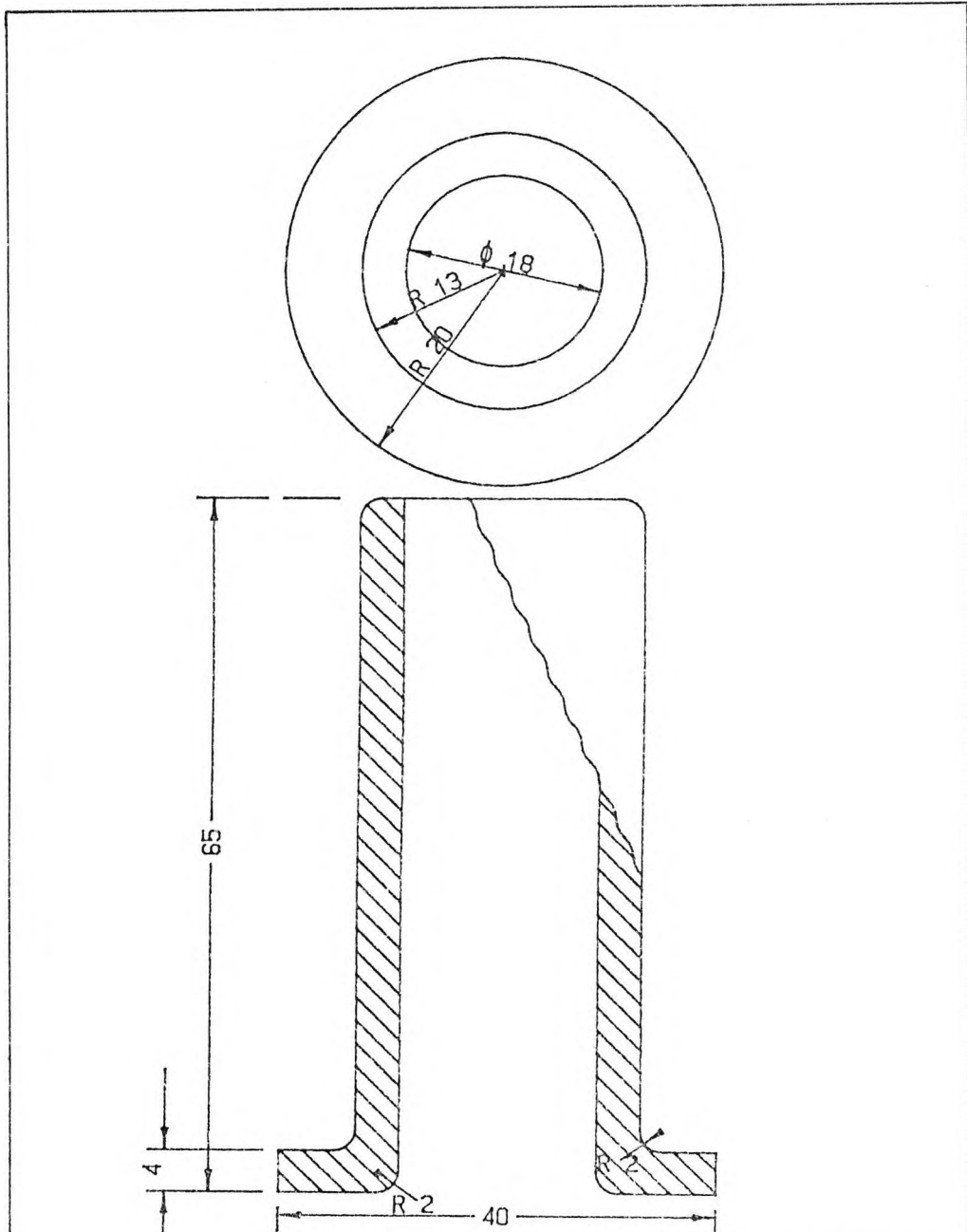


all dimensions in mm

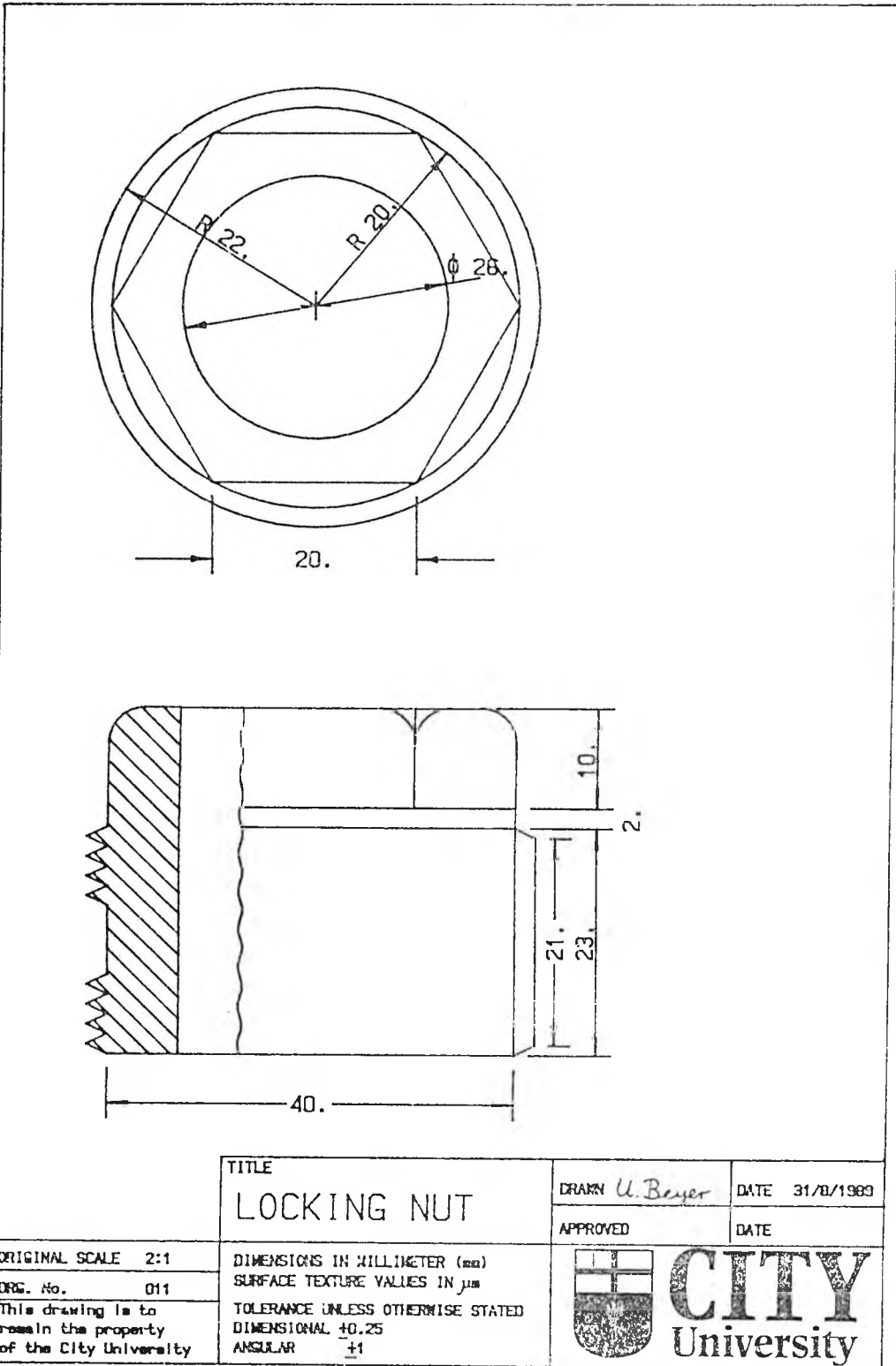
U. Beyer 13/5/1989

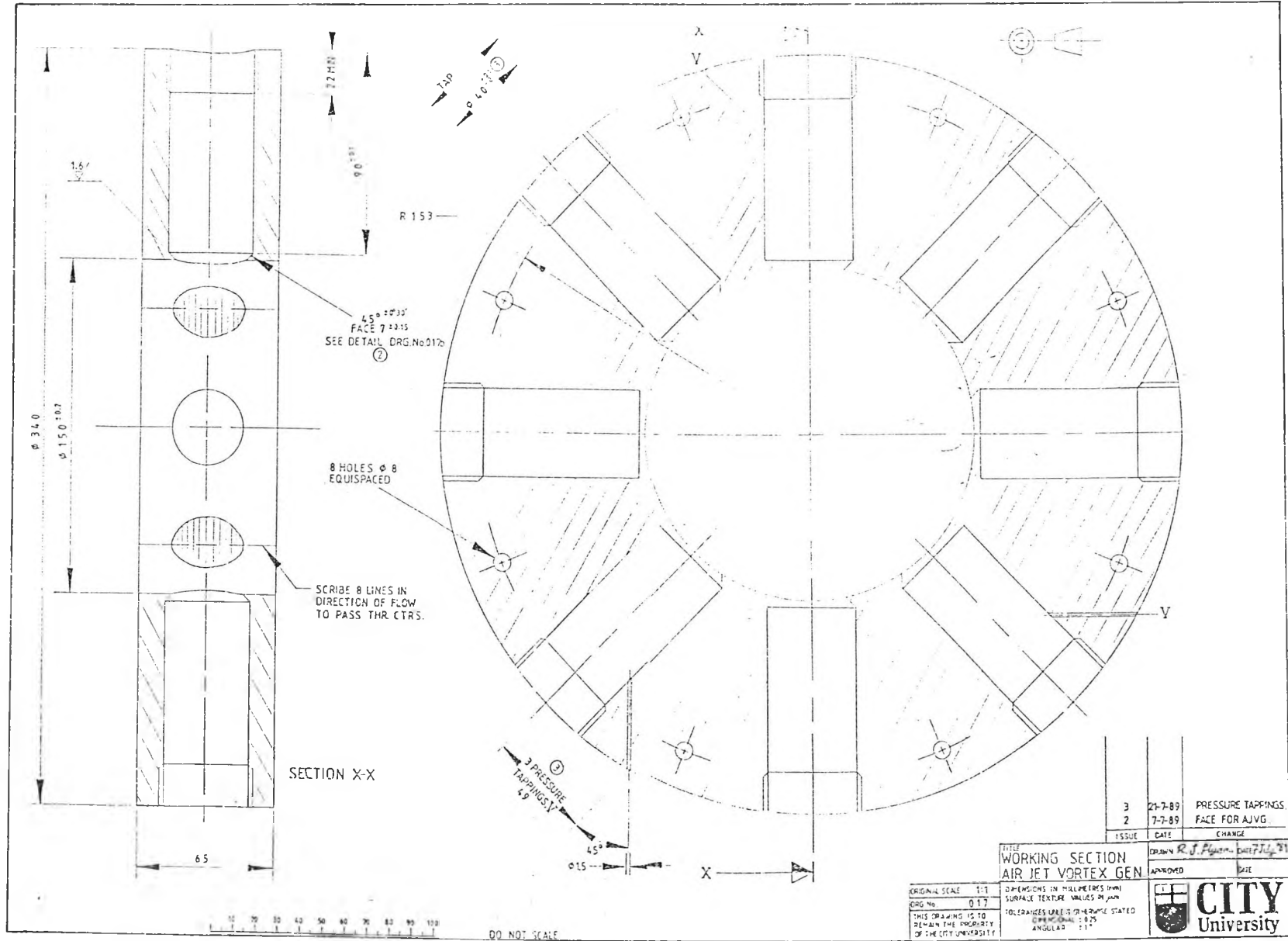
TITLE DIFFUSER (SIDE VIEW)		DRAWN U. Beyer	DATE 13 May 1989
ORIGINAL SCALE 1:1		APPROVED	DATE
ORG. No. 007	DIMENSIONS IN MILLIMETER (mm)	 CITY University	
This drawing is the property of the City University	SURFACE TEXTURE VALUES IN μm		
	TOLERANCE UNLESS OTHERWISE STATED DIMENSIONAL ± 0.25 ANGULAR $\pm 1^\circ$		

Ejector



TITLE		DRAWN <i>U. Beyer</i>		DATE 31/8/1989
CONNECTOR		APPROVED	DATE	
ORIGINAL SCALE 2:1	DIMENSIONS IN MILLIMETER (mm)	 CITY University		
DWG. No. 010	SURFACE TEXTURE VALUES IN μm			
This drawing is to remain the property of the City University	TOLERANCE UNLESS OTHERWISE STATED DIMENSIONAL ± 0.25 ANGULAR ± 1			





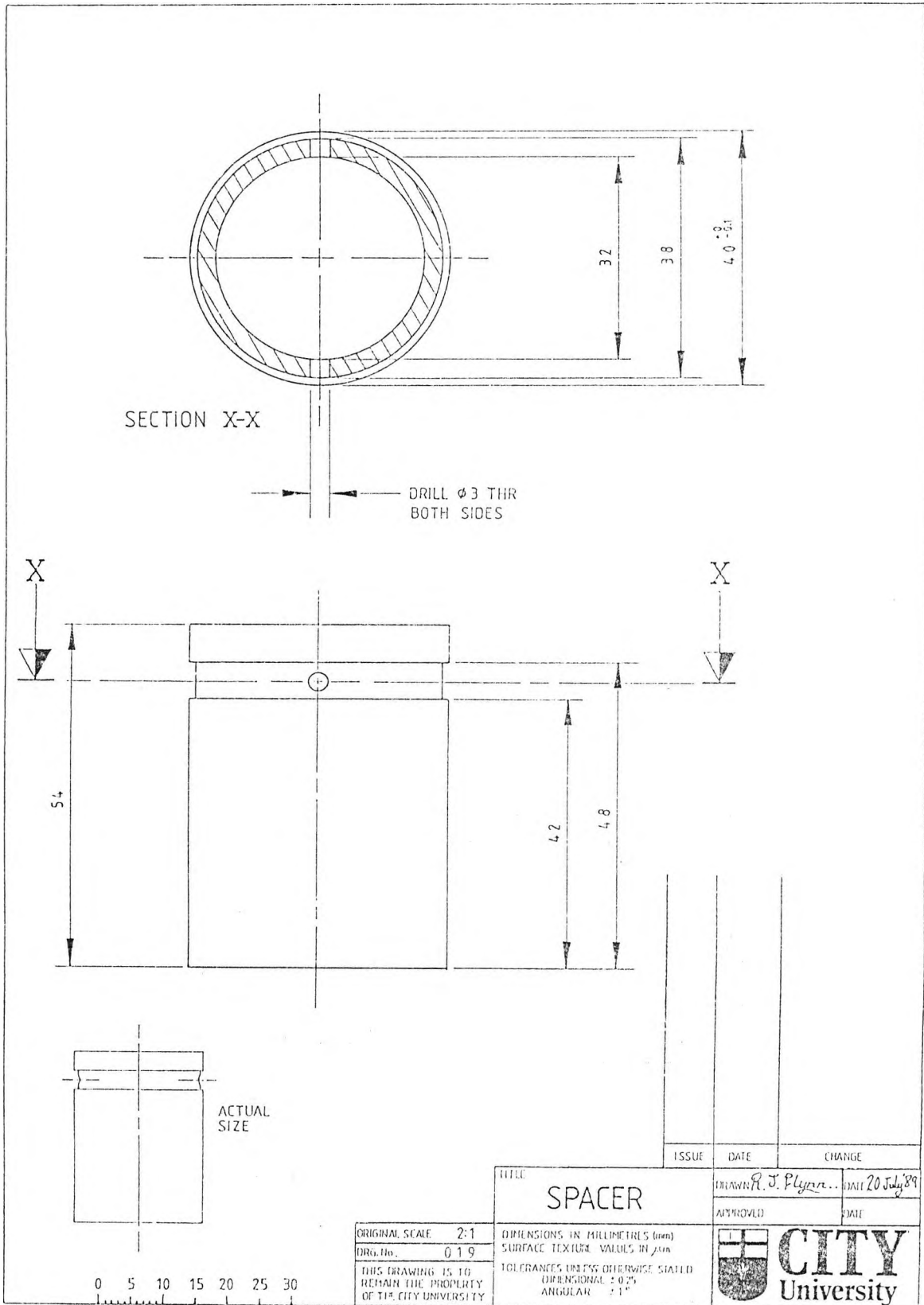
3	21-7-89	PRESSURE TAPPINGS
2	7-7-89	FACE FOR AJVG
ISSUE	DATE	CHANGE

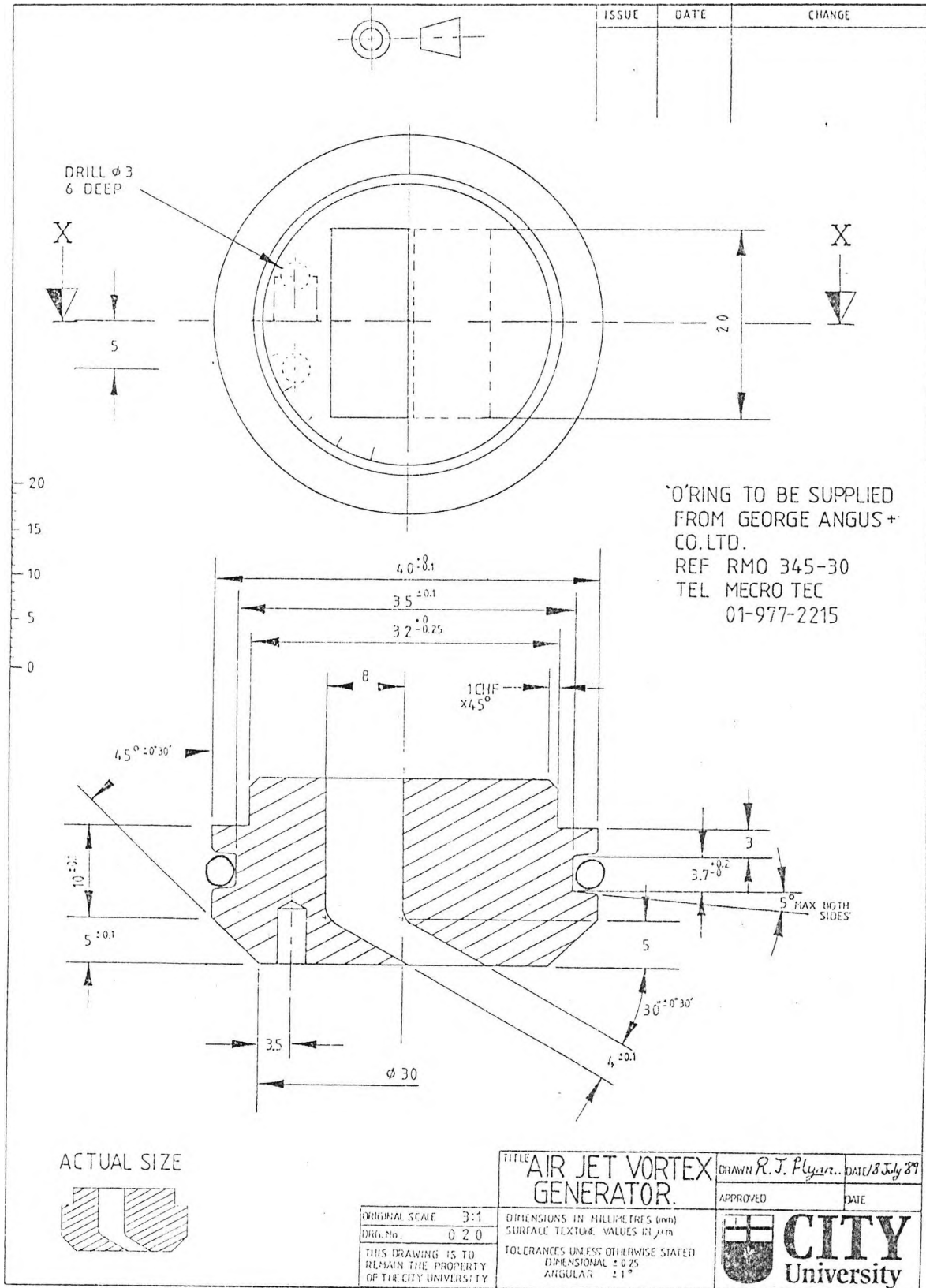
APPROVED *R. J. P...* DATE 7/15/89

ORIGINAL SCALE 1:1
 DIMENSIONS IN MILLIMETRES (MM)
 SURFACE TEXTURE VALUES IN µm
 THIS DRAWING IS TO REMAIN THE PROPERTY OF THE CITY UNIVERSITY

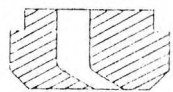
TITLE WORKING SECTION AIR JET VORTEX GEN
 DIMENSIONAL : 0.25
 ANGULAR : 1°





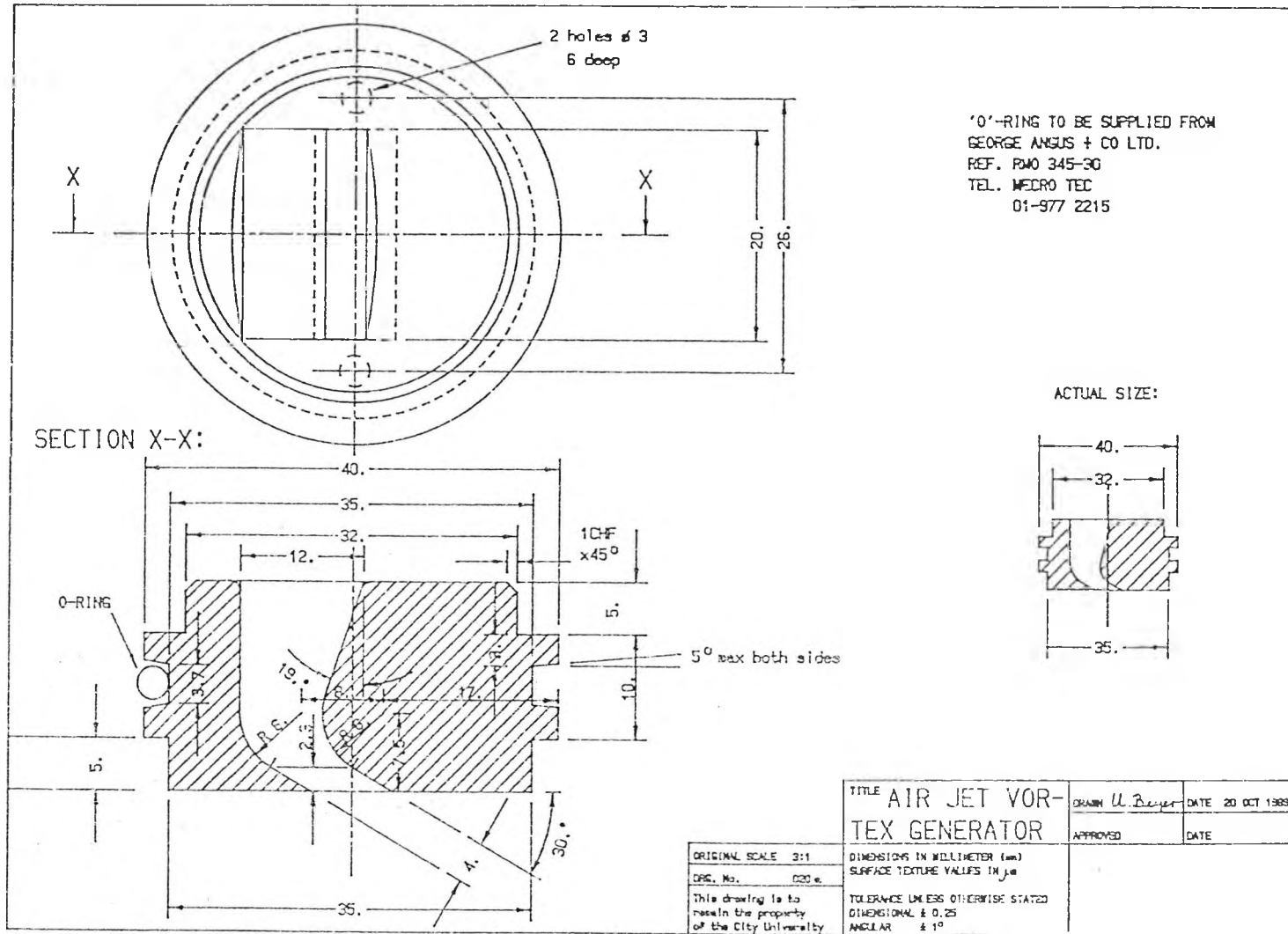


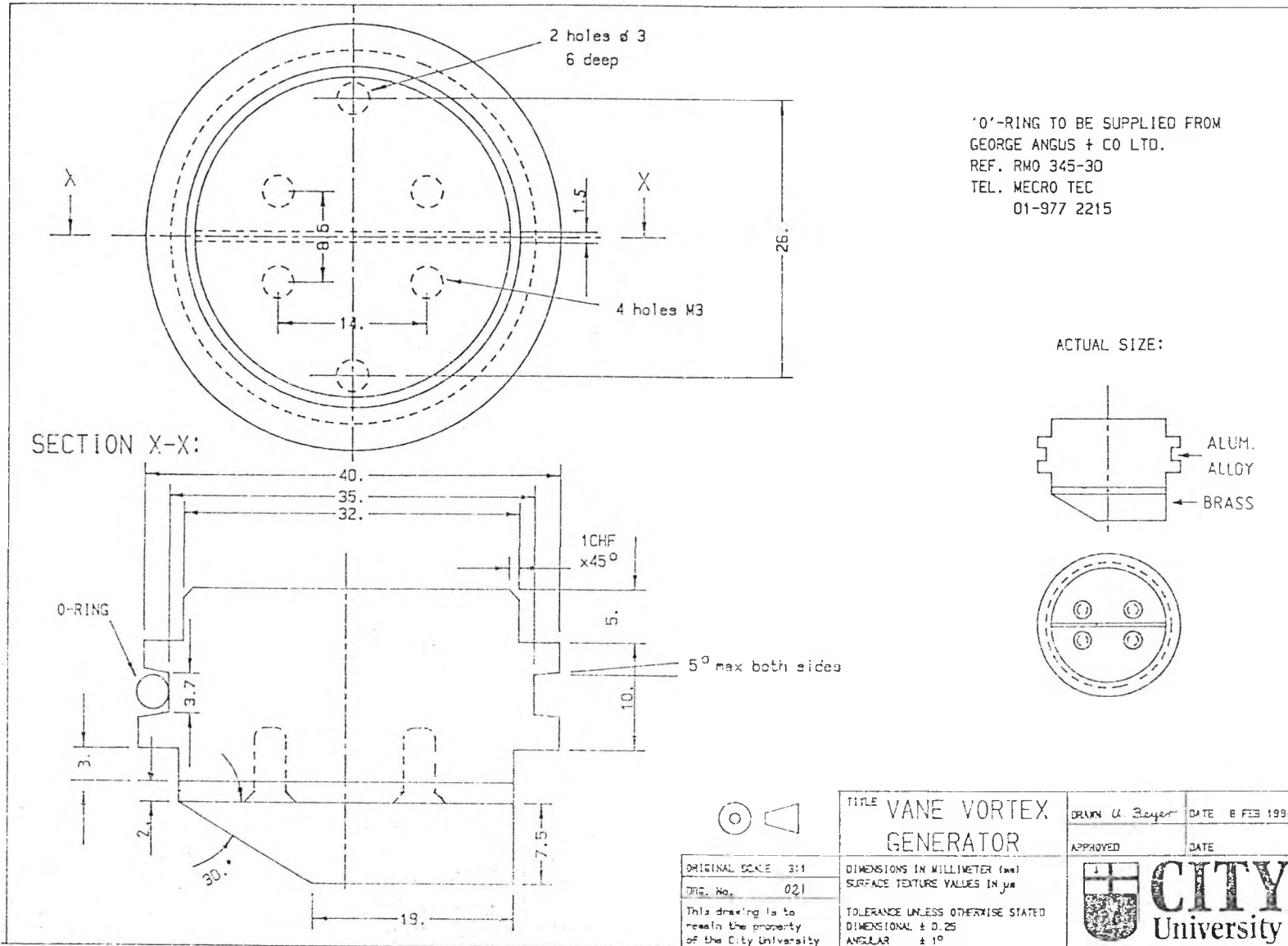
ACTUAL SIZE

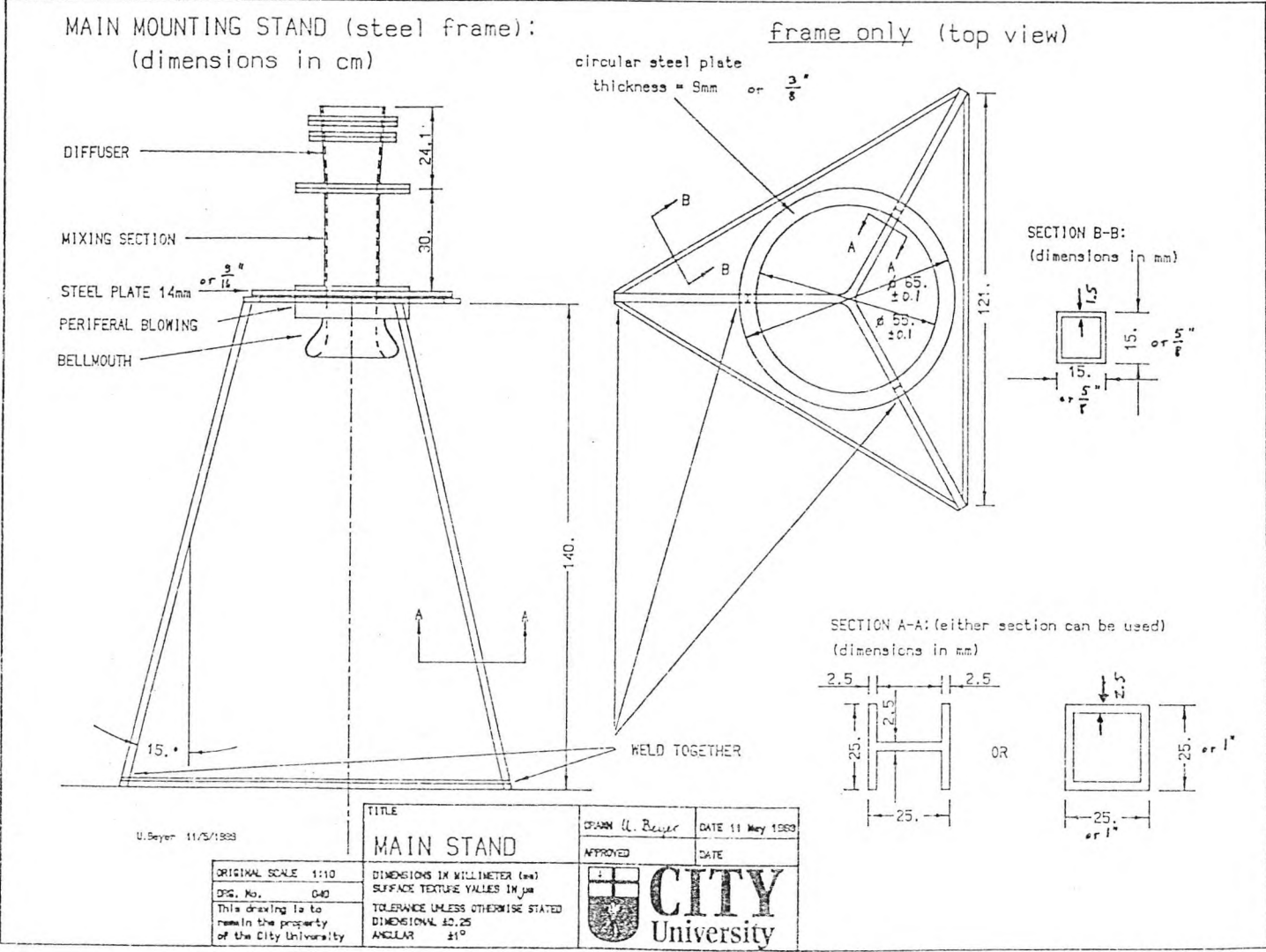


ORIGINAL SCALE 3:1
 DIM. NO. 0 2 0
 THIS DRAWING IS TO REMAIN THE PROPERTY OF THE CITY UNIVERSITY

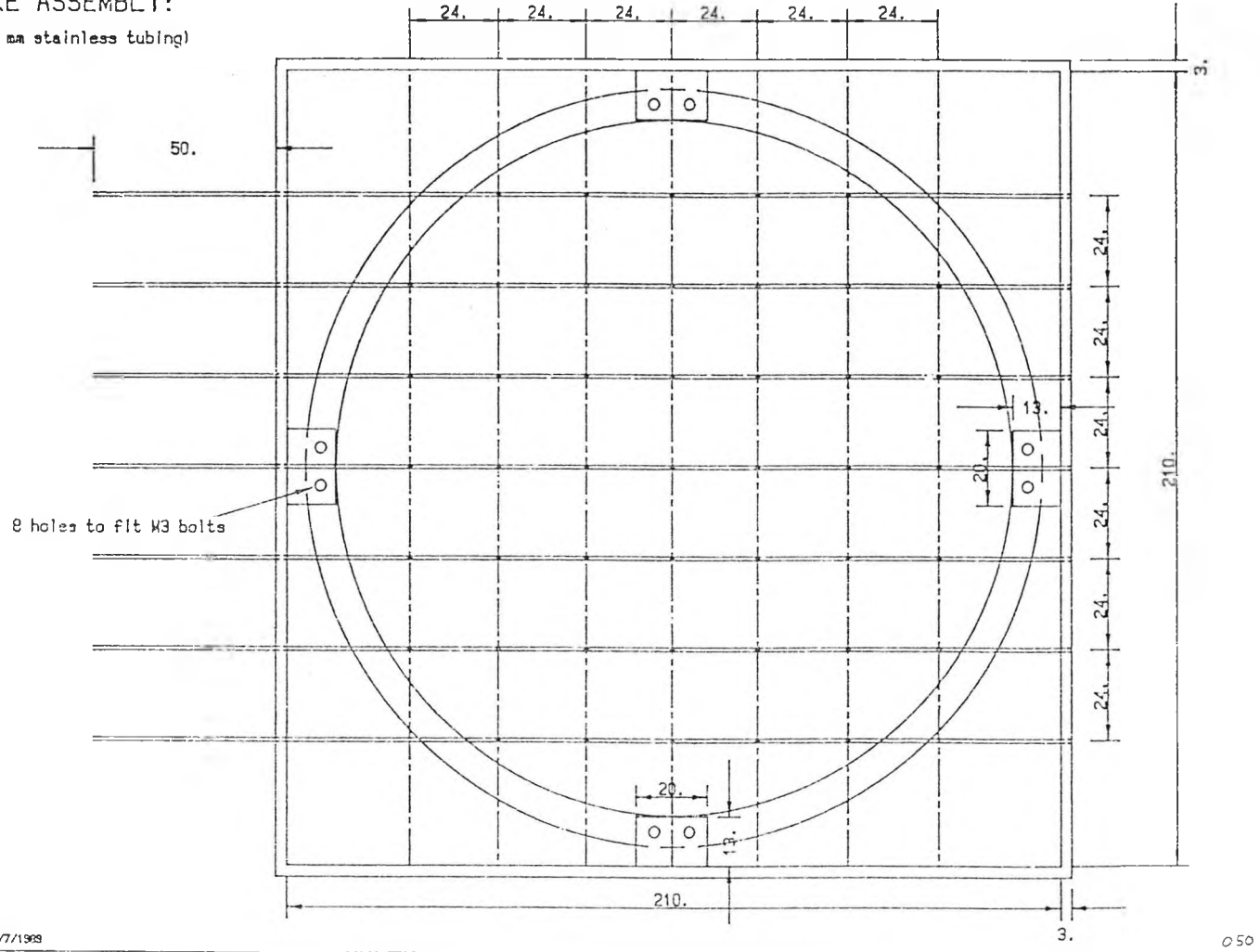
TITLE AIR JET VORTEX GENERATOR.		DRAWN R. J. PLYM...		DATE 18 July 89	
DIMENSIONS IN MILLIMETRES (MM)		APPROVED		DATE	
SURFACE TEXTURE VALUES IN µm				CITY University	
TOLERANCES UNLESS OTHERWISE STATED					
DIMENSIONAL ± 0.25 ANGULAR ± 1°					







RAKE ASSEMBLY:
(1.1 mm stainless tubing)



Section A-A:
hypodermic tubing (brass)

